University of Huddersfield Repository

Russell, Mark A.

Kinetics and mechanisms of steps in anti-sense oligonucleotide synthesis

Original Citation

Kinetics and Mechanisms of Steps in Anti-sense Oligonucleotide Synthesis

by

Mark A. Russell B.Sc. (Hons)

2007

Thesis submitted in partial fulfilment of the requirements for the degree of Doctor of Philosophy

Department of Chemical and Biological Sciences

The University of Huddersfield

Abstract

Mechanistic studies are reported for the detritylation, coupling and sulphurisation reactions involved in oligonucleotide synthesis by the phosphoramidite method.

Detritylation is the acid catalysed removal of a 4,4-dimethoxytrityl protecting group from the 5' protected nucleotide to give the 5' deprotected nucleotide and the 4,4-dimethoxytrityl carbocation. In the absence of water and at high acid concentrations the equilibrium favours carbocation formation. Equilibrium profiles show a sigmoidal shape rather than the expected hyperbolic curves and it is likely that residual water in the system reacts with the carbocation to form the 4,4-dimethoxytrityl alcohol. Results of kinetic studies of the detritylation reaction show that the detritylation reaction proceeds by a concerted general acid catalysis mechanism.

The coupling step is the reaction between an alcohol and a phosphoramidite in the presence of an acidic activator, in this research the salt of saccharin and *N*-methylimidazole. ^{31}P NMR studies have shown that initial activation of the phosphoramidite forms a reactive saccharin adduct bonded through its carbonyl oxygen to phosphorus. Reaction of the alcohol and phosphoramidite in the presence of saccharin/*N*-methylimidazole salt shows second order kinetics. However, at high alcohol concentrations the reaction becomes independent of alcohol. This indicates a change in rate limiting step from the final alcoholysis step to the activation step.

Phosphite sulphurisation was performed with the sulphur transfer reagent 3-amino-1,2,4-dithiazole-5-thione (xanthane hydride). Contrary to the previously reported mechanism of sulphurisation, nucleophilic attack by the phosphorus upon xanthane hydride occurs on the sulphur adjacent to the thiocarbonyl group and not on the sulphur adjacent to the amino group. Kinetic measurements of the sulphurisation reaction show second order kinetics. Reaction constants determined from Hammett and Taft constants for triaryl and trialkylphosphites are -1.09 and -1.20 respectively. These reaction constants indicate partial formation of a positive charge in the transition state. The effect of solvent polarity on the rate of sulphurisation has shown a decrease in rate on increasing the polarity of the solvent. This has been attributed to an increase in the xanthane hydride stability in more polar solvents.

<u>Acknowledgements</u>

Table of Contents

Table of figures

Table of tables

Table of schemes

Table of spectra

Abbreviations

CEO	cyanoethyl group
TH	tetrazole
Xanthane hydride	3-amino-1,2,4-dithiazole-5-thione
XH	3-amino-1,2,4-dithiazole-5-thione
DMTr-OT	4,4-dimethoxytritylthymidine
$DMTr^+$	4,4-dimethoxytrityl carbocation
HA	acid
PTSA	*para*-toluenesulphonic acid
i-Pr	*iso*-propyl group
X^-	non-specific anion
Nuc	nucleophile
SH	saccharin
sac	saccharin
NMI	*N*-methylimidazole
SMI	saccharin/*N*-methylimidazole salt
DIA	diisopropylamine
T-amidite	5'-4,4-dimethoxytritylthymidine-3'-*β*-cyanoethyl-*N,N*-diisopropylphosphoramidite (11)
Sc	specific conductance
Bc	background conductance
Mc	measured conductance
ITC	isothermal titration calorimetery
RF	retention factor
ε	molar extinction coefficient

1   Introduction

1.1   General Introduction

1.1.1   Anti-sense oligonucleotide mode of action

Many diseases are due to the overproduction or mis-production of proteins, the majority of drugs that are used to cure these diseases target these proteins. Proteins have large and complex structures, which makes their mode of action difficult to fully understand. This makes drug design difficult and drug discovery is often left to chance through screening of thousands of compounds.

The natural synthesis of proteins is achieved by two steps: transcription and translation. Transcription is the process by which genetic information is transmitted from DNA to mRNA. The process is facilitated by an enzyme; mRNA polymerase which binds to the DNA chain at the point where transcription is to start. Upon binding of the enzyme, the DNA strand begins to unwind and the mRNA polymerase travels along the template strand, synthesising a ribonucleic acid chain which is a copy of the DNA template strand. The newly transcribed mRNA is released from the mRNA polymerase once the termination stage of its synthesis is reached. The transcription process can be repeated so that numerous mRNA strands are produced from just one DNA strand.[1-5]

The mRNA strands then undergo translation to produce proteins. Translation is initiated by the binding of a ribosomal subunit to the mRNA. The ribosome then moves along the mRNA strand binding amino acids attached to tRNA, producing a complementary nucleotide sequence on the mRNA strand. Once the correct sequence has been achieved the process is terminated and release factors release the new peptide from the ribosome and the other molecules involved are allowed to disperse. This process can then be repeated so that one mRNA strand can produce many peptides (figure 1). These peptides then undergo chain elongation into the target protein.[1-5]
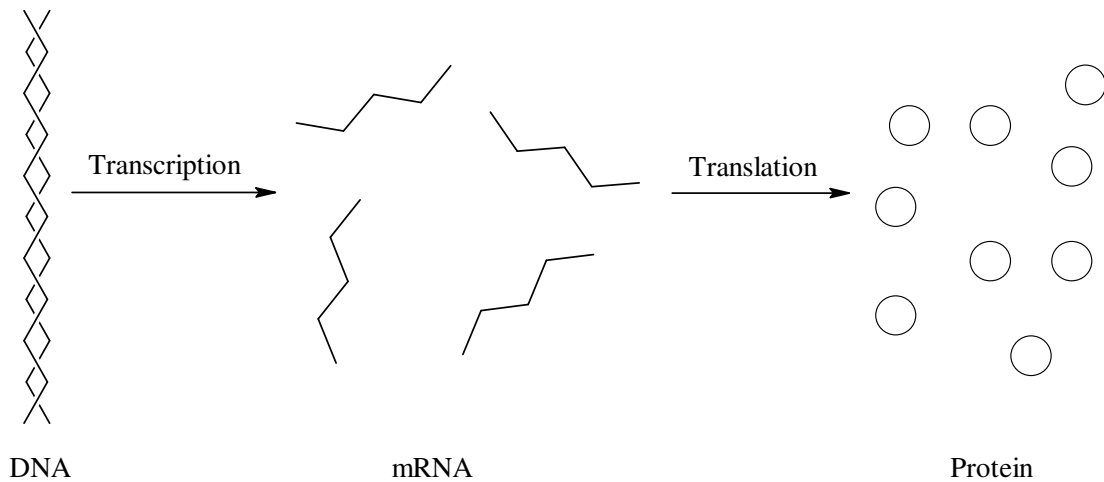
Figure 1: Simplified cartoon of natural protein production via DNA transcription and translation.

In the latter part of the 1970's Zamecnik and Stephenson[6,7] proposed that synthetic oligonucleotides could be used as therapeutic agents. Their early work showed that a synthesised oligodeoxynucleotide complementary to the 13 nucleotides of the terminal sequence of the Rous sarcoma virus could inhibit viral production. They postulated that this occurred through competitive hybridization of the synthetic oligonucleotide with the viral RNA, inhibiting translation and arresting further production.

Since then many studies have focused on synthesising oligonucleotides designed to inhibit production of unwanted genetic material in an aim to alleviate viral, bacterial and cancerous diseases.[5,8]

These synthesised oligonucleotides are designed to bind with a specific mRNA or DNA strand associated with a disease through Watson-Crick base pairing. The target mRNA is often termed the sense-strand which has led to this class of therapeutics being named anti-sense oligonucleotides. Disease alleviation with anti-sense oligonucleotides is potentially highly selective as a single 17 monomer unit anti-sense oligonucleotide would have unique bonding properties with only one mRNA strand, as statistically, a nucleic acid sequence of 17 units only occurs once in the human genome. Therefore, through rational drug design, production of unwanted genetic material can be inhibited if the sequence of nucleic acids in its mRNA can be determined.[4-10]

There have been a number of modes of action proposed for inhibition of protein production by anti-sense oligonucleotides the most popular and widely accepted of these being steric blocking of the mRNA by the anti-sense oligonucleotide and enzyme activation.[5,8,11,12]

1.1.1.1   Steric blocking

Hybridization of the anti-sense oligonucleotide at the terminal end of the mRNA strand by Watson-Crick base pairing forms a stable anti-sense oligonucleotide:mRNA duplex. The presence of the anti-sense oligonucleotide prevents the ribosomes and initiation factors required for translation, from binding to the mRNA, inhibiting the translation and subsequent production of the corresponding protein (figure 2).[4-7]
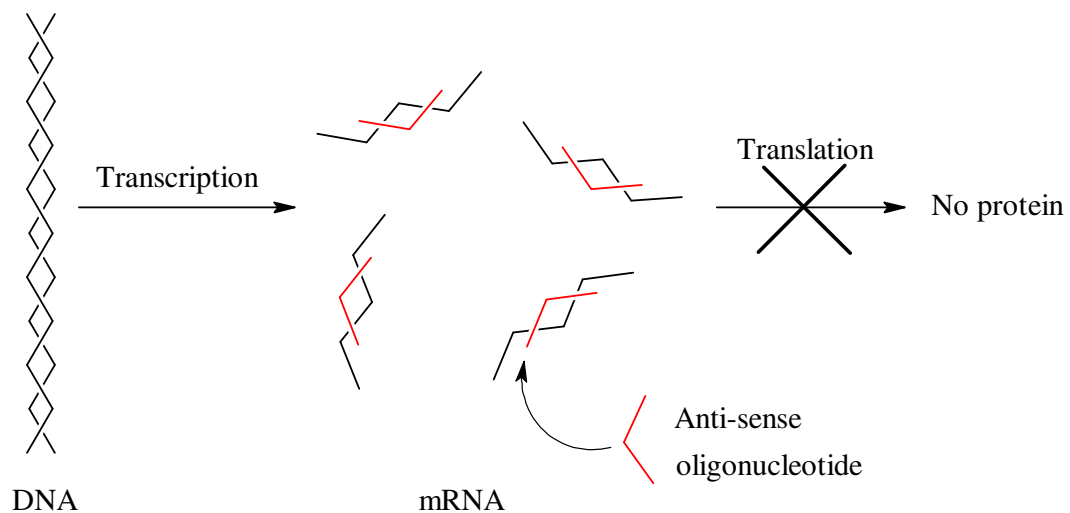
Figure 2: Simplified cartoon of translation inhibition via mRNA steric blocking by anti-sense oligonucleotides.

1.1.1.2   **Enzyme activation**

RNase H is a non-specific enzyme which cleaves the 3'-O-P bond of a growing RNA strand in a RNA:DNA duplex, terminating chain growth. Anti-sense oligonucleotides can activate RNase H to cleave the target mRNA strand by acting as the DNA mimic in the required RNA:DNA duplex. For the anti-sense oligonucleotide to function by this mechanism the RNase H enzyme must recognise the RNA:oligonucleotide duplex. The most effective way of achieving recognition is to incorporate an unmodified DNA gapmer into the anti-sense oligonucleotide. This gapmer is sandwiched between modified oligonucleotides to give the oligonucleotide other desired characteristics such as aqueous solubility, cell permeability and nuclease resistance (figure 3). Anti-sense oligonucleotides which act by this mechanism are catalytic and are therefore highly potent therapeutic agents and are the focus of many studies.[4,5,8,11,12]
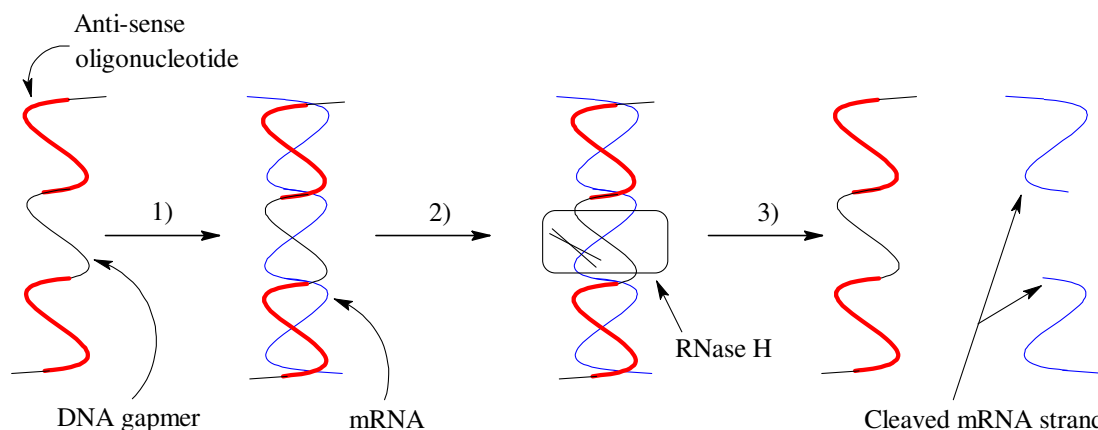
Figure 3: Mechanism of protein inhibition by RNase H activation: 1) anti-sense oligonucleotide containing DNA gapmer binds with target mRNA strand, 2) RNase H enzyme binds with mRNA/DNA duplex and 3) RNase H cleaves the mRNA strand removing its ability to act as a protein template, leaving the anti-sense oligonucleotide to bind with another mRNA strand.

1.1.2 Requirements for an anti-sense oligonucleotide

For an anti-sense oligonucleotide to be effective the oligonucleotide must have a high specificity and affinity for its mRNA target. The simplest way to achieve this is to use the exact copy of the targets complimentary sequence which by definition should have the properties required. However, these un-modified oligonucleotides are susceptible to hydrolysis by extra and intra cellular nuclease enzymes, which renders the oligonucleotide ineffective. They can experience solubility problems due to their high molecular weight and they must also be able to penetrate cell membranes unchanged. These issues can be improved upon by modifications to the natural oligonucleotide template.[4,5,8,9,13]

1.2 Oligonucleotide Modifications

Modifications can be made to either the base, sugar or phosphate backbone of the nucleic acid units which make up the oligonucleotide, all of which show increased resistance towards nuclease enzymes. The increase in nuclease resistance is often at the expense of binding affinity and specificity. Modifications can be made to all of the nucleic acids in the oligonucleotide chain or to just a few to balance out effects depending on the anti-sense requirements.[5,8,9]

1.2.1 Backbone modifications

Modifications to the phosphate backbone are the most common as they are relatively easy to synthesise based on existing un-modified oligonucleotide synthesis methods. Phosphate backbone modifications consist of replacing one or more of the phosphates oxygens with a new substituent.[5,8,9] Figure 4 shows the most frequently studied phosphate backbone modifications.

1. W=O, X=S, Y=O, Z=O   Phosphorthioate

2. W=O, X=S, Y=O, Z=S   Phosphordithioate

3. W=O, X=BH$_3$, Y=O, Z=O   Boranophosphonate

4. W=NH, X=O, Y=O, Z=O   Phosphoamidate

5. W=O, X=CH$_3$, Y=O, Z=O   Methylphosphonate
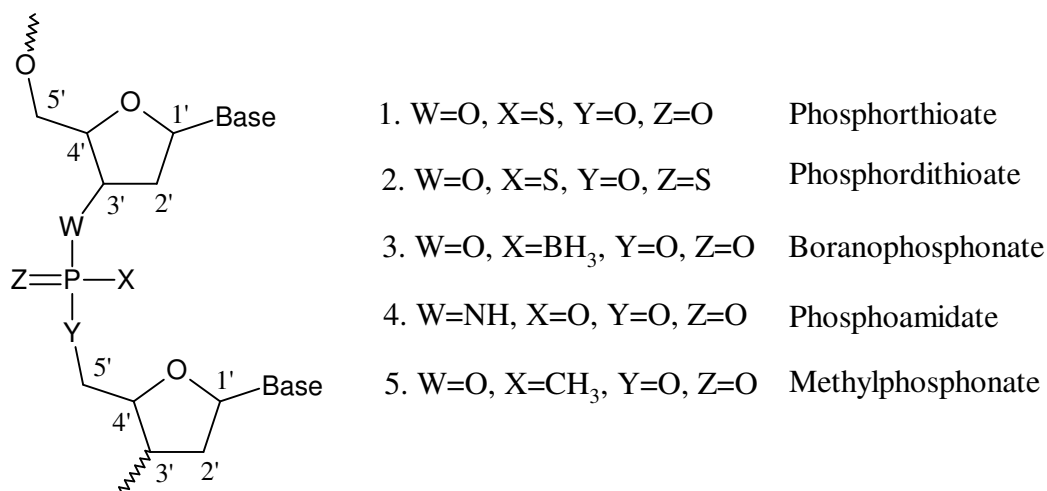
Figure 4: Oligonucleotide phosphate backbone modifications: 1) phosphorthioate, 2) phosphordithioate, 3) boranophosphonate, 4) phosphoamidate and 5) methylphosphonate.

1.2.1.1   Phosphorthioates and phosphordithioates

Phosphorthioate oligonucleotides have the same structure as un-modified oligonucleotides except that one of the non-bridging oxygen atoms of the phosphate backbone is replaced with a sulphur atom. Natural oligonucleotides are negatively charged with the formal charge symmetrically distributed over the two non-bonding oxygens. The phosphorthioates are also negatively charged but crystallography and ^{31}P NMR studies have shown that the charge localisation is unsymmetrical.[14,15] This gives a singly bonded and negatively charged sulphur atom, leaving the other non-bonding oxygen formally with a double bond (figure 5).

6
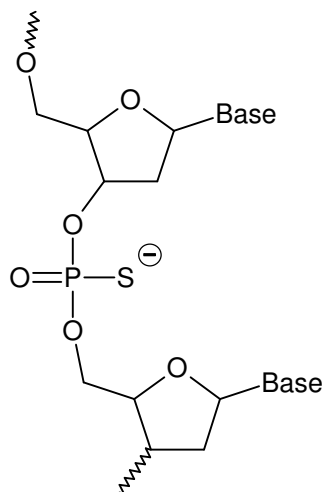
Figure 5: Phosphorthioate oligonucleotide.

Phosphorthioates have increased aqueous solubility, resistance to nuclease enzymes and base catalysed hydrolysis and act as substrates for RNase H enzymes, making them good anti-sense candidates. A reduction in binding affinity is observed with phosphorthioates which has been attributed to the formation of a chiral centre on phosphorus with the introduction of the sulphur atom. Assuming that only one diastereoisomer binds, for one phosphorthioate linkage the binding affinity can be reduced by two if the phosphorthioate is a racemate, with many phosphorthioate linkages in the polymer, reduction in binding affinity can be much greater. The formed diastereoisomers produced during synthesis are impossible to separate which is problematic if the reduction in binding efficiency is very large, if the diastereoisomers show different nuclease resistances or if one of the diastereoisomers is toxic.[8-10,16-19]

The reduction in binding affinity observed for phosphorthioate oligonucleotides is less than observed with the other backbone modifications shown in figure 4. Comparative thermal denaturation studies of these modified oligonucleotides have shown that duplex stability decreases in the order of: un-modified oligonucleotide > phosphorthioate > boranophosphate > methylphosphate.[8]

As well as being used for anti-sense studies phosphorthioates are often used as substrates for elucidating the stereochemistry of enzymic reactions. This and their high nuclease resistance makes them a very popular modification and they are often the foundation for more complex modifications.[14,15]

The chirality problems associated with phosphorthioates can be over come by replacing the second non-bridging oxygen with a sulphur atom to form a symmetrically charged phosphordithioate (figure 6). Phosphordithioates show similar properties to the phosphorthioates including aqueous solubility and nuclease resistance but show increased binding affinities towards their target mRNA.[9,16-18]
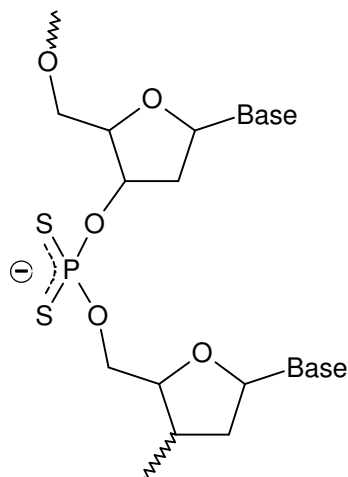
Figure 6: Phosphordithioate oligonucleotide.

1.2.1.2 Boranophosphonates

Boranophosphonates are oligonucleotides with one of the non-bridging oxygens replaced with a borane group (figure 7). These oligonucleotides are negatively charged giving them good aqueous solubility. The borane group is more hydrophobic than oxygen which is thought to give them increased cell permeability. They also show good stability towards nuclease enzymes, chemical hydrolysis and on the whole are more stable than the phosphorthioates.[8,20-22]
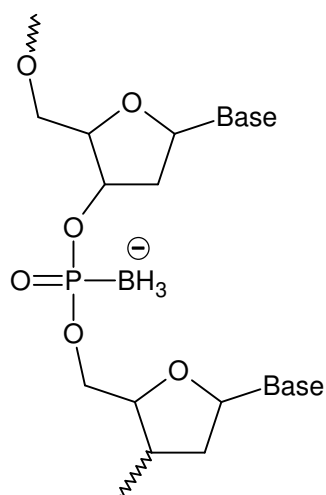
Figure 7: Boranphosphonate oligonucleotide.

1.2.1.3   Phosphoramidates

Replacement of one of the bridging oxygens of an un-modified oligonucleotide with an amide gives a phosphoramidate (figure 8). Phosphoramidates have been shown to be effective sequence specific anti-sense oligonucleotides, with a nuclease resistance similar to that of the phosphorthioates. Phosphoramidate oligonucleotides are chiral around the phosphorus and the mixtures of diastereoisomers present can cause problems. They are also ineffective as RNaseH substrates, but do show good anti-sense properties presumably due to a steric blocking mechanism.[5,8,10,23]
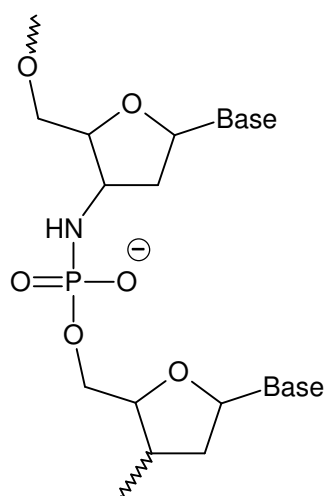
Figure 8: Phosphoramidate oligonucleotide.

1.2.1.4   Methylphosphonates

Alkylphosphonates are a class of anti-sense oligonucleotide where one of the non-bridging oxygen atoms has been replaced with an alkyl group, the most popular of which is the replacement with a methyl group as the relatively small size of the group reduces steric problems. These methylphosphonates (figure 9), and the other alkylphosphonates, are non-ionic and as a consequence the increased hydrophobicity of the neutral molecule should allow for greater cell permeability.[5,24,25] Methylphosphonates have shown specific binding with good binding affinities and act as inhibitors of mRNA translation.[26] The good binding affinities observed by methylphosphonates have been attributed to decrease in charge repulsion between the non-ionic backbone and the negatively charged natural oligonucleotide.[27-30]
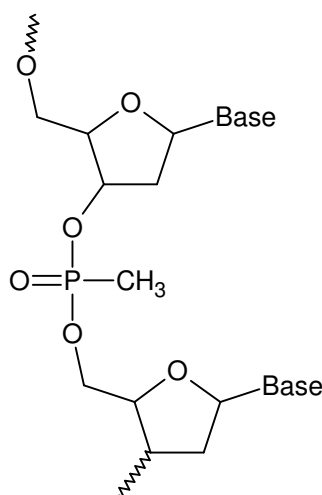
Figure 9: Methylphosphonate oligonucleotide.

Methylphosphonate oligonucleotides are also chiral around phosphorus and therefore the diastereoisomers are likely to have different effects towards binding affinities and nuclease resistance. 2D NMR studies of methylphosphonate duplex stability versus diastereoisomer orientation have shown that when the methyl group was pointing into the major groove of the duplex its binding stability is less than when the methyl group is pointing away from the molecule, which is consistent with steric repulsion.[29]

The methylphosphonate linkage is stable at neutral pH but is susceptible to cleavage under more basic conditions, which has led to studies of other alkylphosphonate type

oligonucleotides such as phenylphosphonates,[31] (dimethoxytrityl)phosphonates,[32] and the more polar (diflouromethyl)phosphonates.[33,34]

1.2.2 Sugar modification

There are a limited number of reported anti-sense oligonucleotide sugar modifications. These consist of restricting the conformation of the sugar ring to improve binding affinity and duplex stability. Examples of these include, 2'-O,4-C-methylene bicyclicribonucleosides (figure 10) which have shown increased binding affinities,[35] and 2'-O,3'-C-linked [3.2.0]bicycloarabinonucleosides which have shown increased duplex stability (figure 10).[36]

2'-O,4-C-methylene bicyclicribonucleoside   2'-O,3'-C-linked [3.2.0]bicycloarabinonucleosides
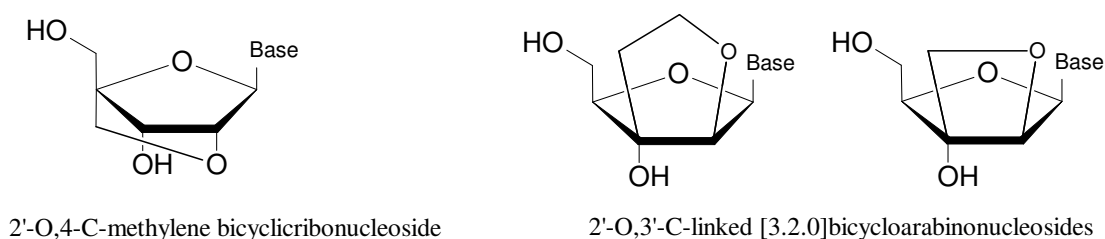
Figure 10: Examples of oligonucleotide sugar modifications.

1.2.3 Base modification

Modifications to the anti-sense oligonucleotides bases to increase the strength of hydrogen bonding have show an increase in duplex binding affinities. Examples of these modifications include, 5-(3-methoxypropynl)-2'-deoxyuridine,[37] 7-deaza-7-methylguanine,[38] 7-propynyl, 7-iodo and 7-cyano-7-deaza-2-aminoadenine (figure 11).[39]
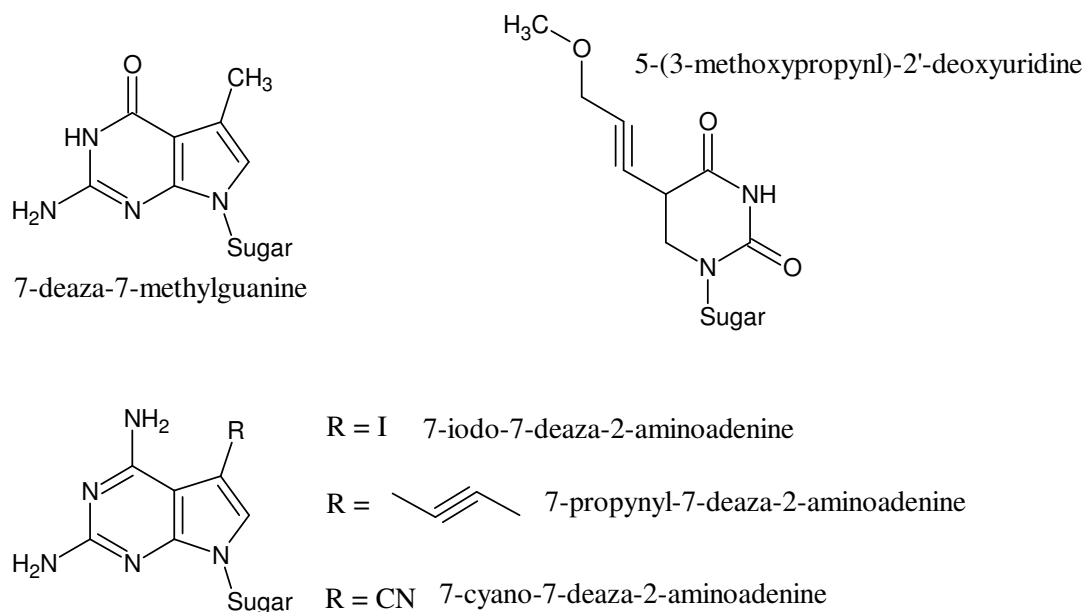
Figure 11: Examples of oligonucleotide base modifications.

1.3 Anti-Sense Oligonucleotide Synthesis

Anti-sense oligonucleotides can be synthesised by a number of methods in solution or with solid support methodologies, where the first nucleoside in the chain is covalently anchored to a solid matrix in a packed column and reagents are pumped through for reaction. At present the use of solid support techniques are the most widely used due to high product yield and purity as well as the extensive automation that the technique allows.

1.3.1 Phosphotriester method

The phosphotriester method of oligonucleotide synthesis was one of the original methods developed by Letsinger[40,41] in the 1960's. Today the phosphotriester method is the most widely used method in solution.[42-44] The synthesis consists of reacting a 5'-dimethoxytrityldeoxynucleoside-3'-(protected)phosphate (1) with the next nucleoside (2) in the oligonucleotide chain in the presence of a condensing agent in anhydrous

pyridine to produce a phosphotriester (scheme 1).[45-47] There are a number condensing agents used for this method, which include arylsulfonylchloride,[45] arylsulfonyl tetrazolide[45] and arylsulfonyl 3-nitro-1,2,4-triazolide.[46] Once the required oligonucleotide chain is synthesised the phosphorus protecting group is removed with aqueous pyridine to produce the natural phosphodiester oligonucleotide. Common protecting groups include *β*-cyanoethyl and the *p*-chlorophenyl.[45]
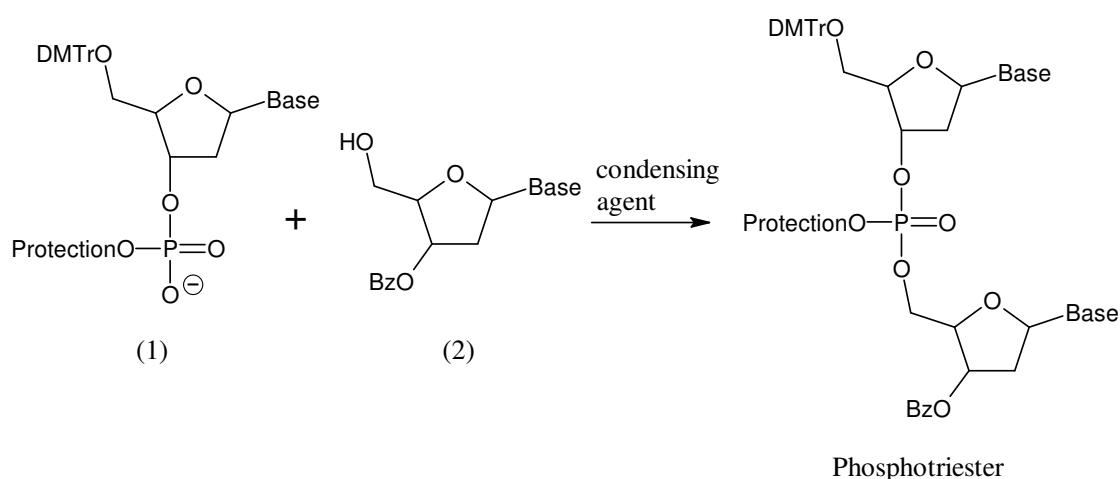
Scheme 1: Phosphotriester method of oligonucleotide synthesis showing formation of the phosphotriester.

The phosphotriester method of oligonucleotide synthesis is useful for synthesising short chain natural oligonucleotides in solution in large quantities.[42,43,48,49] New approaches for synthesising longer chain oligonucleotides have been investigated; the more successful of these were the use of phosphite triesters and phosphodiesters.

1.3.2 Phosphite triester methods

A number of phosphite triester methods of synthesis have been developed which all involve the formation of a phosphite triester in the nucleoside coupling step.

1.3.2.1   Phosphochloridite method

Letsinger developed a method for the synthesis of longer chain oligonucleotides utilising phosphochloridite chemistry. This synthesis was the step wise reaction of the highly reactive phosphochloridites (3) with the corresponding nucleoside alcohol (4) in tetrahydrofuran or pyridine to form a phosphite triester (scheme 2). The phosphite can then be oxidised to a phosphotriester with iodine. These steps are then repeated until the desired chain length is achieved and a final deprotection step with sodium naphthalide produces the natural oligonucleotide.[48,49]
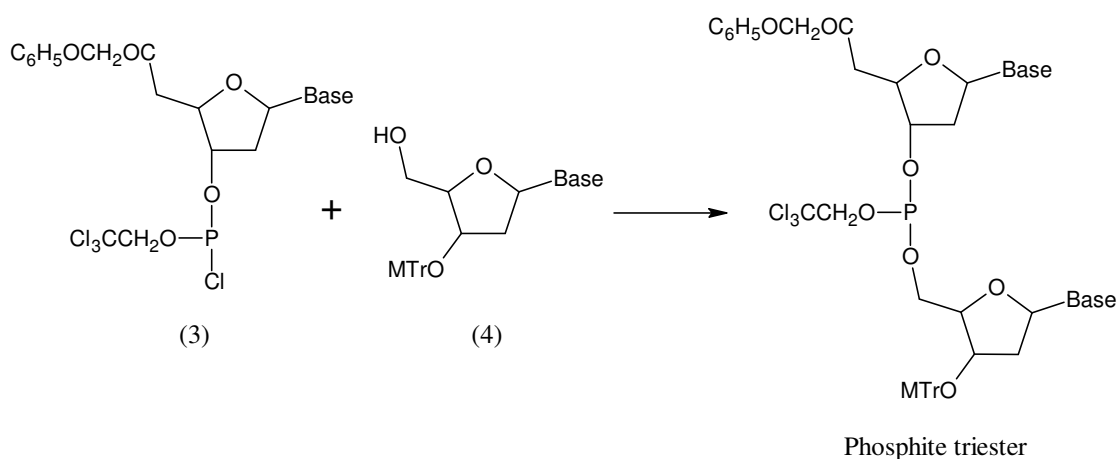
Scheme 2: Phosphochloridite method of phosphite triester formation proposed by Letsinger.

Due to the high reactivity of the phosphochloridites, their instability towards hydrolysis and their oxidation by air was a problem even at sub-zero temperatures. Caruthers *et al* introduced a method of oligonucleotide synthesis to over come these problems, the use of less reactive phosphoramidites.[50]

1.3.2.2   Phosphoramidite method

The phosphoramidite method of oligonucleotide synthesis introduced by Caruthers *et al* in the 1980's involved reaction of a *N,N*-dimethylaminophosphoramidite nucleoside (5) with a 5'-unprotected nucleoside in the presence of the *N,N*-dimethylaniline hydrochloride in chloroform to form the phosphite triester. The phosphite triester could

then be oxidised with iodine and the methoxy group removed under alkaline conditions to produce the natural oligonucleotide. The formation of the phosphite triester is suggested to proceed via a phosphochloridite intermediate (6) (scheme 3) which was susceptible to hydrolysis and oxidation by air.[50]
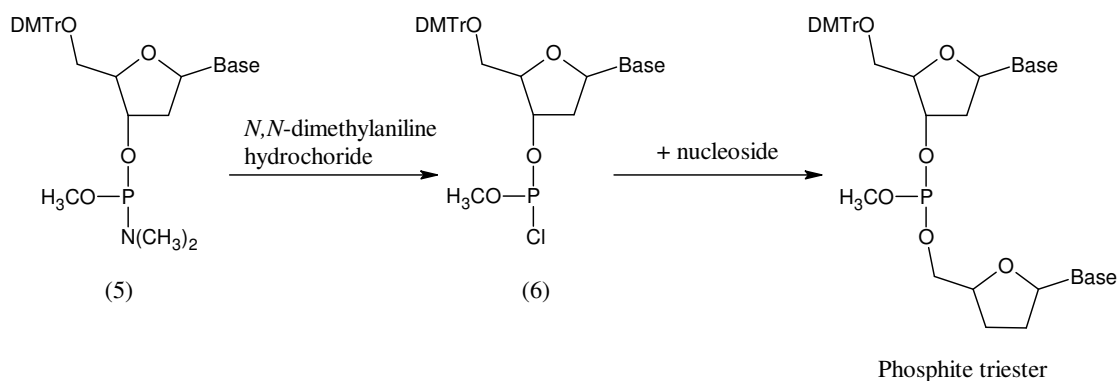
Scheme 3: Phosphoramidite method of phosphite triester synthesis with phosphochloridite intermediate.

Further investigation of possible acidic activating agents other than *N,N*-dimethylaniline hydrochloride by Caruthers *et al* led to the discovery that 1H-tetrazole (figure 12) showed the best characteristics for the coupling of nucleoside units. Coupling with 1H-tetrazole was rapid and near quantitative and 1H-tetrazole itself was a commercially available solid which could be easily purified.[50,51]
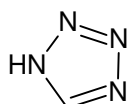
Tetrazole

Figure 12: Structure of 1H-tetrazole.

At present the phosphoramidite method of oligonucleotide synthesis using solid support methodologies is the most widely used due to its high coupling efficiency, stability of starting materials, ease of automation and product purity. The phosphoramidite method can be applied to not only synthesis of natural oligonucleotides but to oligonucleotides with modifications, including phosphorthioates, phosphordithioates, phosphorselenoates, boranophosphonates and also oligonucleotides with mixed functionality.[5,52-55]

1H-tetrazole is still the most popular activating agent but many studies have been undertaken to find new activators as tetrazole is expensive, explosive, toxic and its solubility in acetonitrile, the solvent used for the coupling reaction, is relatively low.[52,56] The *N,N*-dimethylaminophosphoramidite first used by Caruthers *et al*, while much less reactive than the phosphochloridites, were still unstable due to their relatively high reactivity and they were difficult to purify. Today, less reactive 3'-*β*-cyanoethyl *N,N*-diisopropylphosphoramidites are the most popular choice as the bulkier diisopropyl group on the amine reduces the reactivity of the amidite allowing for easier storage and handling.[52,56-60]

The machine assisted solid phase synthesis of oligonucleotides by the phosphoramidite method consists of a four step cycle (scheme 4): 1) detritylation of the 5' oxygen's dimethoxytrityl protecting group of the solid support bound nucleoside, 2) coupling of the solid support bound nucleoside and a 3'-*β*-cyanoethyl *N,N*-diisopropylphosphoramidite with an activating agent, classically 1H-tetrazole, to form a phosphite triester, 3) oxidation of the resulting phosphite triester with iodine to form the phosphotriester and 4) capping of any failed reactions to regulate chain growth by acetylation of unreacted 5'-hydroxyl groups. This cycle is repeated until the required length of oligonucleotide is achieved where a final treatment with alkali to remove the *β*-cyanoethyl protecting group yields the natural phosphodiester oligonucleotide.

The phosphoramidite synthesis method is still susceptible to side reactions through hydrolysis and oxidation with air and strict reagent drying must be undertaken to gain maximum yields of the target oligonucleotides.
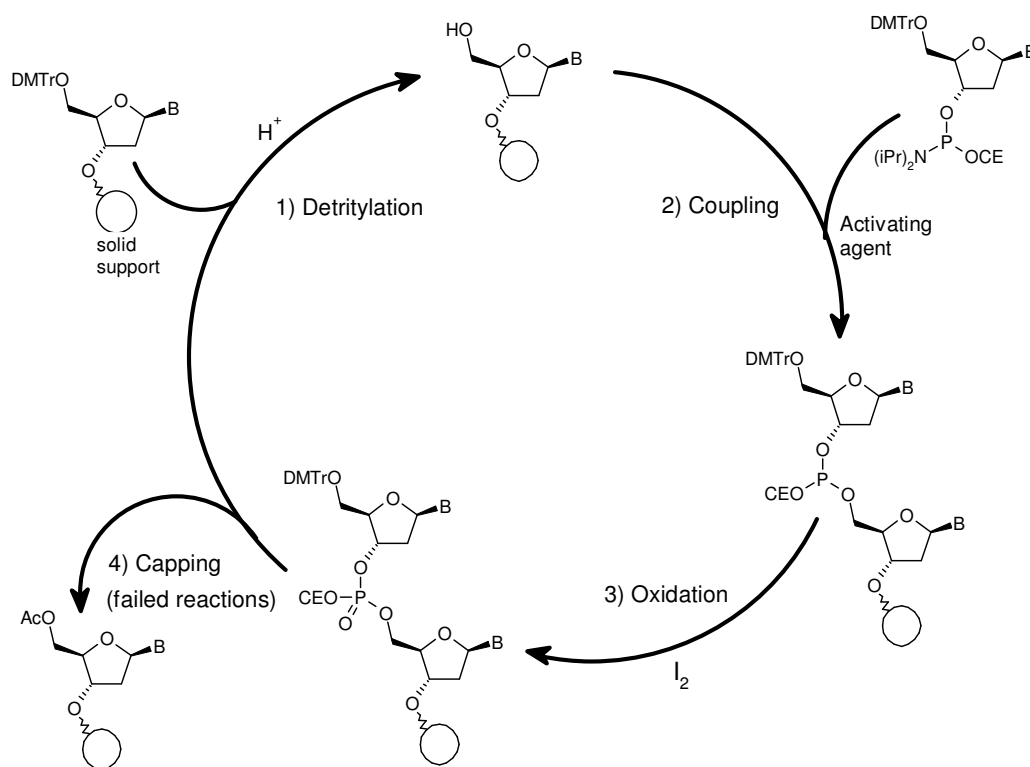
Scheme 4: Phosphoramidite method of oligonucleotide synthesis.

1.3.3 Phosphodiester method

Another method of solid support oligonucleotide synthesis is via the H-phosphonate route. H-phosphonates are stable to moisture and oxidation and are the non-reactive by-products of the phosphoramidite method; therefore their use as an oligonucleotide precursor requires no drying of reagents or other special precautions.

Synthesis via H-phosphonate methods in solution was first described in 1957 by Todd[61] but it wasn't until the 1980's that their use with solid support techniques was first utilised by Froehler *et al*.[19,20] The H-phosphonate method entails: 1) removal of the dimethoxytrityl protecting group of the solid support bound nucleoside and 2) coupling of this nucleoside (8) with a 5'-O-(4,4-dimethoxytrityl)-2'-ribonucleoside 3'-H-phosphonate (7) (scheme 5) with a coupling agent, such as pivaloyl or adamantoyl chloride, to form a coupled H-phosphonate. These steps are repeated until the required

17

chain length has been achieved and then oxidation with iodine produces the natural phosphodiester oligonucleotide.[5,19,20,53]
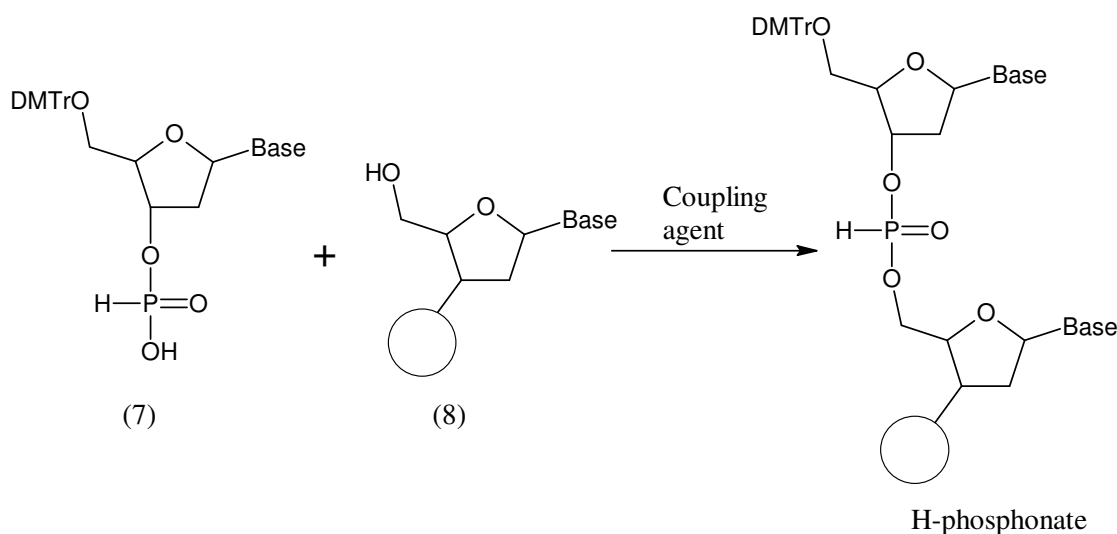
Scheme 5: H-phosphonate coupling reaction.

As well as the stability of the reagents, the H-phosphonate method is seen as a good alternative to the phosphoramidite method because there is no need for further phosphorus protection, therefore less synthetic steps are required and synthesis is also rapid and high yielding.[57,58,62] The H-phosphonate method can be adapted to synthesise modified anti-sense oligonucleotides, for example replacing the final oxidation step of the H-phosphonate approach with a sulphurisation step would yield an oligonucleotide with 100% phosphorthioate functionality. While H-phosphonate chemistry is good for the synthesis of natural phosphodiester oligonucleotides and some modified oligonucleotides, the range of modifications that can be achieved is significantly less than the phosphoramidite method which can be used to produce mixed functionality oligonucleotides due to the step wise nature of the phosphotriester formation step. Another disadvantage to the H-phosphonate method is the presence of side reactions which can significantly reduce yields, such as phosphorus acylation resulting from the reaction of the coupling agent with the phosphorus centre.[19,44,63]

1.4 Phosphorthioate Synthesis by Phosphoramidite Method

Phosphorthioate analogues of oligonucleotides are the focus of considerable research as anti-sense therapeutics and their method of synthesis via the phosphoramidite method is well established. As the need for large quantities of phosphorthioate oligonucleotide is growing to meet research and industrial demands, mechanistic information of the steps involved in their synthesis is required to optimise production procedures.

The method of phosphorthioate synthesis studied here is similar to that described for the synthesis of un-modified oligonucleotides, except that the oxidation step is replaced by sulphurisation (scheme 6).
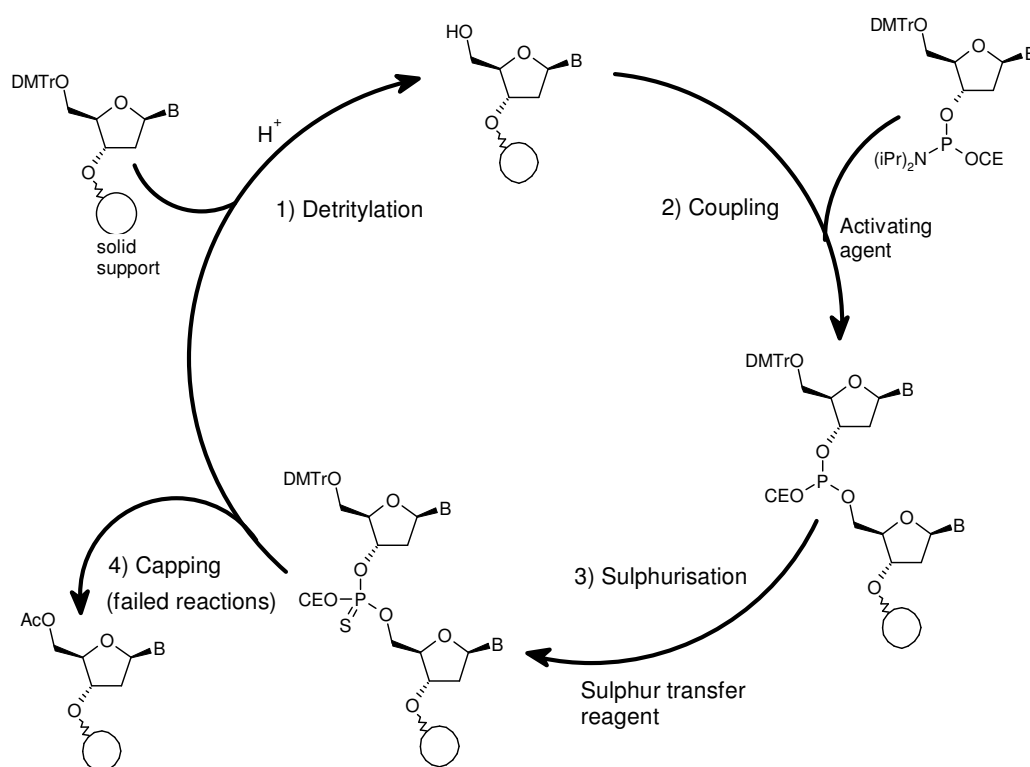
Scheme 6: Phosphorthioate synthesis via the phosphoramidite method.

1.4.1   Detritylation reaction

The detritylation reaction is the acid catalysed removal of the 4,4-dimethoxytrityl protecting group from the 5' oxygen of the solid support bound nucleoside. Removal of the protecting group yields a hydroxy function at the 5' position and a stable 4,4-dimethoxytrityl carbocation (scheme 7). To achieve high yields of the target oligonucleotide, quantitative removal of the protecting group is required as incomplete detritylation causes uncoupled nucleosides that reduce purity and yield.[64,65]
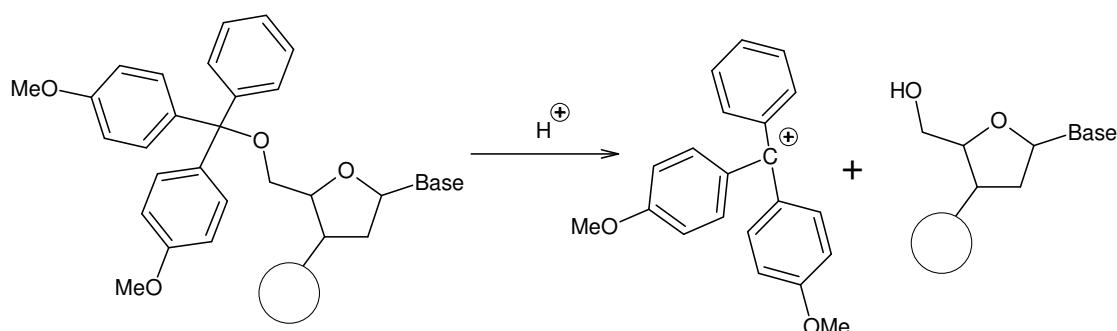
Scheme 7: Detritylation reaction.

High concentrations of a strongly acidic acid are required for rapid and quantitative removal of the protecting group, but under these conditions depurination of guanosine, and to a lesser extent adenosine nucleosides, is frequent. Depurination is the cleavage of the N-glycosyl bond between a purine base and the ribose sugar under acidic conditions (scheme 8).[54,66,67]
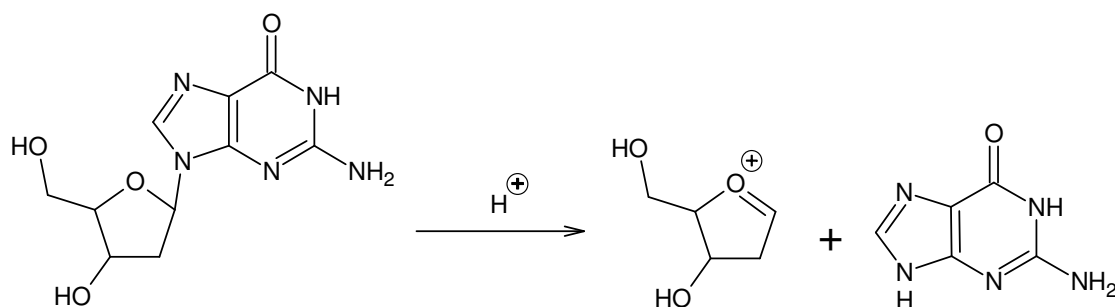
Scheme 8: Depurination reaction.

Classically strong protic acids such as benzenesulphonic acid and trichloroacetic acid have been used to facilitate detritylation, but due to the complication of depurination less acidic alternatives have been sought with dichloroacetic acid being most popular. The use of dilute solutions of a less acidic acid can be used to minimise the extent of depurination but this can cause incomplete detritylation.[54,64,65,68-70] The rate of detritylation is faster than the rate of depurination and therefore, to minimise depurination, detritylation is often performed as quickly as possible.[54,68] The extent of depurination can be reduced by protecting the purine bases such as dialkylformamidinedeoxyadenosine, N^6-phthaloyl-deoxyadenosine and N^6-succinyl-deoxyadenosine (figure 13),[68,71,72] but this introduces even more synthetic steps.

dialkylformamidinedeoxyadenosine N^6-phthaloyl-deoxyadenosine N^6-succinyl-deoxyadenosine
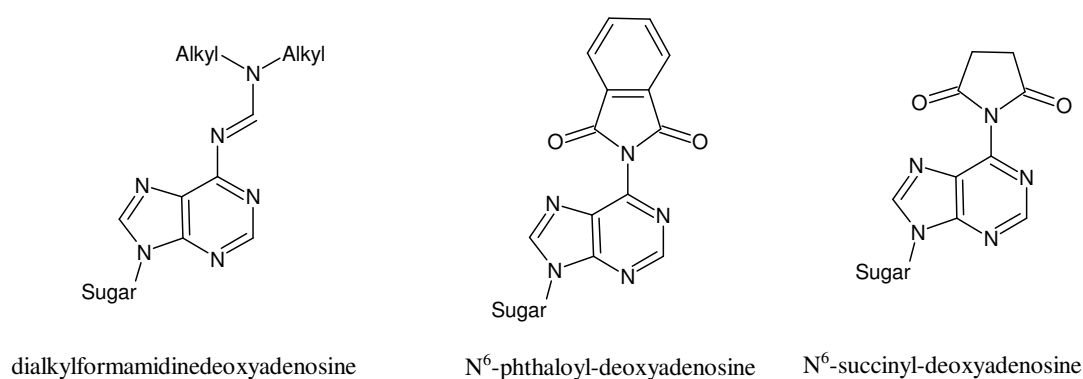
Figure 13: Examples of oligonucleotide base protection.

While there is literature discussing the types of acids and conditions required for optimum detritylation there is little or no mechanistic data available for the deprotection of nucleosides. There are a number of mechanistic studies by Maskill *et al* on the deamination of 4,4-dimethoxytritylamine[73,74] and on the ionisation of 4,4-dimethoxytrityl alcohol[75,76] to the carbocation in aqueous and aqueous/acetonitrile solutions, but their relevance to the detritylation of nucleosides in none aqueous organic solvents maybe questionable.

1.4.2   The phosphoramidite coupling reaction

The coupling reaction of phosphoramidites (scheme 9) involves the irreversible formation of a phosphite triester by a phosphorus (III) nucleophilic substitution reaction. Reaction is between the added nucleoside phosphoramidite, typically a 3'-β-cyanoethyl *N,N*-diisopropylphosphoramidite (9), and the 5'-hydroxy group of the solid support bound nucleoside (10) which displaces the amine from the amidite. The coupling reaction is usually performed in acetonitrile and, due to the stability of *N,N*-diisopropylphosphoramidites needed for easy storage and handling, it only occurs in the presence of an activator.
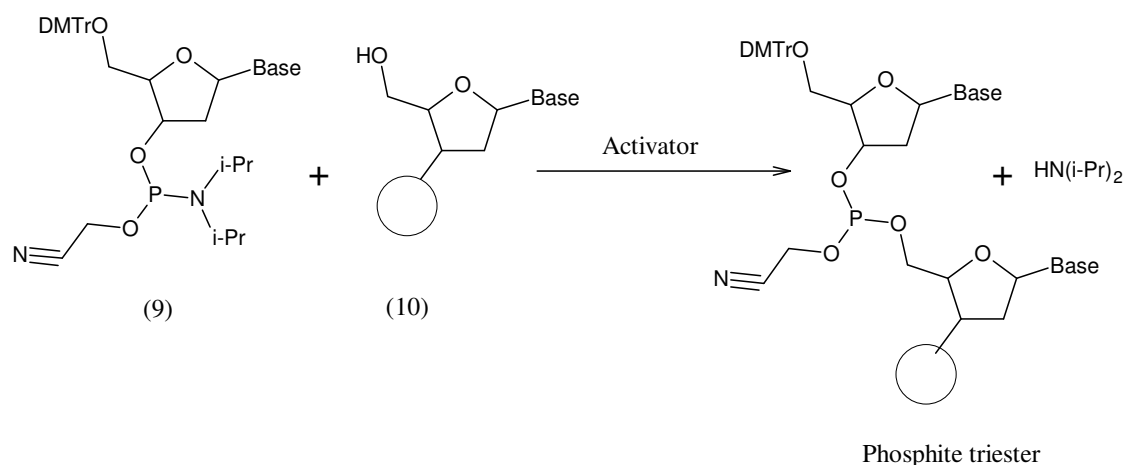
Scheme 9: Coupling reaction.

To achieve high yields of pure oligonucleotide the coupling reaction must be near quantitative. To minimise the possible hydrolytic and oxidative side reactions, coupling must be rapid and therefore the amidite should be highly reactive towards the activator.[52,77] Through screening of a number of acidic compounds Caruthers *et al* discovered that 1H-tetrazole was the most effective activator giving rapid high yielding coupling and is today the most frequently used.[50,51,78]

1H-tetrazole is a weak nitrogen acid with a pK_a in acetonitrile of 14.5[79]. It is widely accepted that activation of amidites is acid catalysed with protonation occurring on either the phosphorus or the nitrogen of the amidite. The 1H-tetrazole could also act as

a nucleophile towards phosphorus displacing the amine group prior to nucleophilic attack by the alcohol or, the alcohol may attack the protonated amidite directly. These mechanistic alternatives are presented in scheme 10.[50,77,80]
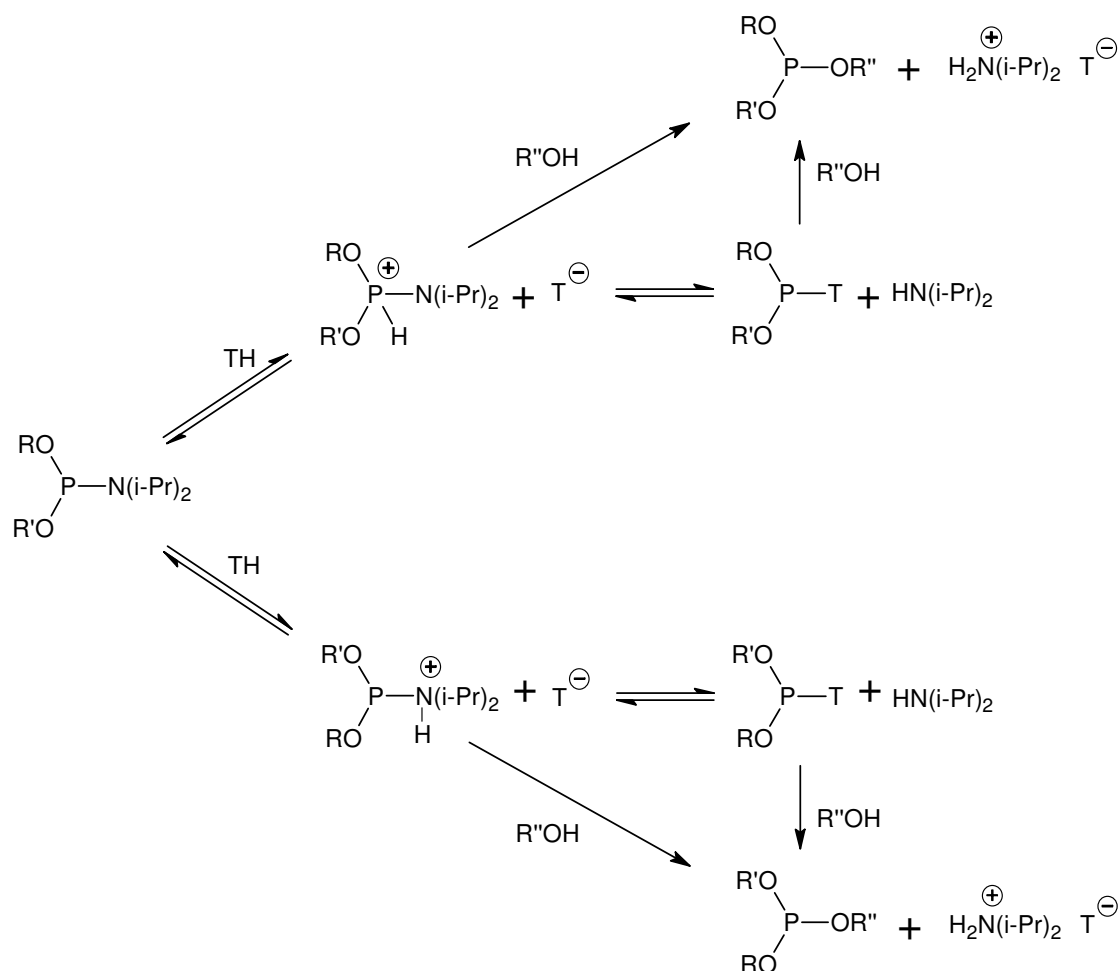
Scheme 10: Mechanistic alternatives for the coupling reaction with tetrazole (TH).

The products of the coupling reaction are the phosphite triester, diisopropylamine and the tetrazole. The basicity of the released diisopropylamine is such that the 1H-tetrazole is not only present as an activator in the reaction but it is also consumed at the end of the reaction in salt formation with the diisopropylamine.[78,81] This means that at least one mole equivalent of 1H-tetrazole is required for complete reaction. Studies performed by Hayakawa *et al*[81] showed that addition of 10Å molecular sieves added to the reaction medium prior to reaction, could remove the generated diisopropylamine allowing the 1H-tetrazole to act in catalytic amounts.

1.4.2.1   Phosphoramidite protonation

Protonation of the phosphoramidite has been proposed on both the phosphorus[77,82-84] and nitrogen atom.[84-86] Molecular modelling by Korkin and Tvetkov[87,88] of a simple model structure, H_2P-NH_2, showed that N-protonation lengthens and weakens the phosphorus nitrogen bond whereas P-protonation shortens and strengthens the bond. This indicates that the reactivity of an N-protonated species would be greater than the reactivity of the P-protonated species. ^{31}P NMR studies by Nurminen *et al*[79,84] showed that P-protonation of non-nucleoside amidites could be achieved with strong acids of pK_as in acetonitrile below 10 but with weak acids no P-protonation is observed. Nurminen also noted that the nucleophilic substitution reaction was slower when the nucleophile was added to an amidite in the presence of a strong acid that could cause P-protonation than to the amidite in presence of a weak acid.

1.4.2.2   Nucleophilic Substitution of the protonated amidite with 1H-tetrazole

There is evidence in the literature that 1H-tetrazole may act as a nucleophile during the coupling reaction to displace the amine of the amidite forming a reactive tetrazolide intermediate. Early studies by Dahl *et al*[77] showed that the rate of coupling was faster when the amidite and tetrazole were premixed rather than when the tetrazole was added to a mixture of amidite and alcohol. This was attributed to the rate limiting formation of the tetrazolide intermediate which was shown to be in equilibrium with the reactants by the addition of diisopropylammonium tetrazolide at the start of the reaction retarding the extent of reaction.
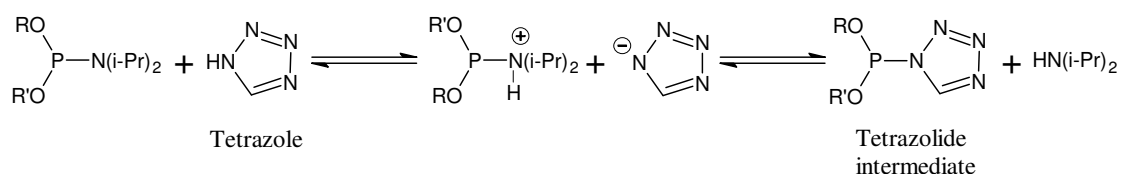
Scheme 11: Formation of the tetrazolide intermediate, assuming N-protonation.

The tetrazolide intermediate has been synthesised and characterised by Caruthers *et al*[51] and Seliger *et al.*[80] Caruthers synthesised a nucleoside tetrazolide species and Seliger a diethoxy-tetrazolophosphane from the reaction of diethoxychlorophosphane and tetrazole. In both cases it was found that the tetrazolide species reacted with alcohols to produce phosphite triesters. The ^{31}P NMR chemical shifts of the tetrazolide species were comparable with those found when the amidite and tetrazole reaction is performed which lends further evidence for nucleophilic attack by tetrazole.

1.4.2.3   Activator acidity

There have been a number of studies of activator acid strength versus the rate of reaction. Seliger *et al*[80] studied the rate of reaction with a range of heterocyclic activators and found that increasing the acidity of the activator increased the rate of alcoholysis. This was also shown with a range of carboxylic acids with varying acidities where activator acidity was closely correlated with activity.[89] Acids with a pK_a of 18 or above were found to be ineffective activators and even acids which were relatively non-nucleophilic showed good activating ability, such as dichloroacetic acid, trichloroacetic acid and triflouroacetic acid. Studies with salts of pyridine and various acids showed reductions in reaction yield with less acidic acids.[90]

These results show that increasing the acidity of the activator increases the rate of reaction. An increase in acidity of reaction system can cause unwanted side reactions namely depurination or premature detritylation of the 5' protected nucleoside amidite.[91,92]

1.4.2.4   Activator nucleophilicity

Bearing in mind the problems with increasing the activator's acidity, studies have been undertaken to evaluate the effect of the activator's nucleophilicity. The use of less acidic but more nucleophilic catalysts by adding *N*-methylimidazole with tetrazole showed a significant increase in coupling yield. Addition of too high a concentration of

N-methylimidazole showed a reduction in coupling yield presumably due to the decrease in acidity.[92]

Nuriminen *et al*[79] studied the rate of alcoholysis of simple alkyl phosphoramidites with various activators of ammonium, pyridinium and azolium salts. These studies showed that the rate of alcoholysis in the presence of a nucleophilic salt was greater than in the presence of a non-nucleophilic salt of equal acidity.

1.4.2.5   Activator choice

It would seem that the best activator for the coupling reaction is a relatively strong acid that does not promote any undesirable side reactions, but strong enough to give high concentrations of protonated amidite. The activator must also be strongly nucleophilic to facilitate rapid conversion to the intermediate as well as being a good leaving group to enable formation of the phosphite triester.

There are many examples of alternative activators with differing acidities and nucleophilicities such as: 2-bromo-4,5-dicyanoimidazole,[93] various carboxylic acids,[89] 4,5-dicyanoimidazole,[92]   2,4-dinitrophenol,[94]   5-phenyltetrazole[95]   and arylsulfonyltetrazoles.[96] Acidic activators like these and 1H-tetrazole do not meet the twin requirements of a good nucleophile and a relatively strong acid; as a strong acid is likely to generate a weakly nucleophilic conjugate base and a strong nucleophile is likely to be derived from a weak acid.[52,97,98]

The use of salts of strong acids and nucleophilic bases are now seen to be more favourable activators. The use of these types of salts should show good protonation of the amidite by the strong acid allowing the conjugate base to act as a nucleophile towards the amidite.[52,97,98]

Again there are many reported activators of this type: salts of benzimidazole with trifluoroacetic acid, tetrafluoroboric acid, hexafluorophosphoric acid and trifluoromethansulphonic acid;[99,100] imidazolium triflate;[101] *N*-methylimidazolium triflate;[102] salts of 4-dimethylaminopyridine with 5-(*o*-nitrophenyl)tetrazole and 5-(*p*-nitrophenyl)tetrazole;[91] pyridinium triflouroacetate;[90] *N*-methylimidazolium triflate and

triflouroacetate; *N*-methylbenzoimidazolium triflate; and *N*-phenylimidazolium triflate.[97]

1.4.3 Sulphurisation

The sulphurisation reaction is the formation of a phosphorthioate linkage from the phosphite triester produced in the coupling step. Sulphurisation is achieved with a sulphur transfer reagent, of which there are numerous examples. These include, sulphur,[103,104] 3H-1,2-benzodithiol-3-one-1,1-dioxide (Beaucage reagent),[105] tetraethylthiuram,[106] bis(*o,o*-diisopropxy phosphinothioyl)disulphide,[107] benzyltriethylammonium tetrathiomolybdate, [108] 1,2,4-dithiazolidine-3,5-dione (DtsNH),[55] 3-ethoxy-1,2,4-dithiazoline-5-one (EDITH),[55] bis(ethoxythiocarbonyl)tetrasulfide[109] and diethyldithiocarbonate disulfide.[110]

Of these sulphurising reagents 3H-1,2-benzodithiol-3-one-1,1-dioxide (figure 14), otherwise called Beaucage reagent, is the most widely used due to its rapid sulphurisation and yield. Beaucage reagent is not easily synthesised and it is potentially an oxidising reagent leading to phosphodiester linkages rather than the target phosphorthioate linkages.[55,111]
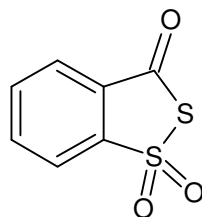
Figure 14: Structure of 3H-1,2-benzodithiol-3-one-1,1-dioxide (Beaucage reagent)

3-Amino-1,2,4-dithiazole-5-thione (xanthane hydride) was first described as an efficient sulphurising agent for synthesis of phosphorthioate oligonucleotides with solid support methodologies by Tang *et al*.[111] Tang proposed a mechanism for the sulphurisation reaction with xanthane hydride for two possible tautomers, but gave no evidence for it (scheme 12).
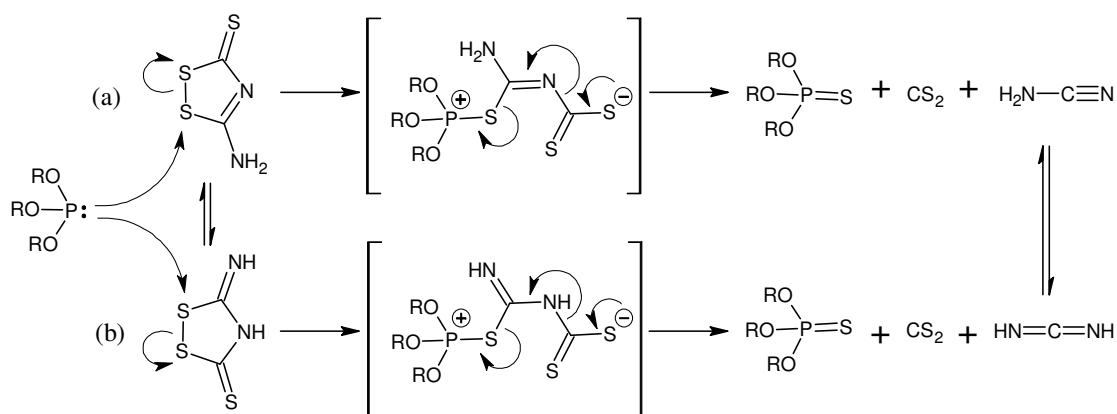
Scheme 12: Mechanism of sulphurisation with xanthane hydride proposed by Tang et al.[111]

X-ray crystallography[112] and MDNO calculations[113] of the most likely tautomeric structures of xanthane hydride (scheme 13) have indicated that the structure shown on the left is the most important. Therefore, it would seem likely that mechanism (a) from scheme 13 would be the most predominant.
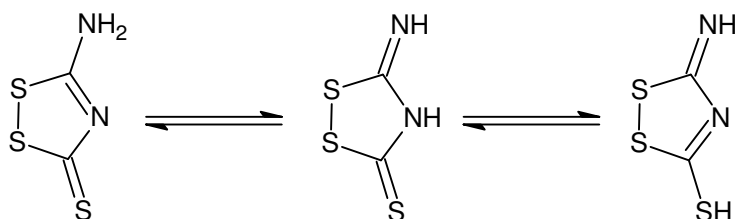
Scheme 13: Possible tautomers of xanthane hydride.

1.4.4 Capping

After the coupling and sulphurisation steps have been performed, there will be a small percentage of nucleotide that has not coupled. These failed reactions are still bound to the solid support and can undergo coupling in subsequent coupling steps, giving an oligonucleotide with one or more less nucleotides than the target as well as the incorrect sequence. These other products would be difficult to separate leading to a final product with varying chain length which is highly undesirable where product

purity is extremely important. Capping of the failed reactions prevents them from participating in further coupling steps, increasing the difference in nucleotide chain length, making them easier to separate.[9,114-116]

The capping reaction is the acetylation of the uncoupled 5'-hydroxyl groups of the solid support bound nucleoside. Capping is usually performed with acetic anhydride/2,6-lutidine/THF (Cap A) and *N*-methylimidazole/THF (Cap B) mixed prior to reaction (scheme 14). The two capping solutions are stored separately and only mixed when required as the combined capping reagent degrades over time. The capping reaction is always performed with the capping reagent in large excess to ensure that all failed reactions are capped. [9,114-116]

| Cap A | Cap B | Capping reagent |

| Uncoupled nucleotide | Capped nucleotide |
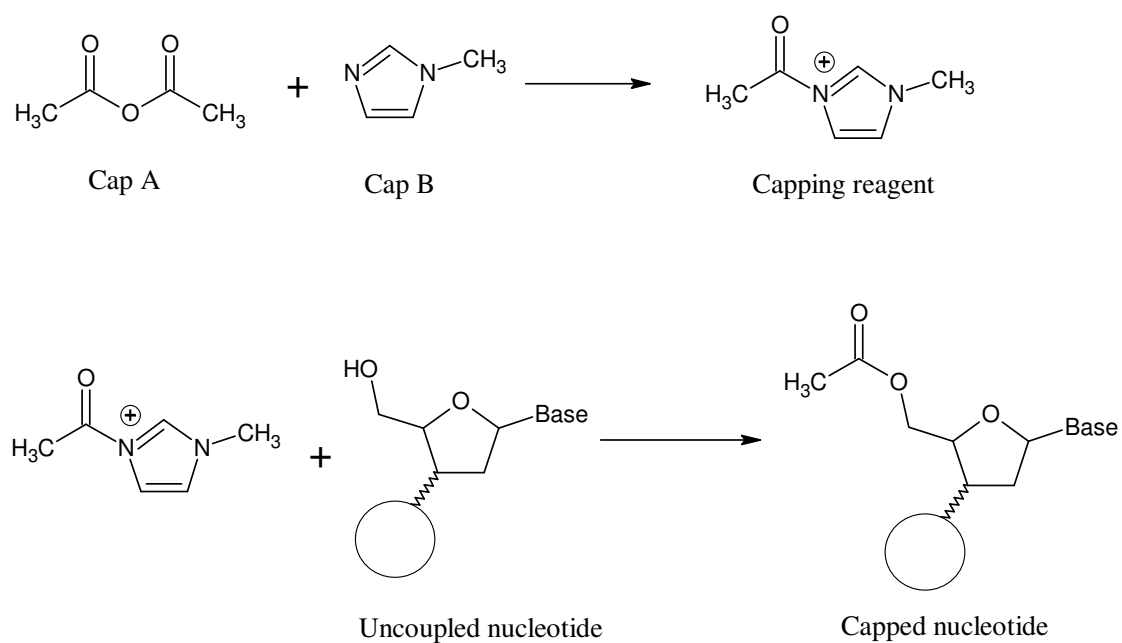
Scheme 14: Capping reaction.

2   Experimental

2.1   Materials

The 4,4-dimethoxytritylthymidine and saccharin/*N*-methylimidazole salt were supplied by Avecia Biotechnology and were used without further purification. Xanthane hydride was also supplied by Avecia Biotechnology but was recrystallised from a 1:4 mixture of DMSO:water prior to use. All other reagents used were analytical grade or an equivalent grade where available. Reagents were supplied by Sigma-Aldrich, Avocado Research Chemicals Ltd or Acros Organics. Deuterated solvents were obtained from Goss Scientific Instruments Ltd.

2.2   Equipment

Ultraviolet spectral measurements were performed on a Cary 1E UV-Visible spectrophotometer with a twelve compartment cell block thermostated by a peltier system with 1 cm quartz cuvettes. Observed rate constants were obtained on this instrument from the generated absorbance versus time data using the Cary Win UV kinetics application Version 02.00. For reactions where the rate was too rapid for use on the Cary instruments, measurements were performed on an Applied Photophysics SX.18 MV-R1 Stop-flow spectrophotometer. Observed rate constants were obtained on this instrument from the generated absorbance versus time data using the installed kinetic fitting software.

^{1}H, ^{13}C and ^{31}P NMR spectra were run on a Bruker-DPX400 spectrophotometer and 2D NMR spectra and ^{15}N NMR spectra were run on a Bruker-AV500 spectrophotometer. 5 mm internal diameter NMR tubes were used in each experiment.

2.3 Detritylation Experimental

2.3.1 UV spectrophotometric equilibrium studies

Equilibrium studies were all performed on a Cary 1E UV-Visible spectrophotometer.

2.3.1.1 Varying solvent: constant water concentration

Typically, a solution of 4,4-dimethoxytritylthymidine (3.6×10^{-5} M, 2 ml) in the solvent understudy was pipetted into a 1 cm quartz cuvette and dichloroacetic acid (12 M, 1-20 μl) was titrated into the cuvette. UV scans from 250-600 nm were performed after each aliquot of acid was added. Water content of reactant solutions was determined by Karl Fischer titration and an average of three results was used.

2.3.1.2 Varying solvent: varying water concentration

The same procedure for determining UV absorbance and water content was used as in section 2.3.1.1, but water was added to reagent stock solutions prior to reaction.

2.3.1.3 Carbocation formation from 4,4-dimethoxytrityl alcohol

In a typical experiment, 4,4-dimethoxytrityl alcohol (3.6×10^{-5} M, 2 ml) in acetonitrile was added to a 1 cm path length quartz cuvette and was titrated with dichloroacetic acid (12 M, 5-20 μl). UV wavelength scans were performed after each addition of acid between the range of 250-600 nm.

2.3.1.4   Varying alcohol concentration in acetonitrile

The same procedure for determining UV absorbance and water content was used as in section 2.3.1.1, but propan-1-ol (0.502-0.903 M) was added to reagent stock solutions prior to reaction

2.3.2   UV stop-flow spectrophotometric rate measurement

All kinetic measurements were performed at 30°C (unless other wise stated) using stop-flow instrumentation with a 25:1 syringe ratio. In a typical experiment, 4,4-dimethoxytritylthymidine (9 x10^{-4} M in acetonitrile) was loaded into the smaller of the two syringes and dicholoroacetic acid (0.2-3.5 M) was loaded into the larger syringe. The concentration of water in the reaction system was determined by sampling of reactant solutions with Karl Fischer titration apparatus, of which an average of three determinations was used. Injection of the contents of the two syringes into the reaction cell initiated the reaction which was followed by measurement of the increase in absorbance at 497 nm. For each concentration of acid an average of 20-30 results was used.

The same procedure was used for kinetic measurements in toluene and dichloromethane.

2.3.3   Solubility of 4,4-dimethoxytritylthymidine

In a typical experiment, 4,4-dimethoxytritylthymidine (1.5 g) was added to acetonitrile (25 ml) and was left with agitation for 30 minutes at ambient temperature to ensure complete equilibration. The sample was then filtered under gravity and the mass of un-dissolved 4,4-dimethoxytritylthymidine was determined. The concentration of water in the filtrate was measured by Karl Fischer titration and an average of three results was used. The same procedure was used for determining the solubility of 4,4-

dimethoxytritylthymidine in acetonitrile with varying concentrations of water and the solubility in toluene and dichloromethane.

2.3.4 Synthesis of 4,4-dimethoxytrityl alcohol
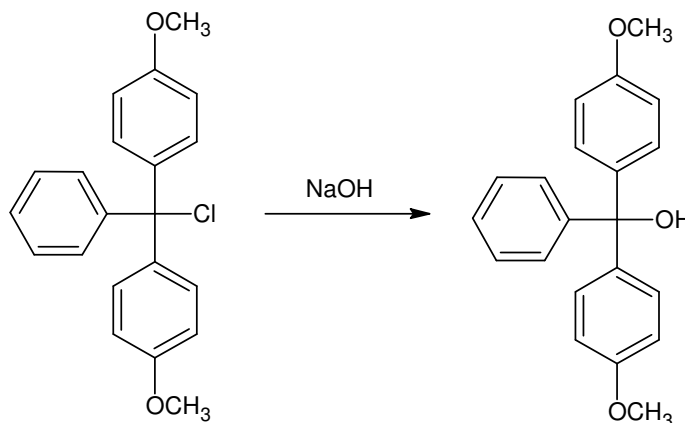
Sodium hydroxide (10 ml, 2.95 mmol) was added to a solution of 4,4-dimethoxytritylchloride (1 g, 2.95 mmol) in acetonitrile (25 ml). As the reaction proceeded the solution was kept basic with further additions of sodium hydroxide (apx. 3 ml). On the addition of water (20 ml) to the solution, a yellow brown oil and a white precipitate was formed. The oil was found to be a crude form of the 4,4-dimethoxytrityl alcohol (0.89 g, 94 %). The oil was dissolved in ether (25 ml) and water (25 ml) and the organic layer extracted with ether (3 x 15 ml). After drying over sodium sulphate and filtration, the solvent was removed and the resulting very viscous orange oil was the 4,4-dimethoxytrityl alcohol (0.76g, 81%).

^{1}H NMR: δ (CD$_3$CN) 7.23 (5H m, aromatic H); 7.12 (4H d, aromatic H J = 2.2 Hz); 6.82 (4H d, aromatic H J = 2.2 Hz); 4.24 (1H s, -OH) (lost on D$_2$O shake); 3.57 (6H s, -OCH$_3$)

^{13}C NMR: δ (CD$_3$CN) 159.9 (2C, aromatic C); 149.0 (1C, aromatic C); 140.9 (2C, aromatic C); 130.0 (4CH, aromatic C); 128.6 (4CH, aromatic C); 127.7 (C, aromatic C); 113.8 (4CH, aromatic C); 81.6 (C, C-OH); 55.8 (2CH$_3$, -OCH$_3$)

IR: 3485.0 (OH); 3058.1 (Ph-H) 2835.3 (OCH$_3$); 1607.5, 1583.1, 1508.7 (Ph) cm^{-1}

2.4   Coupling Experimental

2.4.1   Pre-equilibrium studies of saccharin, *N*-methylimidazole and diisopropylamine

2.4.1.1 ^{1}H NMR studies of acid base equilibria

^{1}H NMR equilibrium studies were performed on a Bruker-DPX400 spectrophotometer. In a typical experiment, saccharin (0.09 M, 0.4 ml) in deuterated acetonitrile and *N*-methylimidazole (0.18 M, 0.2 ml) in deuterated acetonitrile were transferred to an NMR tube and spectra recorded.

2.4.1.2   ITC studies for calculation of pre-equilibrium constants

Isothermal titration calorimetery was performed on a MicroCal VP-ITC microcalorimeter. For determination of the saccharin/diisopropylamine equilibrium constants, saccharin (0.25 mM, 2 ml) in acetonitrile was placed in the cell block and the titrating syringe was loaded with diisopropylamine (7.3 mM, 250 µl) in acetonitrile. Titre volumes of 4 µl were used in this experiment with 150 second delay between titrations. For the determination of the saccharin/*N*-methylimidazole equilibrium constants, saccharin (1 mM, 2 ml) in acetonitrile was placed in the cell block and *N*-methylimidazole (14.6 mM, 250 µl) in acetonitrile was loaded into the titration syringe. In this case, titre volumes of 2 µl were titrated with a 150 second delay between injections.

2.4.1.3   Conductivity studies for calculation of pre-equilibrium constants

Conductivity measurements were performed on a Jenway 4010 conductivity meter. In a typical experiment, acetonitrile (25 ml) was incubated at $30^{\circ}C$. The conductivity probe was immersed in the stirred acetonitrile and saccharin/diisopropylamine solution (0.1616 M, 15 μl) in acetonitrile was titrated into the system. Conductivity readings were taken after approximately 2 minutes to allow for adequate mixing. The experiment was then repeated but titration was performed in to a solution of diisopropylamine (0.1 M, 25 ml) at $30^{\circ}C$. The experiments were repeated, replacing the diisopropylamine with *N*-methylimidazole.

The conductivity data was fitted to equations outlined in the appendix (chapter 7, page 224) using the mathematical fitting program SCIENTIST (Micro Math Scientific Software, Utah, USA, version 3.2).

2.4.1.4   Solubility studies of the saccharin/*N*-methylimidazole salt

Saccharin/*N*-methylimidazole salt (10 g) was added to solutions of *N*-methylimidazole (0-2.5 M, 25 ml) in acetonitrile and was left for 30 minutes with stirring at ambient temperature to ensure complete equilibration. The samples were then filtered under gravity and the mass of un-dissolved saccharin/*N*-methylimidazole was determined.

2.4.2   Phosphoramidite activation equilibrium studies

2.4.2.1   NMR studies

^{1}H, ^{13}C and ^{31}P NMR equilibrium studies were performed on a Bruker-DPX400 spectrophotometer and ^{15}N NMR experiments on a Bruker-AV500 spectrophotometer with 5 mm internal diameter NMR tubes. All reagents were pre-prepared in deuterated acetonitrile or deuterated chloroform and stored over 4Å molecular sieves under dry argon for at least 24 hours before use, and NMR tubes were sealed with rubber septum and flushed with dry argon. All experiments were performed with a total reaction volume of 0.6 ml. In a typical experiment, saccharin/*N*-methylimidazole salt (0.12 M, 0.5 ml) and phosphoramidite (0.6 M, 0.1 ml) was transferred, in a dry argon atmosphere, to the sealed NMR tube. Depending on the reaction, the total concentration of the reaction medium varied due to solubility limits. Saccharin/*N*-methylimidazole salt is only soluble in acetonitrile up to 0.2 M, therefore reactions with excesses of the salt required phosphoramidite concentrations lower than those given above. For example, the reaction performed with five mole equivalents of saccharin/*N*-methylimidazole salt and one mole equivalent of thymidine phosphoramidite, was prepared with 0.5 ml of 0.18 M salt and 0.1 ml of 0.18 M amidite giving a reaction concentration of amidite of 0.03 M.

2.4.2.2   Infra-red   studies   of   dimethyl-*N*,*N*-diisopropylphosphoramidite activation

All reagents were pre-prepared in deuterated acetonitrile and stored over 4Å molecular sieves under dry argon for at least 24 hours before use. In a typical experiment, saccharin (0.08 M, 20 ml) and dimethyl-*N,N*-diisopropylphosphoramidite (0.32 M, 5 ml) was mixed together under a dry argon atmosphere and the resulting mixture was injected into a 1 mm quartz cell which had been flushed with dry acetonitrile (5 ml) and sealed with rubber septa.   Infra red spectra were then obtained on a Thermo Nicolet 380 FT-IR.

2.4.3 Phosphite triester formation with thymidine phosphoramidite and alcohols

2.4.3.1 Alcoholysis equilibrium studies

The same method for studying the activation equilibrium (section 2.4.2.1) was used for the study of the alcoholysis equilibrium with all solutions being pre-dried over 4Å molecular sieves and stored under dry argon before use. In a typical experiment, thymidine phosphoramidite (0.3 M, 0.1 ml), alcohol (0.3 M, 0.1 ml) and saccharin/base (0.075 M, 0.4 ml) were transferred to a sealed NMR tube under a dry argon atmosphere.

2.4.3.2 Alcoholysis kinetic studies

Kinetic measurements for alcoholysis were performed using rapid ^{31}P NMR techniques on a Bruker-DPX400 spectrophotometer. All reagents were pre-prepared in deuterated acetonitrile and stored over 4Å molecular sieves under dry argon for at least 24 hours before use. In a typical kinetic run, two identical samples of saccharin/*N*-methylimidazole salt (0.075 M, 0.4 ml) in deuterated acetonitrile and 4-methoxyphenol (0.3 M, 0.1 ml) in deuterated acetonitrile were prepared in sealed/argon flushed NMR tubes. To one of these samples, the NMR experiments shimming and deuterium locking protocols were performed after addition of thymidine phosphoramidite (0.3 M, 0.1 ml). Thymidine phosphoramidite (0.3 M, 0.1 ml) was then added to the other sample which was placed in the NMR magnet as quickly as possible and the experiment was started. ^{31}P NMR spectra were recorded successively at intervals of 23 seconds. This time base was chosen to gain the maximum number of data points over the kinetic run, but also give adequate signal resolution.

2.4.3.3   Synthesis of ^{15}N labelled saccharin

The ^{15}N labelled saccharin was prepared by a modified method to that described by Fahlberg and Remsen.[117]

2.4.3.3.1   Step 1: synthesis of ^{15}N *ortho*-toluenesulfonylamide
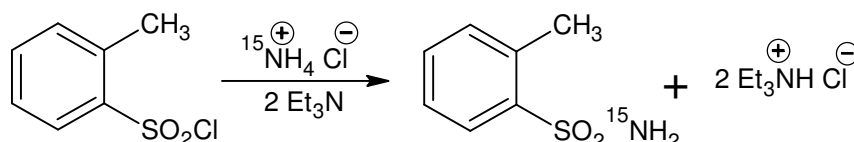
ortho-Toluenesulphonylchloride (2 g, 10 mmol) was dissolved in acetonitrile (5 ml) and cooled to -38°C in an acetonitrile/liquid nitrogen bath. ^{15}N labelled ammonium chloride (5 g, 92 mmol) in acetonitrile (5 ml) was added drop wise over 15 minutes. Triethylamine (18.6 g, 184 mmol) in acetonitrile (5 ml) was then added drop wise over 15 minutes. The solution was allowed to warm to room temperature and the solvent was removed. The residue was dissolved in ether (40 ml) and water (40 ml) and the pH of the solution was adjusted to pH 4 with dilute hydrochloric acid. The organic layer was extracted into ether (3 x 20 ml) and dried over sodium sulphate. After gravity filtration the solvent was removed to yield a white solid which was the ^{15}N labelled *ortho*-toluenesulfonylamide (1.46 g, 81%). ^{1}H NMR has shown that the *ortho*-toulenesulfonylamide was 74% ^{15}N labelled to 26% ^{14}N (which is compatible with the ratio of ^{15}N to ^{14}N in the starting ^{15}N labelled ammonium chloride).

^{1}H NMR: δ (CD$_3$CN) 7.90 (1H d, aromatic H J = 7.8 Hz); 7.48 (1H t, aromatic H J = 7.8 Hz); 7.35 (2H m, aromatic H); 5.67 (2H d, ^{15}NH$_2$ J = 82 Hz); 5.67 (2H s, ^{14}NH$_2$); 2.61 (3H s, CH$_3$)

^{13}C NMR: δ (CD3CN) 141.3 (C, aromatic C); 136.4 (C, aromatic C); 132.4 (2CH, aromatic C); 127.5 (CH, aromatic C); 126.2 (CH, aromatic C); 19.4 (CH$_3$)

^{15}N NMR: δ (CD$_3$CN) 91.2 (t)

ESI-MS: *m/z* 171.02184 (M-H^{+}). Expected: 171.02516

2.4.3.3.2 Step 2: synthesis of ^{15}N labelled saccharin
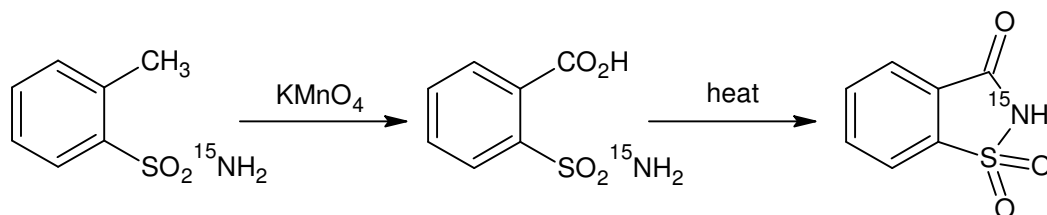
[15]N labelled *ortho*-toluenesulfonylamide (1.4g, 8 mmol) was dissolved in water (50 ml) and after addition of potassium permanganate (5 g), the resulting solution was stirred for 10 hours at 50°C. The solution was then allowed to cool to room temperature and ethanol was added drop wise until all of the un-reacted potassium permanganate had precipitated. After filtration the solvent was reduced to a quarter of its volume and acidified with hydrochloric acid. The precipitate was filtered and recrystalised from water to give a white powdery solid which was the ^{15}N labelled saccharin (0.6497 g, 43%), melting point 215-218°C (220°C).[117]

^{1}H NMR: δ (CD$_3$CN) 7.93 (4H m, aromatic H)

^{13}C NMR: δ (CD$_3$CN) 159.9 (C=O); 139.4 (C, aromatic C); 135.7 (CH, aromatic C); 134.7 (CH, aromatic C); 127.5 (C, aromatic C); 125.1 (CH, aromatic C), 120.9 (CH, aromatic C)

^{15}N NMR: δ (CD$_3$CN) 152.7 (s)

ESI-MS: *m/z* 182.98860 (M-H^{+}). Expected: 182.98877

2.5 Sulphurisation Experimental

2.5.1 UV spectrophotometric rate measurement

Prior to kinetic measurements, wavelength scans of xanthane hydride and the phosphites under study in acetonitrile were performed to determine the presence of UV chromophores (figure 15). All of the phosphites under study strongly absorbed UV wavelengths below 280nm. Xanthane hydride absorbs UV at two main wavelengths: 280nm (ε = 21400 dm^3 mol^{-1} cm^{-1}) and 360nm (ε = 6200 dm^3 mol^{-1} cm^{-1}), which on the addition of at least one mole equivalent of phosphite showed considerable loss of absorbance (figure 15). As some of the triarylphosphites absorbed wavelengths of up to 280nm, kinetic measurements were performed by following the disappearance of the absorbance at 360nm.
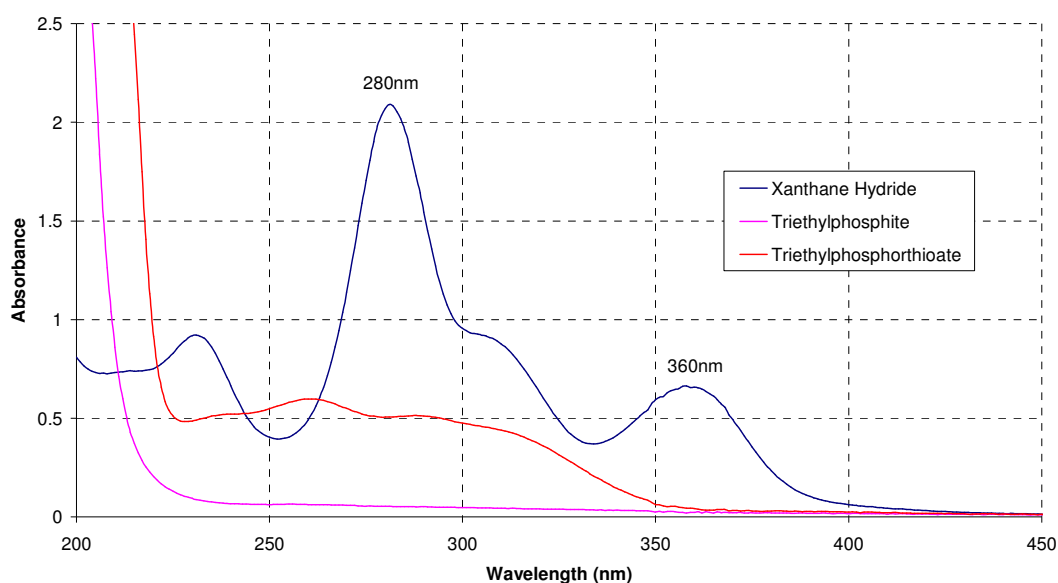
Figure 15: UV traces in acetonitrile of 1 x10^{-4} M xanthane hydride (blue line), 1 x10^{-4} M triethylphosphite (magenta line) and a 1:1 reaction mixture of the two forming the triethylphosphorthioate (red line).

All kinetic measurements were performed at 30°C (unless otherwise stated) using 1 x10^{-4} M xanthane hydride and varying phosphite concentrations in excess of the xanthane hydride to give pseudo first order kinetics. Kinetic measurements of the

sulphurisation of the trialkylphosphites and some of the triarylphosphites were performed using stop-flow instrumentation with 1:1 syringe volume ratio. In a typical experiment, xanthane hydride (2×10^{-4} M in acetonitrile) was loaded into one syringe of the stop-flow and the phosphite under study (1×10^{-3}-2×10^{-2} M in acetonitrile) into the other. Injection of the two syringes into the reaction cell initiated the measurement of the reduction in absorbance at 360 nm. For each concentration of phosphite an average of 20-30 results was used.

For the slower reacting phosphites, kinetic measurements were performed on the standard UV instrumentation. A typical run, 50 μl of xanthane hydride (5×10^{-3} M in acetonitrile) was injected into 2.5 ml of phosphite (5×10^{-4}-1×10^{-2} M in acetonitrile) in a 1 cm cuvette. After quick mixing, the reduction in absorbance at 360 nm was followed. For each concentration of phosphite an average of 3-5 results was used.

For kinetic measurements performed with varying ionic strengths the same procedures were used as above except solutions of xanthane hydride, phosphite and phosphine were prepared in stock solutions of *tetra-n*-propylammonium bromide (5×10^{-3}-3×10^{-2} M) in acetonitrile.

2.5.2 Conductivity measurements of *tetra-n*-propylammonium bromide solution

To ascertain whether the increase in conductance of *tetra-n*-propylammonium bromide solutions in acetonitrile was linear with concentration over the concentration range studied, conductivity studies were undertaken. Conductivity measurements were performed on a Jenway 4010 conductivity meter. In a typical experiment, acetonitrile (25 ml) was incubated at 30°C. The conductivity probe was immersed in the stirred acetonitrile and *tetra-n*-propylammonium bromide (0.505 M, 15-200 μl) in acetonitrile was titrated into the solution. Conductivity readings were taken after approximately 2 minutes to allow for adequate mixing.

2.5.3   Determination of xanthane hydride solubility

Xanthane hydride (0.5 g) was added to solutions of *tetra-n*-propylammonium bromide in acetonitrile (25 ml, 5 x10^{-3}-5 x10^{-2} M) which were then left with agitation for 30 minutes at ambient temperature to ensure complete equilibration. The samples were then filtered under gravity and the absorbance at 360 nm of the filtrate was measured. Using the slope of the calibration graph (figure 16) (which was prepared by measuring the absorbance at 360 nm of xanthane hydride solutions of known concentrations in acetonitrile), the solubility of xanthane hydride was determined.

Calibration Curve for Determination of Xanthane hydride Solubility

$y = 6225.8x + 0.0538$

$R^2 = 0.9989$
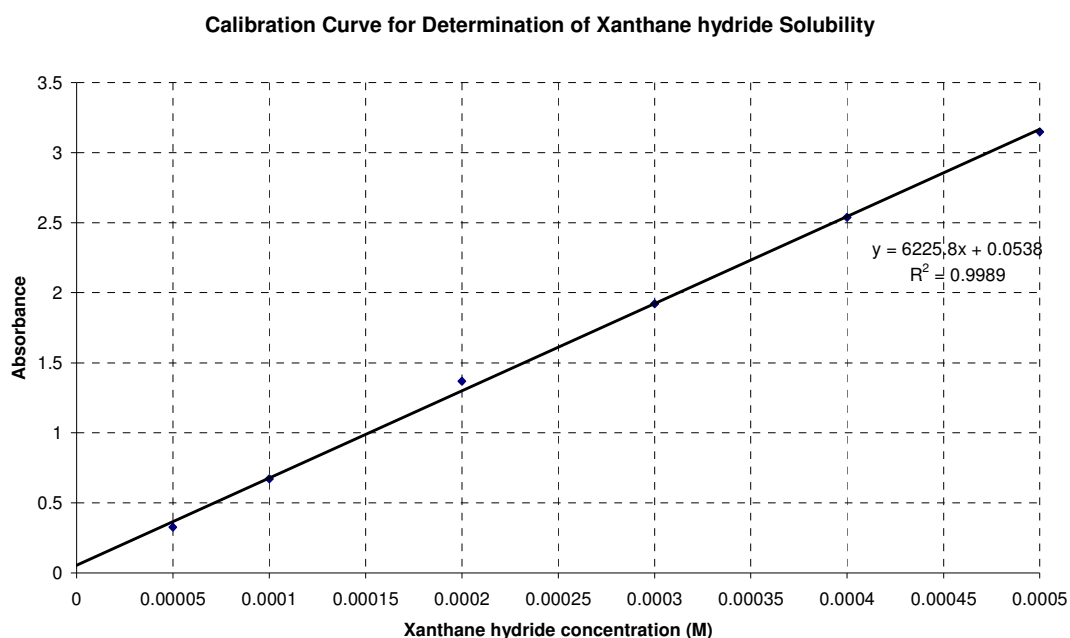
Figure 16: Calibration curve of absorbance versus xanthane hydride concentration in acetonitrile.

2.5.4   Synthesis of 1-(4-nitrophenyl)dithiobiuret
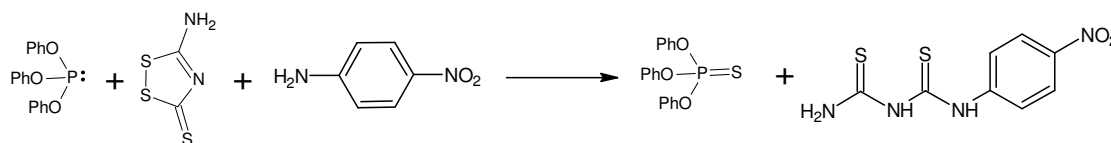
Xanthane hydride (1g, 6.7 mmol) was dissolved in acetonitrile (400 ml) under a nitrogen atmosphere at 30°C and a solution of triphenylphosphite (2.08 g, 1.75 ml, 6.7 mmol) in 100 ml of acetonitrile was added. The reaction mixture was stirred for 6 hours and then 4-nitroaniline (0.92 g, 6.7 mmol) in 20 ml acetonitrile was added. After 18 hours the acetonitrile was removed and the solid residue was quickly extracted with 3 x 40 ml of 3% aqueous potassium hydroxide solution in ether. After filtration the insoluble material was triphenylphosphorthioate. The filtrate was immediately neutralised with concentrated hydrochloric acid and the resulting precipitate, which was found to be 1-(4-nitrophenyl)dithiobiuret, was filtered off and dried (1.56 g, 91%).

^{1}H NMR: δ (DMSO) 13.24 (1H s, H$_2$N-CS-N<u>H</u>-CS-NH-); 11.05 (1H s, H$_2$N-CS-NH-CS-N<u>H</u>-); 9.29 (2H d, <u>H</u>$_2$N-CS-NH-CS-NH- J = 122.1 Hz); 8.26 (2H d, aromatic H J = 9.2 Hz); 7.97 (2H d, aromatic H J = 9.2 Hz)

^{13}C NMR: δ (DMSO) 179.0 (C, H$_2$N-<u>C</u>S-NH-CS-NH-); 177.1 (C, H$_2$N-CS-NH-<u>C</u>S-NH-); 144.1 (C, aromatic C); 143.5 (C, aromatic C); 124.5 (CH, aromatic C); 123.2 (CH, aromatic C)

ESI-MS: *m/z* 254.99942 (M-H$^+$). Expected: 255.000493

2.5.5 Synthesis of 1-phenyldithiobiuret
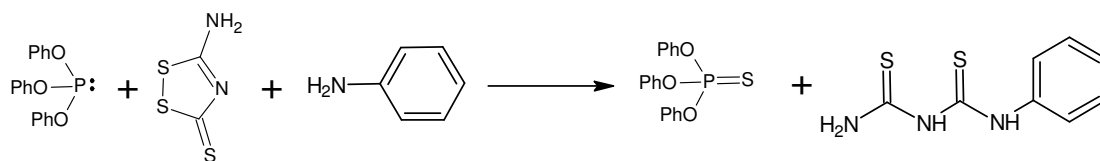
1-phenyldithiobiuret was synthesised via the same procedure as used for synthesis of 1-(4-nitrophenyl)dithiobiuret. Yield 1.13 g, 80 %.

^{1}H NMR: δ (DMSO) 12.72 (1H s, H$_2$N-CS-N<u>H</u>-CS-NH-); 10.83(1H s, H$_2$N-CS-NH-CS-N<u>H</u>-); 9.24 (2H d, <u>H</u>$_2$N-CS-NH-CS-NH- *J* = 53.4 Hz); 7.56 (2H d, aromatic H *J* = 7.5 Hz); 7.40 (2H d, aromatic H *J* = 7.5 Hz); 7.25 (1H d, aromatic H *J* = 7.5 Hz)

^{13}C NMR: δ (DMSO) 179.7 (C, H$_2$N-<u>C</u>S-NH-CS-NH-); 177.7 (C, H$_2$N-CS-NH-<u>C</u>S-NH-); 137.8 (C, aromatic C); 129.3 (CH, aromatic C); 126.8 (C, aromatic C); 124.6 (CH, aromatic C)

ESI-MS: *m/z* 210.01628 (M-H$^+$). Expected: 210.01542

2.5.6 Synthesis of 1-(4-methoxyphenyl)dithiobiuret
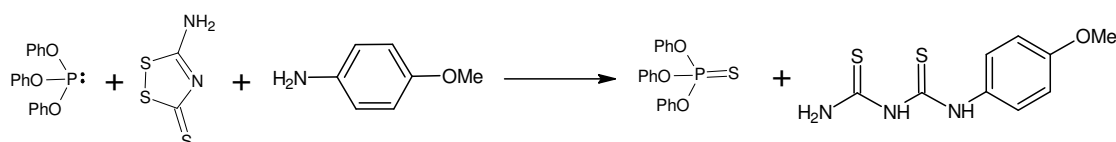
1-(4-methoxyphenyl)phenyldithiobiuret was synthesised via the same procedure as used for synthesis of 1-(4-nitrophenyl)dithiobiuret. Yield 1.41 g, 86 %.

^{1}H NMR: δ (DMSO) 12.48 (1H s, H$_2$N-CS-N<u>H</u>-CS-NH-); 10.78 (1H s, H$_2$N-CS-NH-CS-N<u>H</u>-); 9.20 (2H d, <u>H</u>$_2$N-CS-NH-CS-NH- *J* = 44.0 Hz); 7.40 (2H d, aromatic H *J* = 9.0 Hz); 6.95 (2H d, aromatic H *J* = 9.0 Hz); 3.75 (3H s, -OCH$_3$)

^{13}C NMR: δ (DMSO) 179.7 (C, H$_2$N-C̲S-NH-CS-NH-); 177.6 (C, H$_2$N-CS-NH-C̲S-NH-); 157. 9 (C, aromatic C); 130.2 (C, aromatic C); 126.4 (CH, aromatic C); 114.4 (CH, aromatic C); 55.76 (CH$_3$, -OCH$_3$)

ESI-MS: *m/z* 240.02389 (M-H$^+$). Expected: 240.02598

2.5.7 Synthesis of 1-(4-nitrophenyl)-5,5-dimethyldithiobiuret
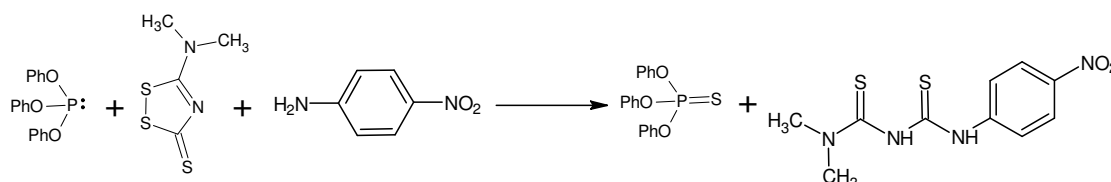
1-(4-nitrophenyl)-5,5-dimethyldithiobiuret was synthesised via the same procedure as used for synthesis of 1-(4-nitrophenyl)dithiobiuret except that the dimethyl derivative of xanthane hydride was used. Yield 1.57 g, 87 %.

^{1}H NMR: δ (DMSO) 11.68 (1H s, (CH$_3$)$_2$N-CS-NH̲-CS-NH-); 10.37 (1H s, (CH$_3$)$_2$N-CS-NH-CS-NH̲-); 8.24 (2H d, aromatic H *J* = 9.2 Hz); 7.96 (2H d, aromatic H *J* = 9.2 Hz); 3.30 (6H s, (CH̲$_3$)$_2$N -CS-NH-CS-NH-)

^{13}C NMR: δ (DMSO) 179.5 (C, (CH$_3$)$_2$N-C̲S-NH-CS-NH-); 179.3 (C, (CH$_3$)$_2$N-CS-NH-C̲S-NH-); 145. 5 (C, aromatic C); 143.7 (C, aromatic C); 124.9 (CH, aromatic C); 122.5 (CH, aromatic C); 42.1 (CH$_3$, (C̲H$_3$)$_2$N-CS-NH-CS-NH-)

ESI-MS: *m/z* 283.03141 (M-H$^+$): Expected: 283.03179

2.5.8   Synthesis of tri(4-methoxyphenyl)phosphite
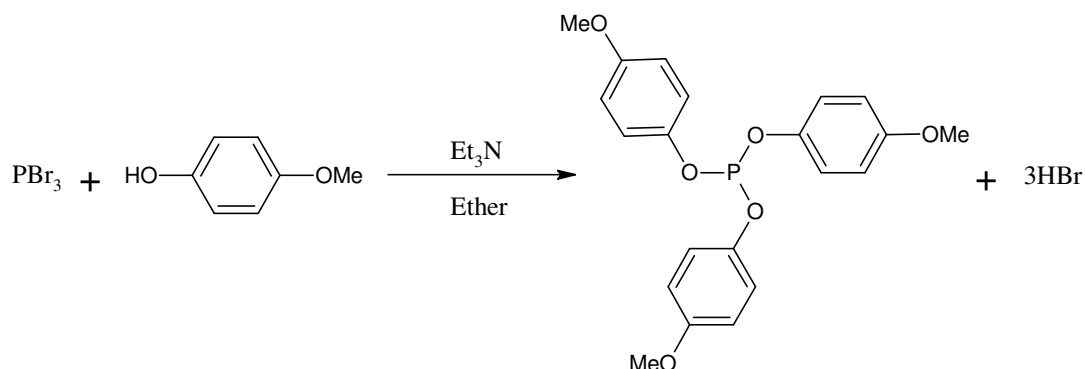
To a 0°c stirred solution of 4-methoxyphenol (8.184 g, 66 mmol) and triethylamine (8.08 g, 80 mmol) in anhydrous ether (80ml) was added drop wise phosphorous tribromide (5.42 g, 20 mmol) in a flame dried round bottom flask. After 30 minutes the white precipitate that had formed was filtered under vacuum and the remaining solution was extracted with 1M HCl (25 ml), a saturated solution of $NaHCO_3$ (25 ml) and finally with brine (25 ml). The solution was then dried with anhydrous sodium sulphate, filtered and reduced on a rotary evaporator at 50°c to give a colourless oily liquid (3.46 g, 43.3%) which was the crude phosphite. Purification was achieved by column chromatography with silica (60 g) as the stationary phase and dichloromethane as the mobile phase (RF = 0.34), the tri(4-methoxyphenyl)phosphite was obtained at a purity of 87% with 13% un-reacted alcohol present.

^{1}H NMR: δ ($CDCl_3$) 7.15 (6H d, aromatic H *J*= 8.9 Hz); 6.90 (6H d, aromatic H *J*= 8.9 Hz); 3.80 (9H s, -OCH_3)

^{13}C NMR: δ ($CDCl_3$) 156.2 (C, aromatic C); 145.1 (C, aromatic C); 121.7 (CH, aromatic C); 114.8 (CH, aromatic C); 55.6 (CH_3, -OCH_3)

^{31}P NMR: δ ($CDCl_3$) 129.6 (P(OR)$_3$)

IR: 3421.1 (OH); 1606.5, 1591.0, 1502.0 (Ph); 1190.0 (P-OPh) cm^{-1}

2.5.9 Synthesis of tri(4-chlorophenyl)phosphite
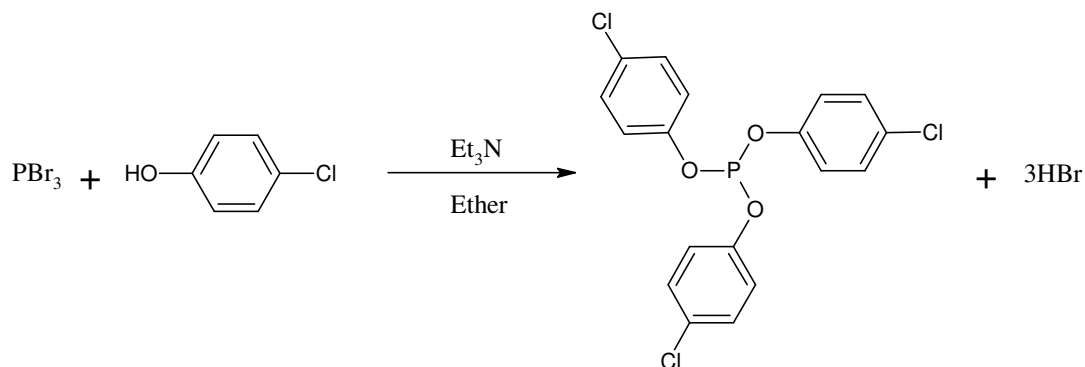
Tri(4-chlorophenyl)phosphite was synthesised via the same procedure as used for synthesis of tri(4-methoxyphenyl)phosphite (RF = 0.42). The tri(4-chlorophenyl)phosphite was obtained at a purity of 82% with 18% un-reacted alcohol.

^{1}H NMR: δ (CDCl$_3$) 7.36 (6H d, aromatic H *J*= 8.7 Hz); 7.11 (6H d, aromatic H *J*= 8.7 Hz);

^{13}C NMR: δ (CDCl$_3$) 154.0 (C, aromatic C); 149.6 (C, aromatic C); 129.7 (CH, aromatic C); 121.8 (CH, aromatic C)

^{31}P NMR: δ (CDCl$_3$) 127.8 (P(OR)$_3$)

IR: 3416.2 (OH); 1638.8, 1590.0, 1484.5 (Ph); 1201.6 (P-OPh) cm^{-1}

2.5.10 Synthesis of tri(4-methylphenyl)phosphite
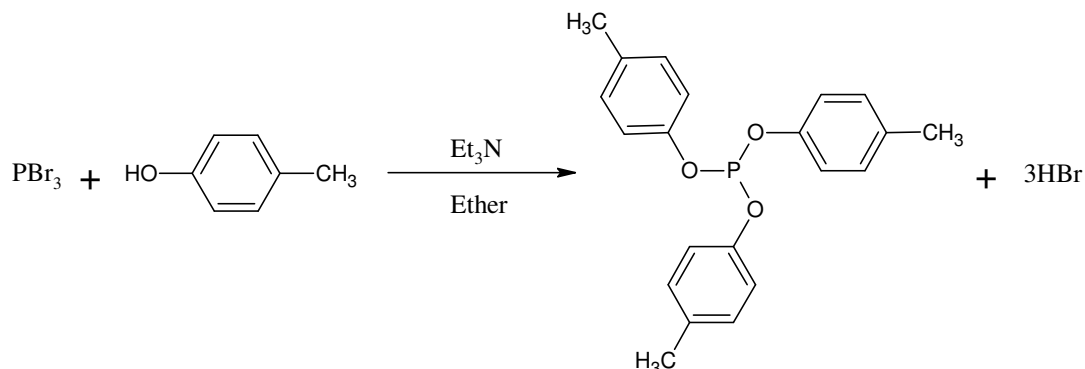
Tri(4-methylphenyl)phosphite was synthesised via the same procedure as used for synthesis of tri(4-methoxyphenyl)phosphite (RF = 0.38). The tri(4-methylphenyl)phosphite was obtained at a purity of 85% with 15% un-reacted alcohol.

^{1}H NMR: δ (DMSO) 7.17 (6H d, aromatic H J= 8.3 Hz); 7.04 (6H d, aromatic H J= 8.3 Hz); 2.28 (9H s, CH_3)

^{13}C NMR: δ (DMSO) 155.5 (C, aromatic C); 149.2 (C, aromatic C); 134.0 (CH, aromatic C); 130.8 (CH, aromatic C); 20.6 (CH_3, CH_3)

^{31}P NMR: δ (DMSO) 129.3 ($P(OR)_3$)

2.5.11   Synthesis of tri(3-methylphenyl)phosphite
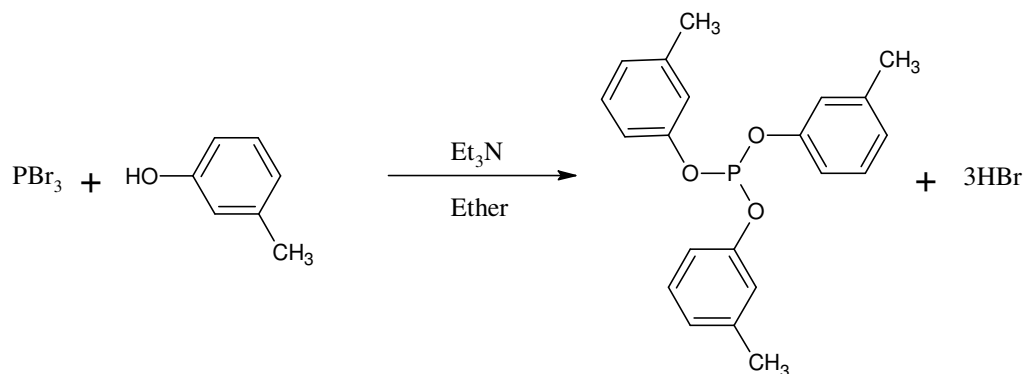
Tri(3-methylphenyl)phosphite was synthesised via the same procedure as used for synthesis of tri(4-methoxyphenyl)phosphite (RF = 0.39). The tri(3-methylphenyl)phosphite was obtained at a purity of 97% with 3% un-reacted alcohol.

^{1}H NMR: δ (DMSO) 7.26 (3H t, aromatic H *J*= 7.7 Hz); 6.98 (9H m, aromatic H); 2.29 (9H s, CH$_3$)

^{13}C NMR: δ (DMSO) 151.4 (C, aromatic C); 140.3 (C, aromatic C); 130.2 (CH, aromatic C); 125.7 (CH, aromatic C); 121.5 (CH, aromatic C); 117.9 (CH, aromatic C); 21.5 (CH$_3$, CH$_3$)

^{31}P NMR: δ (DMSO) 129.3 (P(OR)$_3$)

2.5.12 Synthesis of tri(tri-2,2,2-chloroethyl)phosphite
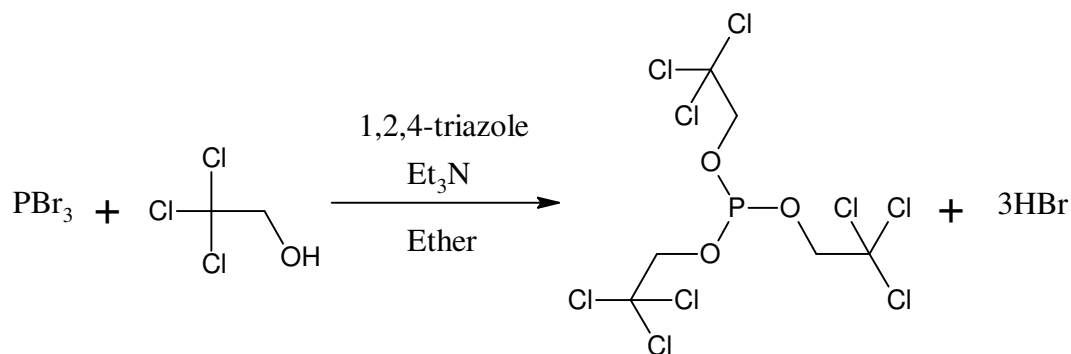
1,2,4-Triazole (8.16 g, 121 mmol, 5.8 moleq), triethylamine (16.97 g, 168 mmol, 8 moleq) and THF (160 ml) were mixed and cooled in an ice/water/salt bath for 30 minutes. Phosphorous tribromide (5.69 g, 21 mmol, 1 moleq) and THF (10 ml) was added drop wise over 30 minutes with a final THF (10 ml) wash. The reaction was allowed to stir for a further 30 minutes in the ice/water/salt bath. Tri-2,2,2-chloroethanol (9.73 g, 65 mmol, 3.1 moleq) was added over 1 hour 30 minutes and left stirring for 2 hours maintaining 0^oc. Once the reaction was complete the mixture was warmed to room temperature and a mixture of water (40 ml) and triethylamine (40 ml) was added with stirring. A solution of DCM (250 ml) and water (325 ml) adjusted to pH 7 with acetic acid and triethylamine was added to quench the reaction. The aqueous and organic layers were separated and the aqueous layer was washed with two lots of DCM (100 ml). The organic and DCM layers were combined and dried over anhydrous sodium sulphate, the reaction was filtered and the solvent removed under vacuum to produce a pale yellow oily liquid (8.6 g, 86%) which was the crude phosphite. The crude product (4 g) was purified by column chromatography (alumina 60 g) (10% MeOH in DCM, RF= 0.82) to afford a colourless oily liquid (2.33 g, 58%) which was the phosphite. The tri(tri-2,2,2-chloroethyl)phosphite was obtained at a purity of 84% with 16% un-reacted alcohol.

^{1}H NMR: δ (CDCl$_3$) 4.55 (6H d, CH$_2$)

^{31}P NMR: δ (CDCl$_3$) 138.1 (PR$_3$)

IR: 3446.2 (OH); 2945.0 (C-H); 1098.2 (P-OCH2); 721.1 (C-Cl) cm^{-1}

2.5.13   Synthesis of tri(2-cyanoethyl)phosphite
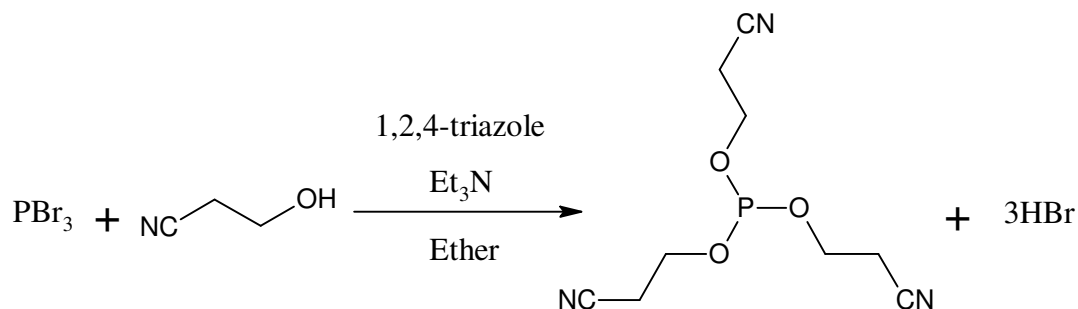
Tri(2-cyanoethyl)phosphite was prepared by the same method as tri(tri-2,2,2-chloroethyl)phosphite.

The crude product (4 g) was purified using reduced pressure distillation. At 1mmHg a colourless oily liquid (1.9 g, 48%) was collected with a boiling range of 90-96 ^{o}C which proved to be the purified phosphite. The tri(2-cyanoethyl)phosphite was obtained at a purity of 51% with 49% un-reacted alcohol.

^{1}H NMR: δ (CDCl$_3$) 4.14 (6H q, CH$_2$ *J*= 2 Hz); 2.74 (6H t, CH$_2$ *J*= 2 Hz)

^{31}P NMR: δ (CDCl$_3$) 138.5 (PR$_3$)

IR: 3439.8 (OH); 2250.4 (C≡N); 1057.7 (P-OCH$_2$) cm^{-1}

3   Results and Discussion: Detritylation

3.1   Detritylation with dichloroacetic acid: equilibrium studies

The detritylation reaction is the acid catalysed removal of the 4,4-dimethoxytrityl protecting group from the 5' oxygen of the protected nucleoside. The commonly assumed mechanism for this reaction is an S_N1 type mechanism with initial protonation of the 5' oxygen to form the intermediate, which then undergoes bond cleavage to give the 4,4-dimethoxytrityl carbocation and the free 5' hydroxyl group (scheme 15).
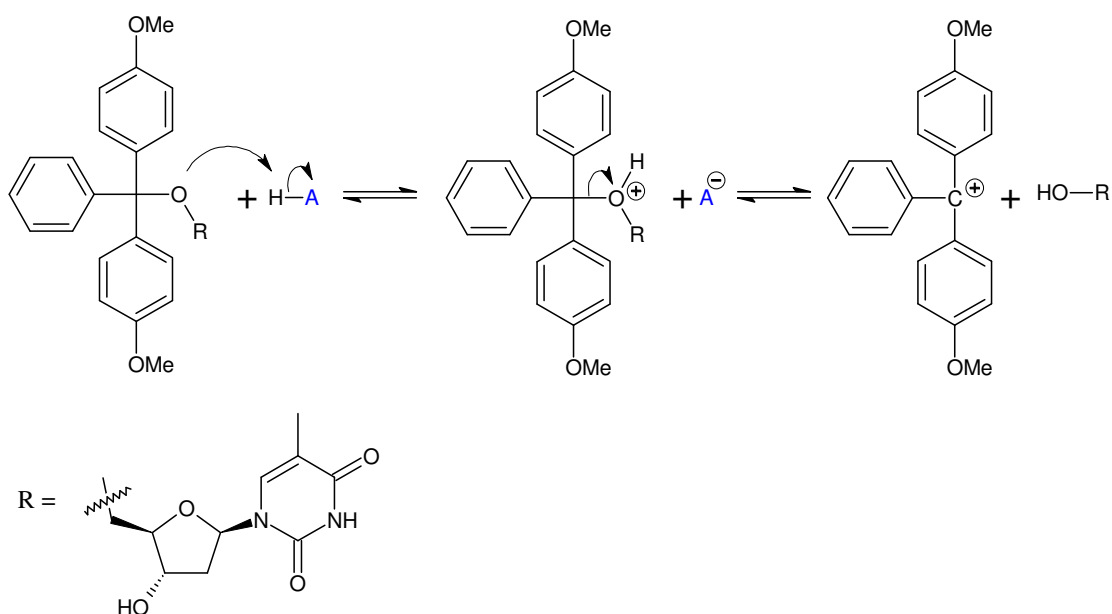
Scheme 15: Detritylation of 4,4-dimethoxytritylthymidine

We wished to investigate this process further, particularly the timing of the bond cleavage and protonation steps and also the equilibrium between the various possible species.

3.1.1   Exploring the equilibrium

The 4,4-dimethoxytrityl cation absorbs UV radiation at a λ_{max} which shows a bathochromic shift on decreasing solvent polarity (dielectric constant taken as a measure of solvent polarity). Table 1 shows the λ_{max} of the 4,4-dimethoxytrityl cation generated from 4,4-dimethoxytritylthymidine and dichloroacetic acid in toluene, dichloromethane and acetonitrile.

Solvent	λ_{max} (nm)	Dielectric constant of solvent
Toluene	510	2.4
Dichloromethane	505	4.8
Acetonitrile	497	37.5

Table 1: Change in λ_{max} of 4,4-dimethoxytrityl cation, generated from 3.6 x10^{-5} M 4,4-dimethoxytritylthymidine and 0.05 M dichloroacetic acid in dichloromethane and 0.5 M dichloroacetic acid in toluene and acetonitrile.

UV measurements of dichloroacetic acid titration to 4,4-dimethoxytritylthymidine in acetonitrile, toluene and dichloromethane give absorbance versus dichloroacetic acid concentration profiles shown below (figure 17).
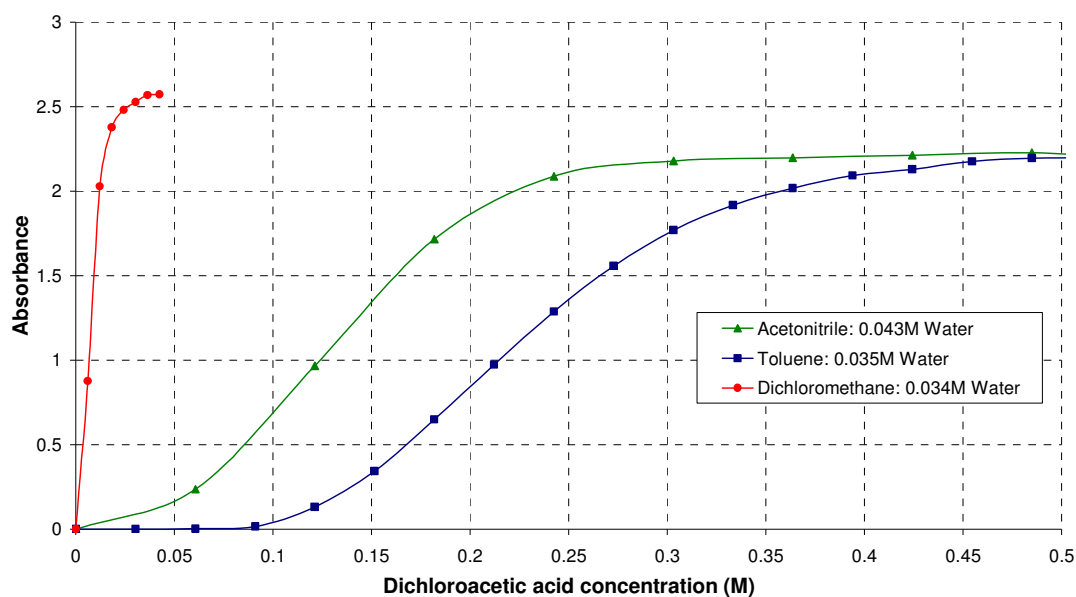
Figure 17: Detritylation of 3.6x10^{-5} M 4,4-dimethoxytritylthymidine with dichloroacetic acid in dichloromethane, acetonitrile and toluene.

The dielectric constants in table 1 show that acetonitrile is by far the most polar of the three solvents studied. Classically, carbocation production is expected to be favoured in polar solvents and it would seem intuitive that the detritylation reaction would also proceed more readily in polar solvents due to stabilisation of the charged product. The absorbance versus acid concentration profiles in figure 17 show that this is not the case, the best solvent for 4,4-dimethoxytrityl carbocation formation being dichloromethane.

In addition to the trityl cation being formed more readily in dichloromethane with a lower concentration of dichloroacetic acid, the molar extinction coefficient also seems to be greater in this solvent than in acetonitrile and toluene, for which it appears similar. This is contrary to expectation and requires further investigation and explanation.

The equilibrium presumably being measured is shown in scheme 16 in its simplest form.

$$DMTr\text{-}OT \ + \ HA \ \xrightleftharpoons{\ K_{detrit}\ } \ DMTr^{\oplus} \ + \ TOH \ + \ A^{\ominus}$$
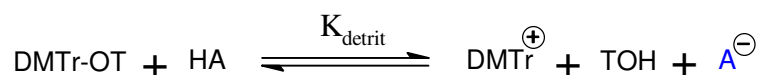
Scheme 16: Detritylation equilibrium.

Where,
$$K_{det\,rit} = \frac{\left[DMTr^+\right]\left[TOH\right]\left[A^-\right]}{\left[DMTr-OT\right]\left[HA\right]}$$

The obvious factors controlling this equilibrium are the stability of the reactants and products in the different solvents. The acidity of dichloroacetic acid is expected to be greatest in acetonitrile, as is the stability of the trityl cation, the alcohol and dichloroacetate anion. It is difficult to conceive significant solvent effects on the reactant ether. It is possible that small traces of water cause differences but the measured concentration is the same in each solvent.

Manipulation of this equation for the equilibrium constant allows determination of K_{detrit}. Assuming that the charges must balance,

$$\left[DMTr^+\right] = \left[A^-\right] = \left[TOH\right]$$

Therefore,

$$K_{det\,rit} = \frac{\left[DMTr^+\right]^3}{\left[DMTr-OT\right]\left[HA\right]}$$

The mass balance for this reaction gives,

$$\left[DMTr-OT\right]_o = \left[DMTr-OT\right]+\left[DMTr^+\right]$$

Rearrangement of the mass balance and substitution into the equation for K_{detrit} gives,

$$K_{det\,rit} = \frac{\left[DMTr^+\right]^3}{\left(\left[DMTr-OT\right]_o - \left[DMTr^+\right]\right)\left[HA\right]}$$

Attempts to fit the data in figure 17 to this equation met with no success. Modelling of the equation gave plots which were hyperbolic in shape (figure 18) rather than the sigmoidal shape found experimentally (figure 17). It appears that the simple equation in scheme 16 does not adequately describe the reaction.
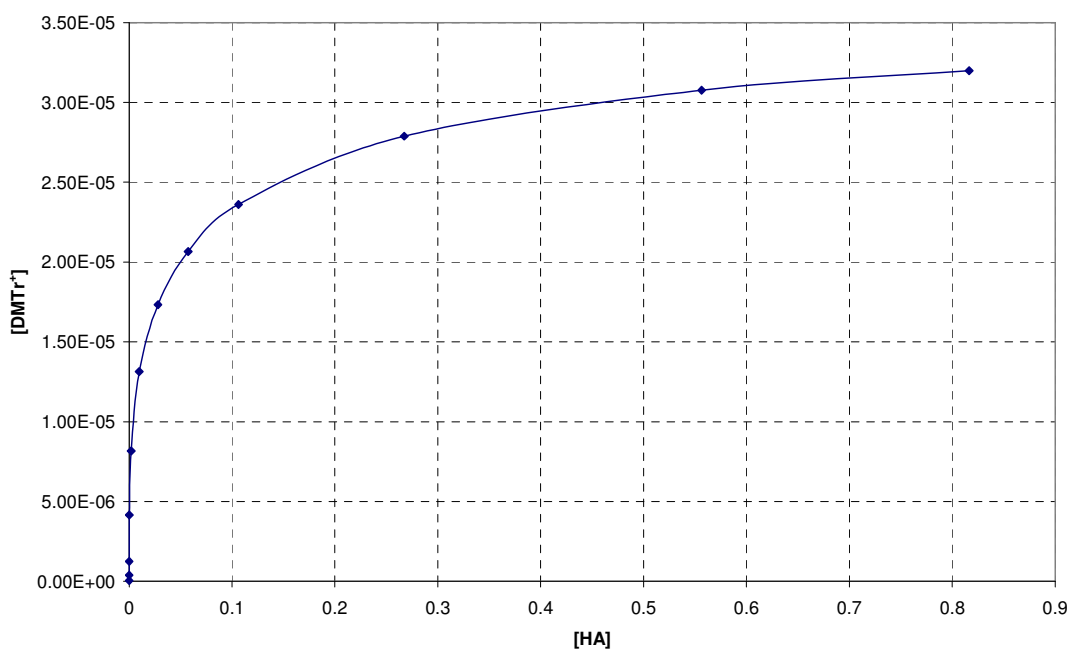
Figure 18: Plot of 4,4-dimethoxytrityl carbocation concentration as a function of dichloroacetic acid concentration determined from the equation for the equilibrium constant K_{detrit}.

Dichloroacetic acid is a strong acid in water with a pK_a of 1.29.[118] In the organic solvents studied here, dichloroacetic acid will be relatively weak, for example in acetonitrile, dichloroacetic acid has a pK_a of 15.8[119] (no pK_a data is available in toluene or dichloromethane). It may, therefore, be more appropriate to discuss the reaction in terms of the dissociated acid concentration which can be determined from the equilibrium constant K_a described in scheme 17, rather than the total concentration of added acid.

$$\text{Solvent} + \text{HA} \; \underset{}{\overset{K_a}{\rightleftharpoons}} \; \text{SolventH}^{\oplus} + \text{A}^{\ominus}$$

$$\text{DMTr-OT} + \text{SolventH}^{\oplus} \; \underset{}{\overset{K_1}{\rightleftharpoons}} \; \text{DMTr}^{\oplus} + \text{TOH} + \text{Solvent}$$
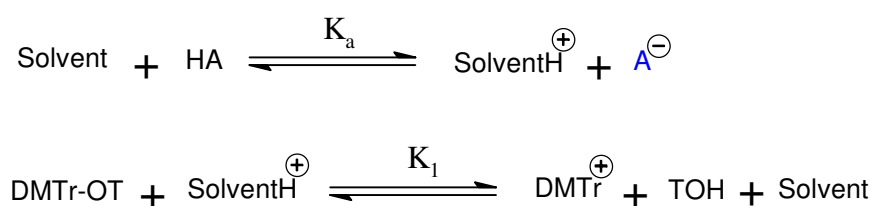
Scheme 17: Equilibria for the dissociation of acid and detritylation.

Where, $$K_a = \frac{[SolventH^+]\,[A^-]}{[Solvent]\,[HA]}$$ and $$K_1 = \frac{[DMTr^+]\,[TOH]\,[Solvent]}{[DMTr-OT]\,[SolventH^+]}$$

The equilibrium constant for detritylation, K_{detrit}, is equal to the product of K_a and K_1, as described below.

$$K_{det\,rit} = K_a.K_1 = \frac{[SolventH^+]\,[A^-]}{[Solvent]\,[HA]} . \frac{[DMTr^+]\,[TOH]\,[Solvent]}{[DMTr-OT]\,[SolventH^+]}$$

Therefore, $$K_{det\,rit} = \frac{[DMTr^+]\,[TOH]\,[A^-]}{[DMTr-OT]\,[HA]}$$

In this equation there are no terms for the dissociated acid concentration or for the solvent. It is identical to the equation presented on page 55 which showed a hyperbolic equilibrium curve. Therefore, discussion of the detritylation reaction in terms of the dissociated acid does not explain the sigmoidal shape found in figure 17.

3.1.2   Effect of water on the detritylation reaction

It is difficult to completely remove traces of water in the solvents and it is possible that this can cause problems when comparing solvents. The effect of changing the concentration of water in the detritylation reaction was therefore studied. Using UV-vis spectroscopy, absorbance versus dichloroacetic acid concentration profiles for each solvent at varying water concentrations were produced (figures 19, 20 and 21). These show that increasing the initial water concentration, increases both the sigmoidal shape of the profiles and the concentration of acid required for complete detritylation. There is also a small reduction in the extinction coefficient at this wavelength on increasing water concentration which is due to a slight shift in the trityl cations λ_{max}, presumably due to an increase in solvent polarity as water is added.

Detritylation of 4,4-dimethyoxytritylthymidne with Dichloroacetic Acid in Acetonitrile
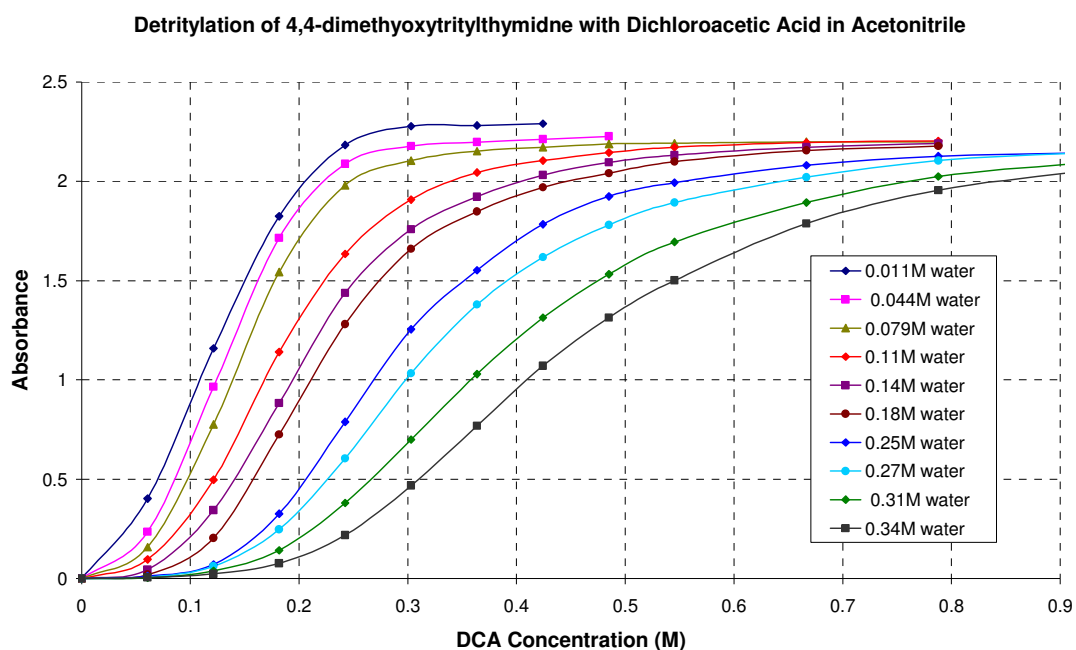
Figure 19: Detritylation of 3.6×10^{-5} M 4,4-dimethoxytritylthymidine with dichloroacetic acid in acetonitrile at varying water concentration.
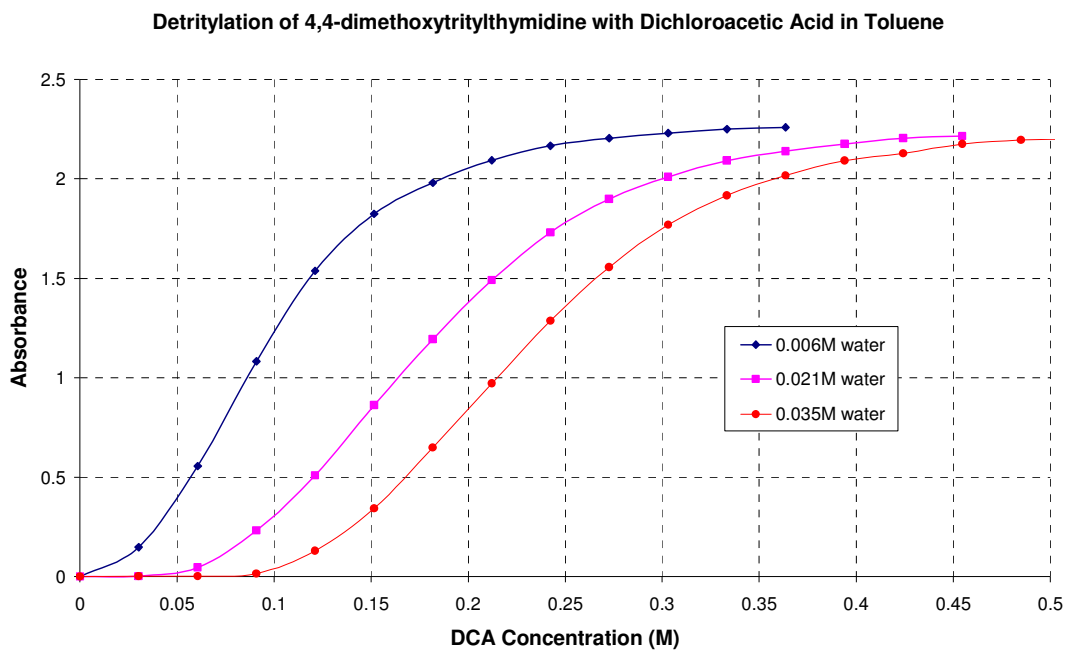
Figure 20: Detritylation of 3.6x10^{-5} M 4,4-dimethoxytritylthymidine with dichloroacetic acid in toluene at varying water concentration.
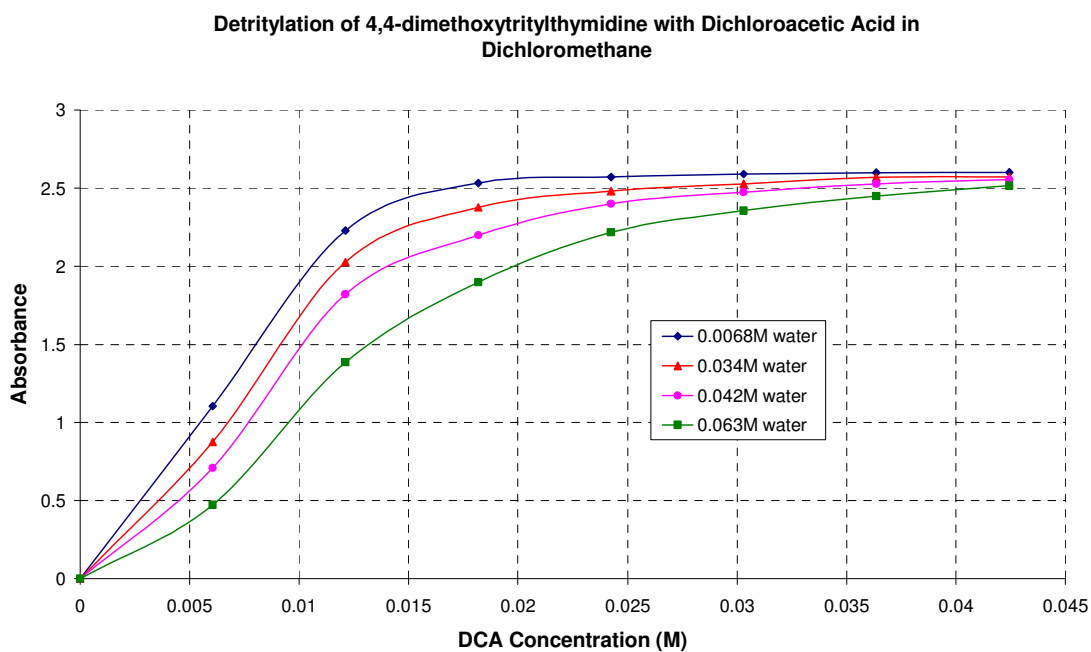
Figure 21: Detritylation of 3.6x10^{-5} M 4,4-dimethoxytritylthymidine with dichloroacetic acid in dichloromethane at varying water concentration.

58

It is clear from these plots that the presence of water in the reaction is having a significant effect on the detritylation equilibrium. It may be that the presence of water, and any other basic impurities within the system, are influencing the degree of acid dissociation, effectively mopping up the first aliquots of acid preventing carbocation formation. This will occur until enough acid is added to neutralise the water after which the acidity of the reaction medium will become sufficient to cause detritylation.

Another possibility is that water is reacting with the 4,4-dimethoxytrityl cation to form 4,4-dimethoxytrityl alcohol (scheme 18).

Scheme 18: Formation of 4,4-dimethoxytrityl alcohol from reaction of the 4,4-dimethoxytrityl carbocation and water.

At low concentrations of acid the cation undergoes hydration with any available water to form the 4,4-dimethoxytrityl alcohol, keeping the measured absorbance close to zero. This occurs until there is a sufficient concentration of acid present to force the equilibrium towards formation of the cation by removal of both the thymidine group of the ether and the hydroxyl group of the alcohol. As the initial concentration of water is increased a greater concentration of dichloroacetic acid is required to cause complete detritylation. A reaction scheme (scheme 19) can be written to show the two equilibria involved.

$$\text{DMTr-OT} + \text{HA} \underset{\longleftarrow}{\overset{K_{detrit}}{\rightleftharpoons}} \text{DMTr}^{\oplus} + \text{A}^{\ominus} + \text{TOH}$$

$$K_{hyd} + H_2O$$

$$\text{DMTr-OH} + \text{HA}$$

Scheme 19: Equilibria between 4,4-dimethoxytrityl ether, 4,4-dimethoxytrityl cation and 4,4-dimethoxytrityl alcohol.

To confirm that an equilibrium exists between the 4,4-dimethoxytrityl cation and alcohol, synthesised 4,4-dimethoxytrityl alcohol was titrated with dichloroacetic acid. The absorbance versus dichloroacetic acid concentration profiles (figure 22) are very similar to the profiles in figure 19 for trityl cation formation from 4,4-dimethoxytritylthymidine. Both sets of profiles show an increase in the concentration of acid required for complete carbocation formation and an increase in the profiles sigmoidal shape as water concentration is increased. There is also again a reduction in the extinction coefficient as the water content is increased.

Dehydration of 4,4-dimethoxytrityl Alcohol with Dichloroacetic Acid in Acetonitrile
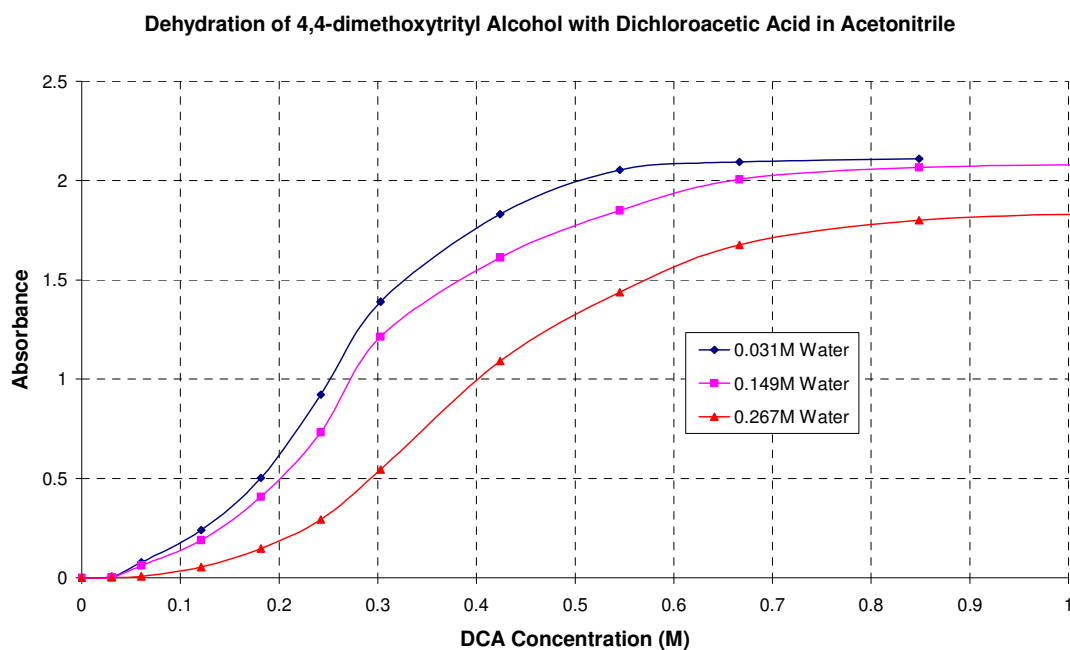
Figure 22: Ionisation of 3.6×10^{-5} M 4,4-dimethoxytrityl alcohol with dichloroacetic acid in acetonitrile.

3.1.3 Modelling of the detritylation equilibria

The effect of water on the shape of the absorbance versus acid concentration profiles can be modelled using the scheme below (scheme 20).

$$\text{DMTr-OT} + \text{HA} \xrightleftharpoons{K_{detrit}} \text{DMTr}^{\oplus} + \text{A}^{\ominus} + \text{TOH}$$

$$\left\updownarrow\, K_{hyd}\right.$$

$$+\ H_2O$$
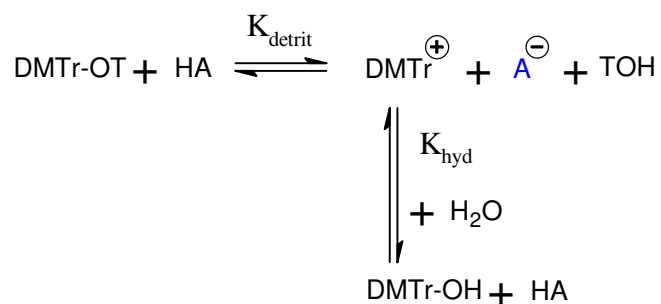
$$\text{DMTr-OH} + \text{HA}$$

Scheme 20: Equilibria between the 4,4-dimethoxytrityl ether, carbocation and alcohol.

The equilibrium constants K_{detrit} and K_{hyd} can be calculated from the equations,

$$K_{det\,rit} = \frac{\left[DMTr^+\right]\left[A^-\right][TOH]}{\left[DMTrOT\right]\left[HA\right]} \qquad \ldots\ldots\ldots.1$$

And,

$$K_{hyd} = \frac{\left[DMTrOH\right]\left[HA\right]}{\left[DMTr^+\right]\left[H_2O\right]\left[A^-\right]} \qquad \ldots\ldots\ldots.2$$

The mass balance for the reaction gives:

$$\left[DMTrOT\right]_o = \left[DMTrOT\right] + \left[DMTr^+\right] + \left[DMTrOH\right]$$

Rearranging equations 1 and 2 gives:

$$[DMTrOT] = \frac{[DMTr^+]\,[A^-]\,[TOH]}{K_{det\,rit}\,[HA]} \qquad\qquad ....3$$

And,

$$[DMTrOH] = \frac{K_{hyd}\,[DMTr^+]\,[H_2O]\,[A^-]}{[HA]} \qquad\qquad ....4$$

Substituting equations 3 and 4 into mass balance gives:

$$[DMTrOT]_o = \frac{[DMTr^+]\,[A^-]\,[TOH]}{K_{det\,rit}\,[HA]} + [DMTr^+] + \frac{K_{hyd}\,[DMTr^+]\,[H_2O]\,[A^-]}{[HA]}$$

$$[DMTrOT]_o = [DMTr^+]\left\{ 1 + \frac{[A^-]\,[TOH]}{K_{det\,rit}\,[HA]} + \frac{K_{hyd}\,[H_2O]\,[A^-]}{[HA]} \right\}$$

$$[DMTrOT]_o = [DMTr^+]\left\{ \frac{K_{det\,rit}\,[HA] + [A^-]\,[TOH] + K_{det\,rit}\,K_{hyd}\,[H_2O]\,[A^-]}{K_{det\,rit}\,[HA]} \right\}$$

The concentration of trityl carbocation can then be calculated from the following equation,

$$\boxed{[DMTr^+] = \frac{K_{det\,rit}\,[HA]}{K_{det\,rit}\,[HA] + [A^-]\,[TOH] + K_{det\,rit}\,K_{hyd}\,[H_2O]\,[A^-]}\,[DMTrOT]_o} \quad ....5$$

If [HA] is large, equation 5 becomes,

$$[DMTr^+] = \frac{K_{det\,rit}[HA]}{K_{det\,rit}[HA]}[DMTrOT]_o$$

$$\boxed{[DMTr^+] = [DMTrOT]_o}$$

Therefore, if there is a large concentration of acid then both equilibria will be over to the carbocation and there will be no dependence on either the acid or water concentration.

If [HA] is small, equation 5 becomes,

$$\boxed{[DMTr^+] = \frac{K_{det\,rit}[HA]}{[A^-][TOH] + K_{det\,rit}K_{hyd}[H_2O][A^-]}[DMTrOT]_o}$$

If the concentration of acid is small then the concentration of carbocation will depend on both equilibria. The cation is proportional to the acid concentration and inversely proportional to the formed alcohol, anion and any water present in the system. But again for a fixed water concentration the concentration of DMTr$^+$ should be linear with acid concentration.

If [H$_2$O] is large, equation 5 becomes,

$$[DMTr^+] = \frac{K_{det\,rit}[HA]}{K_{det\,rit}K_{hyd}[H_2O][A^-]}[DMTrOT]_o$$

$$\boxed{[DMTr^+] = \frac{[HA]}{K_{hyd}[H_2O][A^-]}[DMTrOT]_o}$$

If there is a large concentration of water in the system only K_{hyd} will be important and the concentration of cation will be inversely proportional to the concentration of water.

If [H$_2$O] is small, equation 5 becomes,

$$\left[DMTr^+\right] = \frac{K_{det\,rit}\left[HA\right]}{K_{det\,rit}\left[HA\right] + \left[A^-\right]\left[TOH\right]}\left[DMTrOT\right]_o$$

If there is a low concentration of water in the system then only the equilibrium for the detritylation reaction will be important.

The presence of water in the system acting as a nucleophile towards the trityl carbocation, still does not explain the sigmoidal shape of the absorbance versus acid concentration profiles.

3.1.4   Effect of excess alcohol on the detritylation reaction

Detritylation of 4,4-dimethoxytritylthymidine with dichloroacetic acid was performed in the presence of propan-1-ol to confirm that an equilibrium exists and the product carbocation could be converted back to an ether. The thymidine could not be used due to poor solubility.

Absorbance versus acid concentration profiles (figure 23) of 4,4-dimethoxytritylthymidine detritylation with dichloroacetic acid and varying initial concentrations of propan-1-ol are sigmoidal in shape. The concentration of acid required for complete detritylation is increased with increasing concentrations of propan-1-ol. These profiles are similar to those in figure 19 (page 57) for the formation of the trityl cation with dichloroacetic acid in the presence of varying concentrations of water. Both are sigmoidal and show an increase in the concentration of acid required for complete detritylation on increasing either the water or alcohol concentration.
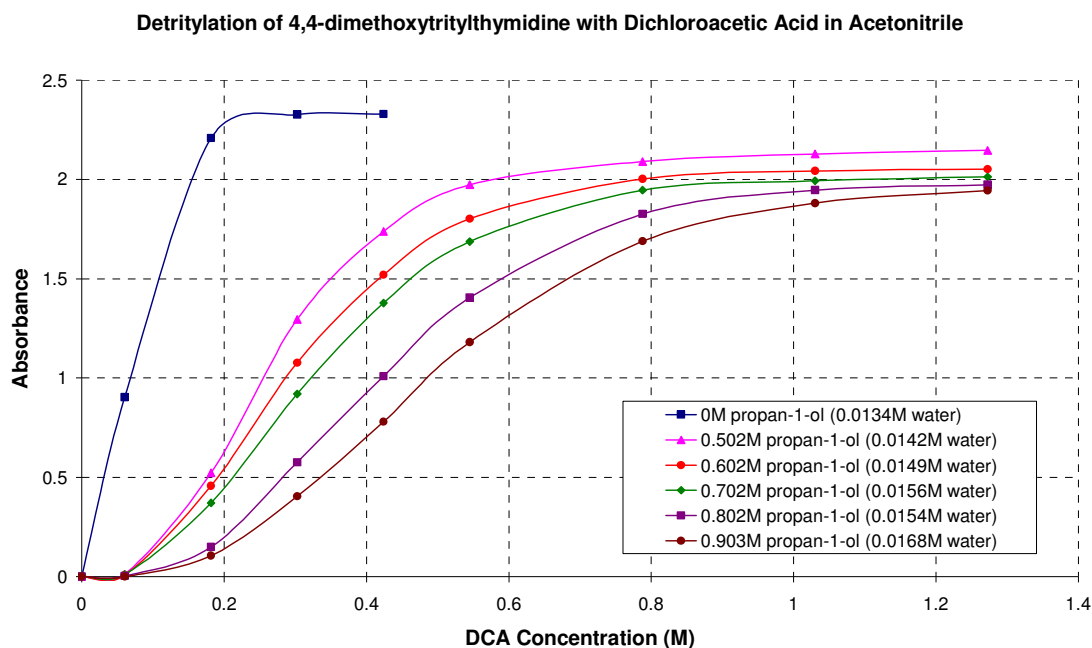
Figure 23: Detritylation of 3.6×10^{-5} M 4,4-dimethoxytritylthymidine with dichloroacetic acid in acetonitrile at varying propan-1-ol concentrations.

3.1.5   Calculation of K_{dehyd} and K_{detrit}

The equilibrium constant K_{dehyd} may be calculated from the absorbance versus acid concentration profile (figure 19, page 57) for detritylation of the 4,4-dimethoxytrityl alcohol in the presence of varying concentrations of water. The equilibrium for the reaction is shown below (scheme 21).

$$\text{DMTr-OH} \; + \; \text{HA} \; \underset{}{\overset{K_{dehyd}}{\rightleftharpoons}} \; \text{DMTr}^{+} \; + \; \text{A}^{-} \; + \; H_2O$$
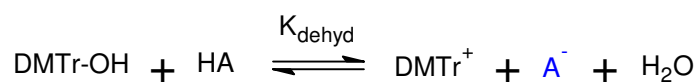
Scheme 21: 4,4-dimethoxytrityl alcohol dehydration equilibrium.

The equilibrium constant can be calculated from the equation,

$$K_{dehyd} = \frac{\left[DMTr^+\right]\left[A^-\right]\left[H_2O\right]}{\left[DMTr-OH\right]\left[HA\right]} \qquad \qquad ....6$$

65

The charges must balance, therefore equation 1 becomes,

$$K_{dehyd} = \frac{[DMTr^+]^2[H_2O]}{[DMTr-OH][HA]} \qquad \ldots\ldots\ldots.7$$

The total concentration of DMTr-OT used was 3.6×10^{-5} mol dm^{-3}; therefore at complete detritylation there will be 3.6×10^{-5} mol dm^{-3} of DMTr$^+$. If water is then added to reduce the concentration of DMTr$^+$ by half then there will be equal concentrations of DMTr$^+$ and DMTr-OH in the system. Therefore, equation 7 will simplify to,

$$K_{dehyd} = \frac{[DMTr^+]_{50\%}[H_2O]_{50\%}}{[HA]_{50\%}} \qquad \ldots\ldots\ldots.8$$

Rearranging for [HA] gives,

$$[HA]_{50\%} = \frac{[DMTr^+]_{50\%}[H_2O]_{50\%}}{K_{dehyd}} \qquad \ldots\ldots\ldots.9$$

Using the data from figure 19 (page 57) a plot of $[HA]_{50\%}$ versus $[H_2O]_{50\%}$ should give a straight line with a slope equal to $[DMTr^+]_{50\%}/K_{dehyd}$ (figure 24). This is only true of the data where there is enough acid to cause complete detritylation at low water concentrations.
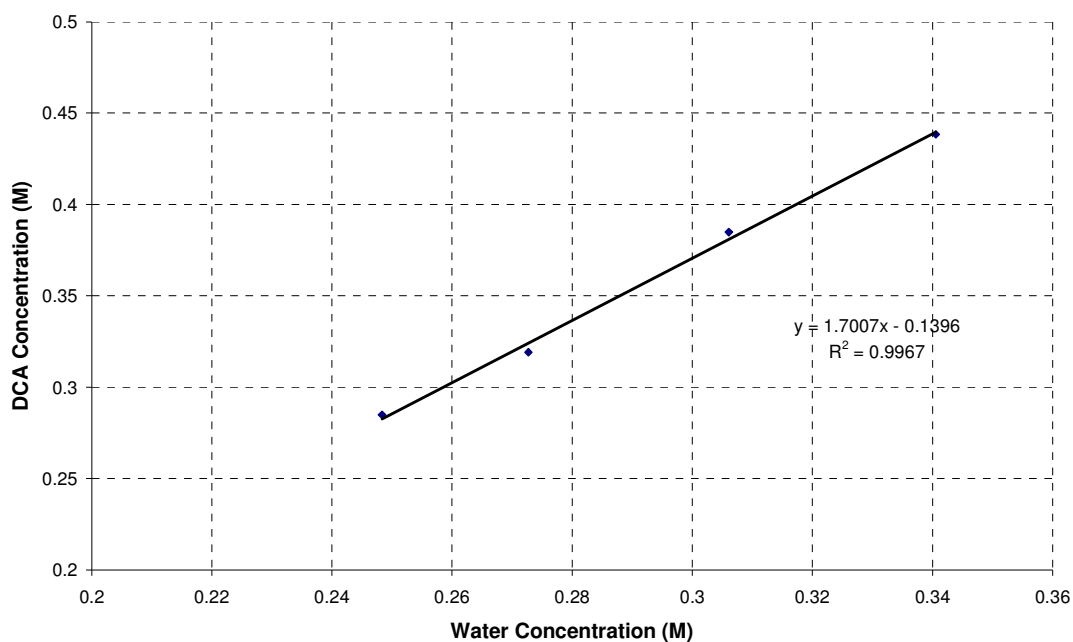
Figure 24: Dichloroacetic acid concentration versus water concentration.

The slope of this plot is 1.70, therefore K_{dehyd} is equal to $[DMTr^+]_{50\%}$/slope, where $[DMTr^+]_{50\%}$ is a constant at 1.80×10^{-5} mol dm^{-3}. Therefore K_{dehyd} is equal to 1.06×10^{-5} mol dm^{-3}.

A similar method has been used to calculate K_{detrit} by using the data gained from the addition of propan-1-ol prior to the acid titration (figure 23, page 65). The equilibrium can be written as in scheme 22.
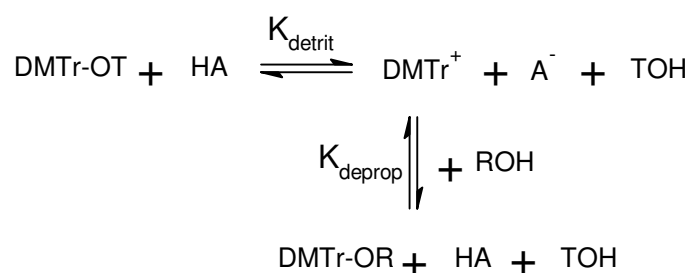
Scheme 22: 4,4-dimethoxytritylthymidine detritylation and ether formation equilibria.

Where ROH represents the propan-1-ol, the equilibrium constant, $K_{deprop,}$ (which is assumed to be comparable to the equilibrium for detritylation, K_{detrit}) can be calculated from,

$$K_{deprop} = \frac{[DMTr^+][A^-][ROH]}{[DMTr-OT][HA]} \qquad ....10$$

Using the same assumptions as for the calculation of K_{dehyd}, equation 10 can be simplified as below at half the carbocation concentration.

$$K_{deprop} = \frac{[DMTr^+]_{50\%}[ROH]_{50\%}}{[HA]_{50\%}} \qquad ....11$$

And rearranging 6 gives,

$$[HA]_{50\%} = \frac{[DMTr^+]_{50\%}[ROH]_{50\%}}{K_{deprop}} \qquad ....12$$

Therefore, a plot of $[HA]_{50\%}$ versus $[TOH]_{50\%}$, using the data from figure 23 (page 65) should give a straight line with a slope equal to $[DMTr^+]_{50\%}/K_{deprop}$ (figure 25). Again this is only true of the data at higher acid concentrations.
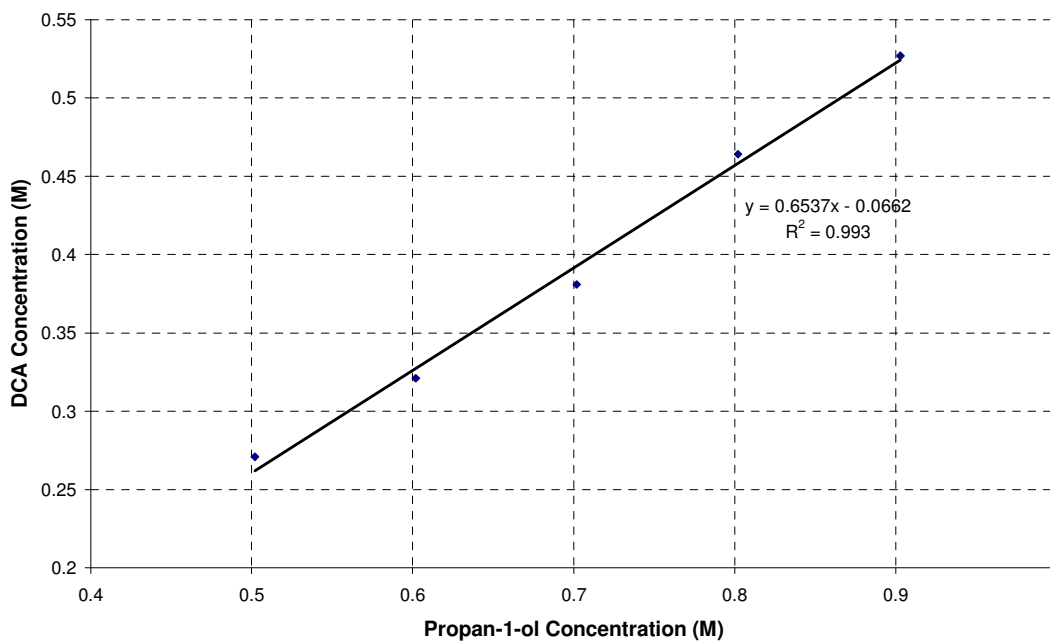
Figure 25: Dichloroacetic acid concentration versus propan-1-ol concentration.

The slope of this plot equals 0.65; therefore K_{deprop} is equal to 2.75×10^{-5} mol dm^{-3}. Overall the equilibrium and constants are shown in scheme 23.
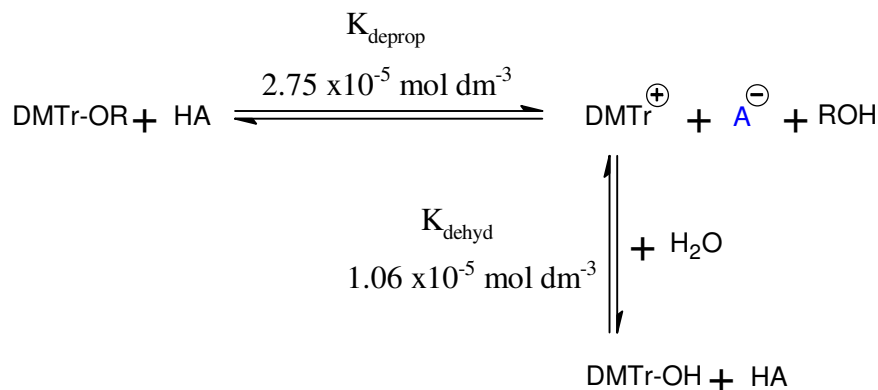
Scheme 23: Equilibria between the 4,4-dimethoxytrityl ether, alcohol and cation.

The equilibrium between the ether and the alcohol (K_{trans}) will be equal to the quotient of the two equilibrium constants K_{deprop} and K_{dehyd}, which equals 2.59 (scheme 24).
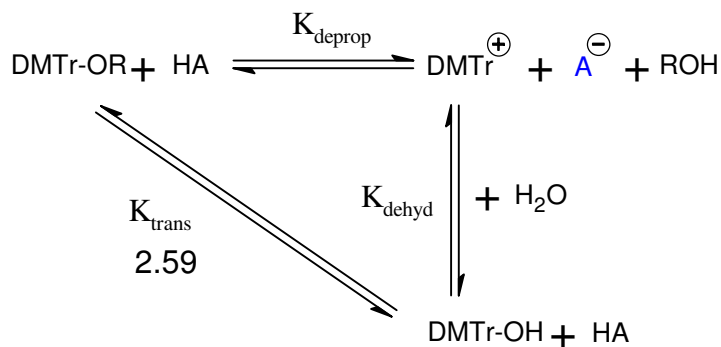
Scheme 24: Equilibria between the 4,4-dimethoxytrityl ether, alcohol and cation.

The equilibrium constant for K_{trans} indicates that the 4,4-dimethoxytrityl alcohol is marginally more thermodynamically stable in acetonitrile than the ether. As well as the stabilities of the 4,4-dimethoxytrityl ether and alcohol, there will also be a thermodynamic contribution from the propan-1-ol, anion and water. The magnitude of K_{trans} can be confirmed by comparison of Figures 19 and 23 where, for example, to reduce the amount of 4,4-dimethoxytrityl carbocation to an absorbance of 0.5 at a dissociated acid concentration of 6×10^{-9} M, a concentration of approximately 0.27 M water or a concentration of approximately 0.72 M propan-1-ol is required. The ratio between the concentration of water and propan-1-ol required for this reduction in carbocation concentration is equal 2.67 which is comparable to the equilibrium constant K_{trans}.

3.2   Detritylation with *para*-toluenesulphonic acid: equilibrium studies

For a comparison with the equilibrium studies of detritylation with dichloroacetic acid similar experiments were performed with *para*-toluenesulphonic acid. *Para*-toluenesulphonic acid is a much stronger acid than dichloroacetic acid, with pK_as of 8.6[120] and 15.8[119] respectively in acetonitrile. The detritylation of 4,4-dimethoxytrityl thymidine with PTSA, yields UV absorbance versus acid concentration profiles (figure 26) which are sigmoidal in shape, comparable to that with dichloroacetic acid.

Detritylation of 4,4-dimethoxytritylthymidne with para-toluenesulphonic Acid in Acetonitrile
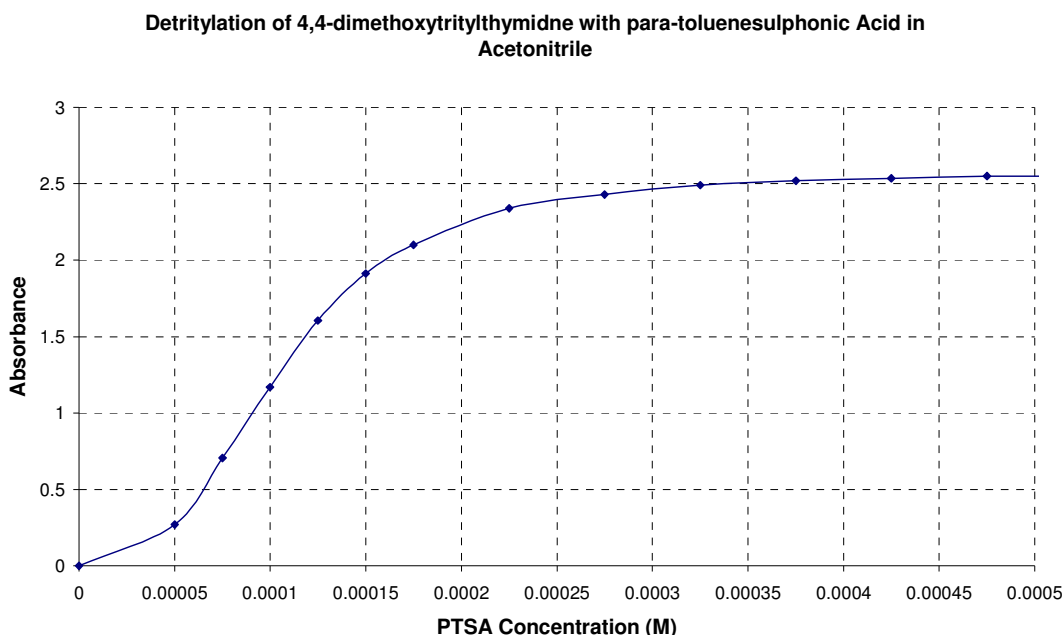
Figure 26: Detritylation of 3.6×10^{-5} M 4,4-dimethoxytrityl thymidine in acetonitrile with *para*-toluenesulphonic acid.

Figure 27 shows the UV absorbance versus acid concentration profiles for the addition of water to the 4,4-dimethoxytrityl thymidine prior to PTSA titration. In comparison with the profiles produced under similar conditions with dichloroacetic acid (figure 19, page 57), the end point of the titration with PTSA does not reach the same concentration of carbocation with increasing water concentration. This indicates that the maximum concentration of carbocation that can be produced with PTSA is reduced as the water concentration is increased.
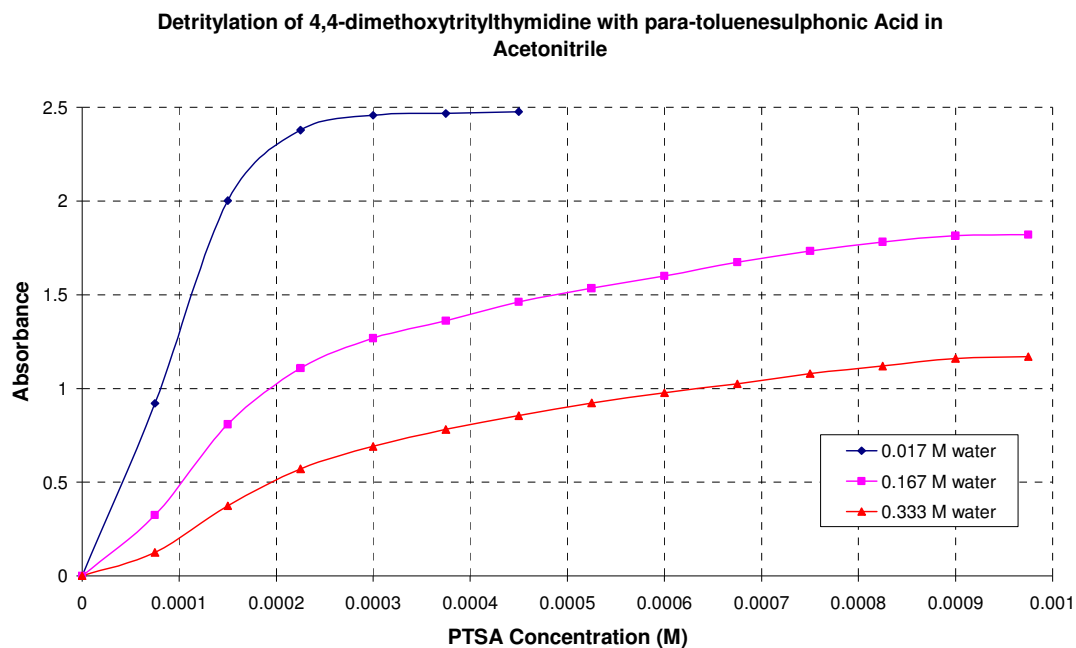
Figure 27: Detritylation of 3.6×10^{-5} M 4,4-dimethoxytrityl thymidine with *para*-toluenesulphonic acid at varying water concentrations.

To confirm that the carbocation formed with PTSA is in equilibrium with the starting ether and alcohol, samples of detritylated 4,4-dimethoxytrityl thymidine were titrated with water, propan-1-ol and butan-1-ol (figure 28). As expected, in each case there was a decrease in carbocation concentration until sufficient water or alcohol had been added to cause its complete carbocation removal. The concentration of water needed to completely remove the carbocation is approximately five times less than the concentration of alcohol required.
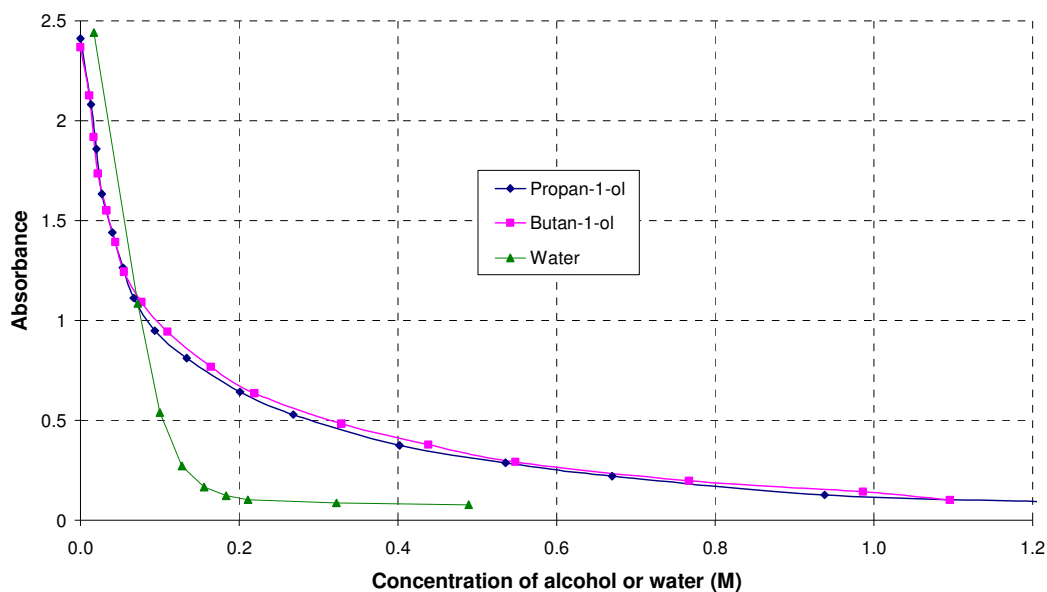
Figure 28: Titration of water, propan-1-ol and butan-1-ol to detritylated 4,4-dimethoxythymidine (3.6×10^{-5} M) with PTSA (3×10^{-4} M) in acetonitrile.

3.3   NMR experiments

The UV experiments in figure 27 have shown that the detritylation reaction with *para*-toluenesulphonic acid does not reach a consistent end point with varying initial concentrations of water. As a consequence, calculation of the equilibrium constants K_{deprop} and K_{dehyd} could not be determined by the same method as with dichloroacetic acid. Therefore, another method of calculating the equilibria was attempted, by determining the ratios of each 4,4-dimethoxytrityl species present at equilibrium by integration of their ^{13}C NMR signals. This method could not be undertaken with dichloroacetic acid, as the vast excess of dichloroacetic acid required to cause a detectable amount of reaction for NMR measurement, would be above dichloroacetic it's solubility in acetonitrile. Also, the dichloroacetic acid signals themselves would swamp others present in the sample. ^{13}C NMR was chosen as there is a notable difference in the chemical shift of the central carbon of the 4,4-dimethoxytrityl group when in its cationic, alcohol and ether form.

72

To determine the chemical shift position of the central carbon, NMR correlation spectroscopy: COSY, HSQC and HMBC experiments were used. Determining the chemical shift of the ether and alcohols carbon (table 2) was relatively straight forward. Determining the chemical shift of the carbocations carbon proved problematic due to overlap of the 4,4-dimethoxytrityls NMR signals with those of PTSA. To overcome this problem methylsulphonic acid was used as an alternative to PTSA, this allowed the chemical shift of the central trityl carbon to be established (table 2).
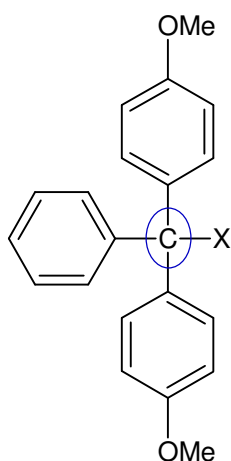
4,4-dimethoxytrityl species	δ of central carbon in deuterated acetonitrile (ppm)
Thymidine	87.3
Alcohol	81.6
Cation	197.3

Table 2: ^{13}C NMR chemical shifts of the central carbon of 4,4-dimethoxytrityl in its ether, alcohol or carbocation adduct.

Unfortunately, due to the large concentration of 4,4-dimethoxytritylthymidine needed to give good signal resolution, it was impossible to achieve a high enough concentration of propan-1-ol or water into solution to observe the reverse reaction, therefore equilibrium constants could not be calculated.

3.4   4,4-dimethoxytrityl detritylation kinetics

In addition to equilibrium studies, a kinetic study of the detritylation reaction was undertaken. The three solvents toluene, acetonitrile and dichloromethane were studied to see what effect their differing polarities had on the reaction kinetics. Stopped-flow UV spectroscopy was used to measure the very fast detritylation reaction. Pseudo-first order rate constants (k_{obs}) were calculated from the generated absorbance versus time data for the production of the 4,4-dimethoxytrityl carbocation, at constant water concentrations in each solvent. The dependence of k_{obs} on the total dichloroacetic acid concentration for each solvent (figure 29) gave a good linear correlation. The second order rate constants calculated from the k_{obs} versus time data in figure 29 are summarised in table 3.
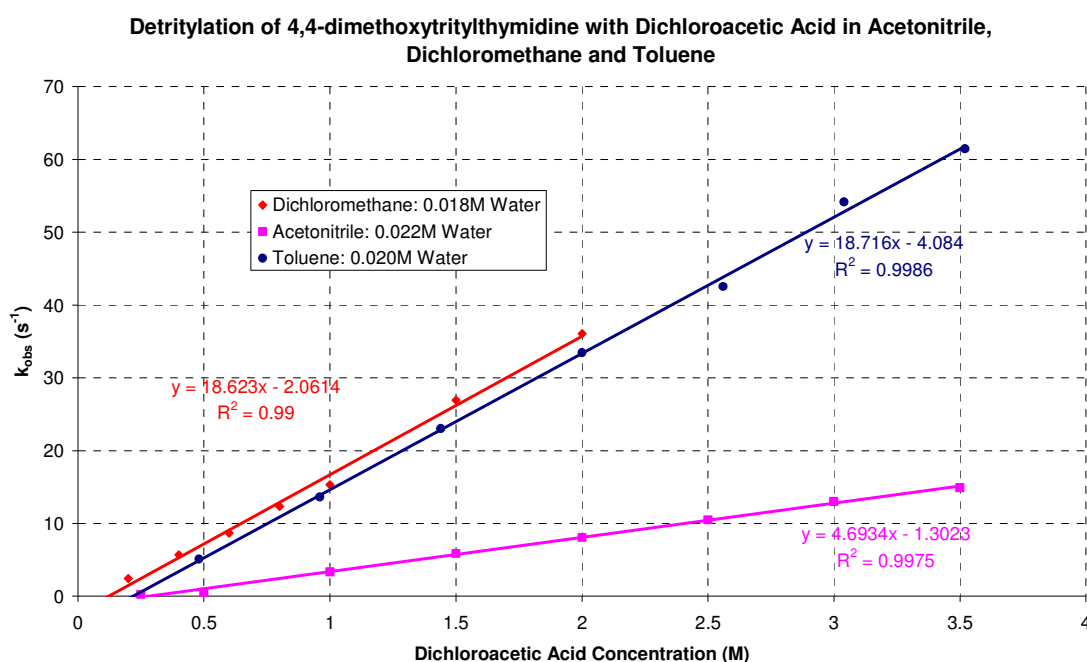
Figure 29: Detritylation of 3.6×10^{-5} M 4,4-dimethoxytritylthymidine at 30°C; the dependence of k_{obs} on total dichloroacetic acid concentration

Solvent	k (M^{-1} s^{-1})	Dielectic constant
Toluene	18.7	2.4
Dichloromethane	18.6	4.8
Acetonitrile	4.7	37.5

Table 3: Second order rate constants for the detritylation of 3.6x10^{-5} M 4,4-dimethoxytritylthymidine with dichloroacetic acid at 30°C.

The rate of reaction in dichloromethane and toluene is almost equal, with second order rate constants of 18.6 and 18.7 M^{-1} s^{-1} respectively. The rate of reaction in acetonitrile is only slightly slower with a second order rate constant of 4.7 M^{-1} s^{-1}, although it would seem intuitive that the greatest rate should be observed in the more polar acetonitrile due to charge stabilisation. However, similarly unexpected results were observed with the equilibrium studies described in the previous section.

Using the equilibrium data from figure 17 (page 53), the concentration of acid required to cause 50% detritylation in each solvent is summarised in table 4.

Solvent	Concentration of dichloroacetic acid required to cause 50% detritylation (M)
Dichloromethane	0.007
Acetonitrile	0.125
Toluene	0.230

Table 4: Concentration of acid required to cause 50% detritylation of 3.6x10^{-5} M 4,4-dimethoxytritylthymidine.

In comparison to the 4 fold reduction in rate observed from performing the reaction in acetonitrile instead of in dichloromethane, the difference in equilibrium position is much larger; 18 times more acid is required to cause 50% detritylation in acetonitrile than in dichloromethane. Even greater differences between kinetics and equilibria are observed with dichloromethane and toluene. The rates of detritylation in dichloromethane and toluene are almost equal but 33 times more acid is needed to cause 50% detritylation in toluene than in dichloromethane.

Typically, carbocation formation should be more favourable in polar solvent due to increased stabilisation of the charged species. It is clear from these equilibrium and kinetic studies that solvent polarity is not having the expected effects on either the rate of reaction or the position of the reactions equilibrium. The 4,4-dimethoxytrityl carbocation is a very stable species due to extensive delocalisation, and it maybe that stabilisation by either solvent or counter-ion has little effect with any changes in the carbocations energy being negligible. In this case, the differences in equilibrium

position and kinetics are likely due to the solvents influence on the other components of the reaction and not on the 4,4-dimethoxytrityl carbocation. Given the large number of possibilities it is difficult to speculate on the major cause of the observed differences.

3.4.1   Effect of water on detritylation kinetics

As discussed in the previous section, in its simplest form, the production of trityl carbocation can be described by two equilibria (scheme 25): K_{detrit} and K_{hyd}. The position of these equilibria is dependent on the concentration of water in the system, with a large excess predominantly forming the trityl alcohol.
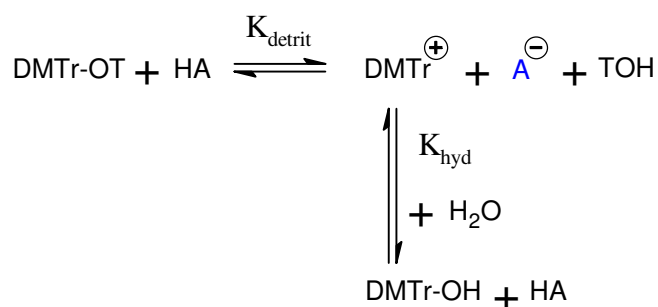
Scheme 25: Equilibria between the trityl ether, carbocation and alcohol.

The effect of changing the concentration of water present during kinetic measurement was studied in acetonitrile. Figure 30 shows the dependence of the observed rate constant on acid concentration at a number of initial water concentrations. These show a good linear correlation with a positive intercept on the x-axis. The second order rate constant for each water concentration is summarised in table 5.

Concentration of water (M)	k ($M^{-1} s^{-1}$)
0.022	4.7
0.078	3.7
0.110	2.2
0.130	1.1

Table 5: Second order rate constants for the detritylation of 3.6x10^{-5} M 4,4-dimethoxytritylthymidine with dichloroacetic acid in acetonitrile at varying concentrations of water at 30°C.
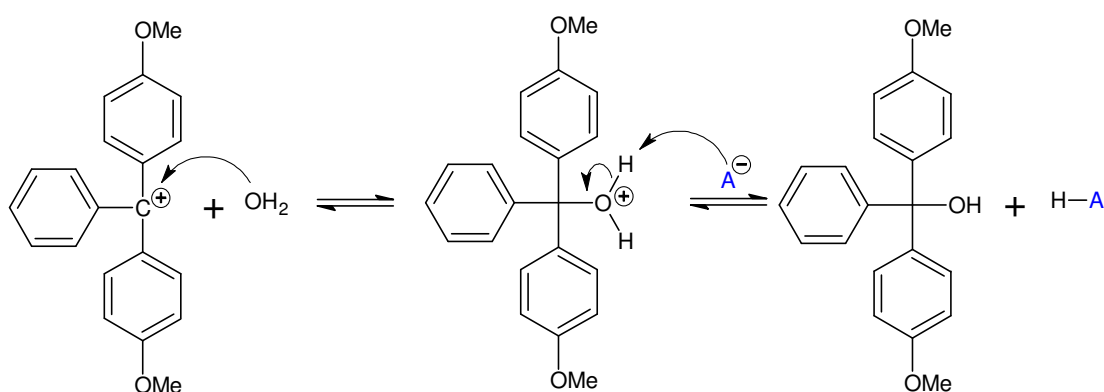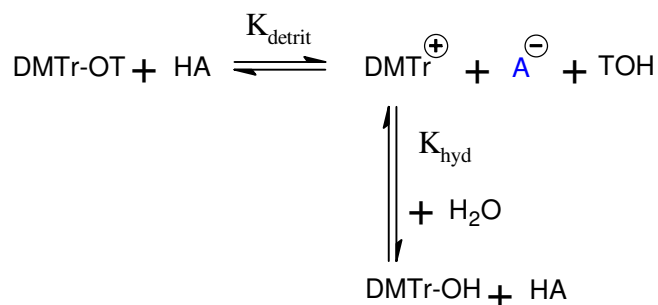
Detritylation of 4,4-dimethoxytritylthymidine with Dichloroacetic Acid in Acetonitrile
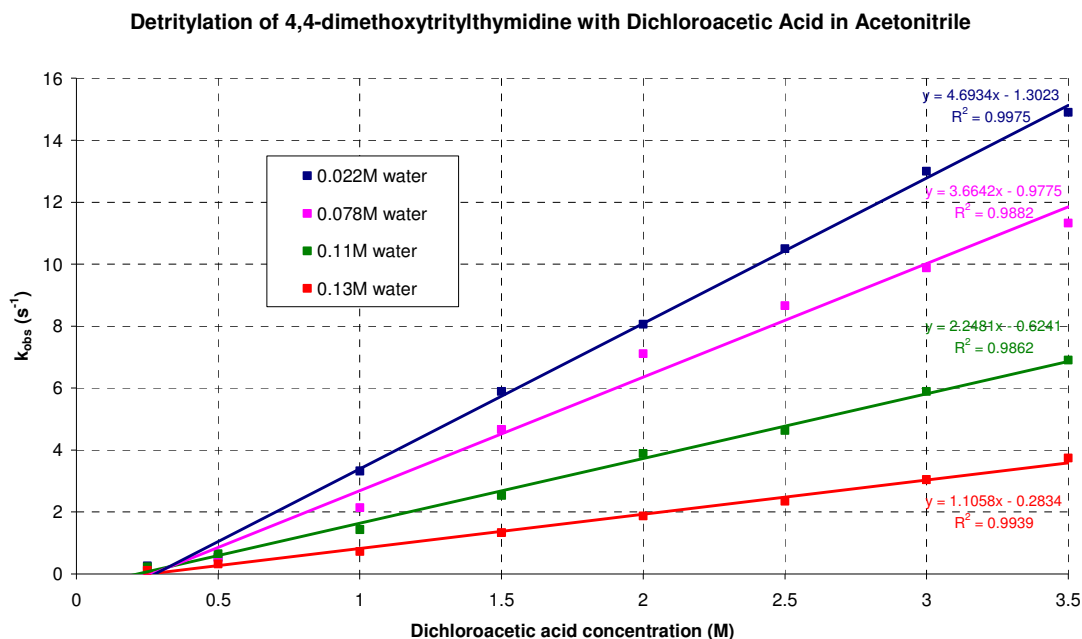
Figure 30: Detritylation of 3.6×10^{-5} M 4,4-dimethoxytritylthymidine at 30°C in acetonitrile; the dependence of k_{obs} on total dichloroacetic acid concentration at varying water concentrations.

Table 5 and figure 30 show that the rate of 4,4-dimethoxytrityl carbocation formation decreases with increasing water concentration, this is further illustrated in figure 31 which is a plot of second order rate constant as a function of water concentration.

Change in Second Order Rate Constant with Water Concentration
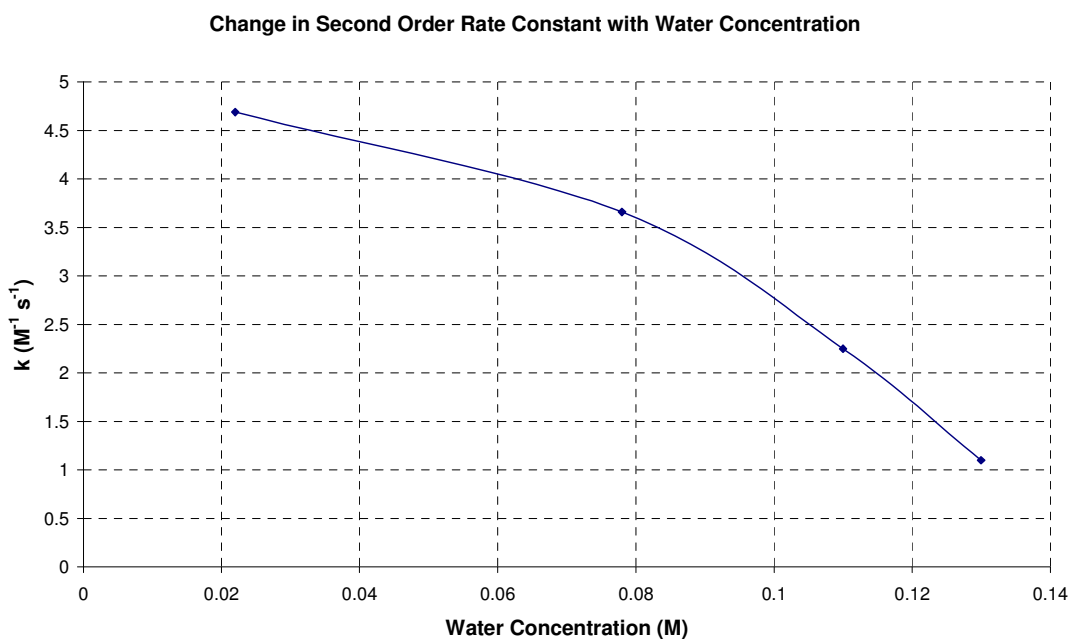
Figure 31: Effect of water on the second order rate constant for detritylation of 3.6×10^{-5} M 4,4-dimethoxytritylthymidine in acetonitrile at 30°C.

77

3.5 Effect of temperature upon the detritylation reaction

The observed equilibrium and kinetic data has shown that the effect of solvent does not follow the expected enhancement with increased polarity due to stabilisation of charged species. Activation energies should also show a difference with changing polarities in systems where there is a change in charge.

Figure 32 shows a plot of the natural log of the second order rate constant (lnk) as a function of temperature for acetonitrile, dichloromethane and toluene.
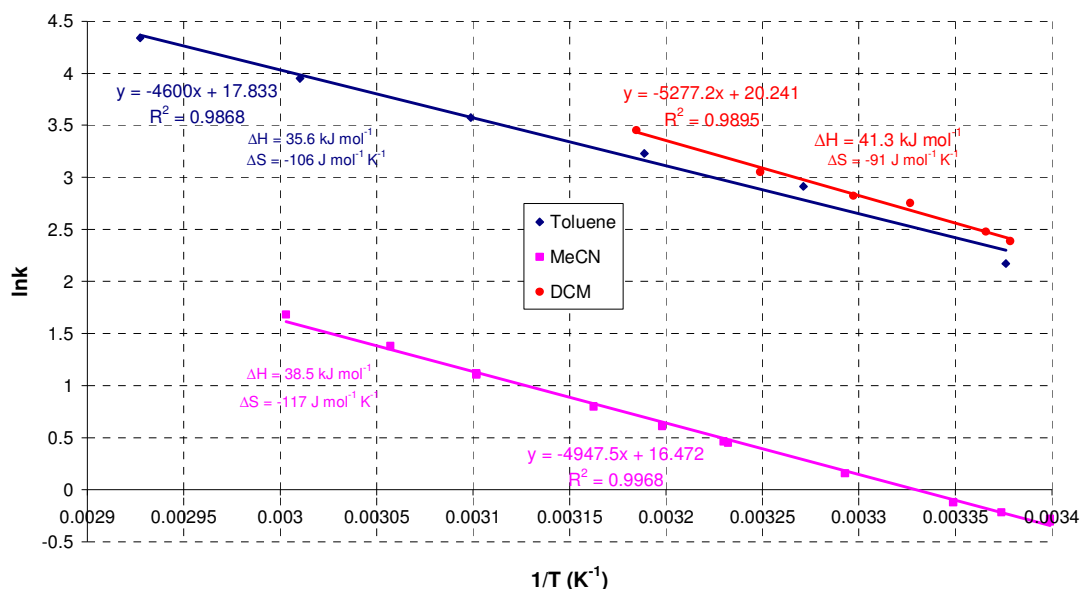
Figure 32: Eyring type plot for detritylation of 3.6×10^{-5} M 4,4-dimethoxytrityl thymidine with 1 M dichloroacetic acid in acetonitrile, toluene and dichloromethane with dichloroacetic acid.

Good linear correlations have been obtained in figure 32, from which enthalpies and entropies of activation have been determined using the Eyring equation (shown below) for each of the solvents, the results of which are summarised in table 6.

$$\ln \frac{k}{T} = \frac{-\Delta H}{R} \cdot \frac{1}{T} + \ln \frac{k_b}{h} + \frac{\Delta S}{R}$$

Solvent	$\Delta S^{\neq}$ (J mol^{-1} K^{-1})	$\Delta H^{\neq}$ (KJ mol^{-1})
Acetonitrile	-117	38.5
Dichloromethane	-106	35.6
Toluene	-91	41.3

Table 6: Entropic and enthalpic data for the detrylation of 4,4-dimethoxytritylthymidine with dichloroacetic acid.

Given the large differences in the polarity of the solvents and their H-bonding ability, the activation energy parameters are remarkably similar. Normally reactions showing changes in charge on going to the transition state are susceptible to solvent effects and, for example, entropies of activation vary enormously. These observations confirm the unusual nature of the 4,4-dimethoxytrityl carbocation and that solvent effects have little effect on its formation.

3.6 Solubility of 4,4-dimethoxytritylthymidine

The effect of solvents on the rates of reactions is often dominated by considering only transition state effects. However, the free energy of activation is the difference between the free energies of the transition state and reactant ground state. Many reactions involving polar transition states developed from neutral reactants have their rates decreased by less polar solvents. Sometimes this is due to increasing the stability of the reactants in the less polar solvent rather than decreasing the stability of the transition state. It is therefore appropriate to investigate the solubilities of the reactants in the different solvents to investigate their relative stabilities.

The solubility of 4,4-dimethoxytritylthymidine has been determined in acetonitrile, toluene and dichloromethane at ambient temperature, the results of which are summarised in table 7.

Solvent	DMTr-OT solubility (M)	Water concentration (M)	Solvent dielectric constant
Acetonitrile	0.015	0.041	37.5
Dichloromethane	0.055	0.018	4.8
Toluene	0.049	0.023	2.4

Table 7: Solubility of 4,4-dimethoxytritylthymidine in acetonitrile, dichloromethane and toluene at ambient temperature.

The solubility of 4,4-dimethoxytritylthymidine in acetonitrile is lower than that in dichloromethane and toluene. However, the concentration of water in acetonitrile is twice that of the other solvents which may have an effect on the measured solubility. A plot of 4,4-dimethoxytritylthymidine solubility in acetonitrile against the concentration of water present in solution (figure 33) shows an increase in solubility with increasing water concentration. Presumably the solubility of 4,4-dimethoxytritylthymidine in acetonitrile at the same, lower, concentration of water as determined for dichloromethane and toluene would be less than the 0.015 M shown in table 7, but not significantly.

Solubility of 4,4-dimethoxytritylthymidine in Acetonitrile as a Function of Water Concentration

$y = 0.0349x + 0.0137$
$R^2 = 0.9952$
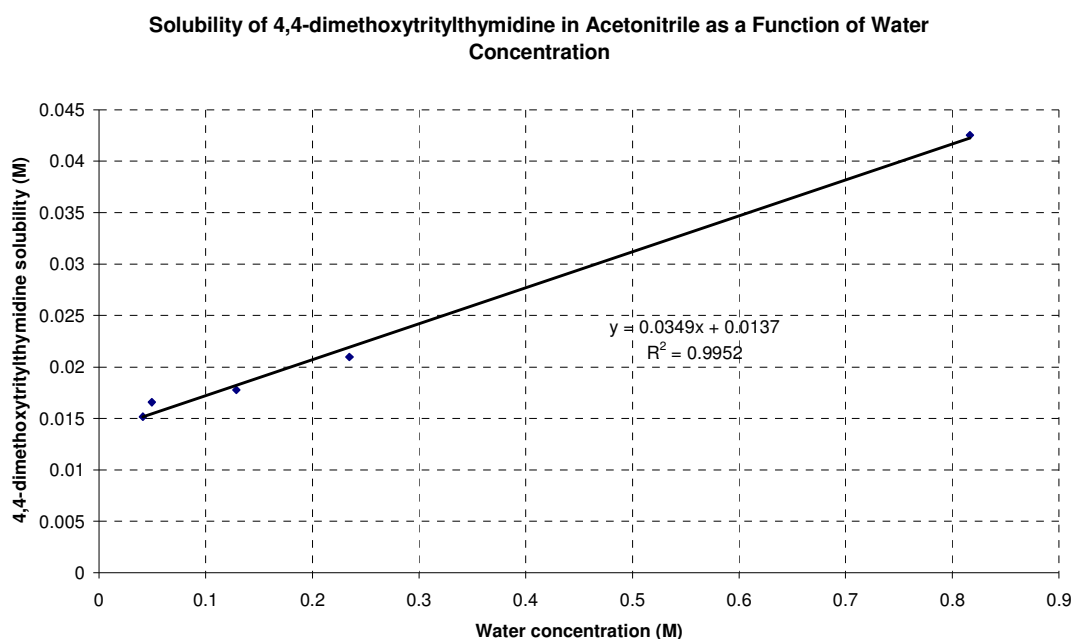
Figure 33: 4,4-dimethoxytritylthymidine solubility in acetonitrile as a function of water concentration at ambient temperature.

It seems likely therefore that the relative stabilities of the 4,4-dimethoxytrityl ether in the different solvents does not make a large contribution to the relative rates of 4,4-dimethoxytrityl carbocation formation

80

3.7   Mechanism of detritylation

In its simplest form, the mechanism of trityl carbocation production (scheme 26) consists of initial detritylation of the trityl ether to form the carbocation which in the presence of water can be consumed to form the trityl alcohol. Both of these processes are in equilibrium.

$$DMTr\text{-}OT + HA \rightleftharpoons DMTr^{\oplus} + A^{\ominus} + TOH \xrightarrow{+ H_2O} DMTr\text{-}OH + HA$$
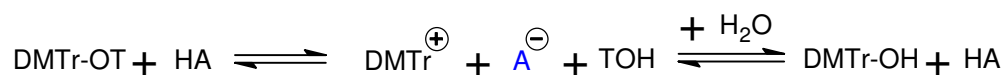
Scheme 26: Reaction between the trityl ether, carbocation and alcohol.

Maskill *et al*, studied the formation of 4,4-dimethoxytrityl carbocation from 4,4-dimethoxytrityl alcohol in aqueous perchloric and nitric acid solutions and the deamination of trityl species by hydronium ions.[73-76] In these studies a step-wise mechanism is reported with protonation of the oxygen occurring prior to carbon-oxygen and carbon-nitrogen bond cleavage.

The reactions studied by Maskill are similar to the ones studied here and incorporation of his step-wise mechanism into the detritylation reaction gives the mechanism shown in scheme 27. For cleavage of the carbon-oxygen bond in the 4,4-dimethoxytrityl ether (II) to occur, initial protonation of the oxygen by the acidic proton must take place, (I). For formation of the 4,4-dimethoxytrityl alcohol, water must first act as a nucleophile upon the carbocation to form a protonated alcohol (III) which then undergoes loss of the acidic proton to form the alcohol (IV).

$$\text{(I)} \quad \text{DMTr-OT} + \text{HA} \underset{k_{-1}}{\overset{k_1}{\rightleftharpoons}} \overset{\oplus}{\underset{|}{\text{DMTr-OT}}} + \overset{\ominus}{\text{A}}$$
$$\overset{}{\underset{\text{H}}{}}$$

$$\text{(II)} \quad \overset{\oplus}{\underset{|}{\text{DMTr-OT}}} \underset{k_{-2}}{\overset{k_2}{\rightleftharpoons}} \overset{\oplus}{\text{DMTr}} + \text{TOH}$$
$$\underset{\text{H}}{}$$

$$\text{(III)} \quad \overset{\oplus}{\text{DMTr}} + \text{H}_2\text{O} \underset{k_{-3}}{\overset{k_3}{\rightleftharpoons}} \overset{\oplus}{\text{DMTrOH}_2}$$

$$\text{(IV)} \quad \overset{\oplus}{\text{DMTrOH}_2} \underset{k_{-4}}{\overset{k_4}{\rightleftharpoons}} \text{DMTrOH} + \overset{\oplus}{\text{H}}$$
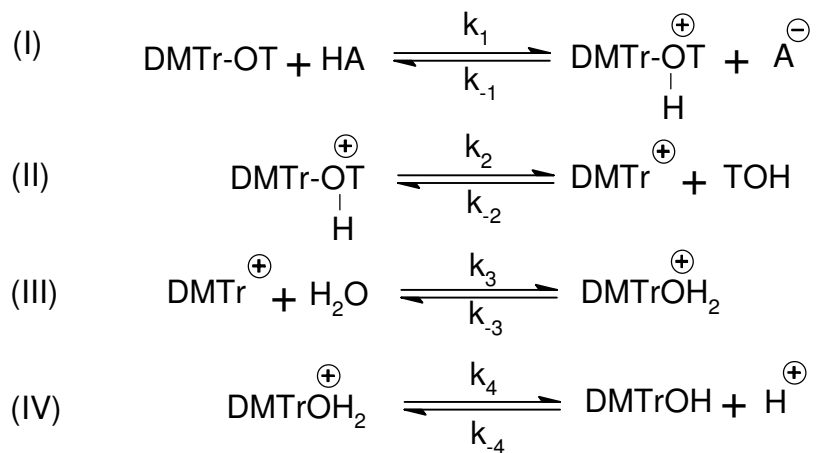
Scheme 27: Possible mechanism of 4,4-dimethoxytrityl carbocation formation.

Maskill also includes elementary steps for changes in solvation of the protonated alcohol and interaction of the acid anion with carbocation species: this was added to account for observed salt effects.

Scheme 28 is an expansion of scheme 27, with the inclusion of solvation changes for the protonated ether (II) and protonated alcohol (V), and the formation of ion pairs between the acid anion and the protonated ether (VII), protonated alcohol (IX) and the 4,4-dimethoxytrityl carbocation (VIII). There is also the possibility of a further step showing formation of a covalently linked 4,4-dimethoxytrityl and acid anion molecule, but, as the anion is non-nucleophilic, no such species was ever detected in the NMR studies performed here.

(I) $\quad$ DMTr-OT $+$ HA $\underset{k_{-1}}{\overset{k_1}{\rightleftharpoons}}$ DMTr-$\overset{\oplus}{\underset{H}{O}}$T $+$ $\overset{\ominus}{A}$

(II) $\quad$ DMTr-$\overset{\oplus}{\underset{H}{O}}$T $\underset{k_{-2}}{\overset{k_2}{\rightleftharpoons}}$ $\overset{\oplus}{DMTr} . \underset{H}{O}$T

(III) $\quad$ $\overset{\oplus}{DMTr} . \underset{H}{O}$T $\underset{k_{-3}}{\overset{k_3}{\rightleftharpoons}}$ $\overset{\oplus}{DMTr}$ $+$ TOH

(IV) $\quad$ $\overset{\oplus}{DMTr}$ $+$ H_2O $\underset{k_{-4}}{\overset{k_4}{\rightleftharpoons}}$ $\overset{\oplus}{DMTr} . OH_2$

(V) $\quad$ $\overset{\oplus}{DMTr} . OH_2$ $\underset{k_{-5}}{\overset{k_5}{\rightleftharpoons}}$ $\overset{\oplus}{DMTrOH_2}$

(VI) $\quad$ $\overset{\oplus}{DMTrOH_2}$ $\underset{k_{-6}}{\overset{k_6}{\rightleftharpoons}}$ DMTrOH $+$ $\overset{\oplus}{H}$

(VII) $\quad$ $\overset{\oplus}{DMTr} . \underset{H}{O}$T $+$ $\overset{\ominus}{X}$ $\underset{k_{-7}}{\overset{k_7}{\rightleftharpoons}}$ $\overset{\oplus}{DMTr} \| \overset{\ominus}{X}$ $+$ TOH

(VIII) $\quad$ $\overset{\oplus}{DMTr}$ $+$ $\overset{\ominus}{X}$ $\underset{k_{-8}}{\overset{k_8}{\rightleftharpoons}}$ $\overset{\oplus}{DMTr} \| \overset{\ominus}{X}$

(IX) $\quad$ $\overset{\oplus}{DMTr} . OH_2$ $+$ $\overset{\ominus}{X}$ $\underset{k_{-9}}{\overset{k_9}{\rightleftharpoons}}$ $\overset{\oplus}{DMTr} \| \overset{\ominus}{X}$ $+$ H_2O
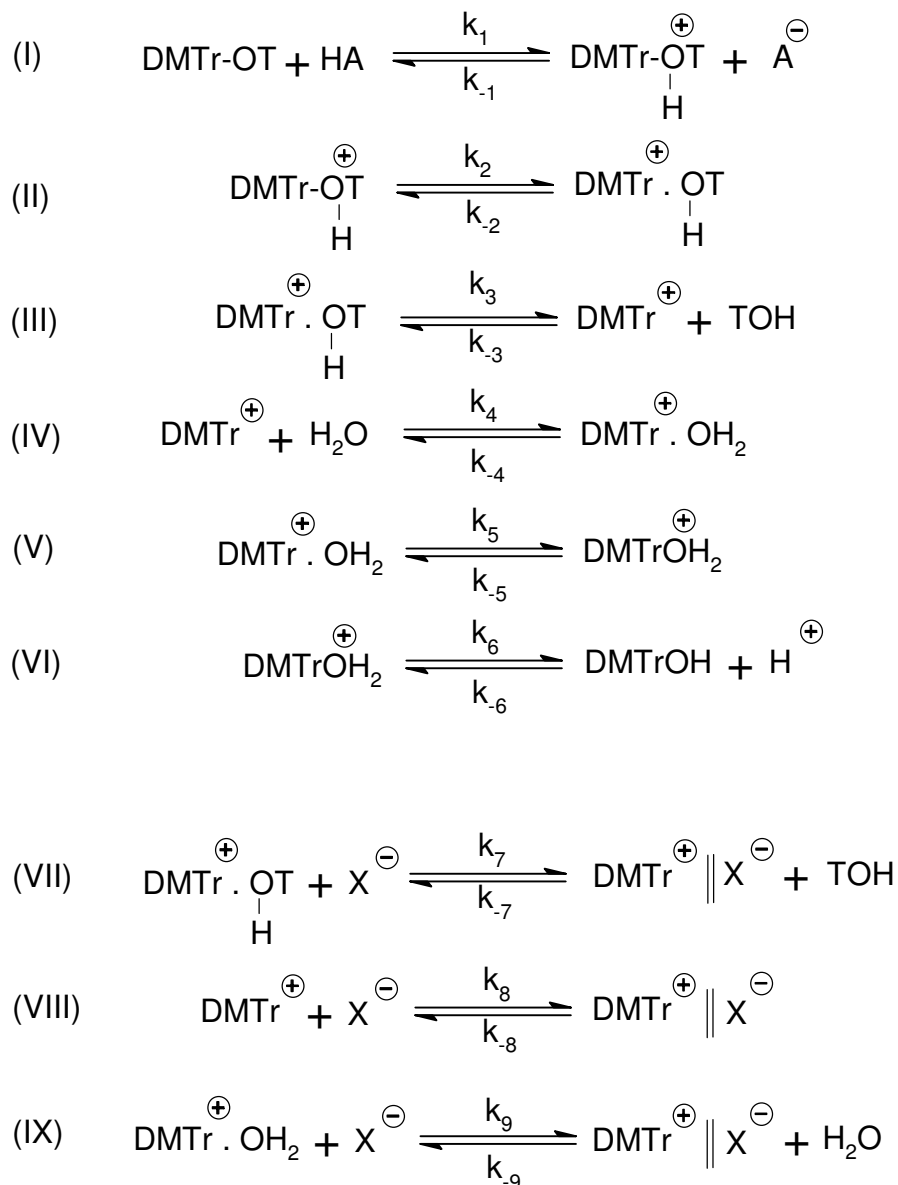
Scheme 28: Possible step-wise mechanism for production of trityl carbocation.

Study of the simplified step-wise mechanism of 4,4-dimethoxytrityl carbocation formation (scheme 29) gives a mechanism with two steps; rate limiting protonation of the 4,4-dimethoxytrityl ether and then bond cleavage to form the 4,4-dimethoxytrityl carbocation, this scheme assumes no reverse reaction for the final step.

DMTr-OT $+$ HA $\overset{K}{\rightleftharpoons}$ DMTr-$\overset{\oplus}{\underset{H}{O}}$T $+$ $\overset{\ominus}{A}$ $\overset{k}{\longrightarrow}$ $\overset{\oplus}{DMTr}$ $+$ TOH
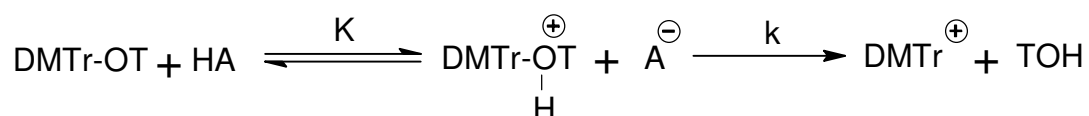
Scheme 29: Simplified step-wise mechanism of detritylation.

The observed rate constant, k_{obs}, for this mechanism will be equal to the product of equilibrium constant for the first step, K, and rate constant for the second step, k. In acetonitrile observed rate constants of approximately 10 M^{-1} s^{-1} have been measured. Estimation of K can be obtained from the dissociation constants of dichloroacetic acid, $K_a^{H^+}$, and the protonated ether, $K_a^{DMTr-OTH^+}$, as described by the equations below.

$$K = \frac{[DMTr-OTH^+][A^-]}{[DMTr-OT][HA]}$$

$$K_a^{H^+} = \frac{[H^+][A^-]}{[HA]}$$

and

$$K_a^{DMTr-OTH^+} = \frac{[DMTr-OT][H^+]}{[DMTr-OTH^+]}$$

Where,

$$\frac{K_a^{H^+}}{K_a^{DMTr-OTH^+}} = \frac{[DMTr-OTH^+]}{[DMTr-OT][H^+]}\frac{[H^+][A^-]}{[HA]} = \frac{[DMTr-OTH^+][A^-]}{[DMTr-OT][HA]} = K$$

The pK_a of dichloroacetic acid is 15.8[119] therefore $K_a^{H^+}$ equals approximately 10^{-16}. There are no pK_a values for protonated ethers in acetonitrile reported but in water they can range between -2 and -6, for example protonated dimethylether and diethylether have pK_as of -2.48 and -2.39 respectively.[121] In acetonitrile pK_as are higher than in water therefore the pK_a of the ether in acetonitrile can be estimated at approximately 3 to 6, which equates to a dissociation constant of 10^{-3} to 10^{-6}.

Inputting these numbers to calculate K, gives,

$$K = \frac{K_a^{H^+}}{K_a^{DMTr-OTH^+}} = \frac{10^{-16}}{10^{-6}} = 10^{-10}$$

Which gives a value for the rate constant of the second step as,

$$k = \frac{k_{obs}}{K} = \frac{10}{10^{-10}} = 10^{11}\, s^{-1}$$

Using a value for $K_a^{DMTr-OTH^+}$ of 10^{-3} gives a value of k of $10^{14}\, s^{-1}$.

An intermediate can only exist if it has a life time longer than that of a molecular vibrational frequency, approximately $10^{13}\, s^{-1}$.[122] The estimated range for the rate constant, k, calculated here is approximately 10^{11} to $10^{14}\, s^{-1}$ which lies either side of this frequency of vibration and therefore intermediate formation seems unlikely, as does a stepwise mechanism. A likely mechanistic alternative for formation of the 4,4-dimethoxytrityl carbocation in acetonitrile is a concerted general acid catalysed mechanism as shown in scheme 30.
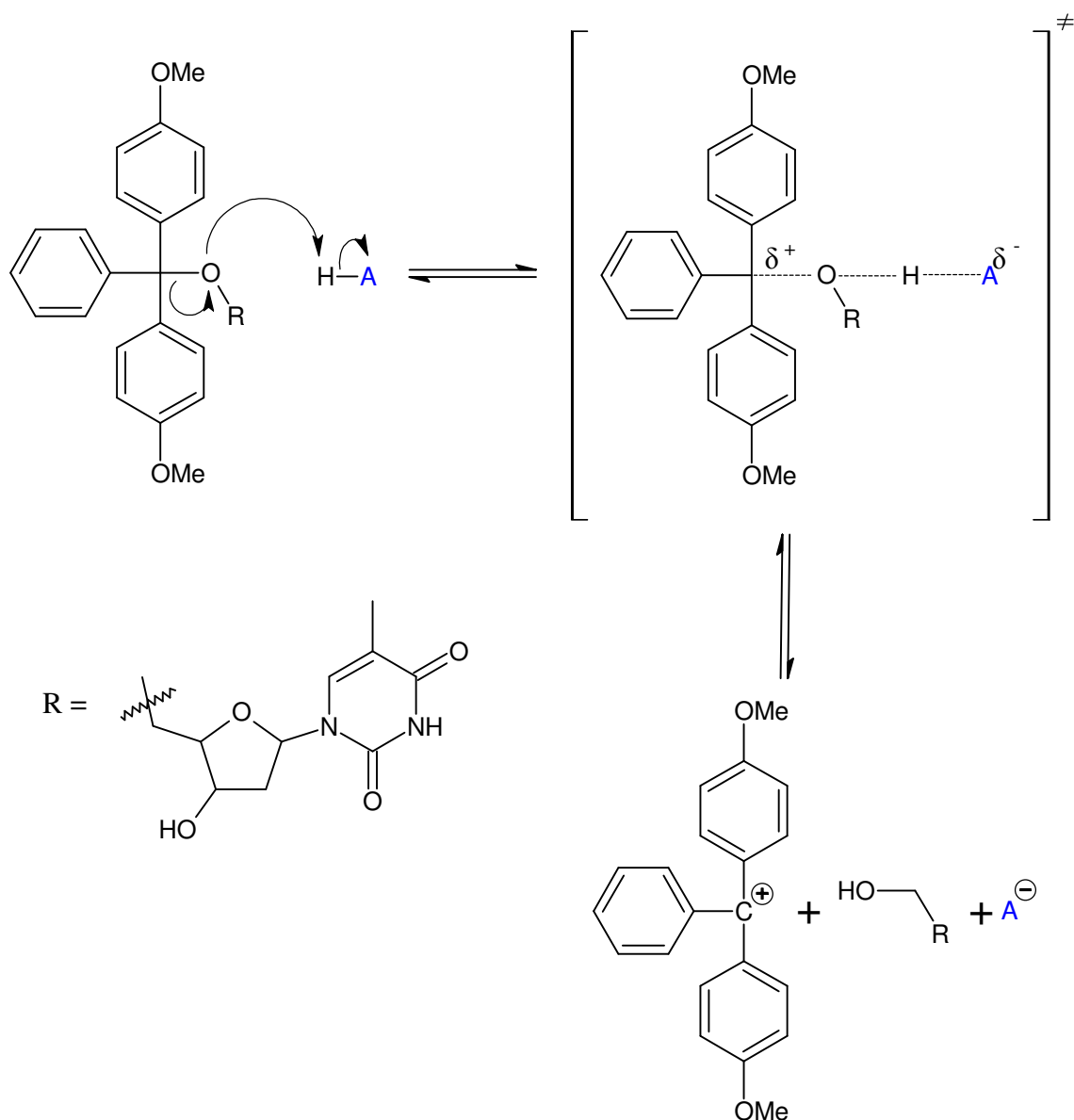
Scheme 30: Concerted mechanism of 4,4-dimethoxytrityl carbocation formation from 4,4-dimethoxytritylthymidine.

Jencks[123] has proposed a number of requirements to identify whether a mechanism will be concerted or stepwise. He stipulates that for a reaction to be a concerted general acid catalysed mechanism there must be a large change in pK_a during the course of the reaction and the catalyst must have pK_a intermediate between the initial and final pK_a values of the substrate site.

During the course of the detritylation reaction there is a large change in pK_a: the pK_a of the protonated ether in acetonitrile is likely to be between 3 and 6 and the pK_a of the thymidine alcohol product will be approximately 22+. The pK_a of dichloroacetic acid is 15.8 which is intermediate between the protonated ether and alcohol.

Fife[124,125] has also proposed a number of requirements for a concerted general acid catalysed mechanism determined from the study of acetal and ketal hydrolysis reactions. These state that for a concerted mechanism to be in effect either the leaving group must be very good or the product carbocation must be stable. The high stability of the 4,4-dimethoxytrityl carbocation is in agreement with Fife's latter requirement.

It seems likely then that the detritylation reaction will proceed by a concerted general acid catalysed mechanism. Though no experimental evidence has been obtained to support this, estimations of rate constants for the step wise mechanism are too large for them to be possible and the requirements for a concerted mechanism proposed by Jencks and Fife are met.

4 Results and Discussion: Coupling

A number of mechanistic studies have been performed on the coupling reaction with tetrazole as the activator.[50,77-80,84,126] It is now widely accepted that activation with tetrazole proceeds via a three step mechanism i) initial protonation of the amine of the phosphoramidite by tetrazole, ii) nucleophilic substitution of the protonated amine with the formed tetrazolide ion to produce a tetrazolide intermediate and then iii) subsequent nucleophilic attack of the tetrazolide by the entering alcohol to produce the phosphite triester. The departing tetrazolide undergoes salt formation with the more basic amine released in the second step (scheme 31). Studies have shown that tetrazole can act catalytically if the amine is removed from the system by molecular sieves.[81]
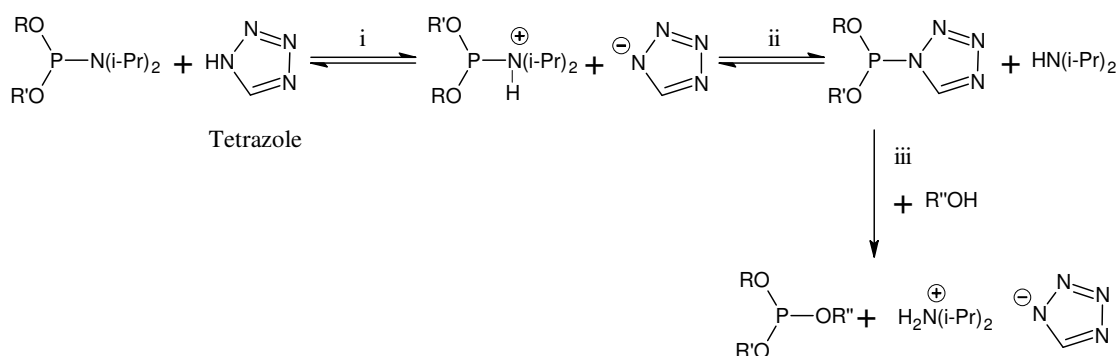
Scheme 31: Proposed mechanism for tetrazole activated coupling reaction.

Most studies into new coupling agents focus on screening possible candidates for coupling efficiency by measuring yields and reaction times. A good activator must be a relatively strong acid that does not promote any undesirable side reactions, but strong enough to protonate the phosphoramidite. The activator must also be strongly nucleophilic to facilitate rapid conversion to the activated phosphite intermediate as well as being a good leaving group to be displaced by the alcohol to give the phosphite triester product. Acidic activators of the HX type like 1H-tetrazole do not generally meet the two requirements of good nucleophile and relatively strong acid simultaneously; as a strong acid is likely to correspond to a weakly nucleophilic conjugate base and a strong nucleophile is likely to be derived from a weak acid.[52,97,98]

Recently many studies have been aimed towards finding activators made up of acid/base salts, as the acidity and nucleophilicity of each component can be altered independently of the other. These salts should consist of relatively strong acids for efficient protonation of the amidite and strongly nucleophilic bases for rapid substitution of the protonated amine (scheme 32). Salts of this type have, on many occasions, shown greater coupling efficiencies than the HX type activators.[52,90,91,97,98,100-102]

$$
\begin{array}{c}
\underset{R'O}{\overset{RO}{{>}}}\!P\!-\!N(i\text{-}Pr)_2 + NucH^{\oplus}\ X^{\ominus} \rightleftharpoons \underset{RO}{\overset{R'O}{{>}}}\!P\!-\!\overset{\oplus}{\underset{H}{N}}(i\text{-}Pr)_2 + Nuc + X^{\ominus} \rightleftharpoons \underset{R'O}{\overset{RO}{{>}}}\!P\!-\!\overset{\oplus}{Nuc} + X^{\ominus} + HN(i\text{-}Pr)_2
\end{array}
$$

$+\ R''OH$

$$
\underset{R'O}{\overset{RO}{{>}}}\!P\!-\!OR'' + H_2\overset{\oplus}{N}(i\text{-}Pr)_2\ X^{\ominus} + Nuc
$$
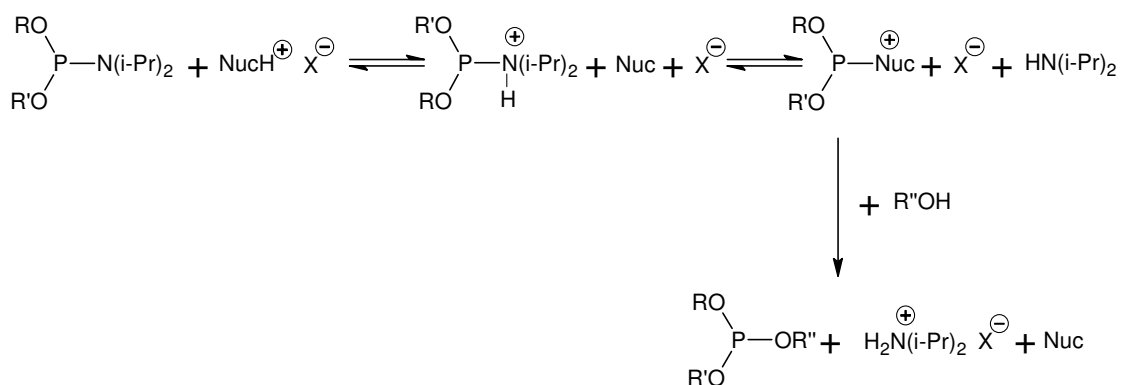
Scheme 32: General mechanism of acid/base salt activated coupling reaction.

One such acid/base salt used for activation of the coupling step within industry is the salt between saccharin and *N*-methylimidazole (scheme 33). Both saccharin and *N*-methylimidazole are readily available and relatively cheap making them a desirable activator choice. As such, the following mechanistic studies on the coupling reaction were performed with activation by saccharin/*N*-methylimidazole salt.
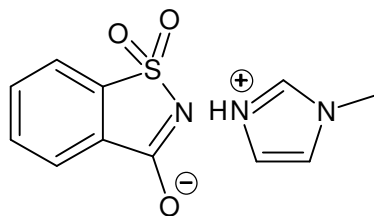
Scheme 33: Saccharin/*N*-methylimidazole salt

4.1   Coupling pre-equilibria

On examination of the phosphoramidite activation and alcoholysis reaction schemes (scheme 34, where sac⁻ = saccharin anion and NMI = *N*-methylimidazole) based on the reaction previously described in the literature, it can be seen that there are two salts which are important: the saccharin/*N*-methylimidazole salt and the saccharin/diisopropylamine salt. Two protons are consumed in each reaction: one to facilitate diisopropylamine cleavage and one for protonation of the released diisopropylamine. In the absence of alcohol two equivalents of saccharin/*N*-methylimidazole salt are required for complete activation. In the presence of alcohol only one equivalent of saccharin/*N*-methylimidazole salt is required.
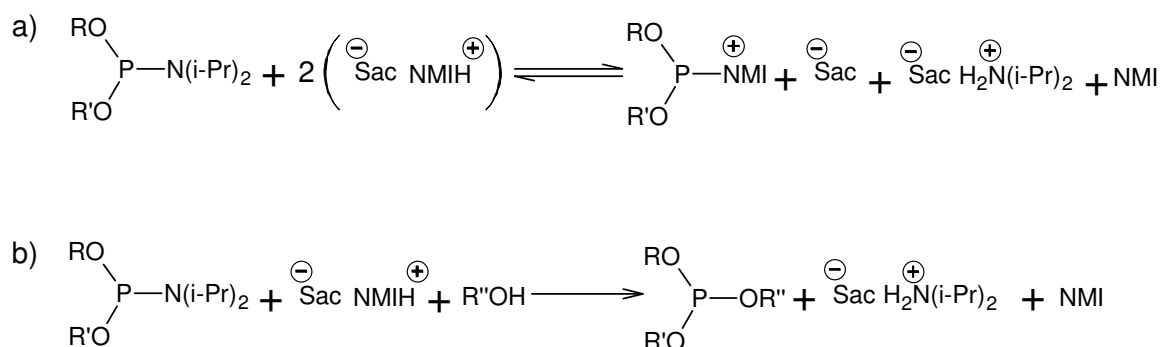
Scheme 34: Phosphoramidite a) activation b) alcoholysis with saccharin/*N*-methylimidazole salt.

The thermodynamics of the reactions are largely controlled by the relative stabilities of the two salts and the increased strength of the P-O bonds in the phosphite triester product versus the P-N bond in the starting amidite. The bond energies for P-O and P-N bonds are shown in table 8 below.

Bond	Bond energy (kJ mol⁻¹)
P-O	360
P-N	230

Table 8: Bond energies of P-O and P-N bonds.[127,128]

The pK$_a$s in water of the acids involved (table 9) indicate that diisopropylamine is more basic than *N*-methylimidazole and as a consequence will form a more stable salt with saccharin. The pK$_a$ of the acids increase in acetonitrile showing that their conjugate bases are much more basic in this solvent (table 9). This is particularly true for saccharin, and as a consequence the differences in pK$_a$s of all three acids in acetonitrile are considerably less than in water.

Acid	pK$_a$ in water	pK$_a$ in acetonitrile
Saccharin	1.6[129]	14.58[120]
N-methylimidazolium	7.12[130]	17.1[79] or 15.4[131]
Diisopropylammonium	11.05[61]	16.5[79]

Table 9: pK$_a$ data in water and acetonitrile.

The pK$_a$ for *N*-methylimidazolium in acetonitrile is considerably different in the two literature sources. The pK$_a$ reported by Nurminen is 17.1[79] which would put *N*-methylimidazoles basicity above that of diisopropylamine, the conjugate base of which has been reported by Nurminen *et al*, to be 16.5.[79] This would suggest that in acetonitrile the salt formed between saccharin and *N*-methylimidazole will be more stable than that of the saccharin and diisopropylamine. However, ^{1}H NMR studies, described in the next section, have shown the reverse of this, with salt formation between saccharin and diisopropylamine taking precedence over the saccharin/*N*-methylimidazole salt. This infers that the reported pK$_a$ values by Nurminen of diisopropylamine and *N*-methylimidazole in acetonitrile are in error.

The other reported pK$_a$ value for *N*-methylimidazole in acetonitrile by Schwetlick *et al* is 15.4,[131] which would make its acidity greater than that of diisopropylammonium; compatible with the ^{1}H NMR studies, described in the next section. This pK$_a$ of 15.4 was not measured experimentally but was determined from extrapolation of pK$_a$ values in dimethylsulphoxide and water.

The reported pK$_a$ of diisopropylammonium (16.5[79]) may also be in error, as a comparative study of the pK$_a$s in water and acetonitrile of aliphatic amines with a similar structure to diisopropylamine (table 10), give an expected pK$_a$ for

diisopropylammonium of at least and possibly greater than 18 in acetonitrile. A pK_a of 18 will place the basicity of diisopropylamine above that of *N*-methylimidazole for both values reported in the literature which is compatible with the preferential salt formation observed between diisopropylamine and saccharin.

Acid	pKa in water	pKa in acetonitrile
Diisopropylammonium	11.05[61]	-
Diethylammonium	10.98	18.75
Triethylammonium	10.65	18.46
Tri-*n*-propylammonium	10.65	18.1
Di-*n*-butylammonium	11.25	18.31
Tri-*n*-butylammonium	10.89	18.09
Diisobutylammonium	10.50	17.88

Table 10: pK_a data for aliphatic amines in water and acetonitrile.[132]

4.1.1 ^{1}H NMR studies of salt formation between saccharin and *N*-methylimidazole and saccharin and diisopropylamine

The ^{1}H NMR spectrum of *N*-methylimidazole in deuterated acetonitrile gives three singlets for the three methyne groups and a singlet due to the methyl group (spectrum 1a, table 11). Hydrogens (b) and (c) (scheme 35) appear as singlets rather than the expected doublets presumably due to the quadrupolar nature of the nitrogen atoms reducing the relaxation time of the two protons.

On addition of one equivalent of saccharin, all the *N*-methylimidazole signals move down field (spectrum 1b, table 11), which is indicative of positive charge formation and proton transfer from saccharin to *N*-methylimidazole (scheme 35). The acidic N-H proton is visible as a broad singlet at δ8.27ppm which is exchangeable with D_2O (spectrum 1c).

92
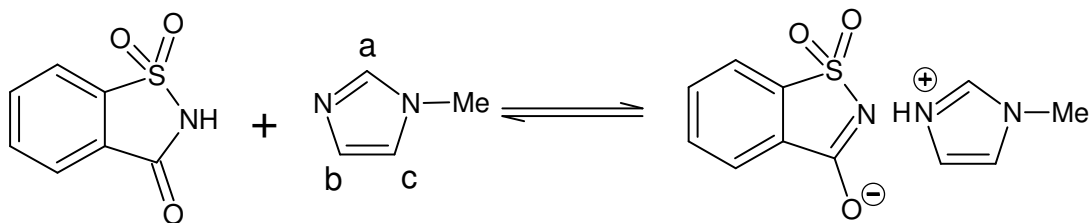
Scheme 35: Salt formation between saccharin and *N*-methylimidazole.

The down field shift in proton (a) is greater than that seen for protons (b) and (c). This is presumably due to the possible resonance structures available to the protonated *N*-methylimidazole (scheme 36). Carbon (a) has a greater positive charge density than that of carbons (b) and (c).
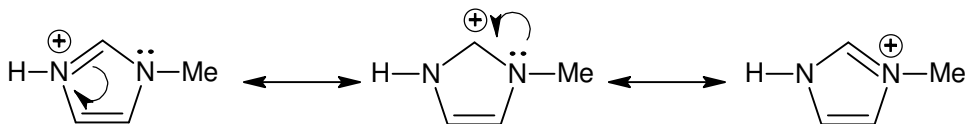
Scheme 36: Resonance structures of protonated *N*-methylimidazole.

On addition of one equivalent of diisopropylamine to a sample of saccharin and *N*-methylimidazole in deuterated acetonitrile the *N*-methylimidazole's protons all move up field towards the position of the un-protonated *N*-methylimidazole (spectrum 1d, table 11). The chemical shifts do not return exactly back to that of the un-protonated form which may be indicative of an interaction or equilibrium between the salts or a small medium effect.

Sample Composition	δ proton (a) (ppm)	δ proton (b) (ppm)	δ proton (c) (ppm)	δ methyl H's (ppm)
1 a) NMI	7.39	6.95	6.90	3.63
1 b) & c) NMI/Saccharin	8.43	7.39	7.27	3.81
1 d) NMI/Saccharin/DIA	7.50	6.98	6.93	3.64

Table 11: ^{1}H NMR chemical shifts of *N*-methylimidazole in acetonitrile.
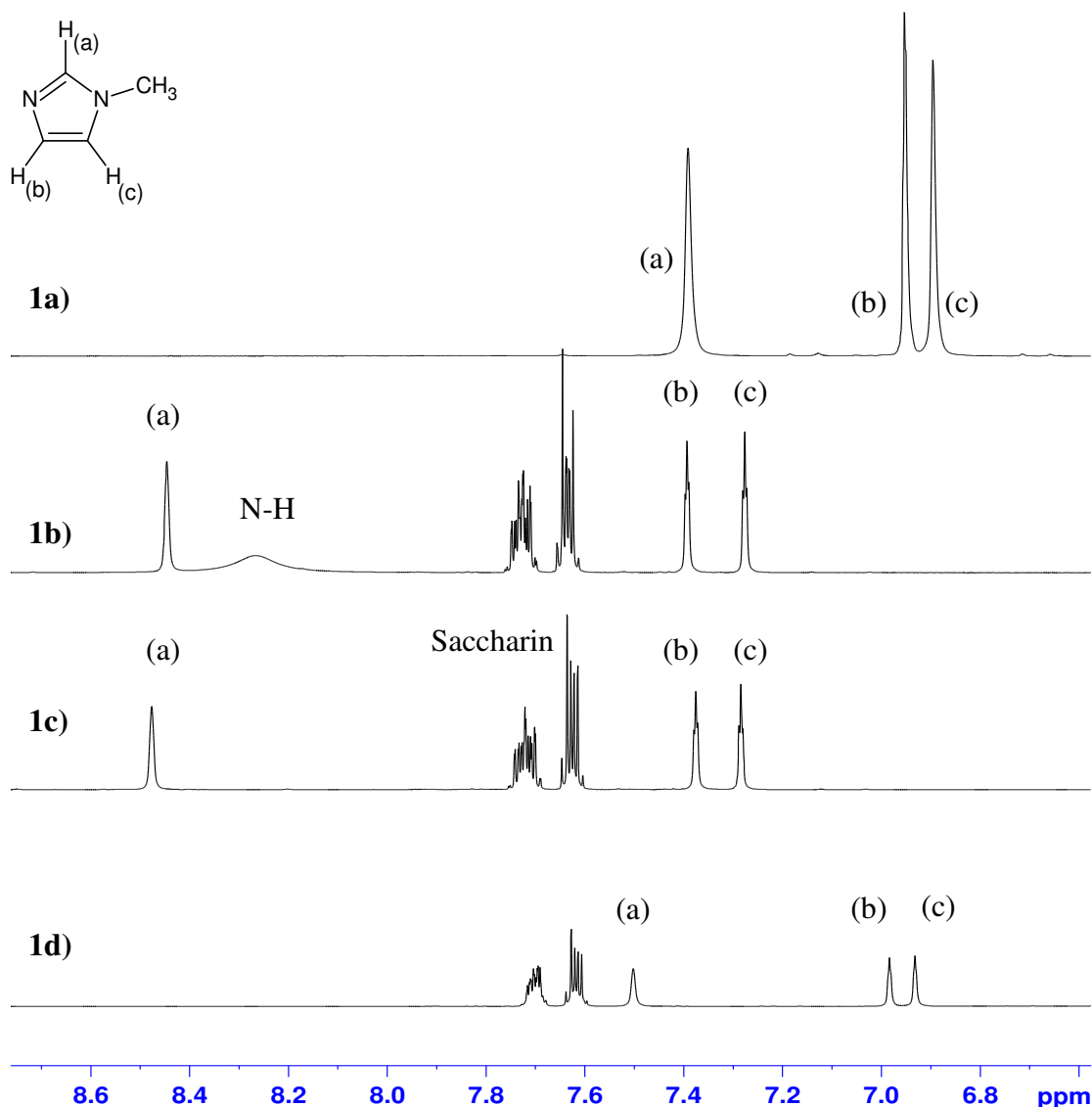
Spectra 1: ^{1}H NMR spectra in acetonitrile of a) 0.06M *N*-methylimidazole, b) 0.06M *N*-methylimidazole and 0.06M saccharin c) 0.06M *N*-methylimidazole and 0.06M saccharin with D$_2$O and d) 0.06M *N*-methylimidazole, 0.06M saccharin and 0.06M diisopropylamine.

The ^{1}H NMR spectrum of diisopropylamine in deuterated acetonitrile gives a heptet for the two methyne hydrogens and a doublet for the four methyl groups (spectrum 2a, table 12). On addition of saccharin these chemical shifts move down field (spectrum 2b, table 12) indicating proton transfer from saccharin to diisopropylamine. On addition of diisopropylamine to a sample of saccharin and *N*-methylimidazole the chemical shifts of the diisopropylamines protons are similar to those of the protonated species (spectrum 2c, table 12). This indicates that salt formation is preferential between saccharin and diisopropylamine as opposed to saccharin and *N*-methylimidazole

94

(scheme 37), which is compatible with diisopropylamine being the strongest base present.

Sample Composition	δ CH protons (ppm)	δ CH$_3$ protons (ppm)
2a) DIA	2.84	0.95
2b) DIA/Saccharin	3.45	1.30
2c) DIA/Saccharin/NMI	3.48	1.31

Table 12: ^{1}H NMR chemical shifts of diisopropylamine (DIA) in acetonitrile.
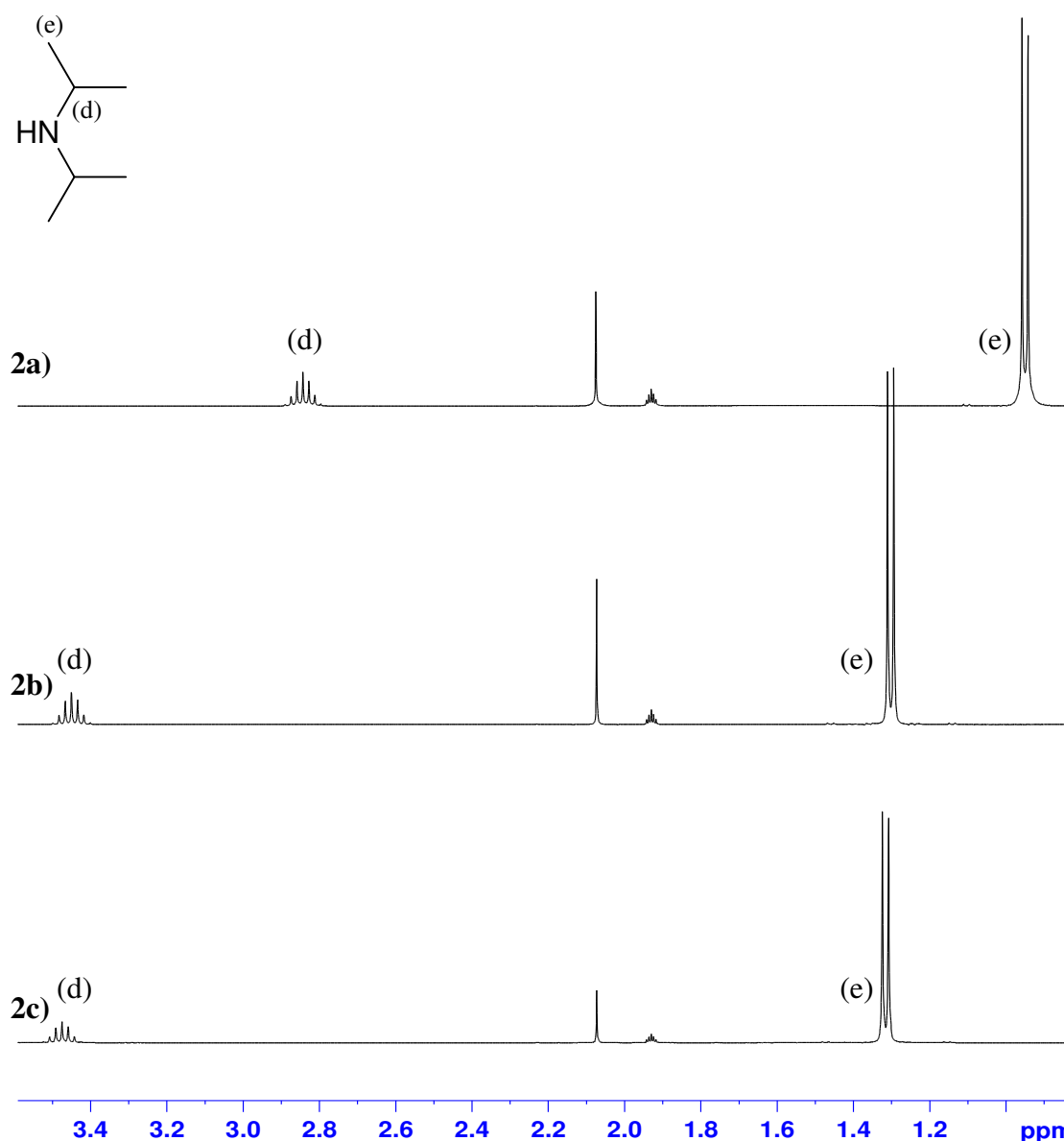
Spectra 2: ^{1}H NMR spectra in acetonitrile of a) 0.06M diisopropylamine, b) 0.06M diisopropylamine and 0.06M saccharin and c) 0.06M diisopropylamine, 0.06M saccharin and 0.06M *N*-methylimidazole.
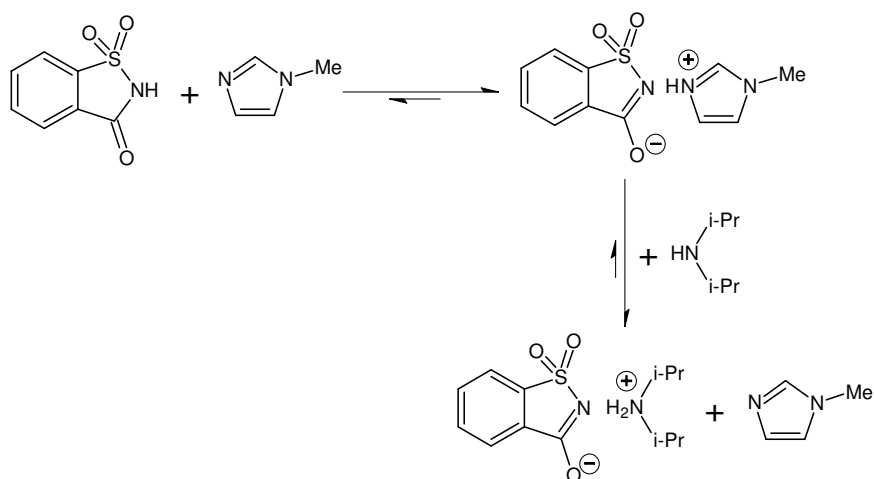
Scheme 37: Preferential salt formation between saccharin and diisopropylamine in the presence of *N*-methylimidazole.

The three equilibrium constants that relate saccharin, *N*-methylimidazole and diisopropylamine together (scheme 38) are: K_{SHNMI}, salt formation between saccharin and *N*-methylimidazole; K_{SHDIA}, salt formation between saccharin and diisopropylamine and; K_{salts}, the equilibrium between the saccharin/*N*-methylimidazole salt and saccharin/diisopropylamine salt.
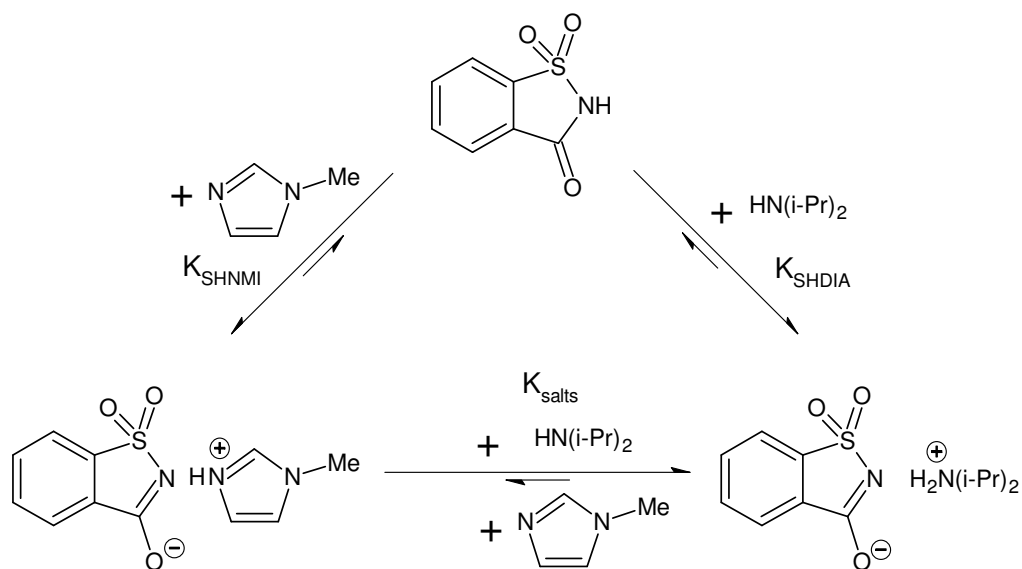
Scheme 38: Salt formation between saccharin, *N*-methylimidazole and diisopropylamine.

4.1.2 Determination of K_{SHNMI}, K_{SHDIA} and K_{salts}

4.1.2.1 Isothermal Titration Calorimetery

The equilibrium constants: K_{SHDIA}, K_{SHNMI}, have been determined at 30°C in acetonitrile by isothermal titration calorimetery.

Calorimetric data obtained by titration of saccharin with diisopropylamine in acetonitrile (figure 34) shows a good fit with the stoichiometery of the reaction (N) being calculated as 1.00. This is expected as one mole of saccharin will react with one mole of diisopropylamine. The equilibrium constant, K_{SHDIA}, was calculated to be 5.59×10^5.

Calorimetric data obtained by titration of saccharin with *N*-methylimidazole in acetonitrile (figure 34) again shows a good fit with the stoichiometery of the reaction (N) being calculated as 1.16. Due to the very low concentrations of reagents used in these experiments it is un-likely that homo-conjugation of *N*-methylimidazolium ions with *N*-methylimidazole molecules will be significant and therefore the stoichiometry of the reaction is expected to be 1.0. The slightly higher calculated stoichiometry is within experimental error for this technique and the equilibrium constant, K_{SHNMI}, was calculated to be 1.27×10^4.

The equilibrium constant, K_{salts}, will be the quotient of K_{SHDIA} by K_{SHNMI}. Therefore K_{salts} is equal to 44, which is compatible with the salt formation between saccharin and diisopropylamine being preferential over the salt formed between saccharin and *N*-methylimidazole.

The calculated equilibrium constant for salt formation based on the pK_a values in table 9 are $\log_{10} K_{SHNMI} = (pK_a\ NMIH^+ - pK_a\ SacH) = (17.1 - 14.6)$ therefore, giving $K_{SHNMI} = 3 \times 10^2$ compared with the ITC value of 1.27×10^4. A pK_a of 18 for diisopropylammonium ion would predict $K_{SHDIA} = 2.5 \times 10^3$ compared with the ITC

value of $5.59x10^5$. The fact that the ITC experiments indicate values much greater than those predicted from the reported pK_a values suggests that salt formation is thermodynamically more stable than simple proton transfer; perhaps indicative of ion-pair formation. Alternatively, the reported pK_a values may be in error.

a)

0.25mM Saccharin in cell with 4μl injections of 7.3mM diisopropylamine

b)

1mM Saccharin in cell with 2μl injections of 14.6mM *N*-methylimidazole
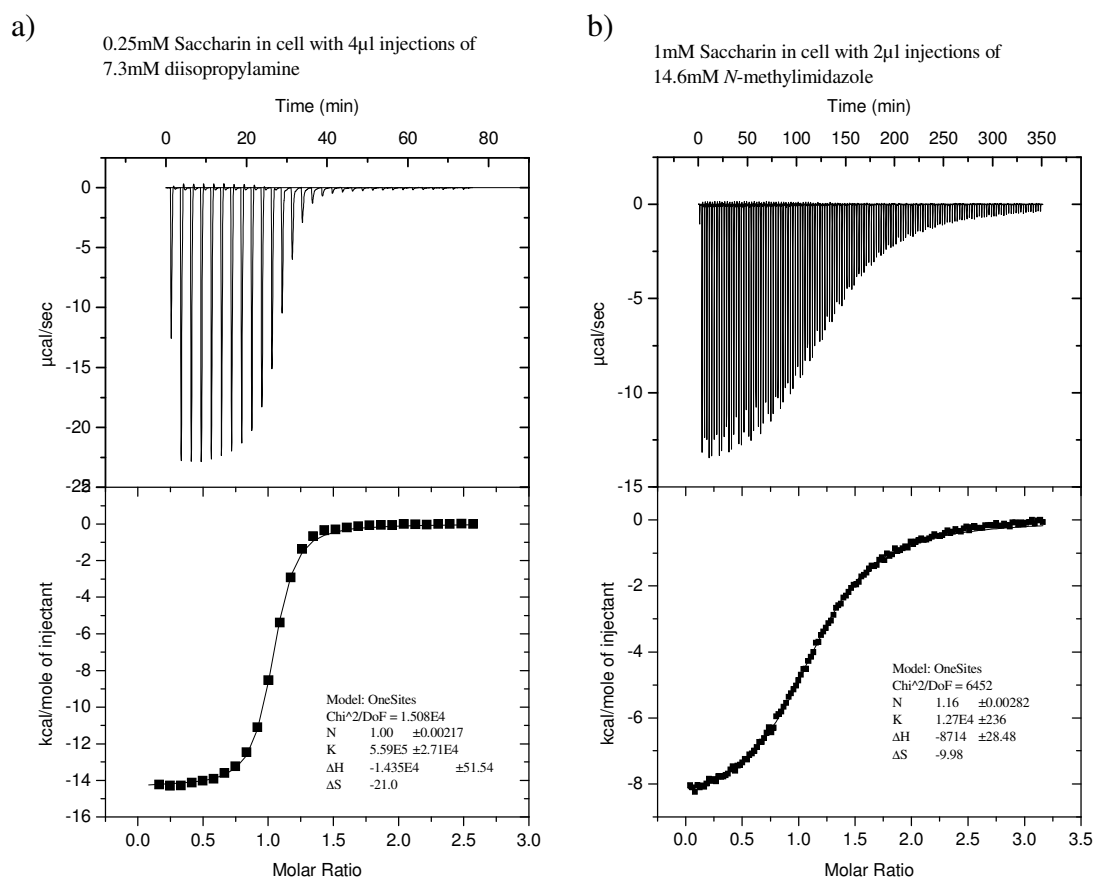
Figure 34: Calorimetric data for titration of saccharin with a) diisopropylamine and b) *N*-methylimidazole.

4.1.2.2   Conductivity

Conductivity measurements were undertaken to determine the equilibrium constants, K_{SHNMI}, K_{SHDIA} and K_{salts}, and to compare them against those determined by ITC and from the literature pK_a values.

Conductivity is proportional to the concentration of free ions in solution. This relationship was checked for each salt by measuring the conductivity on addition of saccharin/*N*-methylimidazole and saccharin/diisopropylamine into acetonitrile. Plots of conductivity versus salt concentration (figure 35) show that the relationship between conductivity and salt concentration is non-linear. A linear relationship was expected based on a direct relationship between conductivity and concentration. A linear relationship would have allowed acid/base titrations to be performed for each salt. As this was not the case more complex calculations were required which are outlined below. It can also be seen from figure 35 that the saccharin/*N*-methylimidazole salt is more conducting than the saccharin/diisopropylamine, which was also unexpected as the more basic diisopropylamine should show more dissociation and therefore more free ion formation.
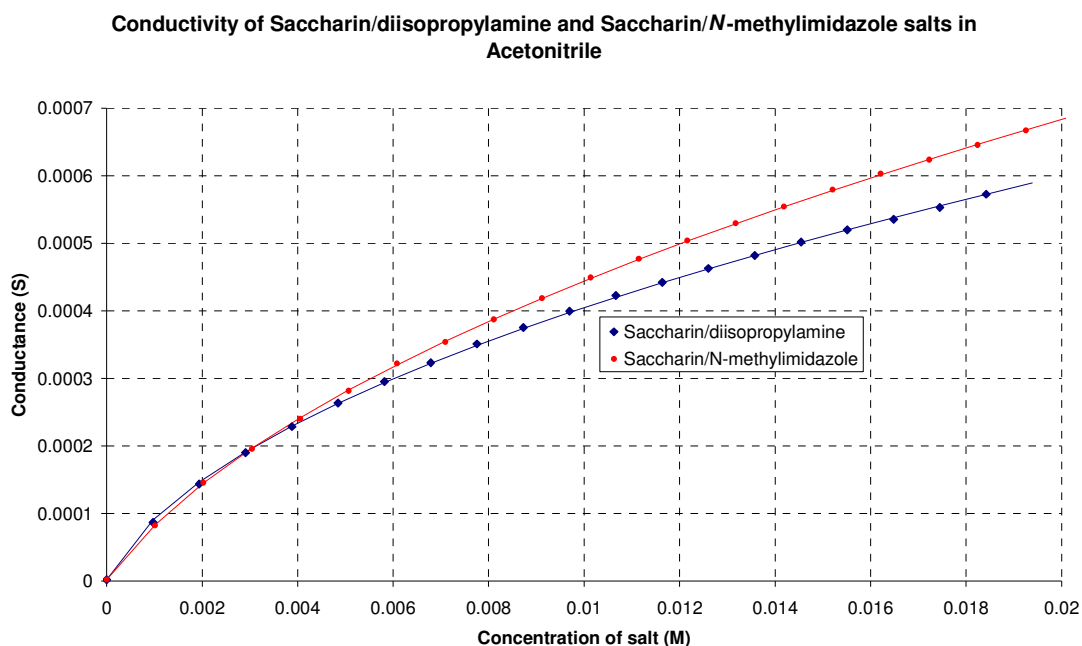
Figure 35: Conductivity of saccharin/diisopropylamine and saccharin/*N*-methylimidazole salts in acetonitrile at 30°C.

99

The non-linear relationship between conductivity and concentration indicates that there are either neutral or non-conducting species present in the system. In non-aqueous solution at least three species are possible for each saccharin-base pair: the un-charged saccharin and base, and, following proton transfer, the ion pairs and solvent separated free ions. Therefore, calculation of K_{SHDIA} and K_{SHNMI} by conductivity must take into account the equilibria between these different species (scheme 39) as conductivity is related only to the concentration of the free ions.
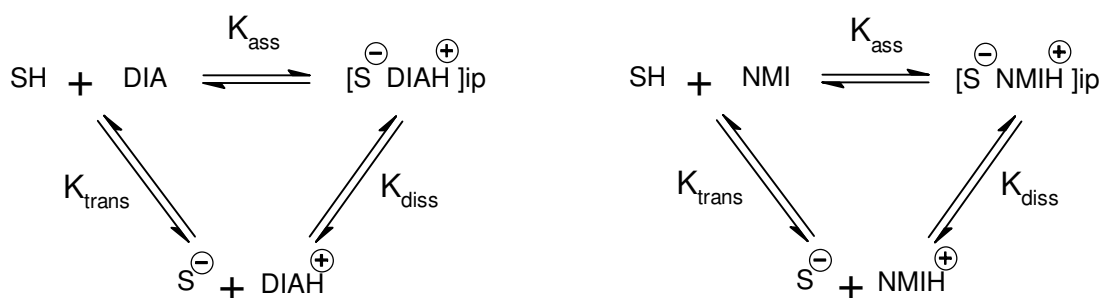
Scheme 39: Equilibria between species in solution.

Conductivity is not a direct measurement of free ion concentration ([S⁻], [DIAH⁺] and [NMIH⁺]). The free ion concentration can be calculated if the background conductance and the specific conductance of the conducting species are taken into account. The equation that relates these is shown below.

$$[S^-] = \frac{(Mc - Bc)}{Sc}$$

Where, Mc = Measured conductance

Bc = Background conductance

Sc = Specific conductance

4.1.2.2.1 Equilibria calculation for the saccharin/diisopropylamine

If the reaction is written as in scheme 40, with initial proton transfer of neutral species to form the ion pair and then formation of the solvent separated ions, the two equilibrium constants can be determined by the following equations:

$$SH \; + \; DIA \; \underset{}{\overset{K_{ass}}{\rightleftharpoons}} \; [S^{\ominus}DIAH^{\oplus}]ip \; \underset{}{\overset{K_{diss}}{\rightleftharpoons}} \; S^{\ominus} \; + \; DIAH^{\oplus}$$
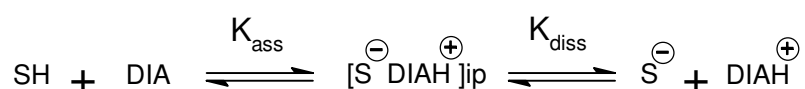
Scheme 40: Possible reaction scheme for interaction between saccharin and diisopropylamine.

$$K_{ass} = \frac{\left[S^- \, DIAH^+\right]_{ip}}{[SH]\,[DIA]} \qquad\qquad K_{diss} = \frac{\left[S^-\right]\left[DIAH^+\right]}{\left[S^-H^+DIA\right]_{ip}}$$

These can be solved with the quadratic equation below, the derivation of which can be found in section 7.2, page 192.

$$[S^-] = \frac{\left(-\left\{ 1 + 1 \middle/ \sqrt{K_{ass}K_{diss}} \right\} + \sqrt{\left\{ 1 + 1 \middle/ \sqrt{K_{ass}K_{diss}} \right\}^2 + 4\left[S^- \, DIAH^+\right]_{added} \middle/ K_{diss}} \right) K_{diss}}{2}$$

This leaves three unknowns in the above quadratic equation: K_{ass}, K_{diss} and Sc, which could not be solved directly. To simplify the calculation, the conductivity measurements were repeated with excess diisopropylamine. With excess diisopropylamine all of the neutral saccharin should be converted to its anion, so that only the ions and ion-pairs need to be considered. Hence, there is no requirement for the K_{ass} term (scheme 41), leaving two unknowns which can be calculated form the quadratic equation below (derivation section 7.1, page 189).

$$\text{[S}^{\ominus}\text{ DIAH}^{\oplus}\text{]}_{ip} \xrightleftharpoons{K_{diss}} \text{S}^{\ominus} + \text{DIAH}^{\oplus}$$

Scheme 41: Equilibrium between saccharin/diisopropylamine ion pair and free ions K_{diss}.

$$\left[S^-\right] = \frac{(Mc - Bc)}{Sc} = \frac{\left(-1 + \sqrt{1^2 + 4\left[S^-\ DIAH^+\right]_{added} \Big/ K_{diss}}\right) K_{diss}}{2}$$

Addition of the saccharin/diisopropylamine salt into pure acetonitrile and acetonitrile containing 0.1 M diisopropylamine yielded conductance versus salt concentration plots shown in figure 36. Both plots are again non-linear and are both similar in magnitude.

Conductance Measurements of Saccharin/Diisopropylamine Salt to Acetonitrile
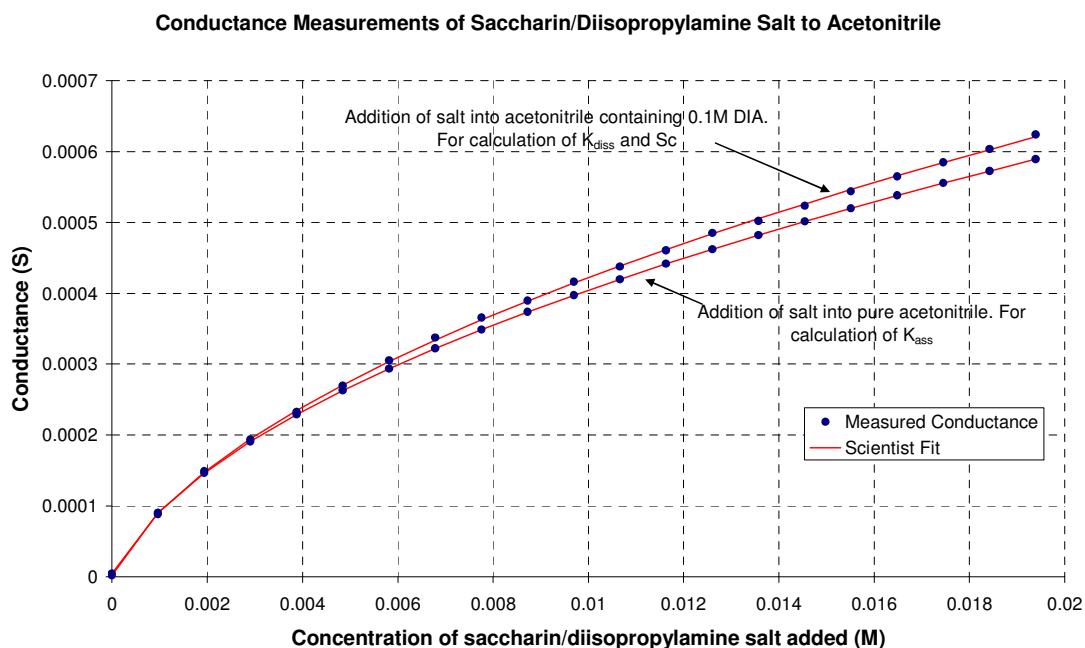
Figure 36: Conductivity data for the addition of saccharin/diisopropylamine salt to pure acetonitrile and 0.1M diisopropylamine in acetonitrile for calculation of K_{diss} and Sc.

K_{diss} was calculated to be 1.74×10^{-3} M with a specific conductivity of 0.1233 S.

The calculated values of K_{diss} and Sc can be put back into the quadratic equation on page 101 to give a value for K_{ass} of 1.55×10^4 M^{-1}.

The large positive K_{ass} indicates that there is almost complete proton transfer from saccharin to diisopropylamine and the very small K_{diss} shows that the ion pair is the most stable species in acetonitrile with few free ions being present.

The product of K_{ass} and K_{diss} will be the equilibrium constant between the neutral molecules and the free ions (K_{trans}) which equals 27.0 (scheme 42). These values can be compared with K_{SHDIA} of 5.59×10^5 obtained from the ITC studies and will be discussed later.
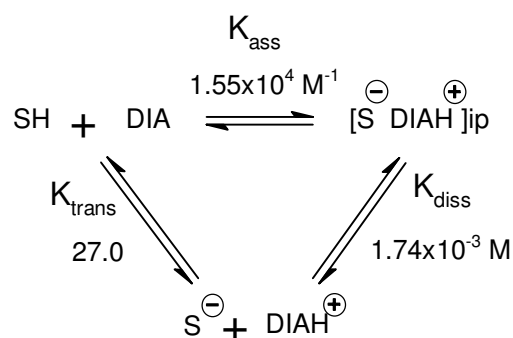
Scheme 42: Saccharin/diisopropylamine equilibria.

4.1.2.2.2 Equilibria calculation for the saccharin/*N*-methylimidazole

A similar method of calculating the equilibrium constants with saccharin/*N*-methylimidazole salt (scheme 43) was used as that with diisopropylamine described previously.

Scheme 43: Reaction scheme used for calculation of equilibrium constants K_{ass} and K_{diss}.

Conductivity measurements of saccharin/*N*-methylimidazole salt addition into an acetonitrile solution containing excess *N*-methylimidazole showed a large change in the conductivity compared with the salt addition to pure acetonitrile (figure 37). This

difference in conductivity is presumably due to homo-conjugation of the excess *N*-methylimidazole. The equilibrium constant for homoconjugation, K_{homo}, has to be added (scheme 44) and has been determined by solubility experiments to be 1.52 M^{-1} (see section 4.1.3, Page 107).

Conductance Measurements of Saccharin/*N*-methylimidazole Salt Addition to Acetonitrile
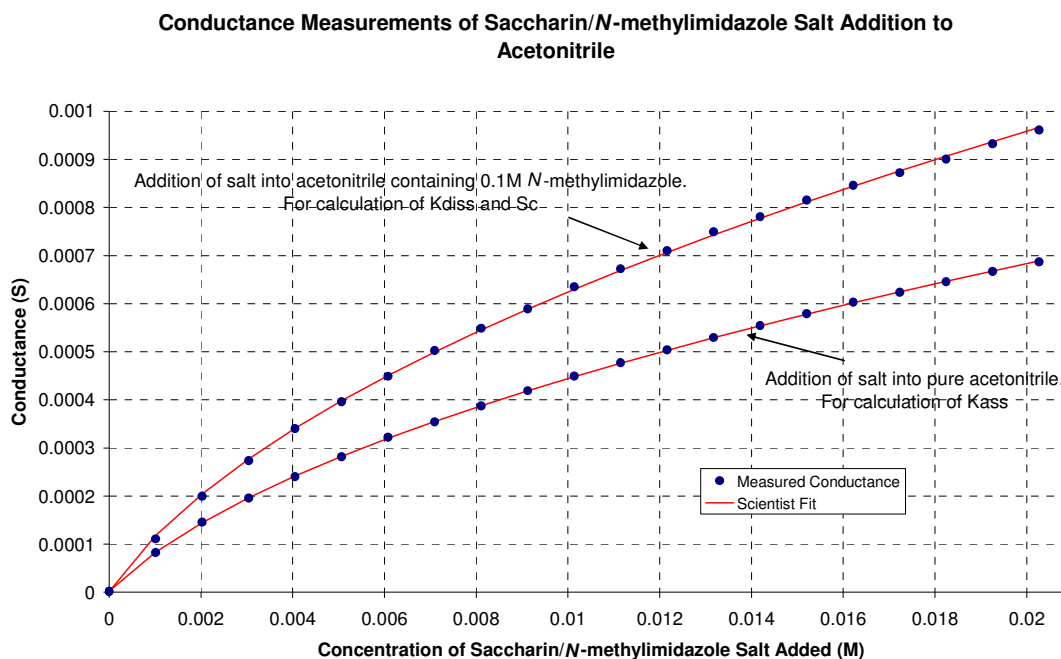
Figure 37: Conductivity data for the addition of saccharin/*N*-methylimidazole salt to pure acetonitrile and 0.1M *N*-methylimidazole in acetonitrile for calculation of K_{diss} and Sc.
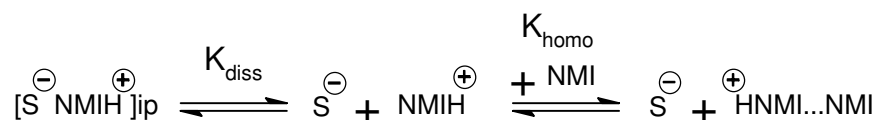
Scheme 44: Equilibria in excess *N*-methylimidazole.

A quadratic equation, shown below, for this scheme can be derived which can be solved for K_{diss} and Sc (derivation section 7.3, page 194).

$$[S^-] = \frac{(Mc - Bc)}{Sc} = \frac{\left(-\left\{ 1 + K_{\hom o}[NMI] \right\} + \sqrt{\left\{ 1 + K_{\hom o}[NMI] \right\}^2 + 4\left\{ 1 + K_{\hom o}[NMI] \right\}\left(-\left[S^- NMIH^+ \right]_{added} \right)/K_{diss}} \right) K_{diss}}{2\left\{ 1 + K_{\hom o}[NMI] \right\}}$$

K_{diss} was determined to be 2.96×10^{-3} M and Sc to be 0.164 S.

K_{ass} can now be calculated using the same quadratic equation as with diisopropylamine, except substituting diisopropylamine with *N*-methylimidazole (derivation section 7.2, page 192).

$$[S^-] = \frac{(Mc - Bc)}{Sc} = \frac{\left(-\left\{ 1 + 1/\sqrt{K_{ass} K_{diss}} \right\} + \sqrt{\left\{ 1 + 1/\sqrt{K_{ass} K_{diss}} \right\}^2 + 4\left[S^- \; NMIH^+ \right]_{added} \Big/ K_{diss}} \right) K_{diss}}{2}$$

The value for Sc determined previously could not be used in these calculations, because specific conductivity is different for each conducting species. In the presence of excess *N*-methylimidazole there are two conducting species: the free *N*-methylimidazolium ion and the charged homo-conjugate. In the absence of excess *N*-methylimidazole there is only one conducting species: the free *N*-methylimidazolium ion. Therefore, the specific conductivity for each experiment will be different.

The above quadratic equation was solved for K_{ass} and Sc and K_{ass} was determined to be 2.74×10^4 M^{-1} and Sc to be 0.110 S. K_{trans}, which is the product of K_{ass} and K_{diss} is equal to 81.1 (scheme 45).
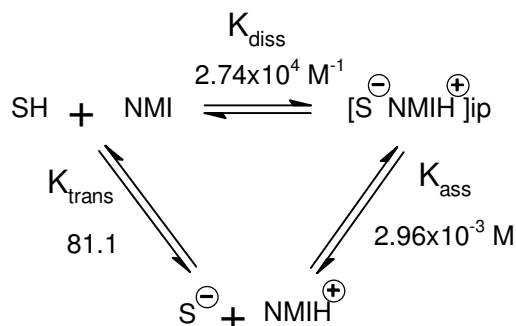
Scheme 45: Saccharin/*N*-methylimidazole equilibria.

The conductivity profiles gained for addition of each salt in acetonitrile (figures 36 and 37) are similar in shape and magnitude. It was expected that the conductivity of the

diisopropylamine system would be higher, as its increased basicity would ensure that charged species predominate compared with *N*-methylimidazole, but, of course, both systems could exist as fully charged species if the difference in pK_as is sufficiently large.

The calculated equilibrium constants for both systems (scheme 46) appear to suggest that *N*-methylimidazole is a stronger base than diisopropylamine. For example, K_{trans} for the *N*-methylimidazole system is three times that of K_{trans} for diisopropylamine. Therefore, more free ions will be present with saccharin/*N*-methylimidazole in acetonitrile than with saccharin/diisopropylamine salt. These results are contrary to those obtained from the ITC data and ^{1}H NMR experiments which showed that a preferential salt between saccharin/diisopropylamine will be formed in the presence of *N*-methylimidazole.
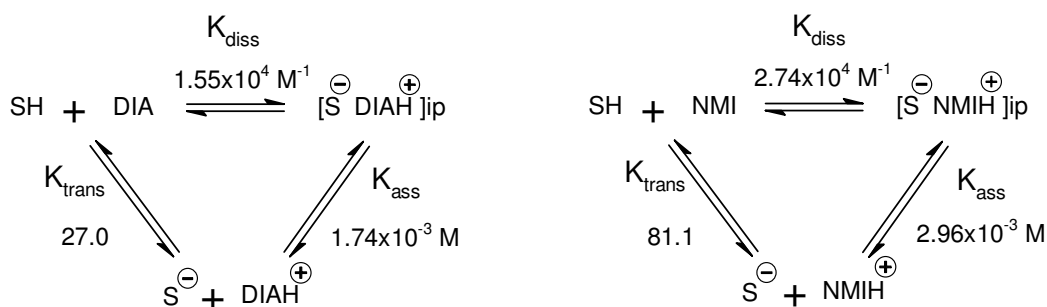
Scheme 46: Calculated equilibrium constants for both saccharin/diisopropylamine and saccharin/*N*-methylimidazole salt formation.

The conductivity calculations have been made under the assumption that the free ions are the only conducting species in solution. This may not be true and therefore the calculated equilibrium constants from the conductivity data may be in error.

4.1.3   Determination of K_{homo}

The solubility of saccharin/*N*-methylimidazole salt in solution is increased on addition of *N*-methylimidazole presumably due to the formation of homo-conjugates. A plot of the solubility of saccharin/*N*-methylimidazole salt as a function of *N*-methylimidazole concentration in acetonitrile (figure 38) shows a linear increase over the concentration range studied. The increase in solubility can be used to determine the equilibrium constant for homo-conjugation, K_{homo}, from the following equation, the derivation of which can be found in section 7.4, page 198.

$$K_{\text{hom}o} = \frac{\left([NMIH^+]_{total\ sol} - [NMIH^+]_{\lim\ sol} \right)}{\left([NMI]_{solution} - [NMIH^+]_{total\ sol} - [NMIH^+]_{\lim\ sol} \right) [NMIH^+]_{\lim\ sol}}$$

K_{homo} has been calculated to be $1.52M^{-1}$ in acetonitrile which indicates the equilibrium is only slightly in favour of the homo-conjugate.
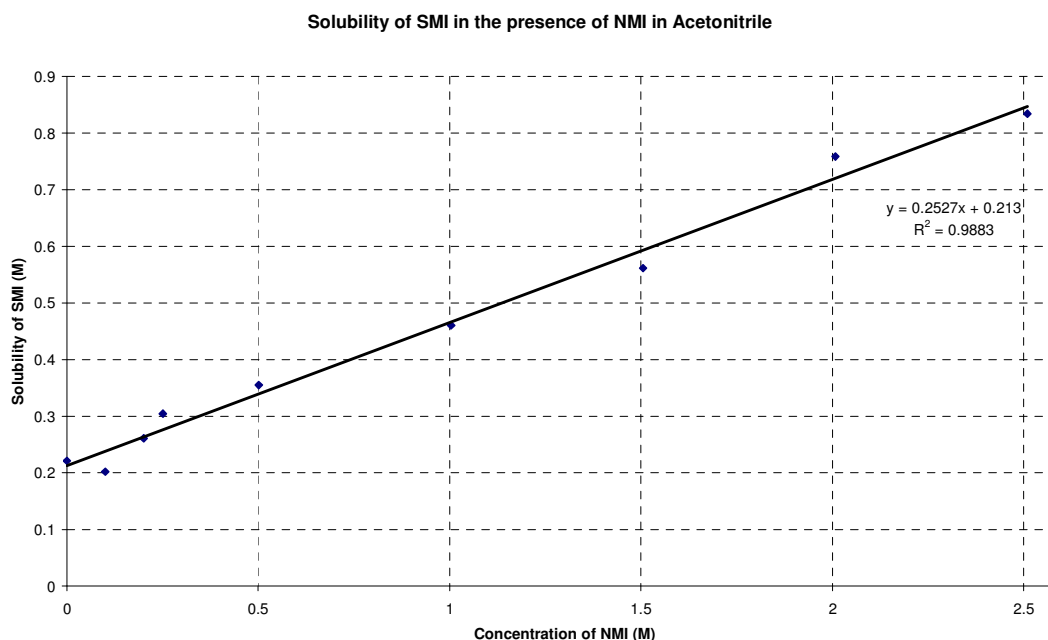
Figure 38: Plot of saccharin/*N*-methylimidazole salt solubility as a function of *N*-methylimidazole concentration.

4.2   Activation

Phosphoramidite activation with saccharin/*N*-methylimidazole salt probably proceeds via a two step mechanism similar to that proposed for the reaction with tetrazole:[77,79,80] 1) initial protonation of the diisopropylamine group of the phosphoramidite and 2) substitution of the protonated amine with either *N*-methylimidazole to form a charged intermediate species or with the saccharin anion, through either its carbonyl oxygen or nitrogen atom, giving two possible neutral intermediates (scheme 47). On the assumption that the liberated diisopropylamine is protonated in the product, the overall reaction has the stoichiometries shown.
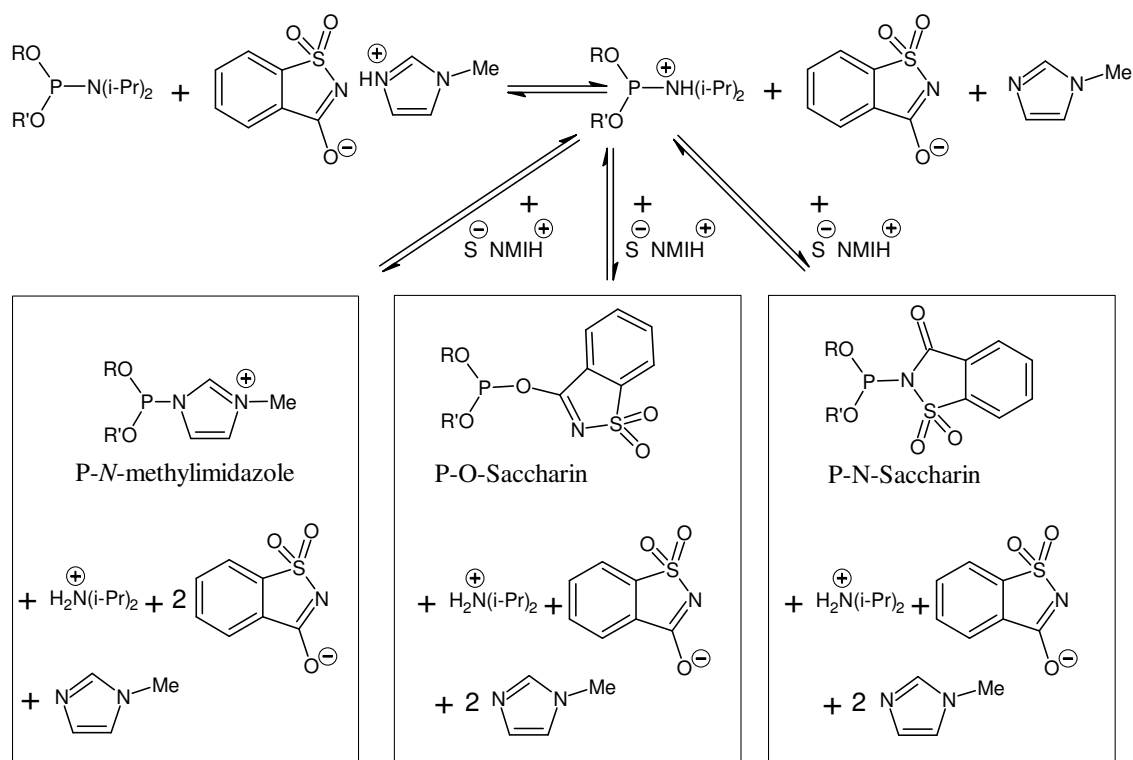
Scheme 47: The three possible activated species: P-*N*-methylimidazole, P-O-saccharin and P-N-saccharin.

The reaction in scheme 47 has been presented with the assumption that in the first step protonation occurs on the nitrogen on the amine rather than on the phosphorus, this assumption will be used throughout the studies on the coupling reaction presented here.

This assumption has been used based on studies performed by two other groups. Korkin and Tvetkov[87,88] used molecular modelling techniques to model a simple structure, $H_2P\text{-}NH_2$. These studies showed that protonation on the nitrogen atom lengthens and weakens the phosphorus nitrogen bond whereas protonation on the phosphorus atom shortens and strengthens the bond. This indicates that N-protonated may be the most prominent for effective reaction. ^{31}P NMR studies by Nurminen *et al*[79,84] showed that P-protonation of non-nucleoside amidites could be achieved by strong acids with pK_as below 10 in acetonitrile. These P-protonated species were then shown to react with nucleophiles significantly slower than the corresponding amidites in the presence of weak acids that showed no P-protonation. This, he proposed, was compatible with weak acids such as 1H-tetrazole protonating the amidite on nitrogen and not phosphorus.

4.2.1 Determination of activated species by ^{31}P NMR (non-nucleoside amidites)

The ^{31}P H-decoupled NMR spectrum (spectrum 3a, table 13) of dimethylphosphoramidite in deuterated acetonitrile gives a singlet at δ149ppm due to the amidite. There are also two other less significant singlets at δ129ppm and δ7ppm. Both of these are due to the reaction of the amidite with water, the latter being the H-phosphonate species and the singlet at δ129ppm is due to a P-O-P anhydride type structure (scheme 48).[79]
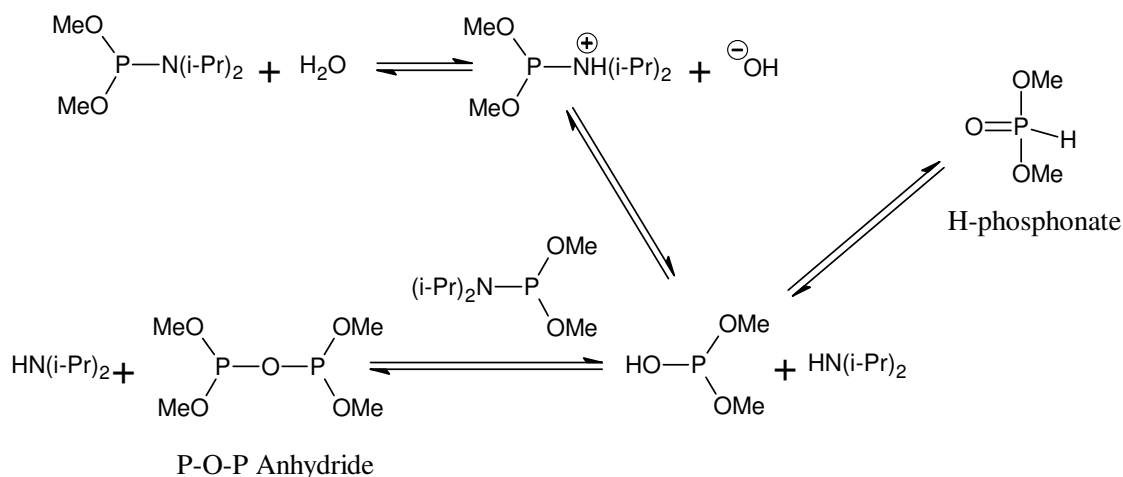
Scheme 48: Reaction of water with phosphoramidites to produce H-phosphonate and P-O-P anhydride.

On addition of one mole equivalent of saccharin to dimethylphosphoramidite in deuterated acetonitrile a very broad signal at δ139ppm is produced (spectrum 3b, table 13). To this sample one mole equivalent of *N*-methylimidazole was added, upon which the δ139ppm signal was replaced by a sharper signal at δ134pppm (spectrum 3c, table 13). Integration of these two spectra showed that addition of *N*-methylimidazole increased the relative amount of starting amidite (40-44%).

In a separate experiment, one mole equivalent of saccharin/*N*-methylimidazole salt was added to dimethylphosphoramidite and the resulting ^{31}P NMR spectrum (spectrum 3d, table 13) showed a relatively broad signal at δ136ppm which on addition of excess *N*-methylimidazole was removed and again the percentage of starting amidite was increased (45-61%) (spectrum 3e, table 13).

Sample Composition	% of amidite (δ 149ppm)	δ of activated species (%)	% of P-O-P (δ 129ppm)	% of H-phosphonate (δ 7ppm)
3a) DiMeN(i-Pr)₂	97	0	1	2
3b) DiMeN(i-Pr)₂/Saccharin	40	19	28	13
3c) DiMeN(i-Pr)₂/Saccharin/NMI	44	10	29	17
3d) DiMeN(i-Pr)₂/SMI	45	19	25	11
3e) DiMeN(i-Pr)₂/SMI/NMI	61	10	0	29

Table 13: ^{31}P NMR spectra of dimethylphosphoramidite with saccharin and *N*-methylimidazole in acetonitrile.
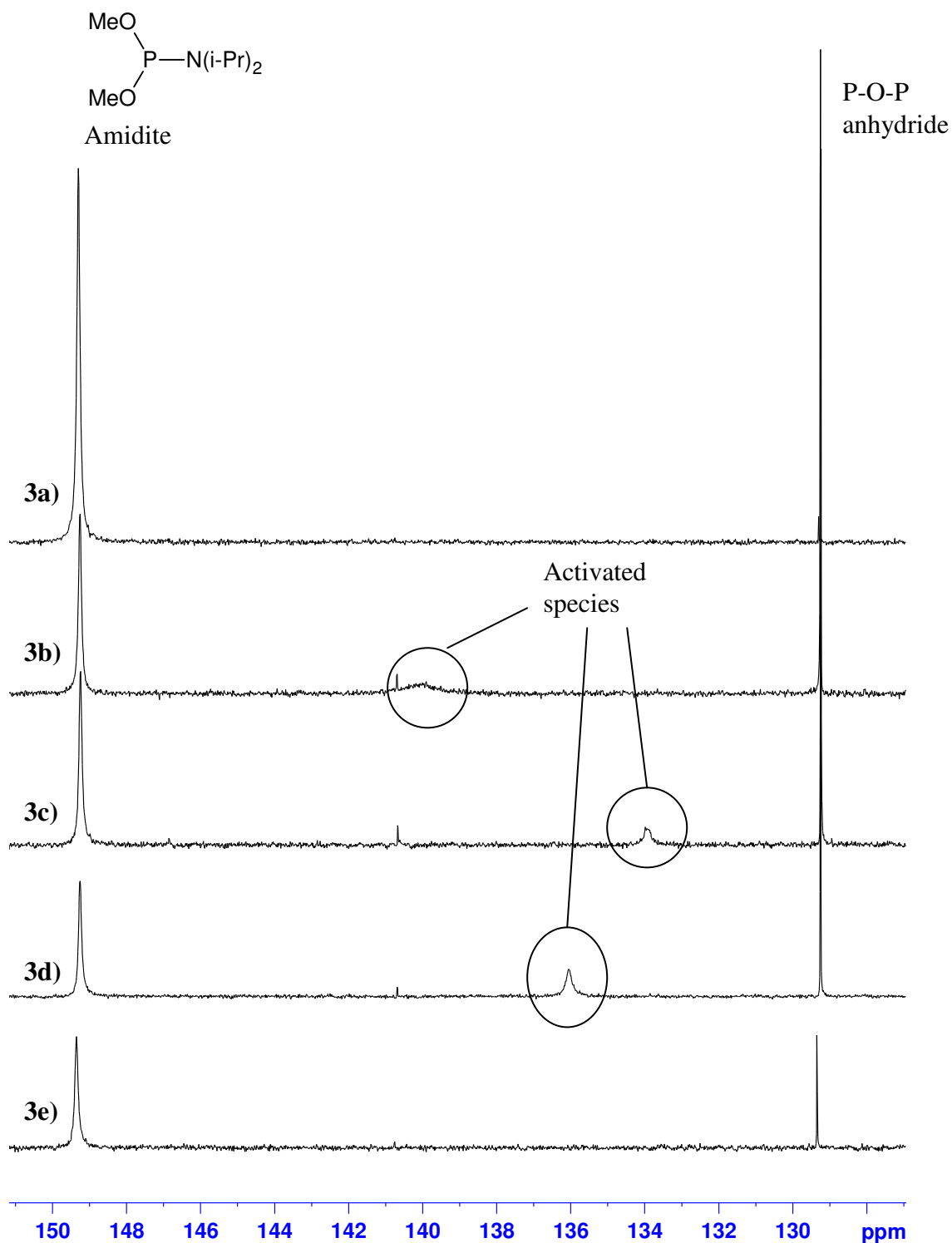
Spectra 3: **^{31}P NMR spectra in deuterated acetonitrile of a) 0.09 M dimethylphosphoramidite, b) 0.09 M dimethylphosphoramidite and 0.09 M saccharin (1:1) c) 0.09 M dimethylphosphoramidite, 0.09 M saccharin and 0.09 M *N*-methylimidazole (1:1:1), d) 0.09 M dimethylphosphoramidite and 0.09 M saccharin/*N*-methylimidazole salt (1:1) and e) 0.09 M dimethylphosphoramidite, 0.09 M saccharin/*N*-methylimidazole salt and 0.09 M *N*-methylimidazole (1:1:1).**

These experiments were repeated in deuterated chloroform. The starting amidite gave a singlet at δ149ppm (spectrum 4a, table 14) which on addition of one mole equivalent of saccharin was reduced and a new signal at δ141ppm was formed (spectrum 4b, table 14). This signal was very sharp in contrast to the broad signal produced in acetonitrile. Addition of one mole equivalent of *N*-methylimidazole to this sample again very clearly showed an increase in the relative concentration of the starting amidite (8-27%) and a reduction in the δ141ppm signal by over half (47-17%) with no change in its position or shape (spectrum 4c, table 14).

One mole equivalent of saccharin/*N*-methylimidazole salt was added to the amidite in deuterated chloroform and the sharp signal at δ141ppm was present in the ^{31}P NMR spectrum (spectrum 4d, table 14). This signal was again reduced in concentration (33-4%) on addition of excess *N*-methylimidazole and the starting amidites concentration was increased (41-75%) (spectrum 4e, table 14).

Sample Composition	% of amidite (δ 149ppm)	% of activated species (δ 141ppm)	% of P-O-P (δ 129ppm)	% of H-phosphonate (δ 7ppm)
4a) DiMeN(i-Pr)₂	97	0	2	1
4b) DiMeN(i-Pr)₂/Saccharin	8	47	2	43
4c) DiMeN(i-Pr)₂/Saccharin/NMI	27	17	8	48
4d) DiMeN(i-Pr)₂/SMI	41	33	3	23
4e) DiMeN(i-Pr)₂/SMI/NMI	75	4	1	20

Table 14: ^{31}P NMR spectra of dimethylphosphoramidite with saccharin and *N*-methylimidazole in chloroform.
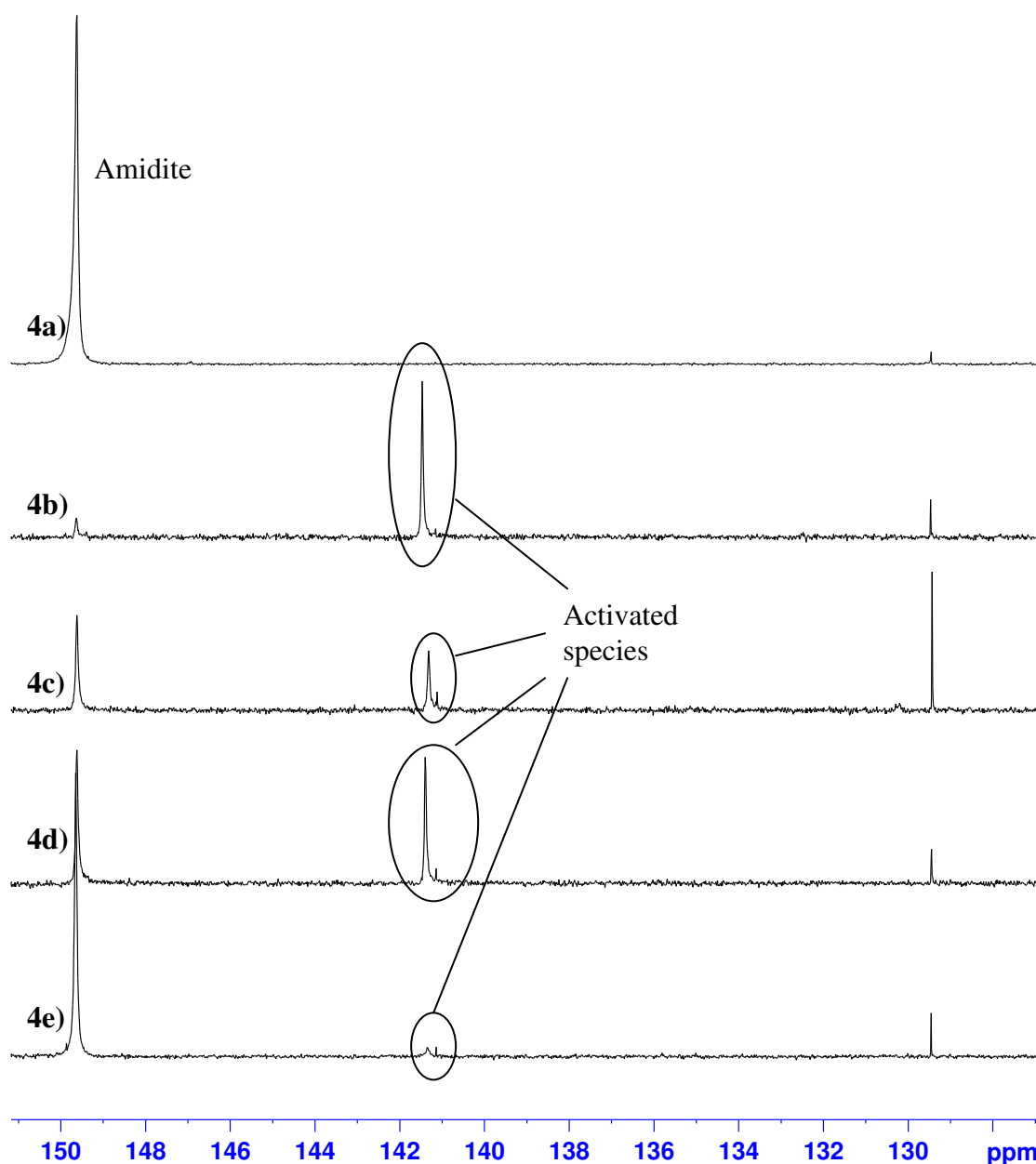
Spectra 4: **^{31}P NMR spectra in deuterated chloroform of a) 0.04 M dimethylphosphoramidite, b) 0.04 M dimethylphosphoramidite and 0.04 M saccharin (1:1), c) 0.04 M dimethylphosphoramidite, 0.04 M saccharin and 0.04 M *N*-methylimidazole (1:1), d) 0.04 M dimethylphosphoramidite and 0.04 M saccharin/*N*-methylimidazole salt (1:1) and e) 0.04 M dimethylphosphoramidite and 0.04 M saccharin/*N*-methylimidazole salt and 0.04 M *N*-methylimidazole (1:1:1).**

On addition of diisopropylamine to a deuterated chloroform solution of the amidite and one mole equivalent of saccharin/*N*-methylimidazole salt, a large decrease in the concentration of the signal at δ141ppm (29-1%) and an increase in starting amidite concentration (24-37%) were observed (spectrum 5b, table 15).

113

Sample Composition	% of amidite (δ 149ppm)	% of activated species (δ 141ppm)	% of P-O-P (δ 129ppm)	% of H-phosphonate (δ 7ppm)
5a) DiMeN(i-Pr)₂/SMI	24	29	4	43
5b) DiMeN(i-Pr)₂/SMI/5DIA	37	1	8	54

Table 15: ³¹P NMR spectra of dimethylphosphoramidite with saccharin and *N*-methylimidazole in chloroform.
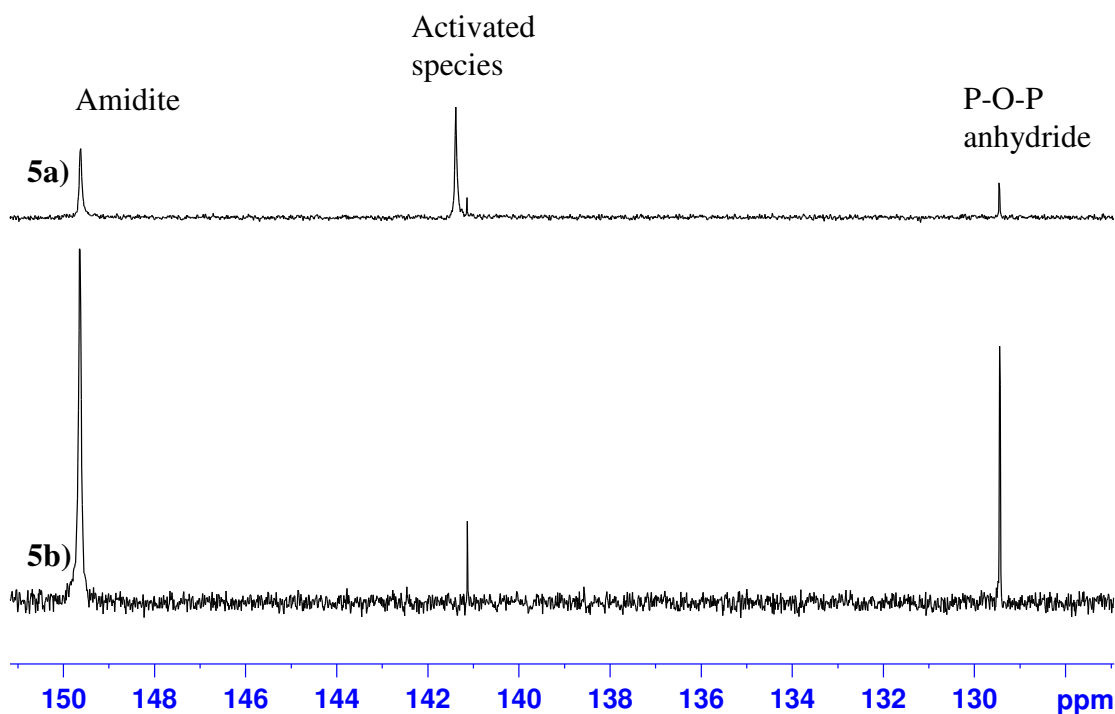
Spectra 5: ³¹P NMR spectra in deuterated chloroform of a) 0.04 M dimethylphosphoramidite and 0.04 M saccharin/N-methylimidazole salt (1:1) and b) 0.04 M dimethylphosphoramidite and 0.04 M saccharin/N-methylimidazole salt and 0.2 M diisopropylamine (1:1:5).

It is clear in both acetonitrile and chloroform that the activation reaction is reversible, with the addition of diisopropylamine and *N*-methylimidazole pushing the reaction back to reactants. *N*-Methylimidazole can form homo-conjugates with the starting saccharin/*N*-methylimidazole salt increasing the salt's stability and reducing its reactivity towards phosphoramidites. Any excess in diisopropylamine will form a stable salt with saccharin removing acidic protons from the system, reducing the degree of activation.

In chloroform only one activated species is formed due to the substitution of the diisopropylamine group with saccharin (scheme 49). On addition of *N*-methylimidazole the signal for the activated species shows only a reduction in concentration with no change in shape or chemical shift, indicating that the *N*-methylimidazole does not form the P-*N*-methylimidazole adduct in chloroform.
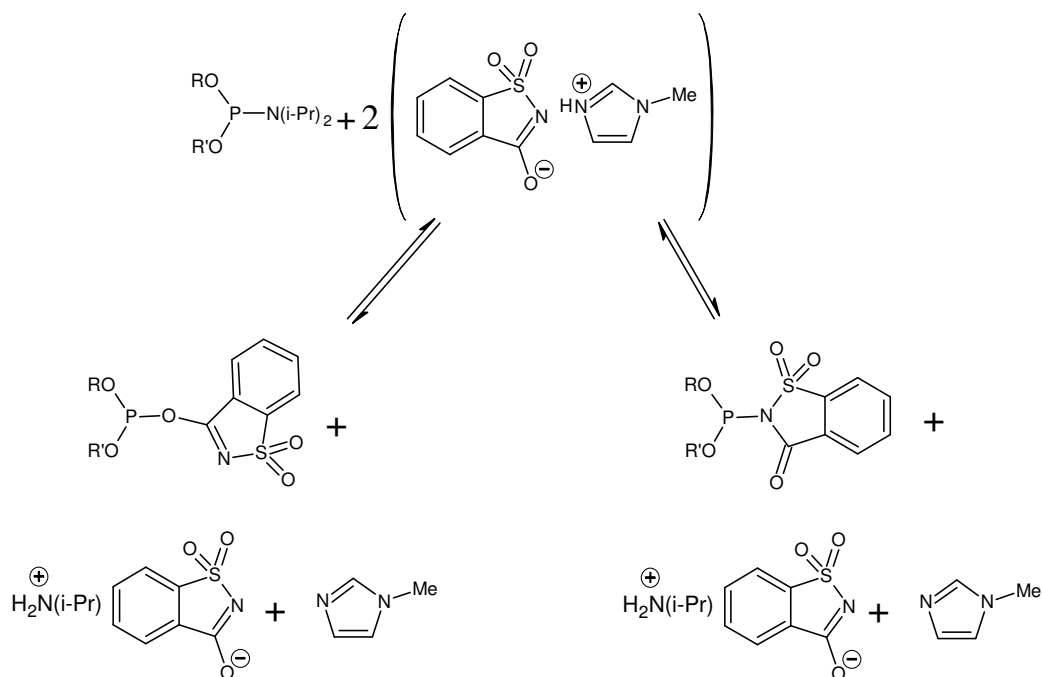
Scheme 49: Phosphoramidite activation in chloroform: formation of P-Saccharin adducts.

The ^{31}P NMR signal for the substitution of diisopropylamine with saccharin is very broad in acetonitrile possibly suggesting a relatively slow exchange process between the P-O-Saccharin and P-N-Saccharin species. On addition of *N*-methylimidazole this signal becomes sharper and a change in chemical shift is observed. The change in chemical shift indicates that the *N*-methylimidazole has an effect on the activated species and there may be an equilibrium in acetonitrile between P-O-Saccharin, P-N-Saccharin and the P-*N*-methylimidazole. The sharpening of the ^{31}P NMR signal indicates that the rate of exchange between the activated species has increased.

The differences observed in the two solvents could be explained by their differing polarities. The P-*N*-methylimidazole adduct is a charged molecule whose formation

will be unfavourable in non-polar solvents such as chloroform (dielectric constant of 4.7), but relatively favoured in the more polar solvent acetonitrile (dielectric constant 37.5). Therefore, in chloroform only the neutral P-Saccharin adducts will form, which are possibly in equilibrium (scheme 50). In acetonitrile all three species could potentially exist in equilibrium owing to the broadness of the NMR signals. If the formation of the P-*N*-methylimidazole adduct was faster than the formation of the P-Saccharin species, and in turn the P-Saccharin species could form faster via the P-*N*-methylimidazole adduct rather than through direct substitution with the amidite, an increase in exchange rate and a sharper ^{31}P NMR signal may be expected (scheme 50).
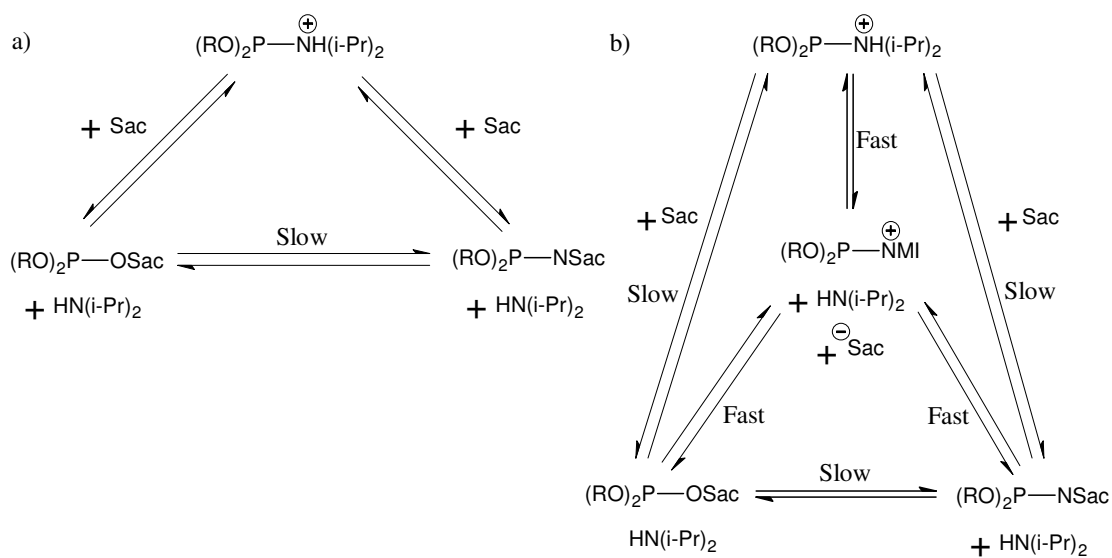
Scheme 50: Exchange between activated species a) in the absence of *N*-methylimidazole b) in the presence of *N*-methylimidazole.

4.2.2   Determination of activated species by ^{31}P NMR (nucleoside amidites)

The ^{31}P NMR H-decoupled spectrum of the 5'-4,4-dimethoxytritylthymidine-3'-β-cyanoethyl-*N,N*-diisopropylphosphoramidite (11) (scheme 51) in deuterated acetonitrile (spectrun 6a, table 16) has two singlets at δ147.90 and 147.83ppm, due to diastereoisomers of the molecule: chiral centres on the phosphorus and carbon 3 of the sugar.
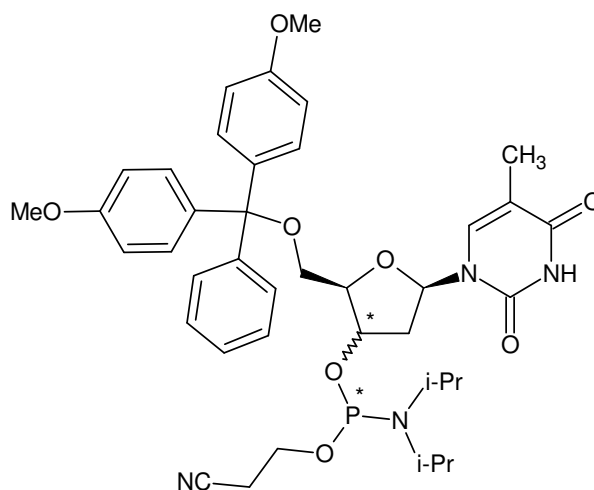
Scheme 51: Thymidine phosphoramidite (11) (chiral centres marked *).

The nucleoside amidites contain a 4,4-dimethoxytrityl protecting group on the sugar's 5' oxygen. This protecting group is acid labile and saccharin is a strong enough acid in acetonitrile to cause de-protection. The *N*-methylimidazole is therefore required to reduce the overall acidity of the reaction mixture and prevent detritylation.

Addition of saccharin/*N*-methylimidazole salt to the thymidine phosphoramidite (11) gives rise to a number of new signals (spectra 6b-6e, table 16). The signals that account for the majority of the phosphorus content are: a broad single peak at δ134ppm which increases in concentration on addition of excess salt, and a set of three signals at δ129ppm whose concentration is independent of salt concentration and is likely due to the P-O-P anhydride type species and its diastereoisomers. There are also two singlets at δ7ppm which show direct phosphorus-hydrogen coupling on a [31]P H-coupled spectrum and must be due to the H-phosphonate species.

117

Sample Composition	% of amidite (δ 149ppm)	% of activated species (δ 134ppm)	% of P-O-P (δ 129ppm)	% of H-phosphonate (δ 7ppm)
6a) T-amidite	100	0	0	0
6b) T-amidite/1SMI	42	12	36	10
6c) T-amidite/2SMI	20	35	38	7
6d) T-amidite/3SMI	4	30	38	28
6e) T-amidite/4SMI	0	55	21	24

Table 16: ^{31}P NMR spectra of thymidine phosphoramidite (11) with varying molar equivalents of saccharin/*N*-methylimidazole salt in acetonitrile
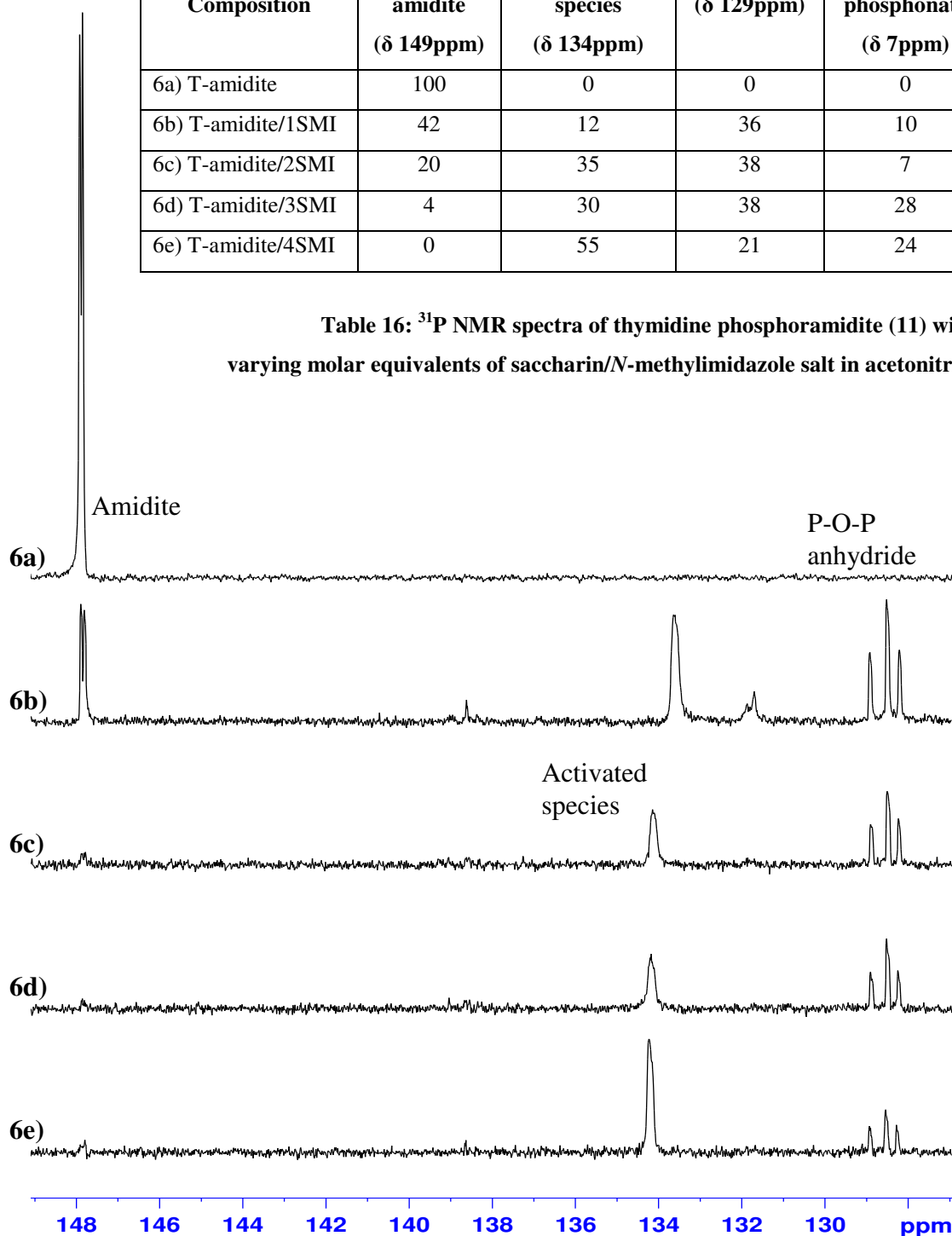
Spectra 6: ^{31}P NMR spectra in deuterated acetonitrile of a) 0.1 M thymidine phosphoramidite (11), b) 0.1 M thymidine phosphoramidite (11) with 0.1 M saccharin/*N*-methylimidazole salt (1:1), c) 0.1 M thymidine phosphoramidite (11) with 0.2 M saccharin/*N*-methylimidazole salt (1:2), d) 0.05 M thymidine phosphoramidite (11) with 0.15 M saccharin/*N*-methylimidazole salt (1:3) and e) 0.0375 M thymidine phosphoramidite (11) with 0.15 saccharin/*N*-methylimidazole salt (1:4).

A study of the phosphoramidite activation mechanism indicates that two equivalents of saccharin/*N*-methylimidazole are required to supply the two protons needed to form the final saccharin/diisopropylamine salt. The experiments described above, show that most of the amidite does react with two equivalents but that three equivalents of the saccharin/*N*-methylimidazole salt are required for complete loss of starting material, indicating that the starting amidite is in equilibrium with the activated species.

The broad signal at δ134ppm is the only signal which is saccharin/*N*-methylimidazole salt dependent and therefore represents the activated species. The signal is comparable in shape and chemical shift to the product of the reaction of dimethylphosphoramidite with the saccharin/*N*-methylimidazole salt (spectra 3). It seems likely then that the signal at δ134ppm is due to the equilibrium between P-O-Saccharin, P-N-Saccharin and P-*N*-methylimidazole.

Additions of diisopropylamine and excess *N*-methylimidazole (spectrum 7, table 17) leads to a reduction in the signal at δ134ppm and an increase in the percentage of starting amidite, again showing that the reaction is reversible and in equilibrium.

Sample Composition	% of amidite (δ 149ppm)	% of activated species (δ 134ppm)	% of P-O-P (δ 129ppm)	% of H-phosphonate (δ 7ppm)
7a) T-amidite/2SMI	20	35	38	7
7b) T-amidite/2SMI/5NMI	44	0	26	30
7c) T-amidite/4SMI	0	32	33	35
7d) T-amidite/4SMI/4DIA	27	0	29	44

Table 17: ^{31}P NMR spectra of thymidine phosphoramidite (11) with saccharin/*N*-methylimidazole salt and excess *N*-methylimidazole and diisopropylamine in acetonitrile.
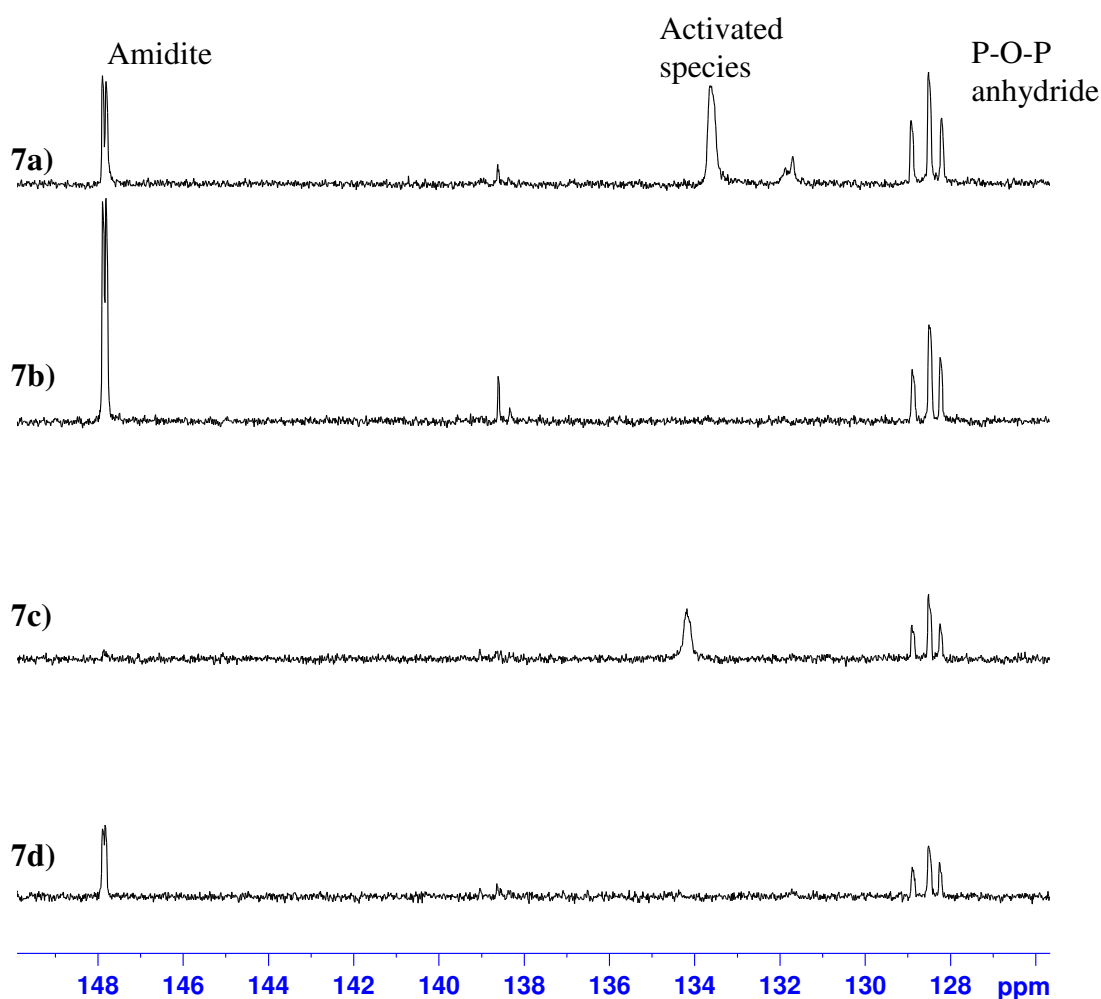
Spectra 7: **^{31}P NMR spectra in deuterated acetonitrile of a) 0.1 M thymidine phosphoramidite (11) with 0.2 M saccharin/*N*-methylimidazole salt (1:2), b) 0.1 M thymidine phosphoramidite (11) with 0.2 M saccharin/*N*-methylimidazole salt and 0.5 M *N*-methylimidazole (1:2:5), c) 0.0375 M thymidine phosphoramidite (11) with 0.015 M saccharin/*N*-methylimidazole salt (1:4) and d) 0.0375 M thymidine phosphoramidite (11) with 0.15 M saccharin/*N*-methylimidazole salt and 0.15 M diisopropylamine (1:4:4).**

Addition of diisopropylamine to thymidine phosphoramidite (11) prior to saccharin/*N*-methylimidazole salt addition shows a decrease in the extent of reaction upon addition of the salt (spectra 8, table 18). This does not necessarily show an equilibrium process as the diisopropylamine will undergo protonation by the saccharin/*N*-methylimidazole salt reducing the amount of activation possible. Unfortunately in these experiments the signal for the activated species is not present as the concentration of water in each sample is high enough to react with all of the activated species to form either the H-phosphonate or P-O-P anhydride species.

120

Sample Composition	% of amidite (δ 149ppm)	% of activated species (δ 134ppm)	% of P-O-P (δ 129ppm)	% of H-phosphonate (δ 7ppm)
8a) T-amidite/DIA/3SMI	11	6	38	43
8b) T-amidite/2DIA/3SMI	21	0	22	56
8c) T-amidite/3DIA/3SMI	91	0	0	9

Table 18: ³¹P NMR spectra of thymidine phosphoramidite (11) with varying molar equivalents of diisopropylamine and saccharin/*N*-methylimidazole salt in acetonitrile.
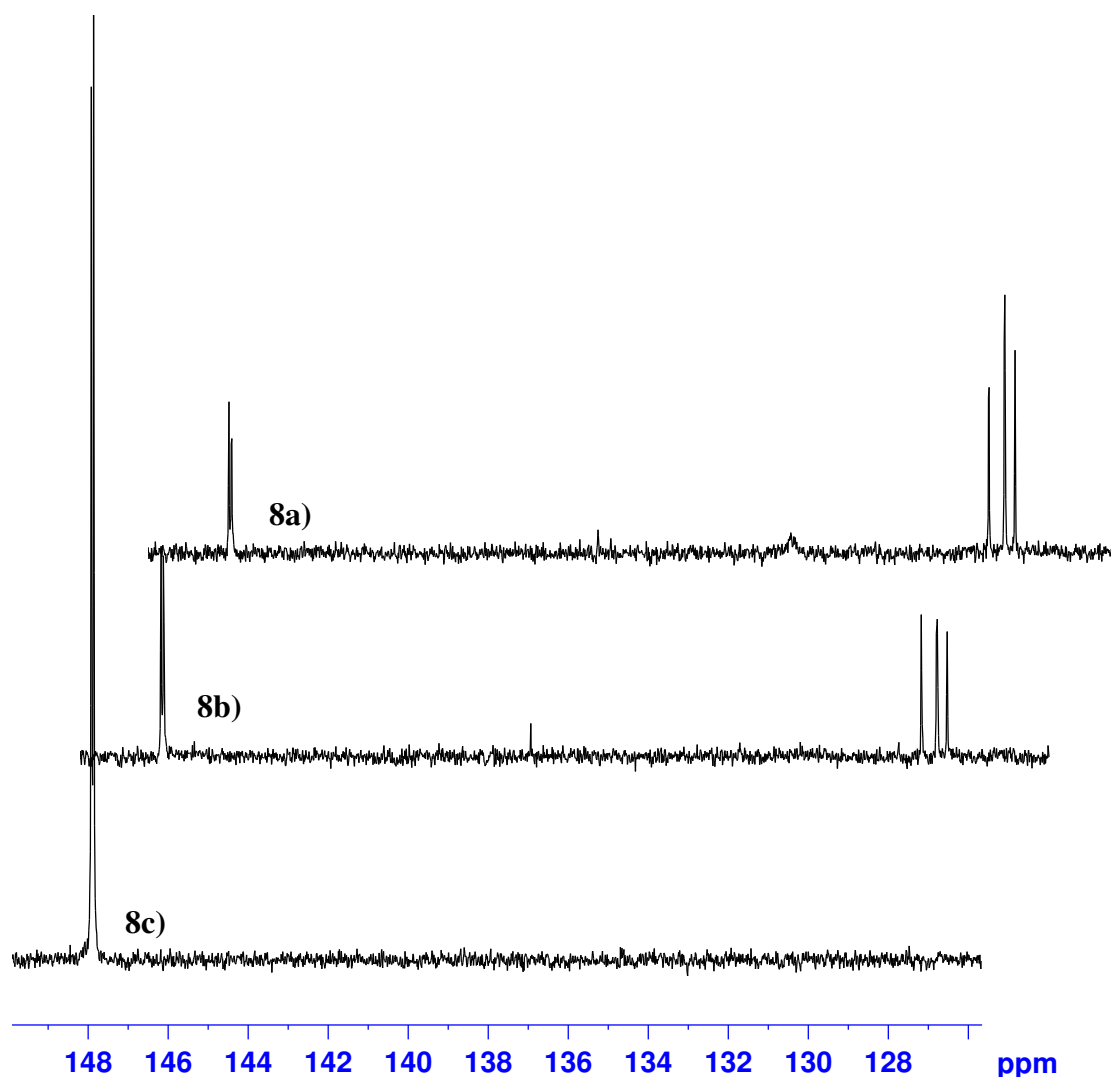
Spectra 8: ³¹P NMR spectra (with off set) in deuterated acetonitrile of a) 0.05 M thymidine phosphoramidite (11) with 0.05 M diisopropylamine and 0.015 M saccharin/N-methylimidazole salt (1:1:3), b) 0.05 M thymidine phosphoramidite (11) with 0.1 M diisopropylamine and 0.15 M saccharin/N-methylimidazole salt (1:2:3) and c) 0.05 M thymidine phosphoramidite (11) with 0.15 M diisopropylamine and 0.15 M saccharin/N-methylimidazole salt (1:3:3).

The addition of saccharin/*N*-methylimidazole to thymidine phosphoramidite (11) in deuterated chloroform gives ^{31}P NMR signals (spectra 9, table 19) that are similar to those produced by dimethylphosphoramidite and the saccharin/*N*-methylimidazole salt (spectra 4). The thymidine phosphoramidite (I) gives signals for the H-phosphonate and P-O-P anhydride at δ7ppm and δ129ppm respectively and a sharp signal at δ135ppm due to the activated P-saccharin species.

Sample Composition	% of amidite (δ 149ppm)	% of activated species (δ 135ppm)	% of P-O-P (δ 129ppm)	% of H-phosphonate (δ 7ppm)
9a) T-amidite	100	0	0	0
9b) T-amidite/SMI	44	22	4	30

Table 19: ^{31}P NMR spectra of thymidine phosphoramidite (11) with saccharin/*N*-methylimidazole salt in chloroform.
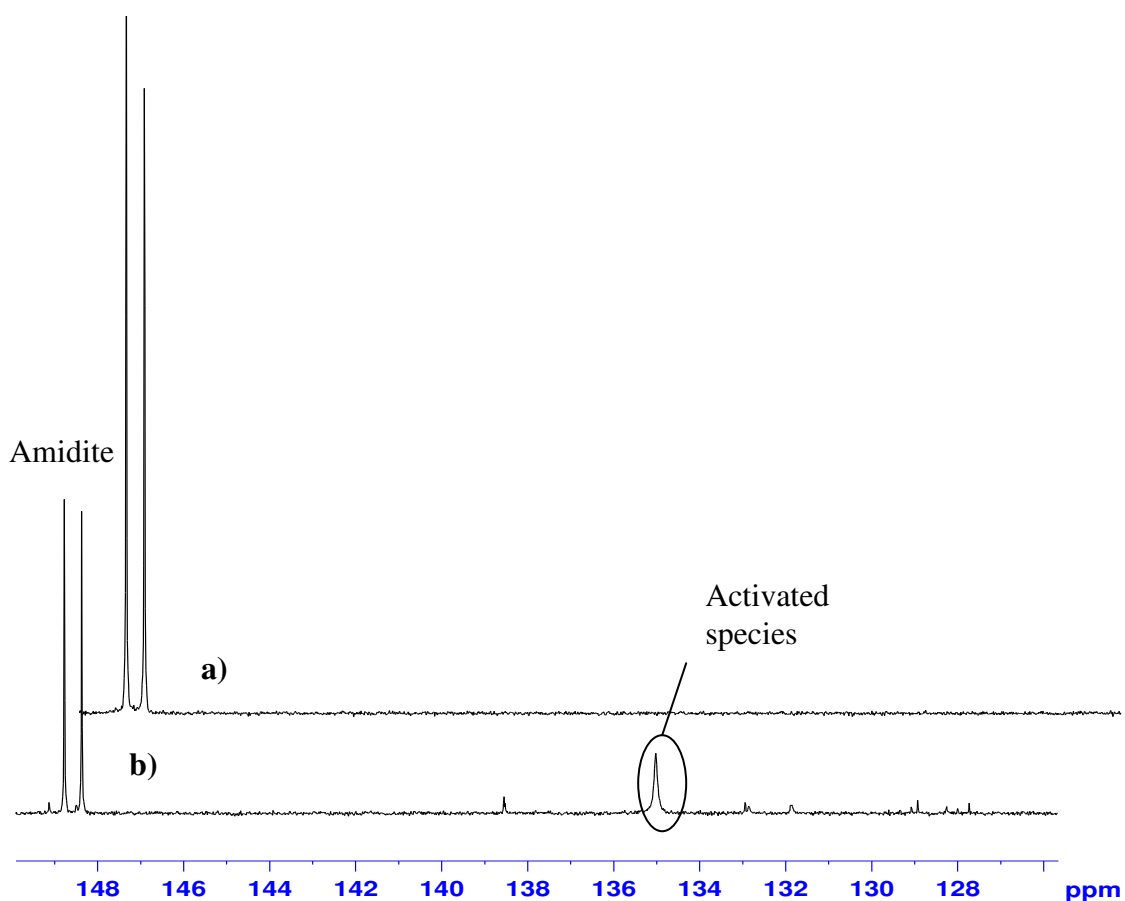
Spectra 9: ^{31}P NMR spectra (with off set) in deuterated chloroform of a) 0.04 M thymidine phosphoramidite (11) and b) 0.04 M thymidine phosphoramidite (11) and 0.04 M saccharin/N-methylimidazole salt (1:1).

4.2.3 Formation of P-O-C bonds with acetic acid and thymidine phosphoramidite (11)

To identify the ^{31}P NMR chemical shift of P-O-C system in a similar compound to those under study, acetic acid was used in place of the saccharin/*N*-methylimidazole salt. Acetic acid was chosen as its acidity is not high enough to cause detritylation and can only bond to phosphorus via its carbonyl oxygen.

On addition of acetic acid to thymidine phosphoramidite (11) in deuterated acetonitrile, two new signals at δ131.74 and δ131.11ppm were present (spectra 10, table 20) which increased in concentration on addition of excess acetic acid. The two signals are presumably due to replacement of the diisopropylamine group with acetic acid to form a new P-O-C system (scheme 52). Two signals are observed because of the two possible diastereoisomers. The activated species formed in this reaction is more stable than the species formed with saccharin/*N*-methylimidazole salt as indicated by the much slower formation of H-phosphonate: no H-phosphonate was detectable after 20 minutes; 27% H-phosphonate was detected after 20 hours (spectra 11, table 21). The chemical shift of δ132ppm can be compared with the δ134/139ppm observed with saccharin and saccharin/*N*-methylimidazole, compatible with P-O bond formation.
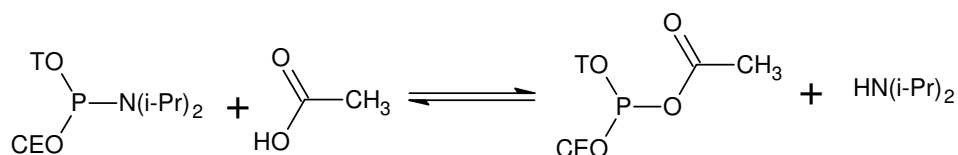
Scheme 52: Reaction between thymidine phosphoramidite (11) and acetic acid.

Sample Composition	% of amidite (δ 149ppm)	% of activated species (δ 132ppm)	% of H-phosphonate (δ 7ppm)
10a) T-amidite	100	0	0
10b) T-amidite/2 acetic acid	45	55	0
10c) T-amidite/3 acetic acid	23	73	4
10d) T-amidite/4 acetic acid	12	85	3

Table 20: ^{31}P NMR spectra of thymidine phosphoramidite (11) with acetic acid in acetonitrile.
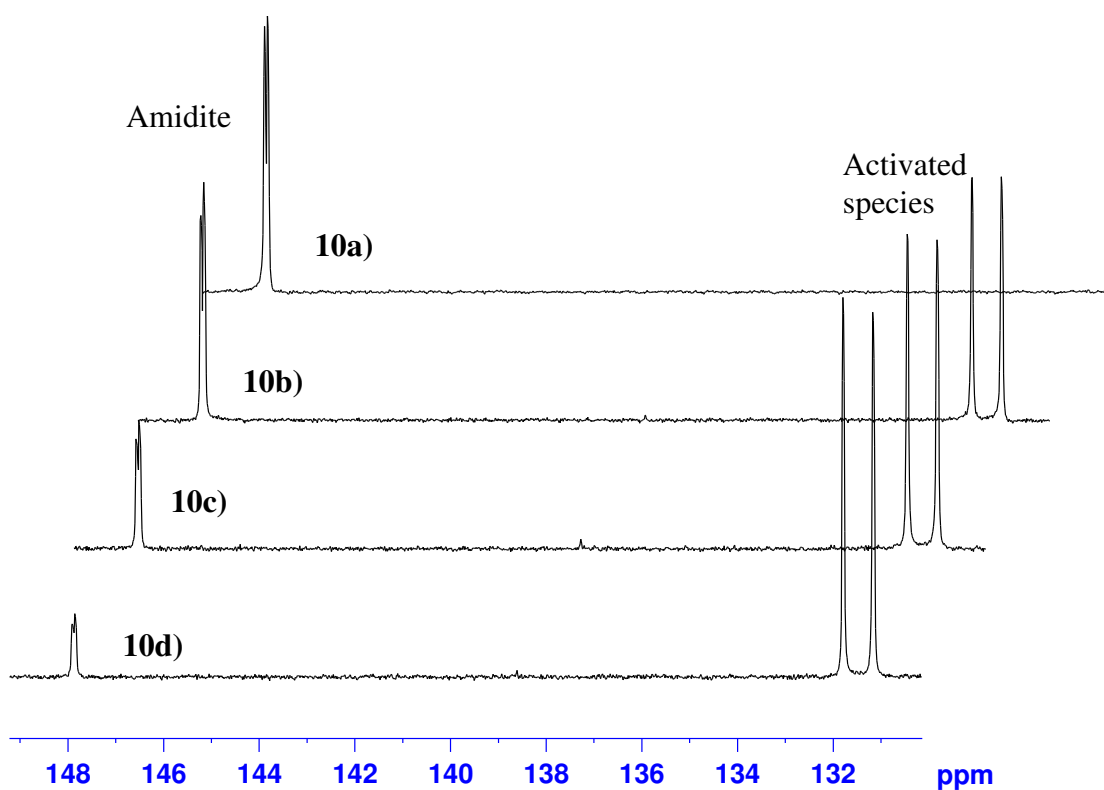
Spectra 10: **^{31}P NMR spectra (with off set) in deuterated acetonitrile of 0.1 M thymidine phosphoramidite (11) with increasing concentrations of acetic acid: a) no acetic acid, b) 0.2 M (1:2), c) 0.3 M (1:3) and d) 0.4 M (1:4).**

Sample Composition	% of amidite (δ 149ppm)	% of activated species (δ 132ppm)	% of H-phosphonate (δ 7ppm)
11a) T-amidite/2 acetic acid (20 mins)	45	55	0
11b) T-amidite/2 acetic acid (20 hrs)	4	67	29

Table 21: ^{31}P NMR spectra of thymidine phosphoramidite (11) with acetic acid in acetonitrile.
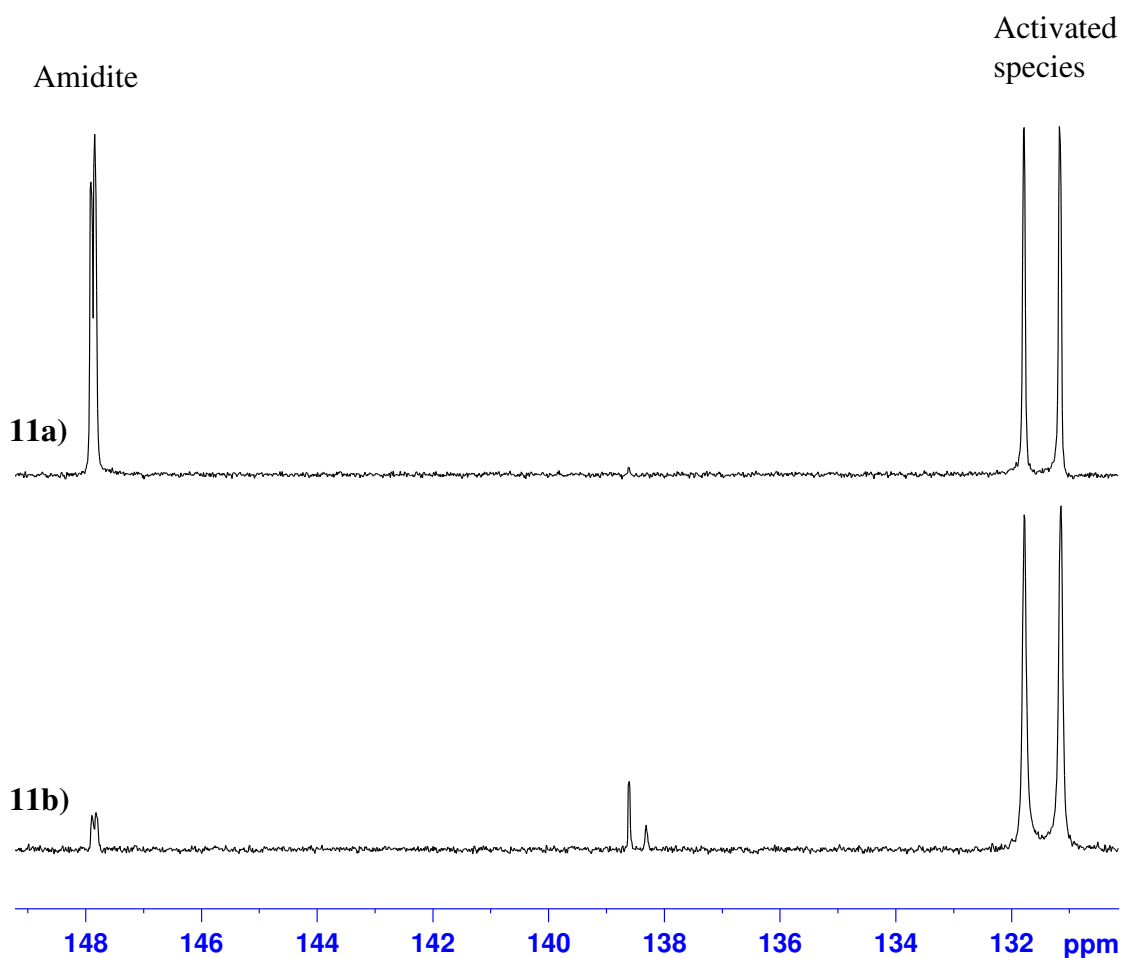
Spectra 11: ^{31}P NMR spectra in deuterated acetonitrile of 0.1 M thymidine phosphoramidite (11) with 0.2 M acetic acid (1:2) after a) 20 minutes and b) 20 hours.

4.2.4 Formation of P-N-C Bonds with *N*-methylimidazole and diethylchlorophosphite

To identify the ^{31}P NMR chemical shift of P-N-C systems in a similar compound to those under study, diethylchlorophosphite was reacted with *N*-methylimidazole in deuterated acetonitrile.

Diethylchlorophosphite gives a singlet at δ167ppm in a ^{31}P H-decoupled NMR spectrum (spectra 12, table 22). On addition of one mole equivalent *N*-methylimidazole this signal is completely replaced by a broad signal at δ162ppm presumably due to the substitution of the chloro group with an *N*-methylimidazole molecule (scheme 53).

There are also two other signals: one at δ128.38ppm and one at δ7ppm due to H-phosphonate.
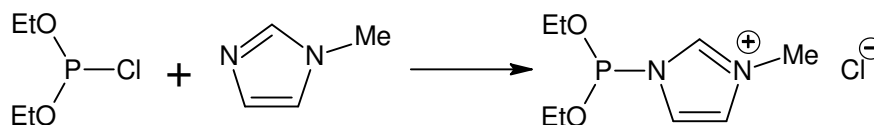
Scheme 53: Reaction between diethylchlorophosphite and *N*-methylimidazole.

On addition of excess *N*-methylimidazole the broad signal at δ162ppm moves up-field by a few ppm and becomes broader and less symmetrical. The signal at δ128ppm stays at the same position and shape and is probably due to the P-O-P anhydride type species (spectra 12, table 22).

The δ162ppm signal which broadens and moves up-field could be the time averaged signal for equilibrium between diethylchlorophosphite and P-*N*-methylimidazole species or alternatively homo-conjugation of excess *N*-methylimidazole molecules. In the 1:1 sample the bonded *N*-methylimidazole will 'pull' electrons from the phosphorus to stabilize its own positive charge, leaving the phosphorus with a partial positive charge. As the concentration of *N*-methylimidazole is increased, the excess *N*-methylimidazole could associate with the phosphorus bonded *N*-methylimidazole (scheme 54). If this self-association was more effective than solvation by acetonitrile in reducing the charge on the ion, then this may decrease the positive charge density on phosphorus. This reduction in positive charge will shift the ^{31}P NMR up-field. The same pattern can be seen on the ^{1}H NMR spectra of the same sample: as the concentration of *N*-methylimidazole is increased the chemical shift of the *N*-methylimidazole protons move up-field.
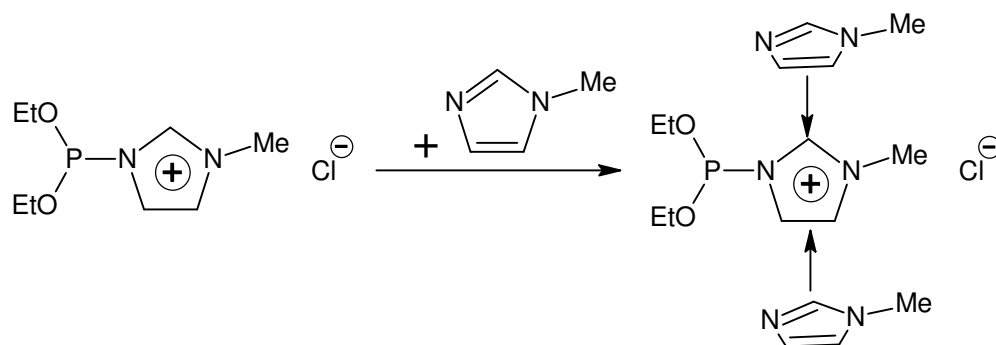
Scheme 54: Self-association of *N*-methylimidazole molecules through Π-Π stacking of *N*-methylimidazole.

Self-association of imidazole and *N*-methylimidazole has been described in aqueous solvents.[133] The planar and aromatic features of imidazole and its *N*-substituted derivatives, allow stacking of the molecules through π-π interactions. There is also the possibility of stacking via hydrogen bonding, but this can only occur in the un-substituted imidazole as the presence of a substituent on nitrogen removes a hydrogen bond donor site.[133]

Sample Composition	δ of main species (ppm)
12a) diethylcholorophosphite	167
12b) diethylcholorophosphite/NMI	162
12c) diethylcholorophosphite/2NMI	161
12d) diethylcholorophosphite/3NMI	159
12e) diethylcholorophosphite/4NMI	155
12f) diethylcholorophosphite/5NMI	151

Table 22: ^{31}P NMR spectra of diethylchlorophosphite with varying molar equivalents *N*-methylimidazole in acetonitrile.

Spectra 12: ^{31}P NMR spectra of 0.1 M diethylchlorophosphite in deuterated acetonitrile with increasing concentrations of *N*-methylimidazole: a) no *N*-methylimidazole, b) 0.1 M (1:1), c) 0.2 M (1:2), d) 0.3 M (1:3), e) 0.4 M (1:4) and f) 0.5 M (1:5) of *N*-methylimidazole.

To further study the system a sample of diethylchlorophosphite with five equivalents of *N*-methylimidazole was cooled to -35°C. At room temperature the broad signal was at δ156.3ppm. On cooling this signal became sharper and moved up-field to δ128.1ppm (spectra 13, table 23). There is an impurity that can be seen in the spectra at approximately δ138ppm which remains at the same chemical shift upon cooling as does the signal for the P-O-P anhydride, therefore the large change in chemical shift observed for the activated species must indicate some change in its nature. This lends further evidence to self-association of *N*-methylimidazole molecules: as the temperature is lowered the *N*-methylimidazole molecules will become more stable in their associated form, reducing the amount of positive charge on the phosphorus and shifting the NMR signal up-field and increasing its sharpness.

The decrease in temperature also affected the chemical shifts of the protons on both the *N*-methylimidazole and diethylchlorophosphite. The protons of *N*-methylimidazole all moved down-field, whereas the protons of diethylchlorophosphite showed a slight up-field shift. Association of *N*-methylimidazole protons would cause a down-field shift in the protons because as the associated form becomes more stable with decreasing temperature the positive charge will be shared out, effectively reducing the magnitude of the charge, shifting the ^{1}H NMR signals down-field.

Spectra Number	Temperature of Sample (K)	δ of signal (ppm)
13a)	295	156.3
13b)	285	150.4
13c)	273	144.2
13d)	268	141.0
13e)	263	137.9
13f)	258	135.3
13g)	253	132.7
13h)	248	130.8
13i)	243	129.3
13j)	238	128.1

Table 23: ^{31}P NMR spectra of diethylchlorophosphite with 5 molar equivalents *N*-methylimidazole at various temperatures in acetonitrile.
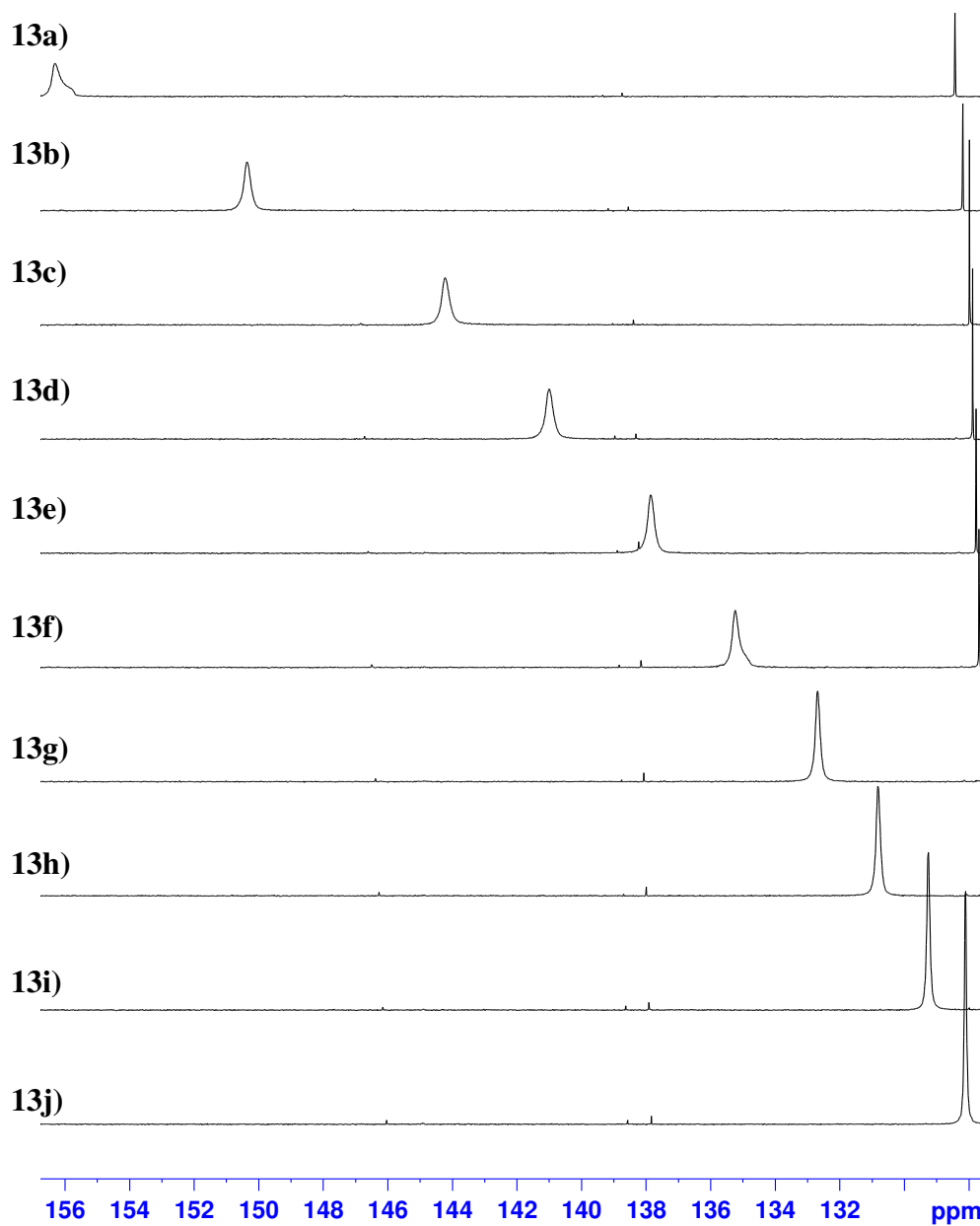
Spectra 13: ^{31}**P NMR spectra of 0.1 M diethylchlorophosphite in deuterated acetonitrile with 0.5 M** *N*-**methylimidazole (1:5) at various temperatures: a) 295K, b) 285K, c) 273K, d) 268K, e) 263K, f) 258K, g) 253K, h) 248K, i) 243K and j) 238K.**

4.2.5   Formation of P-N-C bonds with dimethylaminopyridine and diethylchlorophosphite

One equivalent of dimethylaminopyridine was added to a sample of diethylchlorophosphite in deuterated acetonitrile which gave a ^{31}P NMR spectrum (spectra 14, table 24) with a broad signal at δ142ppm, a signal at δ128.28ppm due to the P-O-P anhydride and a negligible amount of H-phosphonate. The broad signal at δ142ppm is presumably due to the replacement of the chloro group with the dimethylaminopyridine (scheme 55).
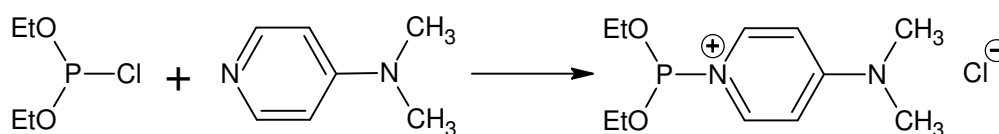
Scheme 55: Reaction between diethylcholorophosphite and dimethylaminopyridine.

Sample Composition	% at δ 166ppm	% of activated species (δ 142ppm)
14a) diethylchlorophosphite	97	0
14b) diethylcholorophosphite/DMAP	0	72

Table 24: ^{31}P NMR spectra of diethylchlorophosphite with dimethylaminopyridine in acetonitrile.
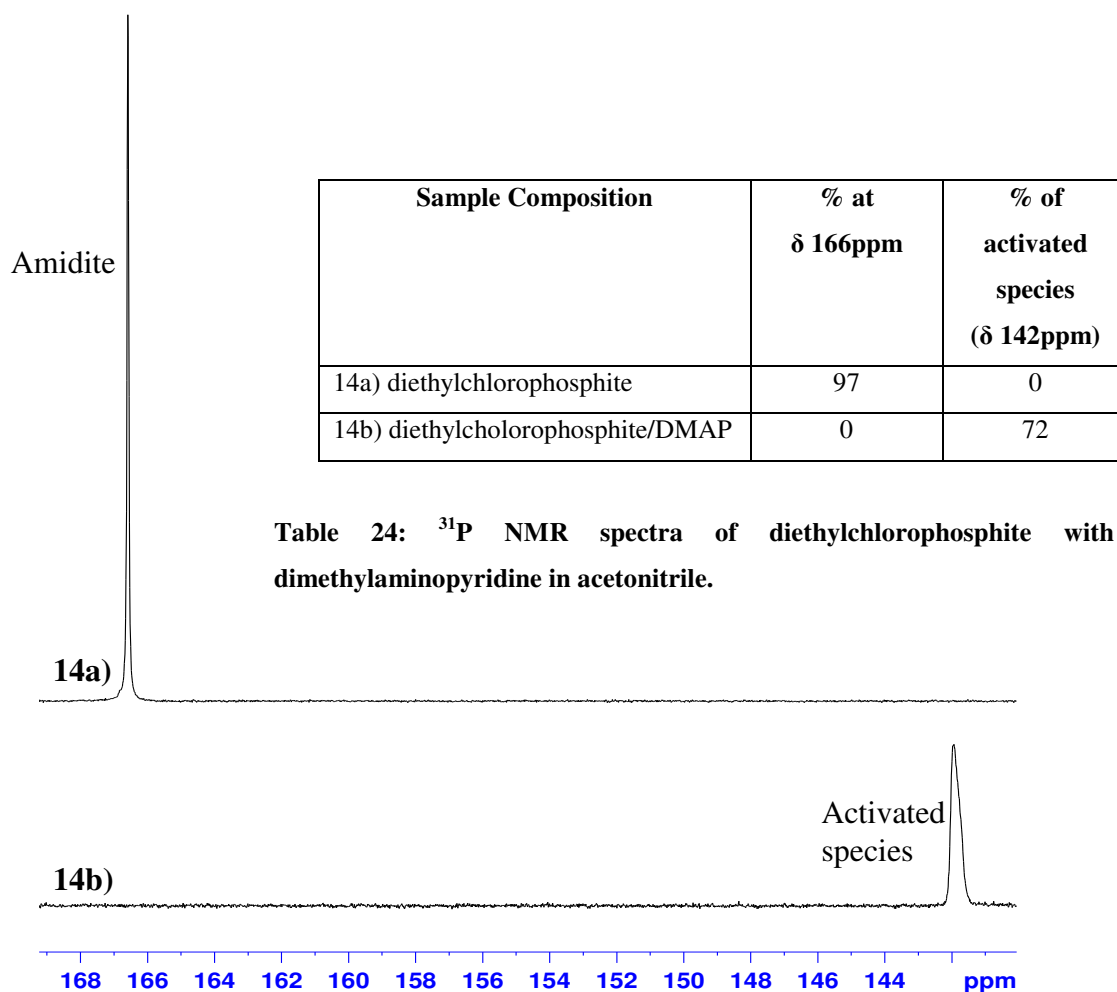
Spectra 14: ^{31}P NMR spectra in deuterated acetonitrile of a) 0.2 M diethylchlorophosphite and b) 0.2 M diethylchlorophosphite and 0.2 M dimethylaminopyridine.

Table 25 summarises the ^{31}P NMR chemical shifts in acetonitrile of the reactions described previously. The chemical shift of P-N species resonate between δ142-162ppm and P-O species resonate further up-field at approximately δ132ppm. The chemical shifts of the P-saccharin intermediate resonate at approximately δ135ppm and it seems likely that this indicates bonding through the saccharin's carbonyl oxygen atom.
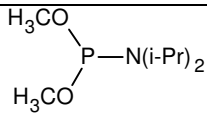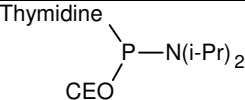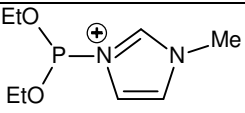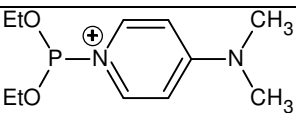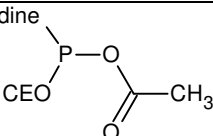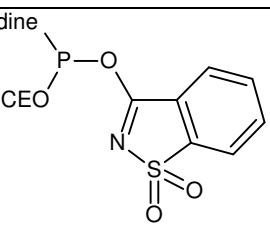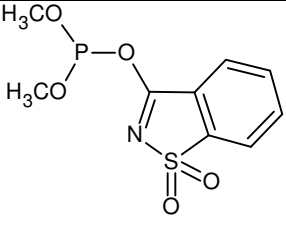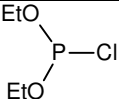
Sample composition	Probable structure	^{31}P NMR chemical shift (ppm)
Dimethylphosphoramidite	H₃CO, H₃CO–P–N(i-Pr)₂	149
Thymidine phosphoramidite (11)	Thymidine, CEO–P–N(i-Pr)₂	149
Diethylchlorophsphite + *N*-methylimidazole	EtO, EtO–P–⊕N (N-methylimidazolium)–Me	150-162 Varies with concentration of *N*-methylimidazole.
Diethylchlorophosphite + Dimethylaminopyridine	EtO, EtO–P–⊕N (pyridinium)–N(CH₃)₂	142
Thymidine phosphoramidite (11) + acetic acid	Thymidine, CEO–P–O–C(=O)–CH₃	132
Thymidine phosphoramidite (11) + saccharin/*N*-methylimidazole	Thymidine, CEO–P–O–(benzisothiazole S,S-dioxide)	134
Dimethylphosphoramidite + saccharin + *N*-methylimidazole	H₃CO, H₃CO–P–O–(benzisothiazole S,S-dioxide)	136-140 Varies with order saccharin and *N*-methylimidazole added.
Diethylchlorophophite	EtO, EtO–P–Cl	166

Table 25: Summary of ^{31}P NMR chemical shifts.

4.2.6   P-O-saccharin versus P-N-saccharin: activation with ^{15}N labelled saccharin

In order to distinguish between P-O saccharin and P-N saccharin, ^{15}N labelled saccharin was synthesised as discussed in section 2.4.3.3. The ^{15}N NMR spectrum for the labelled saccharin gave a sharp signal at δ153ppm. Addition of *N*-methylimidazole to the saccharin saw the disappearance of this signal and the presence of a broader signal at δ203ppm (spectrum 15a, table 26), compatible with proton transfer from saccharin to *N*-methylimidazole. Addition of thymidine phosphoramidite (11) saw further broadening of the signal and a slight down field shift to δ205ppm (spectra 15b, table 26).

Sample Composition	δ position (ppm)
[15]N-saccharin	152.7
15a) ^{15}N-Saccharin/*N*-methylimidazole	203.4
15b) ^{15}N-Saccharin/*N*-methylimidazole/T-amidite	205.0

Table 26: ^{15}N NMR spectra of synthesised ^{15}N-saccharin with *N*-methylimidazole and thymidine phosphoramidite (11).
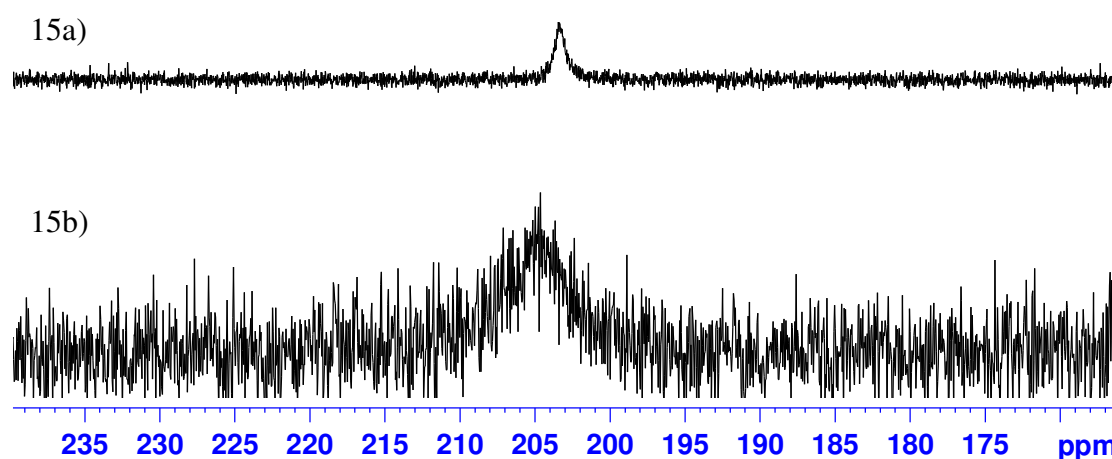
Spectra 15: ^{15}N NMR spectra of synthesised 0.09 M ^{15}N-saccharin with a) 0.09 M N-methylimidazole (1:1) and b) 0.09 M *N*-methylimidazole and 0.09 M thymidine phosphoramidite (11) (1:1:1).

If there was any P-N-Saccharin present in the sample then the ^{15}N NMR signal would be visible as two peaks due to coupling with the phosphorus atom but this is not the case. The only possible evidence of any P-N formation is the broadening of the signal which could suggest an exchange process between P-N and P-O-Saccharin.

The ^{31}P NMR spectra (spectrum 16) of the same samples also showed no coupling between phosphorus and the labelled nitrogen, only the signal at δ134ppm seen previously with the non-labelled saccharin was present. This indicates the P-N-saccharin formation is not significant that the P-O-saccharin is the predominant species.
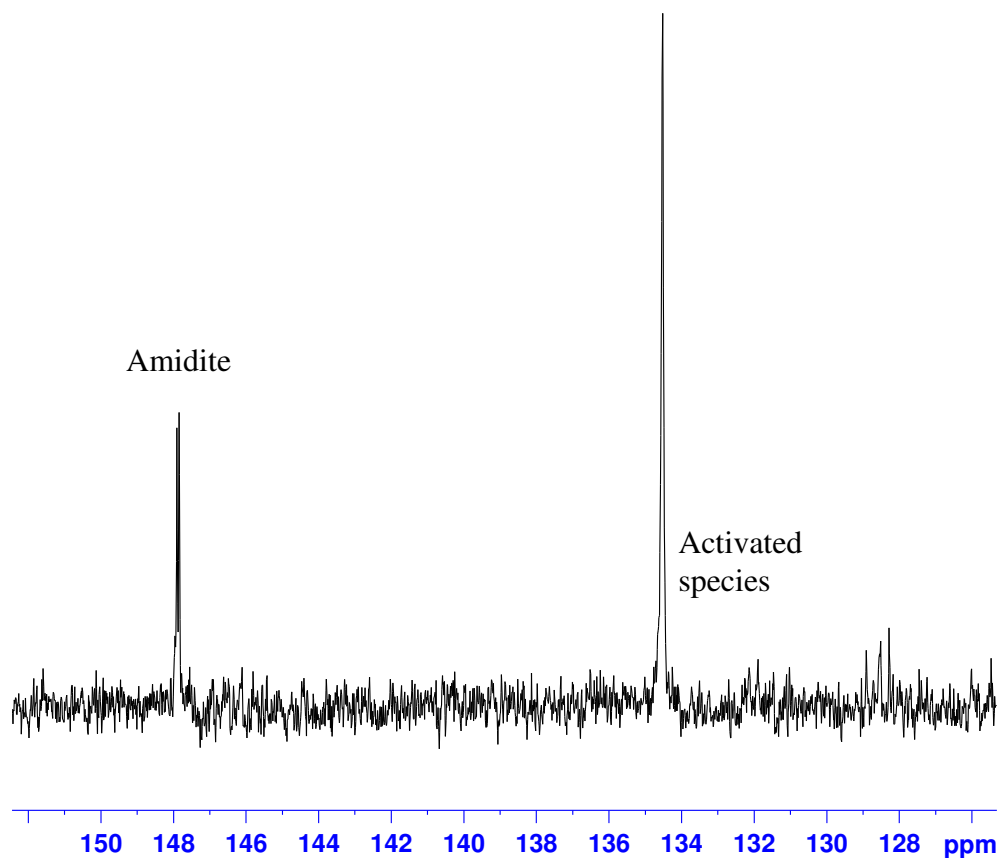
Spectra 16: ^{31}P NMR spectrum of 0.09 M ^{15}N-saccharin/N-methylimidazole salt with 0.09 M thymidine phosphoramidite (11) (1:1).

4.2.7 P-O-saccharin versus P-N-saccharin: infrared studies

To determine whether saccharin is bonded through its oxygen or nitrogen atom to the phosphorus of dimethylphosphoramidite, FT-IR studies were undertaken in deuterated acetonitrile. Similar experiments could not be performed in chloroform due to poor solubility of reagents.

P-O-saccharin   P-N-saccharin
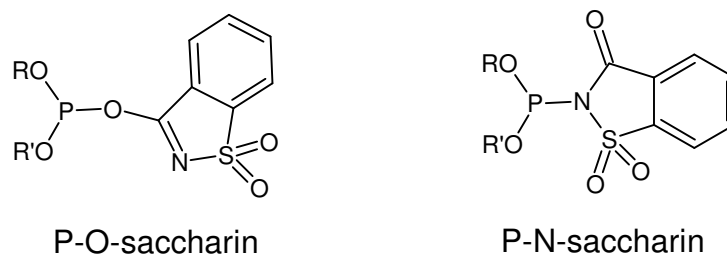
The carbonyl bond of saccharin absorbs IR radiation at 1744cm^{-1} (figure 39). On addition of *N*-methylimidazole this signal is lost (figure 40), compatible with proton transfer and anion formation resulting in a loss of double bond character in the carbonyl group. This also indicates that the saccharin anion carries its negative charge predominately on oxygen in the saccharin/*N*-methylimidazole salt. Another tautomer of the saccharin anion is that with the negative charge on nitrogen (scheme 56). If there was significant negative charge density on nitrogen, then presumably a carbonyl stretching frequency would be observed in the normal range.
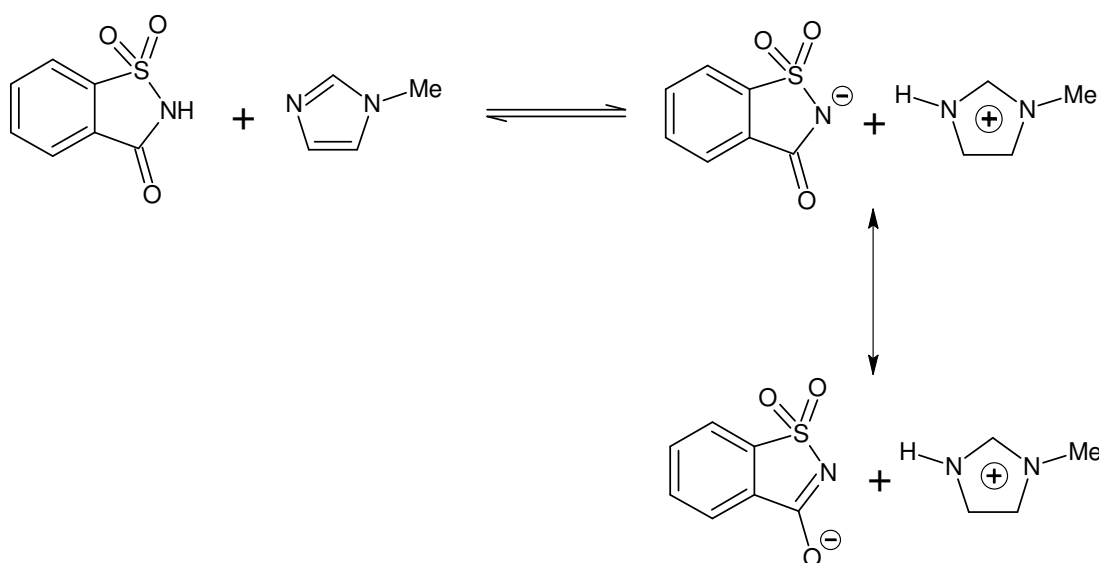
Scheme 56: Salt formation between saccharin and *N*-methylimidazole.

135

On addition of 1 equivalent of dimethylphosphoramidite to a sample of saccharin the resulting IR spectrum (figure 41) showed the absence of the carbonyl stretch, indicating that the saccharin anion has reacted by oxyanion attack, resulting in P-O bond formation. This is expected based on the greater bond strength of P-O bonds compared with P-N bonds.[127,128]

Excess water was added to the sample to promote formation of the H-phosphonate and the carbonyl signal of the neutral saccharin was observed. Reformation of the neutral saccharin also occurred when methanol was added to form trimethylphosphite.

Samples of dimethylphosphoramidite were reacted with 0.5, 1, 1.5, 2 and 2.5 equivalents of saccharin in acetonitrile (figures 42-46). A reaction appears to occur even in the absence of *N*-methylimidazole, but reaction is not complete and, as can be seen from these spectra the carbonyl does not appear until there is two equivalents of saccharin present in the system. This is compatible with the stoichiometric requirement to form the protonated amine (scheme 57).
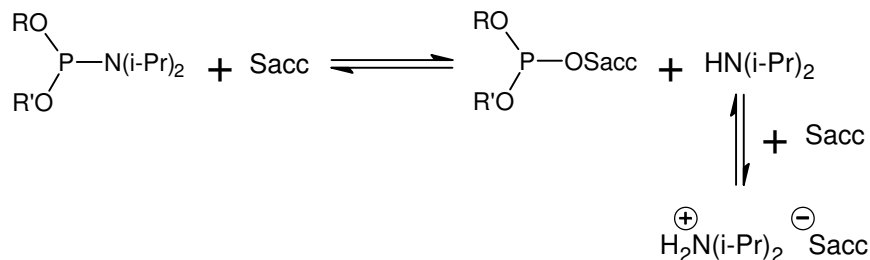
Scheme 57: Amidite activation with two equivalents of saccharin.
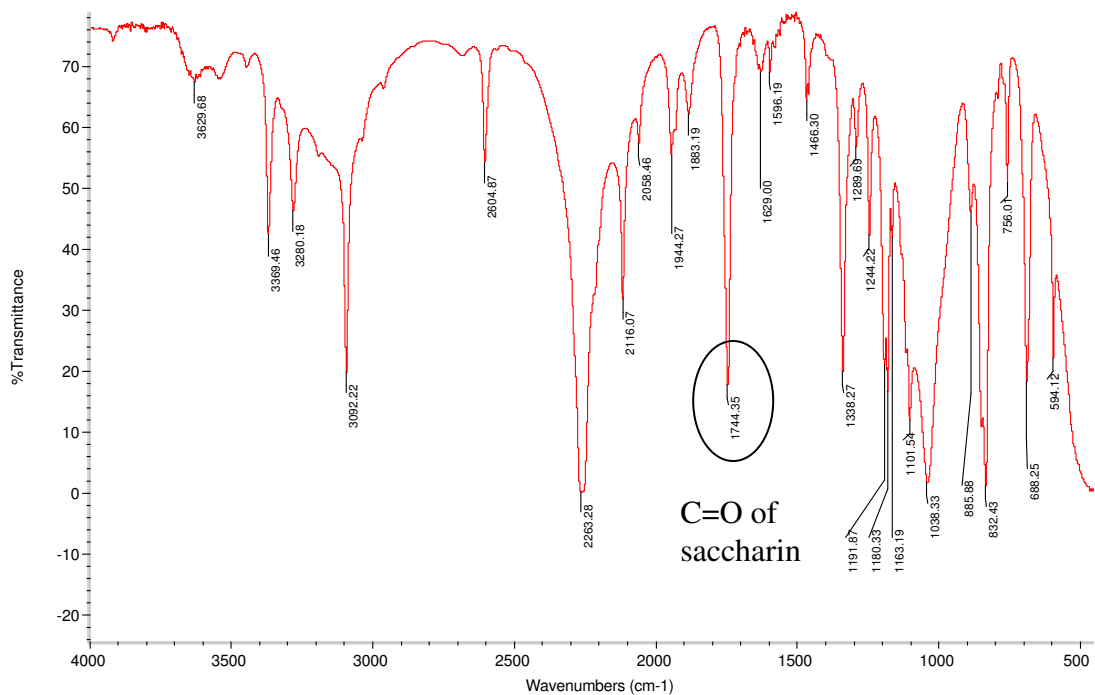
Figure 39: FT-IR spectrum of 0.08 M saccharin in deuterated acetonitrile.
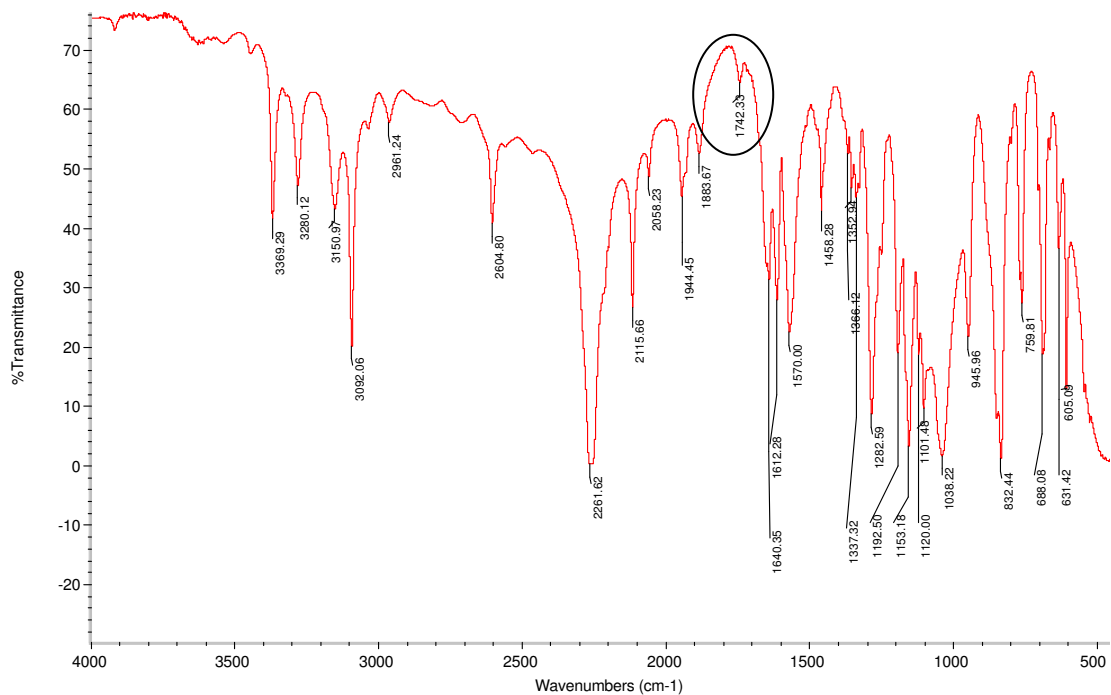
Figure 40: FT-IR spectrum of 0.08 M saccharin/*N*-methylimidazole in deuterated acetonitrile.
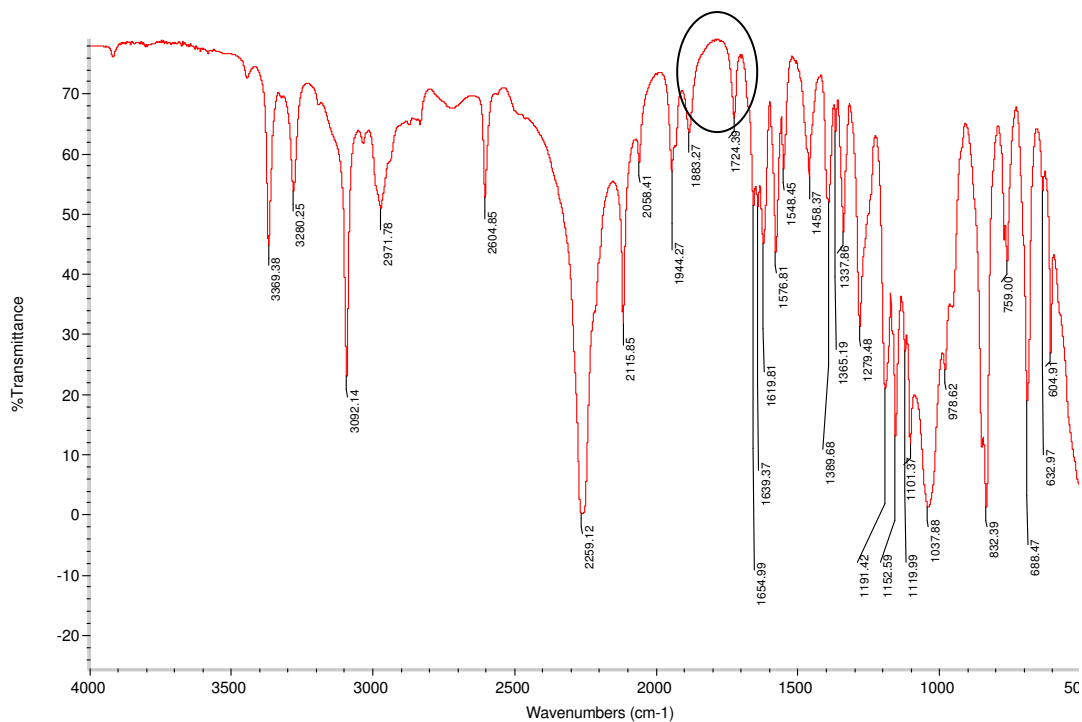
Figure 41: FT-IR spectrum of 0.08 M dimethylphosphoramidite with 0.08 M saccharin (1:1) in deuterated acetonitrile
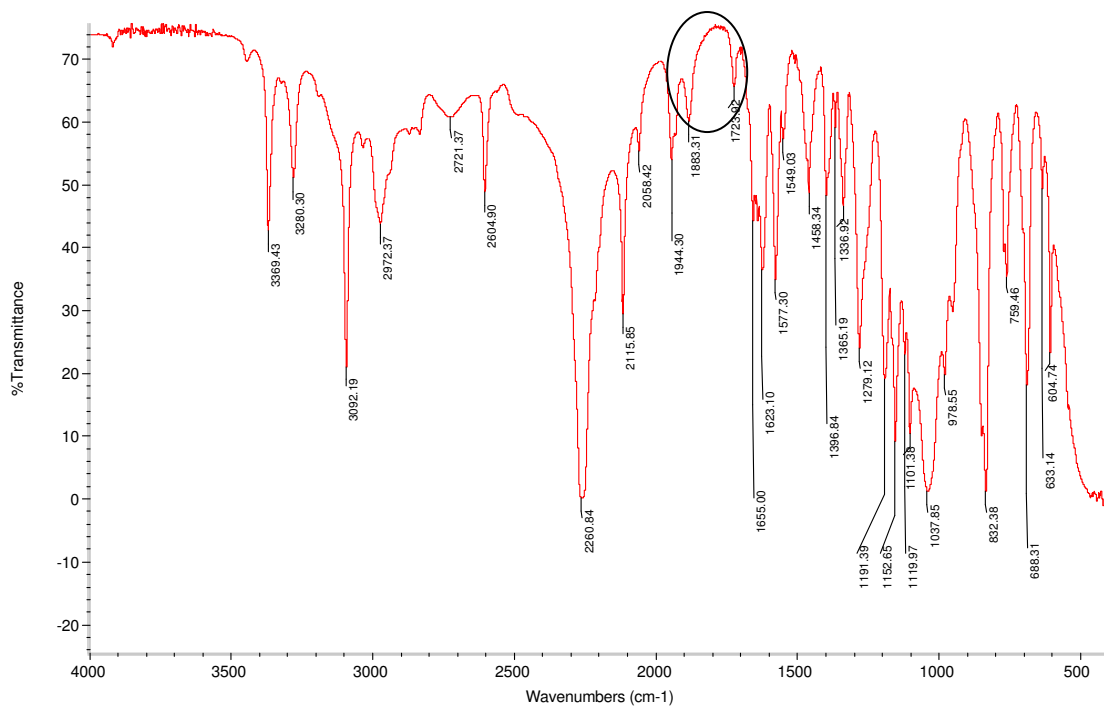
Figure 42: 0.16 M dimethylphosphoramidite with 0.08 M saccharin (1:0.5) in deuterated acetonitrile.

138
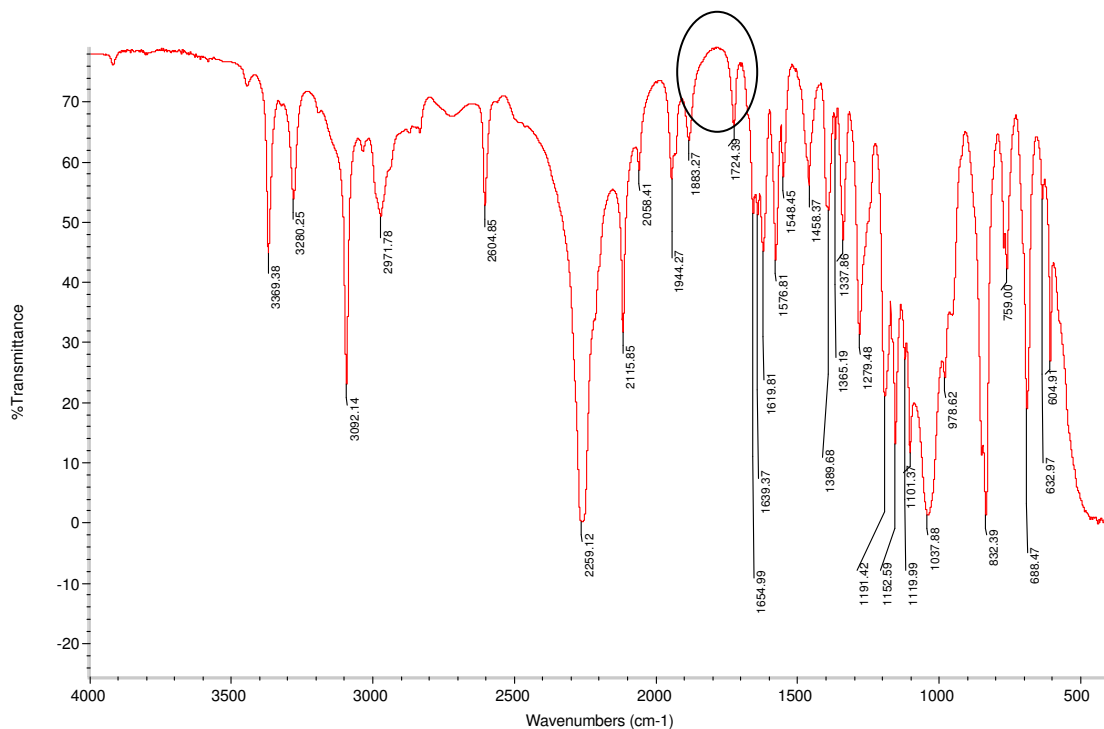
Figure 43: 0.08 M dimethylphosphoramidite with 0.08 M saccharin (1:1) in deuterated acetonitrile.
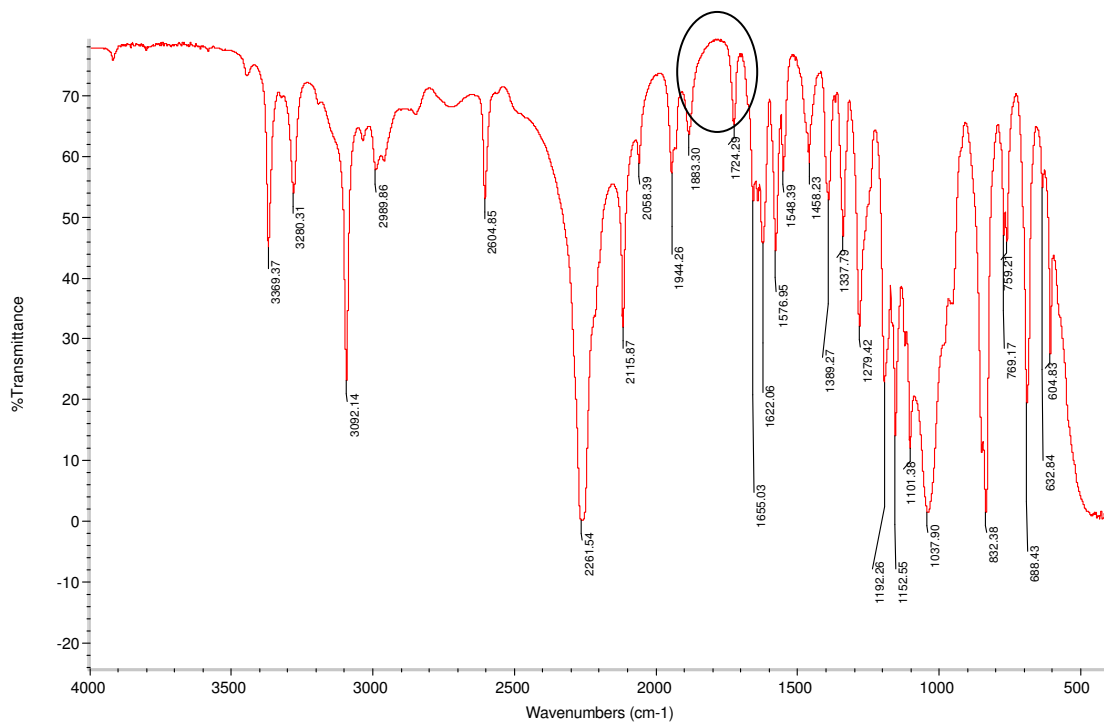
Figure 44: 0.053 M dimethylphosphoramidite with 0.08 M saccharin (1:1.5) in deuterated acetonitrile.
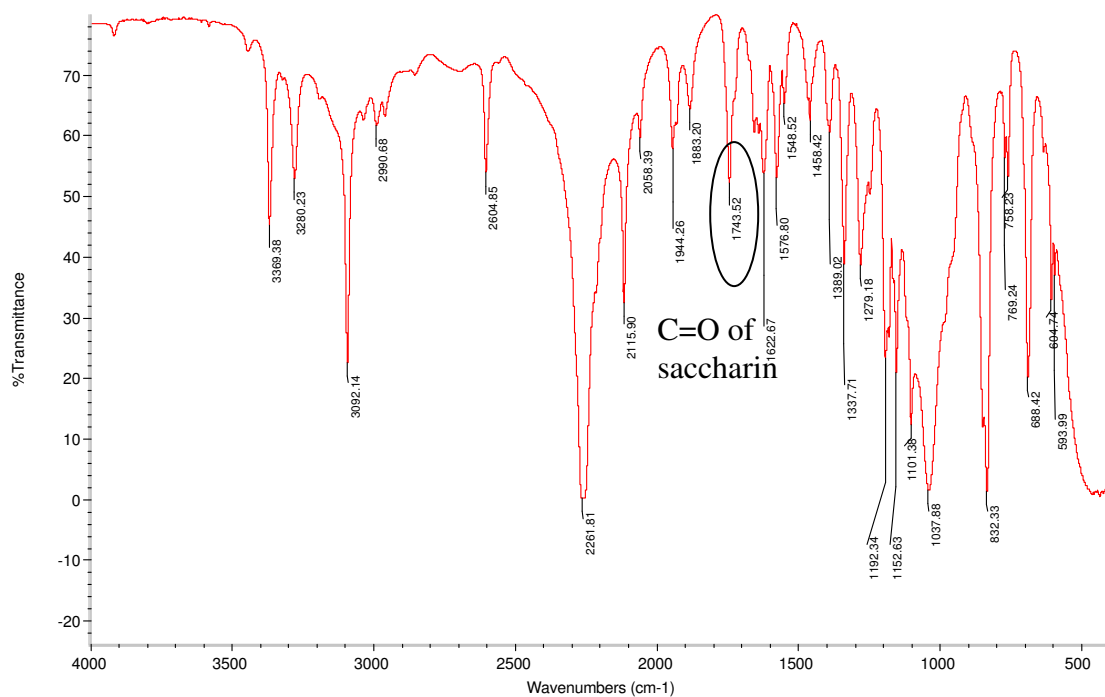
Figure 45: 0.04 M dimethylphosphoramidite with 0.08 M saccharin (1:2) in deuterated acetonitrile.
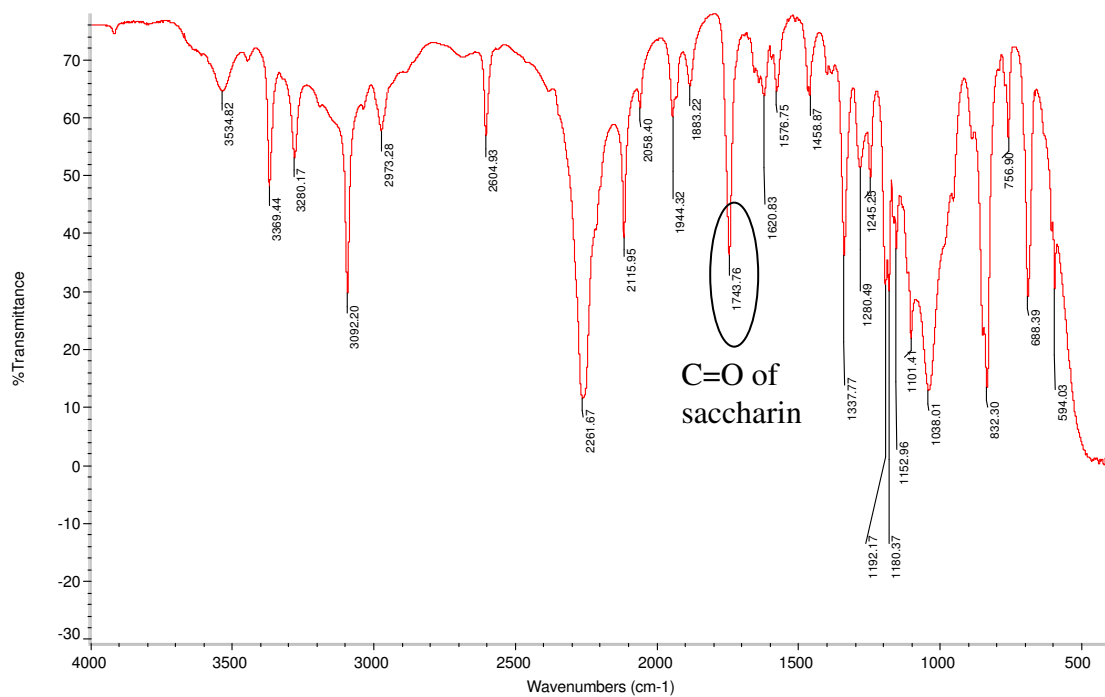
Figure 46: 0.032 M dimethylphosphoramidite with 0.08 M saccharin (1:2.5) in deuterated acetonitrile.

4.2.8   Summary of the nature of the activated species

In chloroform, the phosphorus NMR of solutions of phosphoramidite, saccharin and *N*-methylimidazole indicate that the activated species is an adduct of saccharin, with the same sharp signal being formed in the presence or absence of *N*-methylimidazole. Adding *N*-methylimidazole to a solution of phosphoramidite and saccharin or saccharin/*N*-methylimidazole forms a salt with saccharin, effectively reducing the concentration of activator resulting in a decrease in substitution of the starting amidite. There are two possible P-saccharin analogues: one where saccharin is linked through oxygen and the other where saccharin is linked through nitrogen. In chloroform, there is no evidence distinguishing between the formation of the P-O or P-N-saccharin. One possibility is that there is rapid exchange between the two possible analogues and the NMR signal is the time average of the two.

In acetonitrile, the phosphorus NMR shows that on addition of saccharin to dimethylphosphoramidite the P-saccharin species is formed and the chemical shift data is compatible with P-O bond formation. The ^{31}P NMR signal for this species is very broad which may be indicative of a relatively slow exchange between the P-O and P-N-saccharin adducts. However, the infra red experiments show complete loss of saccharin's carbonyl absorption in the presence of the amidite, which is compatible with P-O-saccharin formation in acetonitrile.

The experiments performed with the ^{15}N labelled saccharin show no coupling of the nitrogen with phosphorus, in either the ^{15}N NMR spectra or the ^{31}P NMR spectra. Again, this indicates that the P-O-saccharin is predominant and the major component of the equilibrium mixture.

The formation of P-O-saccharin bonds over P-N-saccharin bonds is not unexpected on the basis of thermodynamics as the difference in bond energies between P-O and P-N is relatively large: P-O bonds = 360 kJ mol^{-1} and P-N bonds = 230 kJ mol^{-1}.[127,128] Therefore, there will be an enormous thermodynamic driving force for the formation of the P-O-saccharin adduct.

It is clear that the predominant activated species in these systems is the P-O-saccharin adduct. This is contrary to what was expected based on proposed mechanisms in literature which indicated that the basic component of the activator salt should act as the nucleophile for optimum reaction. It seems that the main function of *N*-methylimidazole in this system is to reduce the overall acidity of the reaction to prevent unwanted side reactions such as premature detritylation or depurination.

4.3   Phosphoramidite alcoholysis

Alcoholysis of dimethylphosphoramidite with one mole equivalent of saccharin/*N*-methylimidazole salt and methanol in deuterated acetonitrile leads to complete removal of the starting amidite after only a few minutes, as shown by ^{31}P NMR spectra. The product trimethylphosphite appears as a singlet at δ141ppm.

The alcoholysis reaction (scheme 58), as with activation, requires two proton transfers for complete reaction. One of these protons comes from the alcohol and therefore only one equivalent of the saccharin/*N*-methylimidazole activator is required. Alcoholysis can occur via two routes: either by direct displacement of the protonated amidite or by saccharin acting as a nucleophilic catalyst to generate the activated species which subsequently reacts with the alcohol. Using saccharin/*N*-methylimidazole, complete removal of the starting amidite occurs with one mole of activator and one mole of alcohol.
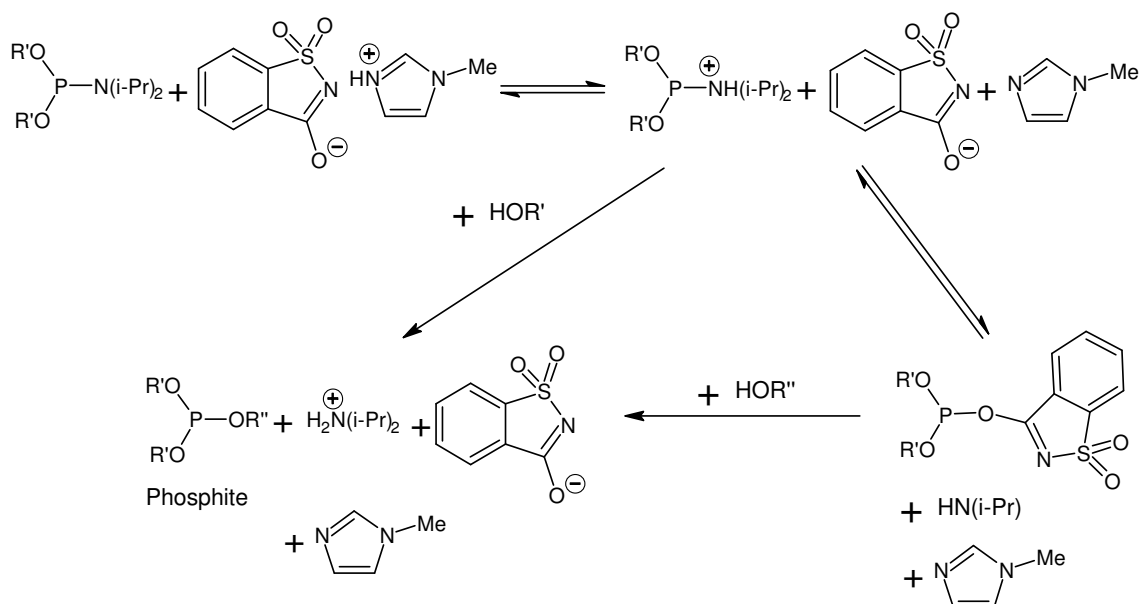
Scheme 58: Phosphoramidite alcoholysis by either nucleophilic displacement of the protonated amine or of the saccharin activated species.

4.3.1 Alcoholysis of thymidine phosphoramidite: changing of activator base

The rate of the alcoholysis reaction can be decreased by using a more acidic alcohol, such as a phenol, so that it can be monitored more easily. A study of the effect of the acidity of the activator acid-base pair was undertaken by monitoring the reaction of thymidine phosphoramidite (11) and 4-methoxyphenol in the presence of saccharin and a number of tertiary amines. The pK_a of the bases in acetonitrile are shown in table 27, together with those in water.

Base	pK_a in acetonitrile	pK_a in water
4-methylmorpholine	15.7[134]	7.41[61]
N,N-dimethylbenzylamine	16.6[134]	-
Tri-*n*-butylamine	18.09[132]	10.89[132]
Triethylamine	18.46[132]	10.65[132]

Table 27: pK_a of bases used for activation in acetonitrile.

The reactions progress was monitored over one week by ^{31}P NMR. The spectra showed in each case the presence of the phosphite triester product and a negligible concentration of H-phosphonate. Tables 28 and 29 show the percentage of the reactant thymidine phosphoramidite (11) and the product phosphite triester present over the one week period.

Base Time (hr)	4-methylmorpholine % (11)	*N,N*-dimethylbutylamine % (11)	tri-*n*-butylamine % (11)	Triethylamine % (11)
0.5	10	23.5	75	91
24	2.5	7.5	49	66
128	0	0	11	24
154	0	0	10	25

Table 28: The percentage of thymidine phosphoramidite (11) with time for the alcoholysis of thymidine phosphoramidite (11) with 4-methoxyphenol, saccharin and base in acetonitrile at 30°C.

Base\Time (hr)	4-methylmorpholine % phosphite	N,N-dimethylbutylamine % phosphite	tri-n-butylamine % phosphite	Triethylamine % phosphite
0.5	90	76.5	25	9
24	97.5	92.5	51	34
128	100	100	89	76
154	100	100	91	75

Table 29: The percentage of phosphite triester with time for the alcoholysis of thymidine phosphoramidite (11) with 4-methoxyphenol, saccharin and base in acetonitrile at 30°C.

The data shows that the equilibrium has been reached in each reaction over the time studied. Tables 28 and 29 and figures 47, 48 and 49, show that increasing the basicity of the activator base, decreases the rate at which an equilibrium is reached. The basicity of the activator base also changes the position of the reactions equilibrium: the extent of reaction is decreased with increasing basicity.

A plot of extent of reaction as a function of amine pK_a after one week (figure 49), shows that below a pK_a of approximately 17.5 there is complete removal of the starting amidite. At pK_as greater than 17.5 the extent of reaction becomes less as the basicity of the amine increases.
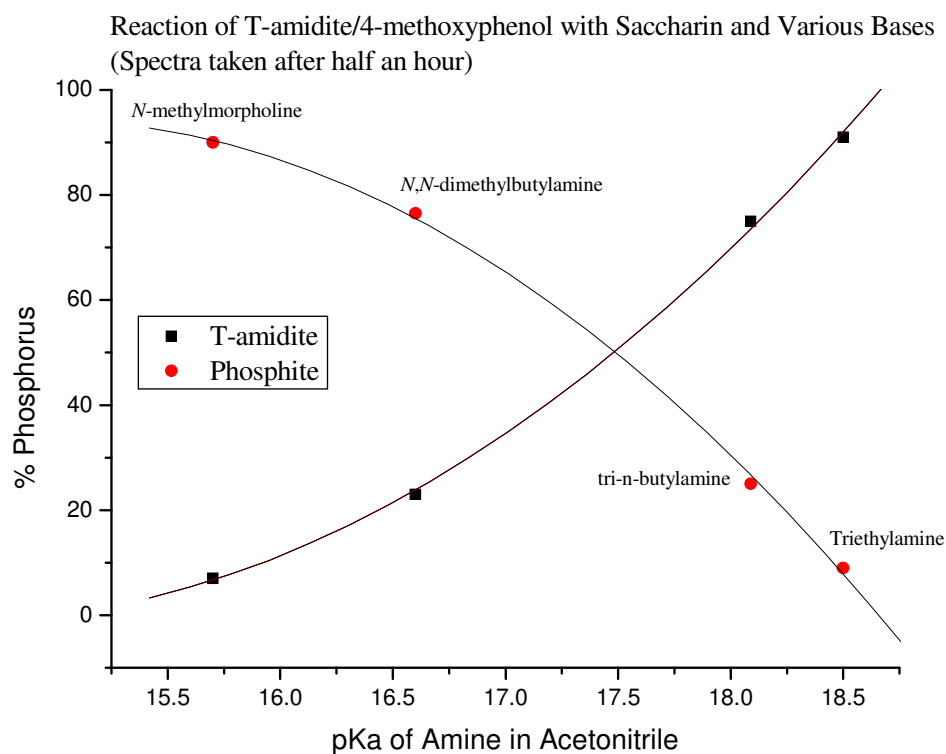
Figure 47: Extent of reaction as a function of amine pK$_a$ for alcoholysis of thymidine phosphoramidite (11) with 4-methoxyphenol and saccharin after half an hour at 30°C.
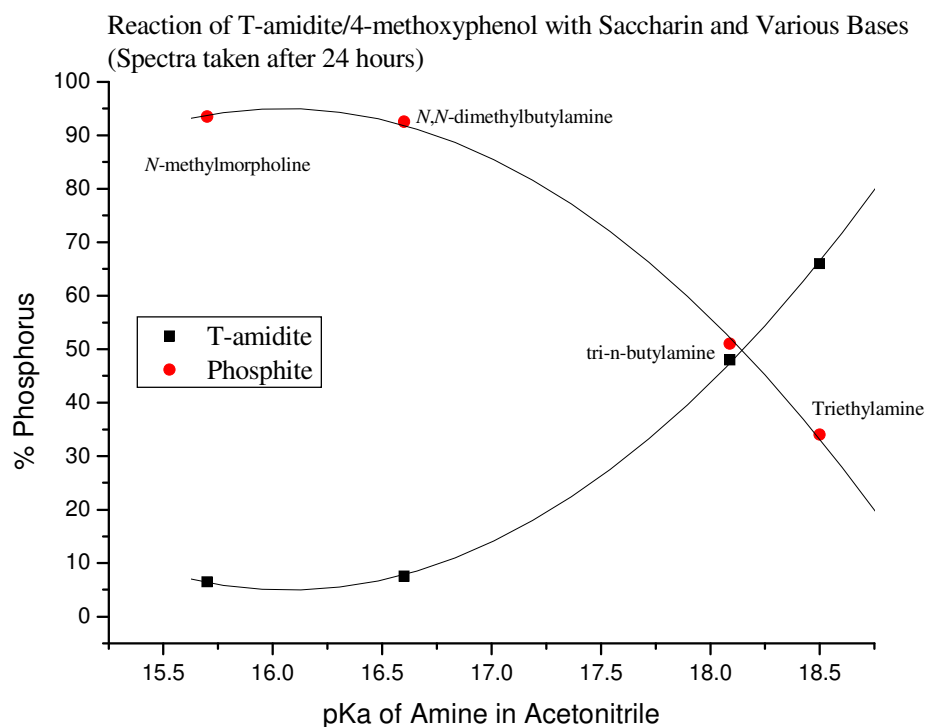
Figure 48: Extent of reaction as a function of amine pK$_a$ for alcoholysis of thymidine phosphoramidite (11) with 4-methoxyphenol and saccharin after 24 hours at 30°C.

Reaction of T-amidite/4-methoxyphenol with Saccharin and Various Bases
(Spectra taken after 154 hours)
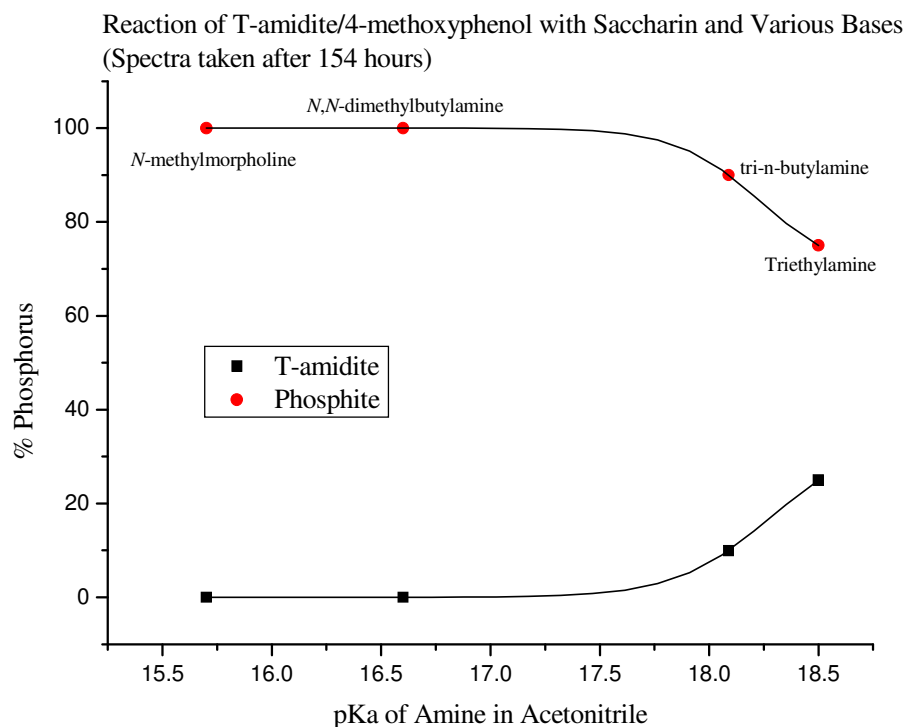
Figure 49: Extent of reaction as a function of amine pK$_a$ for alcoholysis of thymidine phosphoramidite (11) with 4-methoxyphenol and saccharin after one week (154 hours) at 30°C.

With respect to the basicity of the activator base, the alcoholysis reaction is largely controlled by the relative stabilities of the activator salt and the protonated diisopropylamine product. The produced diisopropylamine salt must be more stable than the starting activator salt to drive the reaction to completion. If the pK$_a$ of the starting base is equal to or greater than that of diisopropylamine there may be incomplete reaction because of a reduction in driving force for the reaction.

The pK$_a$ of the conjugate acid of diisopropylamine is 18.4 in acetonitrile and that of triethylamine is 18.5. This suggests that there will be little difference in stabilities between the two possible salts with saccharin and therefore less driving force for the reaction. Figure 49 shows that there is approximately 80% conversion of the amidite to phosphite after one week, which indicates, as expected, that the phosphite triester is thermodynamically more stable than the amidite. This is due to P-O bonds being stronger than P-N bonds which is enough to drive the reaction to partial completion (see table 8, page 90 for P-O and P-N bond energies).

As the pK_a of the conjugate acid of the starting base decreases, the extent of reaction increases due to the saccharin/diisopropylamine salt becoming increasingly more thermodynamically stable than the activator salt, driving the reaction further to completion. Depending on the rate limiting step of the reaction the basicity of the activator base may also be involved in determining the rate of reaction.

In scheme 58 (page 143), the activator base is only involved in initial activator salt formation, but on product formation the activator base will be in equilibrium with the protonated diisopropylamine (scheme 59). In the case of *N*-methylimidazole the equilibrium will be greatly in favour of the protonated diisopropylamine, as described by the large difference in pK_as. As the basicity of the activator base is increased the equilibrium with the protonated diisopropylamine will be progressively more towards the protonated activator base.
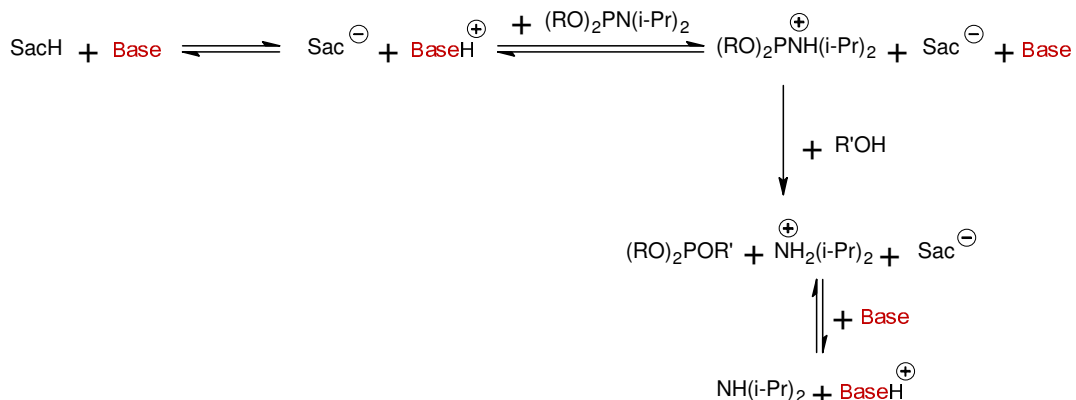
Scheme 59: Phosphoramidite alcoholysis reaction showing equilibrium between protonated diisopropylamine and activator base.

4.3.2 Alcoholysis of thymidine phosphoramidite: Kinetics

Rapid ^{31}P NMR techniques have been used to obtain concentration versus time data for the alcoholysis of thymidine phosphoramidite (11) using saccharin/*N*-methylimidazole salt as the activator and a number of alcohols and phenols. Spectra were recorded every 23 seconds and the concentration of the phosphite formed plotted as a function of time. The concentration versus time plots have been fitted to a second order rate equation for the formation of product and an example of the fits can be seen in figure 50.

Reaction Between Thymidine phosphoramidite, SMI and 4-methoxyphenol in acetontrile
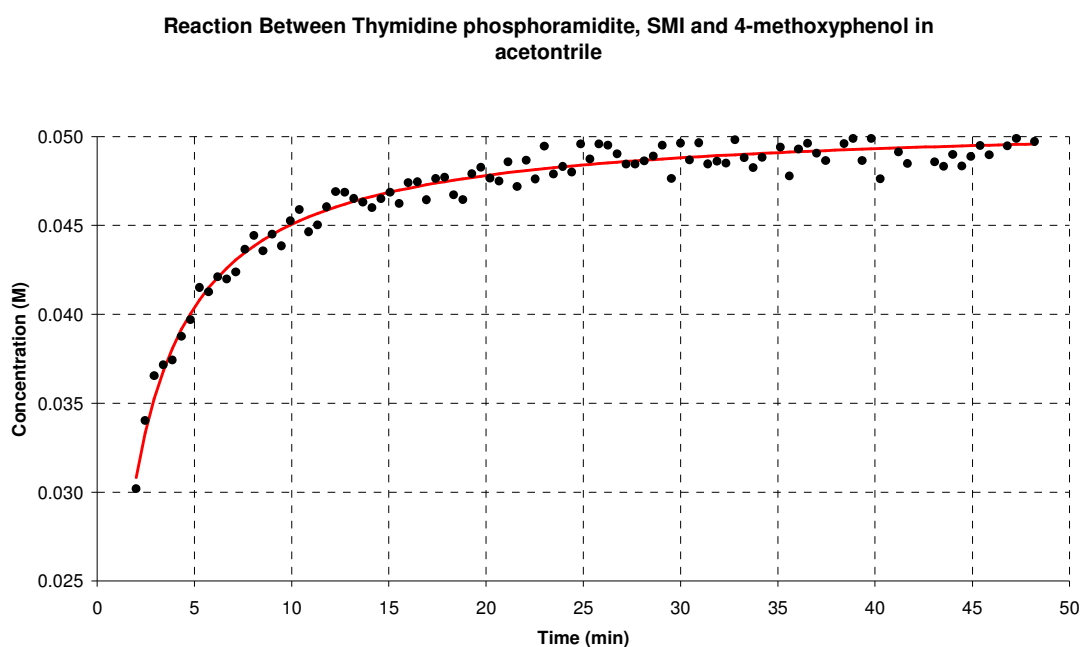
Figure 50: Concentration/time data for the alcoholysis of 0.05M thymidine phosphoramidite (11) with saccharin/*N*-methylimidazole salt and 4-methoxyphenol in deuterated acetonitrile at 22°C, with second order fit.

One equivalent of saccharin/*N*-methylimidazole salt was used for these kinetic measurements, as any excess of the activator produced reactions which were too fast to be followed by ^{31}P NMR methods.

The effect of changing alcohol concentration was studied using a range of 4-methoxyphenol concentrations. Over the range of concentrations studied all of the data showed good fits with second order kinetics. Table 30 and figure 51 shows the dependence of second order rate constants (k_{obs}) on 4-methoxyphenol concentration for

the alcoholysis of thymidine phosphoramidite (11) with one mole equivalent of saccharin/*N*-methylimidazole.

4-methoxyphenol concentration (M)	k_{obs} (M^{-1} min^{-1})
0.05	13.8
0.1	17.1
0.15	18.4
0.2	19.8
0.3	24.2
0.4	25.0
0.5	24.0
0.75	24.6

Table 30: Rate data for varying 4-methoxyphenol concentration.

Alcoholysis of T-amidite with SMI and 4-methoxyphenol in acetonitrile
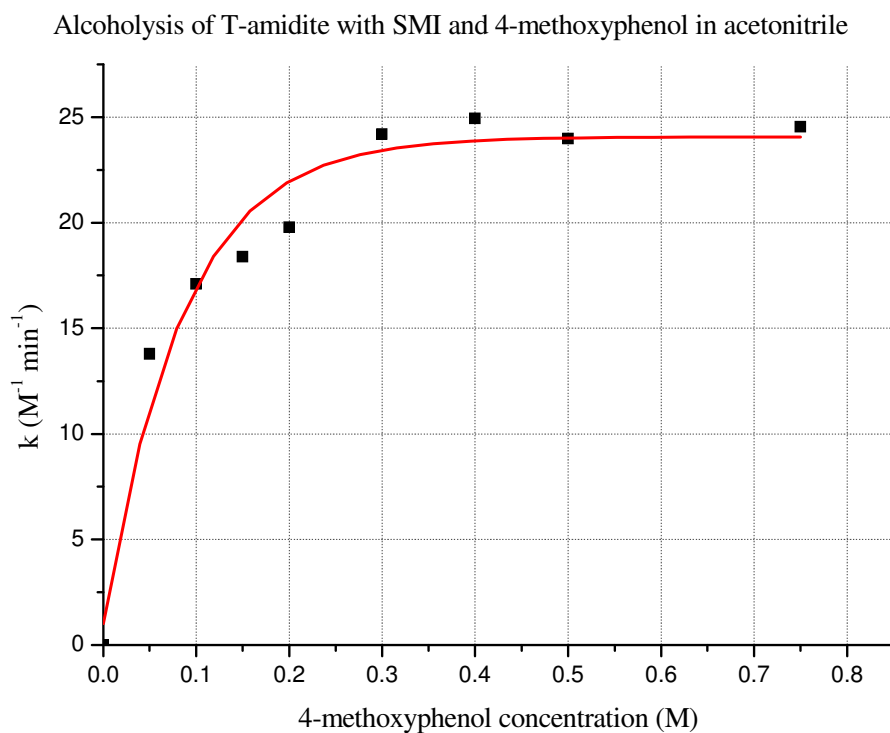
Figure 51: Second order/4-methoxyphenol concentration profile for the alcoholysis of 0.05M thymidine phosphoramidite (11) with 0.05M saccharin/*N*-methylimidazole salt in acetonitrile at 22°C.

Figure 51 shows that there is a non-linear dependence on 4-methoxyphenol concentration. At 4-methoxyphenol concentrations below 0.25M, the observed rate

constants are dependent on 4-methoxyphenol concentration, with an increase in concentration causing an increase in k_{obs}. Above 0.25M 4-methoxyphenol, the rate of phosphite formation becomes independent of the phenol concentration. This change in phenol concentration dependence is an indication of a change in rate limiting step and signifies the presence of an intermediate on the reaction pathway.

Assuming that phosphoramidite (PA) activation involves nucleophilic catalysis by saccharin to form an intermediate P-saccharin by displacement of diisopropylamine (DIA) and that alcoholysis proceeds via a two step mechanism, there are two elementary reaction steps involved in phosphite formation (POR).

$$\text{PA} + \overset{\ominus}{\text{Sac}} \ \overset{\oplus}{\text{NMIH}} \underset{k_{-1}}{\overset{k_1}{\rightleftharpoons}} \text{PSac} + \text{DIA} + \text{NMI}$$

$$\text{PSac} + \text{HOR} \xrightarrow{k_2} \text{POR}$$
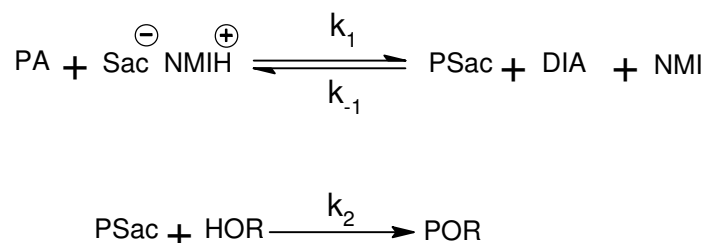
The rate of phosphite triester formation can be expressed as follows:

$$\frac{d[POR]}{dt} = k_2 [PSac]\,[ROH] \qquad\qquad \text{..........1}$$

The formation and loss of intermediate, PSac, can be expressed at steady state as:

$$\frac{d[PSac]}{dt} = k_1 [PA]\,[Sac^- NMIH^+] - k_{-1}[PSac]\,[DIA]\,[NMI] - k_2 [PSac]\,[HOR] = 0$$

$$\text{..........2}$$

Rearranging and simplifying equation 2

$$[PSac] = \frac{k_1 [PA]\,[Sac^- NMIH^+]}{\left(k_{-1}[NMI]\,[DIA] + k_2 [ROH]\,\right)} \qquad\qquad \text{..........3}$$

Substitute 3 into 1 for [PSac]

$$\frac{d[POR]}{dt} = \frac{k_1 k_2 [PA] [ROH] [Sac^- NMIH^+]}{k_{-1}[NMI] [DIA] + k_2 [ROH]} \qquad \ldots\ldots\ldots 4$$

At low [ROH]

k_{-1} [NMI] [DIA] > k_2 [ROH]

$$\boxed{\frac{d[POR]}{dt} = \frac{k_1 k_2 [PA] [ROH] [Sac^- NMIH^+]}{k_{-1}[NMI] [DIA]}} \qquad \ldots\ldots\ldots 5$$

Therefore, k_2 is the rate limiting step, as formation of the intermediate PSac is reversible and reverts to reactants faster than it reacts with alcohol to give the product. The rate is therefore dependent on alcohol concentration.

At high [ROH]

k_2 [ROH] > k_{-1} [NMI] [DIA]

$$\frac{d[POR]}{dt} = \frac{k_1 k_2 [PA] [ROH] [Sac^- NMIH^+]}{k_2 [ROH]}$$

$$\boxed{\frac{d[POR]}{dt} = k_1 [PN] [Sac^- NMIH^+]} \qquad \ldots\ldots\ldots 6$$

Therefore, k_1 is the rate limiting step, because the intermediate now reacts faster with alcohol than it reverts to reactants and the rate is independent of alcohol concentration even though it is consumed during the overall reaction.

In summary, at low alcohol concentrations the dependence of the reaction rate on alcohol concentration is due to k_2 being the rate limiting step (equation 5). As the alcohol concentration is increased $k_2[ROH]$ will become faster to a point where the initial activation (k_1) is rate limiting (as in equation 6). When k_1 becomes rate limiting the term for the alcohol is removed from the rate equation and alcoholysis becomes independent of alcohol concentration.

The overall rate equation (equation 4) contains terms for *N*-methylimidazole and diisopropylamine and can also be reduced to equation 7 if [NMI] or [DIA] are large and so $k_{-1}[NMI][DIA] > k_2[ROH]$.

$$\frac{d[POR]}{dt} = \frac{k_1 k_2 [PA] [ROH] [Sac^- NMIH^+]}{k_{-1} [NMI] [DIA]}$$ ……….7

This shows that when the concentration of *N*-methylimidazole or diisopropylamine is large then the rate of reaction will be inversely proportional to the concentrations of *N*-methylimidazole and diisopropylamine.

Kinetic measurements of a sample of thymidine phosphoramidite (11), one mole equivalent of saccharin, two mole equivalents of *N*-methylimidazole and one mole equivalent of 4-methoxyphenol in acetonitrile show a reduction in rate in comparison with measurements performed under the same conditions but with one mole equivalent of *N*-methylimidazole (figure 52).
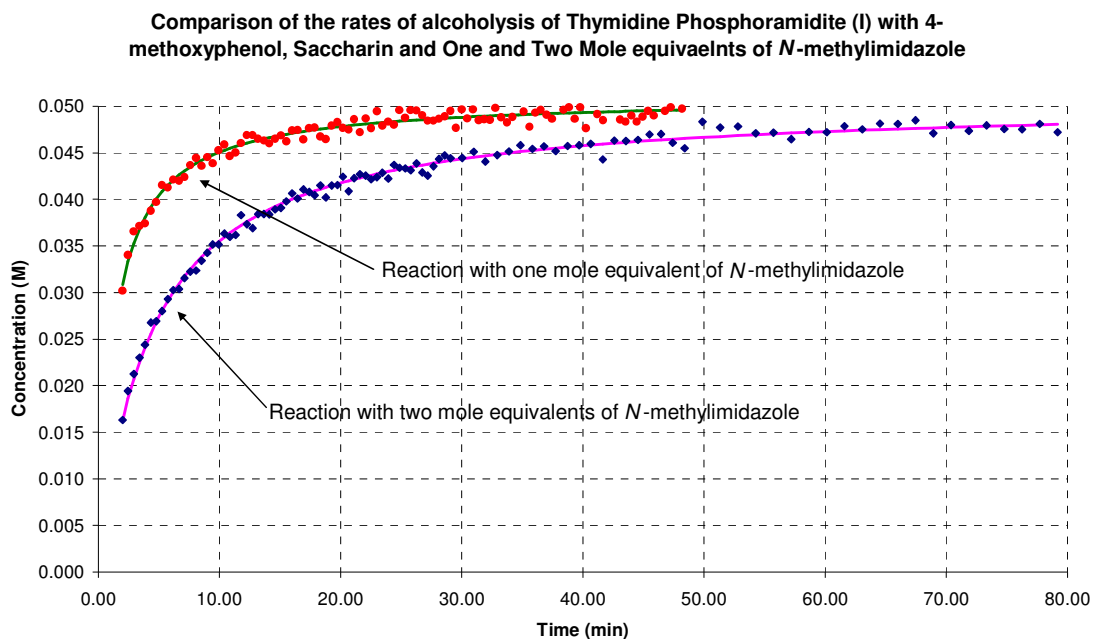
Figure 52: Rate profiles for the alcoholysis of 0.05M thymidine phosphoramidite (11) with 0.05M 4-methoxyphenol, 0.05M saccharin with 0.05M and 0.1M of *N*-methylimidazole in acetonitrile at 22°C.

The calculated rate constants for the two reactions are summarised in table 31, and they show that there is nearly a three fold reduction in rate on doubling the concentration of *N*-methylimidazole, this is compatible with the rate law of equation 4 describing the reaction conditions.

Number of mole equivalent of *N*-methylimidazole	k_{obs} (M^{-1} min^{-1})
One	13.7
Two	4.7

Table 31: Calculated rate constants for the alcoholysis of thymidine phosphoramidite (11) with 4-methoxyphenol and saccharin with one and two equivalents of *N*-methylimidazole in acetonitrile at 22°C.

4.3.3 Electronic and steric effects on the alcoholysis reaction

Changing the substituent at the *para* position of the phenol has remarkably little or no effect on the rate of alcoholysis of thymidine phosphoramidite (11) in the presence of one mole equivalent of saccharin/*N*-methylimidazole (table 32). Even changing to alcohols rather than phenols has a negligible effect (table 32). The only significant difference is with *t*-butanol which has a slightly lower observed rate constant but even this is too small to be attributed to increased steric effects.

Alcohol (0.05M, one mole equivalent)	k_{obs} (M^{-1} min^{-1})
4-cyanophenol	14.2
4-chlorophenol	13.6
Phenol	13.6
4-methylphenol	13.1
4-methoxyphenol	13.7
Propan-2-ol	14.3
t-butanol	11.1

Table 32: Observed rate constants for alcoholysis of 0.05M thymidine phosphoramidite (11) and saccharin/*N*-methylimidazole.

The observed rate constants calculated for these alcohols are in the region where the second step is expected to be rate limiting, as observed previously for 4-methoxyphenol in figure 51. Therefore, a change in rate would be expected on changing the electronic and steric effects of the alcohol. As this is not the case, it is likely that increasing the acidity of the phenol has shifted the rate-limiting step to the formation of the intermediate. This is not unexpected if it is the phenoxide anion that acts as the nucleophile. Similarly alcohols may be more nucleophilic under these conditions compared with phenols leading to a faster second step. Another possibility, though less likely, is that the transition state of the reaction is early on the reaction coordinate and therefore no discrimination between nucleophiles is observed except for when the steric bulk is very large, as with *t*-butanol.

At high alcohol concentrations the first step is rate limiting and as a consequence there is no dependence of rate on alcohol concentration. Changing the substituents on phenol or changing the types of alcohol should also have no effect on the observed rate constant if the first step is rate limiting. Kinetic measurements performed in the presence of high alcohol concentrations with different alcohols, have shown this to be true within experimental error, the results of which are summarised in table 33.

Alcohol (0.5M, ten mole equivalent)	k_{obs} (M^{-1} min^{-1})
Phenol	22.9
4-methoxyphenol	24.0
Propan-2-ol	24.8

Table 33: Alcoholysis of 0.05M thymidine phosphoramidite (11) with saccharin/*N*-methylimidazole and 10 mole equivalents of alcohol in acetonitrile at 22°C.

There is a lack of kinetic data in the literature for the coupling of phosphoramidites with alcohols in the presence of an acidic activator. The reasons for this are likely due to the difficulties in measurement of these rate constants: by definition the activation process should proceed quickly to avoid unwanted hydrolysis side reactions which also make kinetic measurement problematic.

The most relevant studies have been by Nurminen *et al*[78] who used ^{31}P NMR to measure the rate of alcoholysis of diisopropyl *N,N*-diisopropylphosphoramidites with tetrazole as activator in tetrahydrofuran. Tetrahydrofuran was used as solvent to slow down the reaction; in acetonitrile the rate of reaction was too fast for measurement. His studies showed that the phosphoramidite activation reaction gave over all third order kinetics with a first order dependence on the amidite and second order dependence on tetrazole. The second order dependence on tetrazole was attributed to the fact that one molecule of tetrazole acts a proton donor and another as the incoming nucleophile. Nurminen also observed that the alcoholysis reaction was second order overall with first order dependences in respect to the phosphoramidite and tetrazole and independent of the alcohol concentration. He also found that rate of alcoholysis was almost equal to the rate of tetrazolide intermediate formation.

5 Results and Discussion: Sulphurisation

Phosphorthioate analogues of oligonucleotides are synthesised via sulphurisation of the formed nucleotide-phosphite triester with an appropriate sulphurising agent. Throughout these studies the sulphurising agent of choice has been 3-amino-1,2,4-dithiazole-5-thione (xanthane hydride) (scheme 60). Crystallographic studies by Hordvik[112] showed that in the crystal, xanthane hydride has the structure of (12). Later Butler and Glidewell[113], using NMR and MNDO calculations in solution confirmed this, but also postulated that two other tautomers may be possible (structures 13 and 14 of scheme 60).

(12)   (13)   (14)
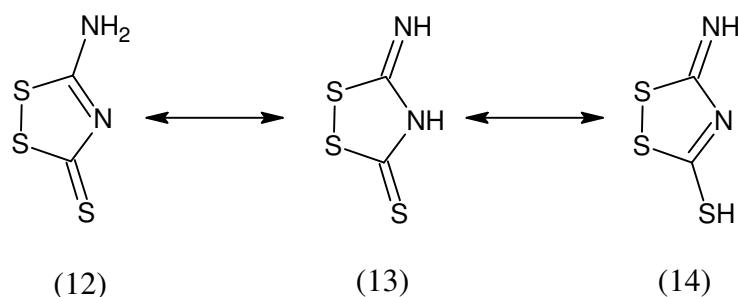
Scheme 60: Tautomers of 3-amino-1,2,4-dithiazole-5-thione (xanthane hydride).

It has been reported by Tang *et al* that the sulphurisation of phosphites proceeds via nucleophilic attack of the phosphite at the sulphur adjacent to the amino group forming a charged phosphonium ion intermediate.[111] This intermediate then breaks down to form the phosphorthioate and the by-products carbondisulphide and cyanamide (scheme 61). However, no evidence for this mechanism was provided, and as there are two electrophilic sulphurs eligible for nucleophilic attack, a study of the reactions products was undertaken to differentiate between them.
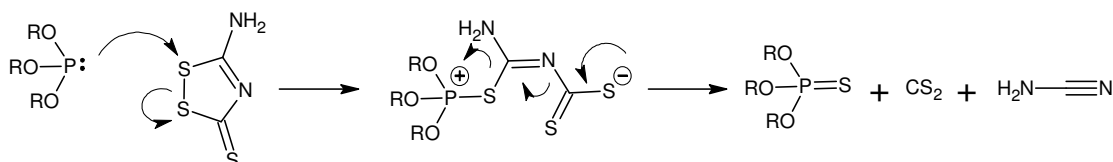
Scheme 61: Mechanism of sulphurisation proposed by Tang *et al*. Nucleophilic attack of the phosphite at the sulphur atom adjacent to the amino group yielding the phosphorthioate, carbon disulphide and cyanamide.[111]

5.1 Sulphurisation product analysis

The reactions of a number of triaryl and trialkylphosphites with xanthane hydride in acetonitrile, were analysed by ^{1}H, ^{13}C, ^{31}P NMR spectroscopies, IR spectroscopy and mass spectroscopy to determine the products of the sulphurisation reaction. In all cases the formation of the phosphorthioate was almost stoichiometric but the presence of the other suggested products, carbondisulphide and cyanamide, could not be identified. This suggested that an alternative mechanism to that proposed by Tang *et al* may occur. No other product, except the phosphorthioate, was detectable using these analytical techniques.

An alternative mechanism for the sulphurisation reaction is nucleophilic attack of the phosphite on the sulphur adjacent to the thiocarbonyl group (scheme 62). This mechanism would again form a charged phosphonium intermediate and ultimately yield the phosphorthioate but thiocarbamoyl isothiocyanate as the other product.
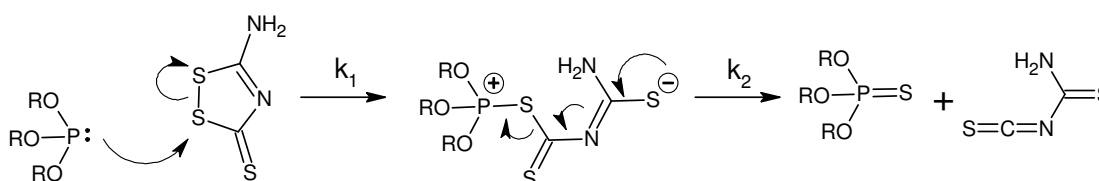
Scheme 62: Sulphurisation via nucleophilic attack of the phosphite on the sulphur adjacent to the thiocarbonyl group, yielding the phosphorthioate and thiocarbamoyl isothiocyanate.

Thiocarbamoyl isothiocyanate has not been described in the literature presumably due to its instability and high reactivity. The dimethyl derivative, *N,N*-dimethylthiocarbamoyl isothiocyanate, has been successfully synthesised and characterised at -15°C. At room temperature *N,N*-dimethylthiocarbamoyl undergoes a [4+2] cycloaddtion to form the dimer 2-dimethylamino-5-dimethylthiocarbamoyl-1,3,5-thiadiazine-4,6-dithione.[135]

5.2 Trapping of sulphurisation by-products

A number of external nucleophiles were added to reaction mixtures of triphenylphosphite and xanthane hydride (for experimental see sections 2.5.4-2.5.7) in an attempt to trap the reactive thiocarbamoyl isothiocyanate. The nucleophiles chosen were aniline, 4-methoxyaniline and 4-nitroaniline. After work up of the reactions, accurate mass spectroscopy, ^{1}H and ^{13}C NMR confirmed that as well as the phosphorthioate the other major product of the reactions was the corresponding dithiobiuret; 1-phenyldithiobiuret; 1-(4-methoxyphenyl) dithiobiuret; and 1-(4-nitrophenyl) dithiobiuret.

Dithiobiurets can be formed from nucleophilic attack of the anilines on the thiocarbamoyl isothiocyanate (scheme 63).
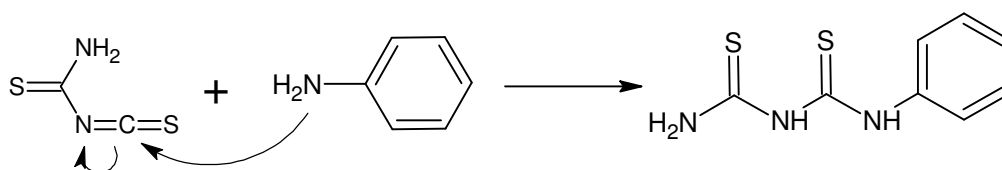
Scheme 63: Formation of 1-phenyldithiobiuret from reaction of thiocarbamoyl isothiocyanate and aniline.

The formation of dithiobiurets in the reaction mixtures is good evidence for a mechanism of nucleophilic attack of the phosphite on the sulphur adjacent to the thiocarbonyl group of xanthane hydride to yield the phosphorthioate and thiocarbamoyl isothiocyante and not, as previously reported, by nucleophilic attack of the sulphur adjacent to the amino group. In the absence of an external nucleophile, it is possible that the thiocarbamoyl isothiocyanate will react with any water to generate thiourea and carbonyl sulphide. It has also been reported that neat thiocarbamoyl isothiocyanates can undergo dimerization (scheme 64) and presumably this is possible in dilute solutions.[135]
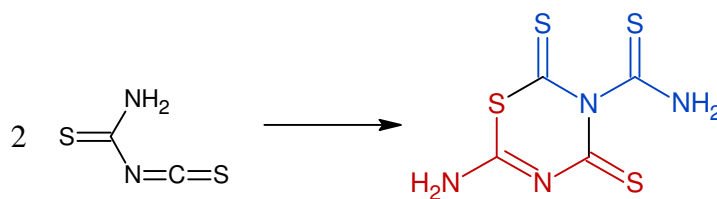
Scheme 64: Dimerization of thiocarbamoyl isothiocyanate.

Similar trapping experiments were performed with the dimethyl derivative of xanthane hydride and 4-nitroaniline. After work up, accurate mass spectroscopy, ^{1}H and ^{13}C NMR showed the presence of the phosphorthioate and 1-(4-nitrophenyl)-5,5-dimethyldithiobiuret. Again this is consistent with attack of the phosphite on the sulphur adjacent to the thiocarbonyl group forming the *N,N*-dimethylthiocarbamoyl isothiocyanate, which is then subsequently trapped by the 4-nitroaniline, producing the dithiobiuret (scheme 65).
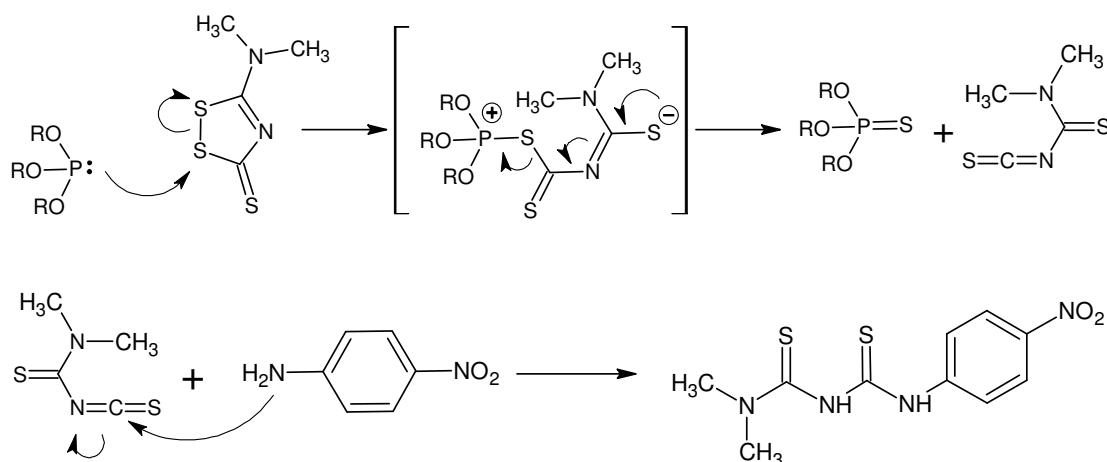
Scheme 65: Sulphurisation with dimethyl xanthane hydride and subsequent trapping of the formed *N,N*-dimethylthiocarbamoyl isothiocyanate with 4-nitroaniline.

5.3 Previously reported evidence for attack of sulphur adjacent to the thiocarbonyl group

Studies on the site of phosphorus attack on xanthane hydride were performed with the selenium derivative of xanthane hydride, 3-amino-1,2,4-thiaselenazole-5-thione, which was synthesised within our group. The reaction between triphenylphosphine and the selenium derivative of xanthane hydride was studied by ^{31}P NMR. The results from these experiments showed that in deuterated acetonitrile, 96% of the product was the triphenylphosphine sulphide and 4% was the triphenylphosphine selenide species (scheme 66).[136] The preferential formation of the sulphide over the selenide is consistent with nucleophilic attack of the phosphorus on the sulphur adjacent to the thiocarbonyl group.
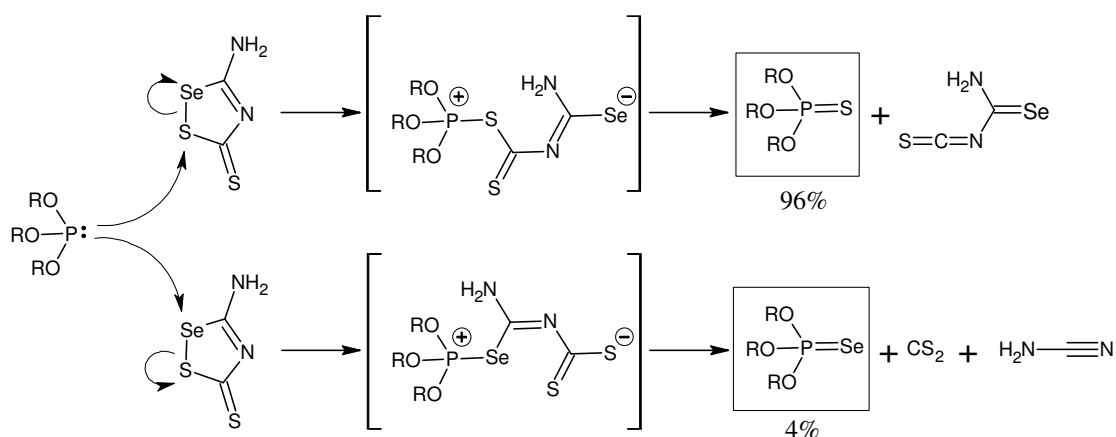
Scheme 66: Phosphite sulphurisation by 3-amino-1,2,4-thiaselenazole-5-thione, the two possible mechanisms.

The site of attack on sulphur adjacent to the thiocarbonyl is predicted from computational calculations-GAUSSIAN 03, of xanthane hydride and dimethyl xanthane hydride, described previously.[136] The most stable tautomers calculated are shown in scheme 67 with Mulliken charges and charges calculated using natural bond analysis (NBO) for the two sites of attack included.
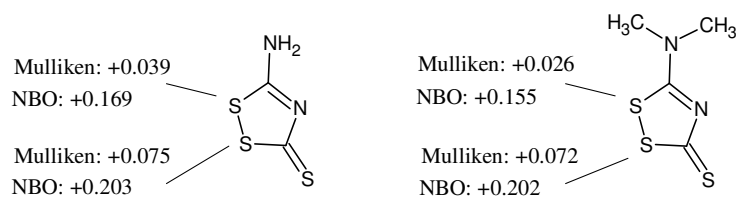
Scheme 67: Mulliken charges and natural bond analysis (NBO) charges of xanthane hydride and dimethyl xanthane hydride in acetonitrile.

In both the xanthane hydride and dimethyl xanthane hydride the Mulliken charge and NBO calculations show that the sulphur adjacent to the thiocarbonyl has a lower electron density than the sulphur adjacent to the amino group and as a consequence will be more susceptible to nucleophilic attack.

5.4 Sulphurisation: kinetics

Initial UV spectroscopic studies of the sulphurisation reaction showed that xanthane hydride absorbs UV at two wavelengths: 280nm and 360nm, which are both removed on addition of phosphite. The majority of phosphites absorb UV at wavelengths which overlap the signal at 280nm therefore the signal at 360nm was monitored to follow the reaction.

Kinetic studies were undertaken with a range of triaryl and trialkylphosphites in acetonitrile. The extent of reaction was followed by monitoring the decrease in the xanthane hydride concentration at 360nm in the presence of excess phosphite. The generated absorbance versus time data showed an exponential decay of the xanthane hydride absorbance which provided pseudo first order rate constants in each case. Plots of k_{obs} as a function of phosphite concentration (figure 53 trialkylphosphites, figure 54 substituted triethylphosphites and figure 55 triarylphosphites) show a linear dependence of k_{obs} on phosphite concentration.

The trialkylphosphites, trimethyl, triethyl, tri-*iso*propyl and tri-*t*-butyl, and the unsubstituted triphenylphosphite were chosen as they were commercially available. Tri(2-cyanoethyl)phosphite was studied to determine the effect of the cyano group upon the sulphurisation reaction, as the phosphites used in oligonucleotide synthesis have a cyanoethyl protecting group upon the phosphorus. The tri(tri-2,2,2-chloroethyl)phosphite was studied as the electron withdrawing nature of the chloro groups would slow the very fast reactions. The substituted triphenylphosphites were chosen for ease of synthesis; the more electron withdrawing the substituent on the starting phenol the more problematic synthesis became and a reduction in the stability of the phosphite product was observed.
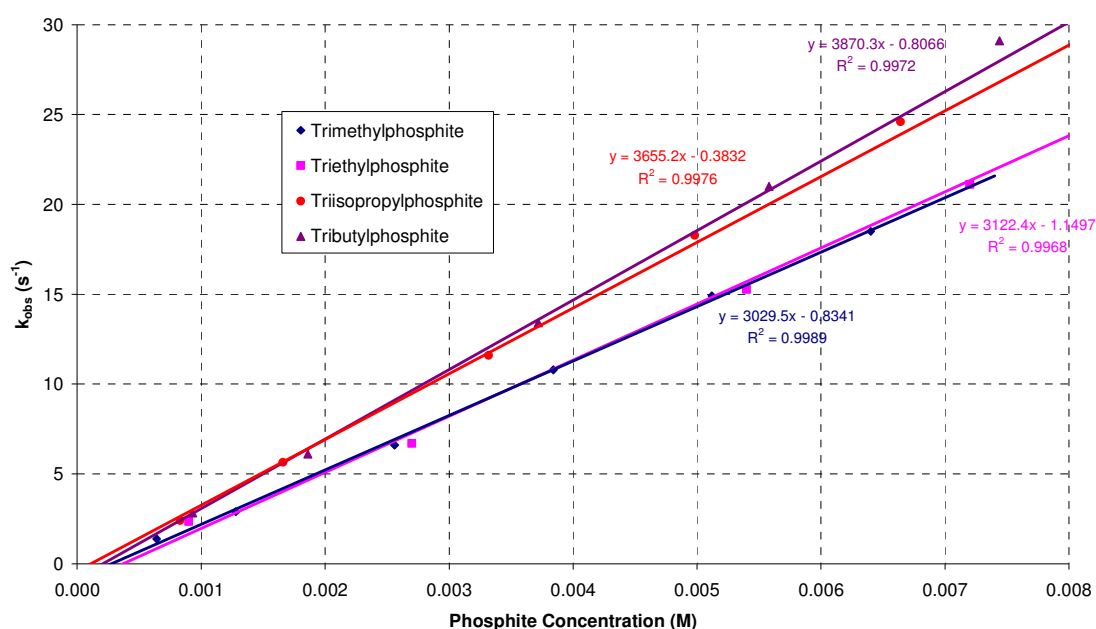
Figure 53: Observed rate constant as a function of phosphite concentration for the sulphurisation of trialkylphosphites in acetonitrile.
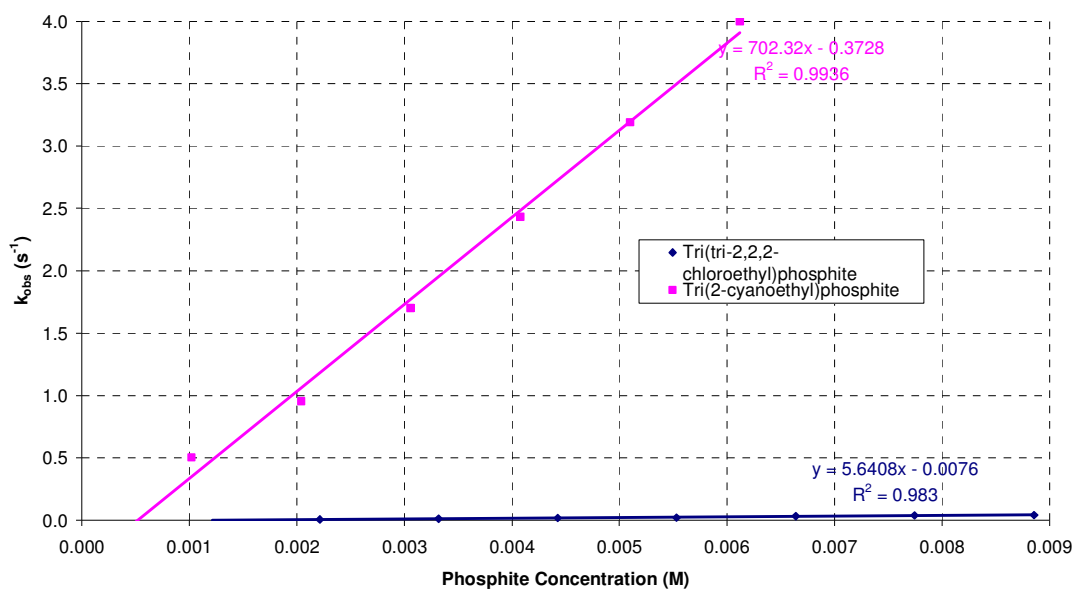
Figure 54: Observed rate constant as a function of phosphite concentration for the sulphurisation of substituted triethylphosphites in acetonitrile.
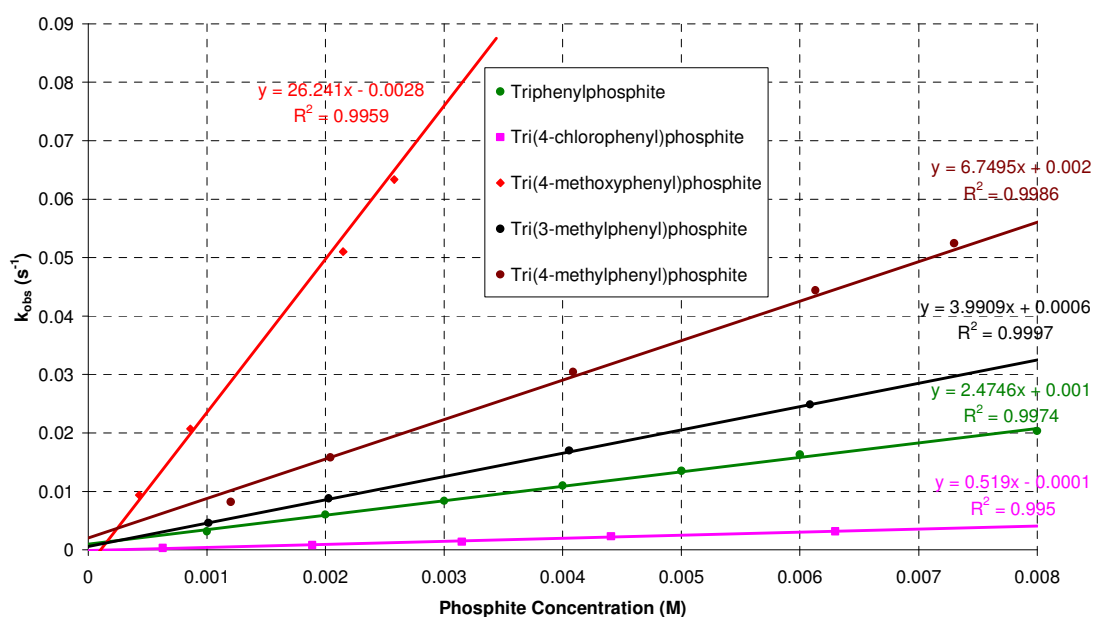
Figure 55: Observed rate constant as a function of phosphite concentration for the sulphurisation of triarylphosphites in acetonitrile.

The calculated second order rate constants determined the plots of observed rate constant versus phosphite concentration for the sulphurisation of each phosphite is summarised in table 34.

164

Phosphite	Second order rate constant ($M^{-1} s^{-1}$)	σ_I[137]	σ[138]
Trimethylphosphite	3030	-0.040	-
Triethylphosphite	3122	-0.051	-
Triisopropylphosphite	3655	-0.062	-
Tri-*t*-butylphosphite	3870	-0.073	-
Tri(2-cyanoethyl)phosphite	702	-	-
Tri(tri-2,2-chloroethyl)phosphite	5.6	-	-
Tri(4-methoxyphenyl)phosphite	26	-	-0.27
Tri(4-methylphenyl)phosphite	6.7	-	-0.17
Tri(3-methylphenyl)phosphite	4.0	-	-0.07
Triphenylphosphite	2.5	0.12	0
Tri(4-chlorophenyl)phosphite	0.5	-	0.23

Table 34: Second order rate constants for the sulphurisation of phosphites with xanthane hydride in acetonitrile and the corresponding substituent constant for each phosphite.

It can be clearly seen that the rate of sulphurisation is dependent on the nature of the substituents in the phosphite triester. The second order rate constants for the trialkylphosphites are approximately three orders of magnitude greater than those for the triarylphosphites which is indicative of a significant inductive effect of the more electron donating alkoxy groups increasing the nucleophilicity of the phosphorus. There is no significant effect on the rate by increasing the size of the substituents of the alkylphosphites. Due to the oxygen bridge between the phosphorus and the alkyl groups it is probable that the steric effects are similar for each of the phosphites studied and the small increase in rate is likely due to the increased inductive effects of the more substituted alkyl groups.

A plot of the second order rate constant for the sulphurisation of trialkylphosphites as a function of Taft's constants for the inductive effects of alkyl groups (σ_I) shows a surprisingly good linear dependence for the four alkyl phosphites (figure 56). Although based on only four data points covering a small range of rates, the slope of this plot gives a reaction constant, ρ_I, of -1.2 which is compatible with an increase in rate on increasing electron donation of the alkyl group.

The substituents on the substituted triethylphosphites are electron withdrawing and despite their considerable distance from the reaction centre, a large decrease in sulphurisation rate is observed. The most electron withdrawing tri(tri-2,2,2-chloroethyl)phosphite has a second order rate constant 3 orders of magnitude less than that of the un-substituted triethylphosphite.

Sulphurisation of Trialkylphosphites with Xanthane Hydridie in Acetonitrile

$y = -1.1744x + 3.3326$
$R^2 = 0.9349$
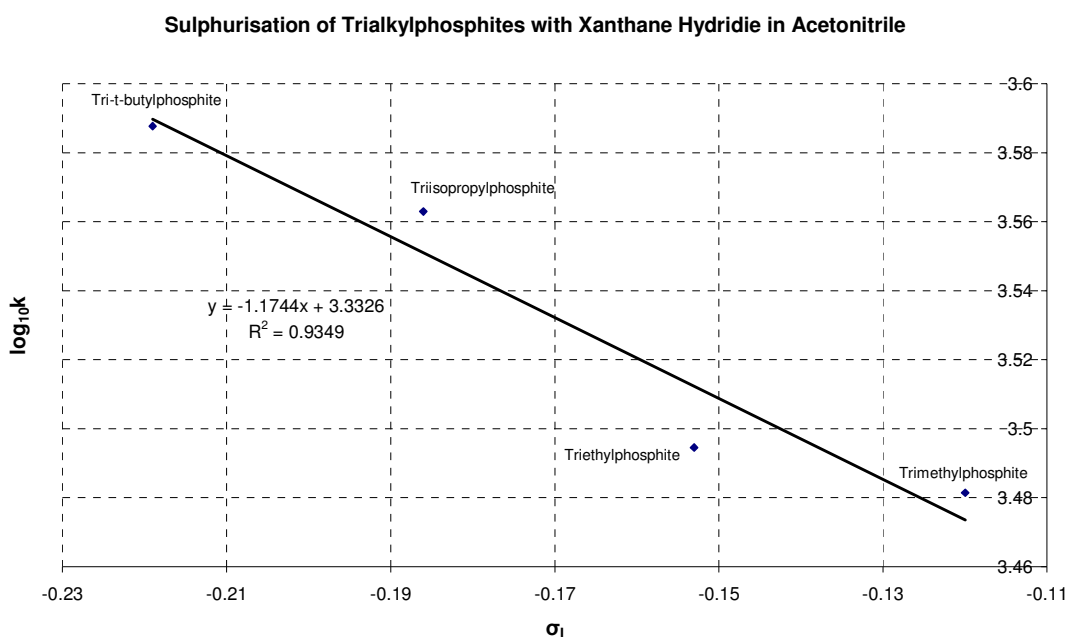
Figure 56: Plot of second order rate constant for the sulphurisation of trialkylphosphites in acetonitrile as a function of Taft's inductive effects (σ_I).

The rate of sulphurisation of the triarylphosphites is slow in comparison to the trialkylphosphites. As expected, electron donating groups upon the phenyl ring increase the size of the second order rate constant and electron withdrawing groups reduce the rate of sulphurisation. A Hammett plot for the triarylphosphites (figure 57), which is the logarithm of the second order rate constant as a function of the substituent constant (σ), shows a linear dependence of the rate constant, the slope of which gives a reaction constant, ρ, of -1.09.

Sulphurisation of Triphenylphosphites with Xanthane Hydride in Acetonitrile
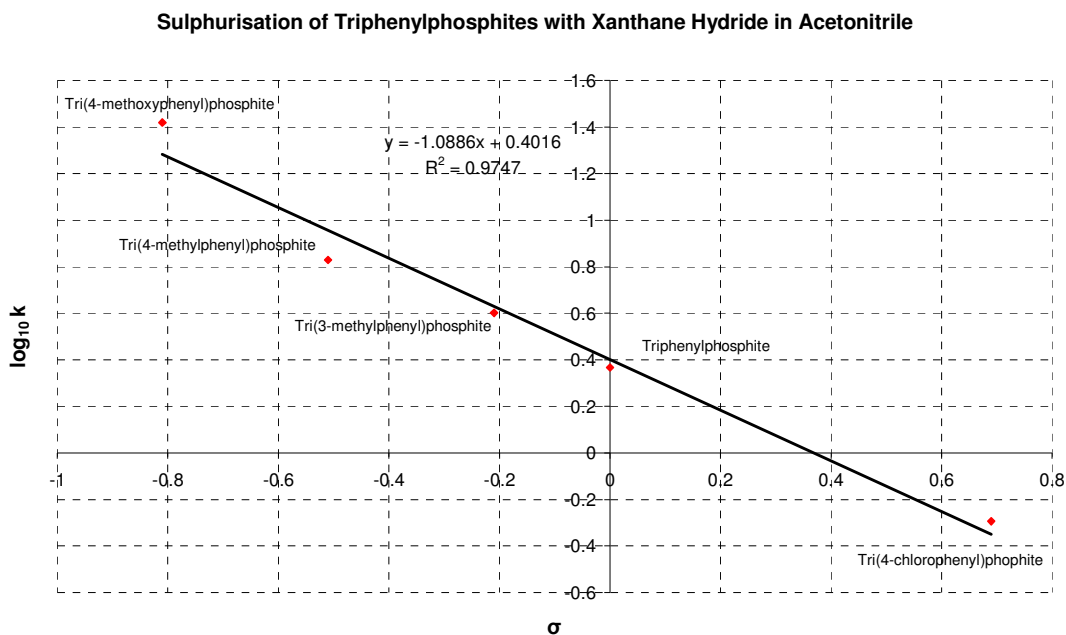
Figure 57: Hammett plot for the sulphurisation of triarylphosphites with xanthane hydride in acetonitrile.

The reaction constant, ρ, for this reaction is equal to -1.09. This is comparable to sulphurisation of trialkylphosphites with xanthane hydride discussed previously, ρ_I = -1.2, triarylphosphines with xanthane hydride and its dimethyl derivative performed by others in our group which generated reaction constants of -0.82 and -0.92 respectively.[136,139]

There are a limited number of Hammett correlations in the literature for reactions of phosphites and phosphines with sulphur derivatives, but among is include the reaction of triarylphosphines with elemental sulphur in benzene, reaction constant -2.5;[140] and the reactions of triarylphosphines and diisopropylphenylphosphonites with diphenyl trisulphide in toluene, reaction constants of -1.1 were determined in each case.[141] The protonation of tertiary phosphines in water gives pK_as which correlated with Taft substituent constants, gave a reaction constant of -2.67.[142]

Comparison of the reaction constant of -2.67 for full charge build up upon the phosphorus, the reaction constants determined here of -1.09 for sulphurisation of triarylphosphites and -1.2 for trialkylphosphites indicate only moderate positive charge

formation on the phosphorus and suggests either an early transition state and the first step being rate limiting or a late transition state and the second step being rate limiting.

5.4.1   Kinetic model

The mechanism for phosphite sulphurisation by xanthane hydride (XH) proposed in scheme 66 can be summarised as below in scheme 68.
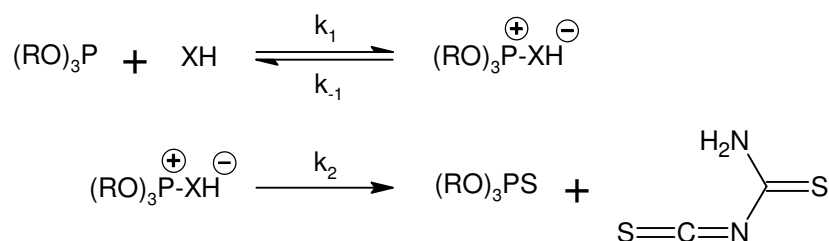
Scheme 68: Mechanism of phosphite sulphurisation.

The rate of phosphorthioate production is given by the following equation:

$$\frac{d[PS]}{dt} = k_2 \left[(RO)_3 P^+ XH^- \right] \qquad \qquad \text{.........1}$$

If the concentration of the intermediate $(RO)_3P^+XH^-$ is assumed to be constant and very small, then applying the steady state assumption gives:

$$\frac{d\left[(RO)_3 P^+ XH^- \right]}{dt} = k_1 \left[(RO)_3 P \right] \left[XH \right] - k_{-1} \left[(RO)_3 P^+ XH^- \right] - k_2 \left[(RO)_3 P^+ XH^- \right] = 0$$

$$k_1 \left[(RO)_3 P \right] \left[XH \right] = \left[(RO)_3 P^+ XH^- \right] \left(k_{-1} + k_2 \right)$$

$$\left[(RO)_3 P^+ XH^- \right] = \frac{k_1 \left[(RO)_3 P \right] \left[XH \right]}{\left(k_{-1} + k_2 \right)} \qquad \qquad \text{.........2}$$

Substituting equation 2 into 1 for [$(RO)_3P^+XH^-$] gives the rate equation:

$$\frac{d[PS]}{dt} = \frac{k_1 k_2 [(RO)_3 P]\,[XH]}{(k_{-1} + k_2)}$$

……….3

If k_{-1} is negligible compared with k_2 i.e. $k_2 \gg k_{-1}$

$$\frac{d[PS]}{dt} = k_1 [(RO)_3 P]\,[XH]$$

Then the rate equation becomes that of a simple second order reaction, and the k_1 step, formation of the intermediate, is rate-limiting.

If k_2 is small compared with k_{-1} i.e. $k_{-1} \gg k_2$

$$\frac{d[PS]}{dt} = \frac{k_1}{k_{-1}} k_2 [(RO)_3 P]\,[XH] = K_1 k_2 [(RO)_3 P]\,[XH]$$

Under these conditions, formation of the intermediate is reversible and the k_2 step is rate-limiting. Then k_{obs} is the product of both the first equilibrium constant and the second step.

5.4.2 Determination of activation parameters

Activation parameters for the sulphurisation of triphenylphosphite with xanthane hydride have been determined in acetonitrile. From a typical plot of the natural logarithm of the second order rate constant as a function of the reciprocal of the temperature (figure 58) the enthalpy and entropy values have been calculated at 30°C as: 36.5 kJ mol^{-1} and -115 J mol^{-1} K^{-1}, respectively, using the Eyring equation shown below.

$$\ln \frac{k}{T} = \frac{-\Delta H}{R} \cdot \frac{1}{T} + \ln \frac{k_b}{h} + \frac{\Delta S}{R}$$

The large negative entropy is indicative of an increase in order from reactants to transition state and is compatible with a bimolecular process. Due to the polarity of acetonitrile there is likely to be an entropic contribution from solvation of the polar transition state.

y = -3881.6x + 14.352
R^2 = 0.9985
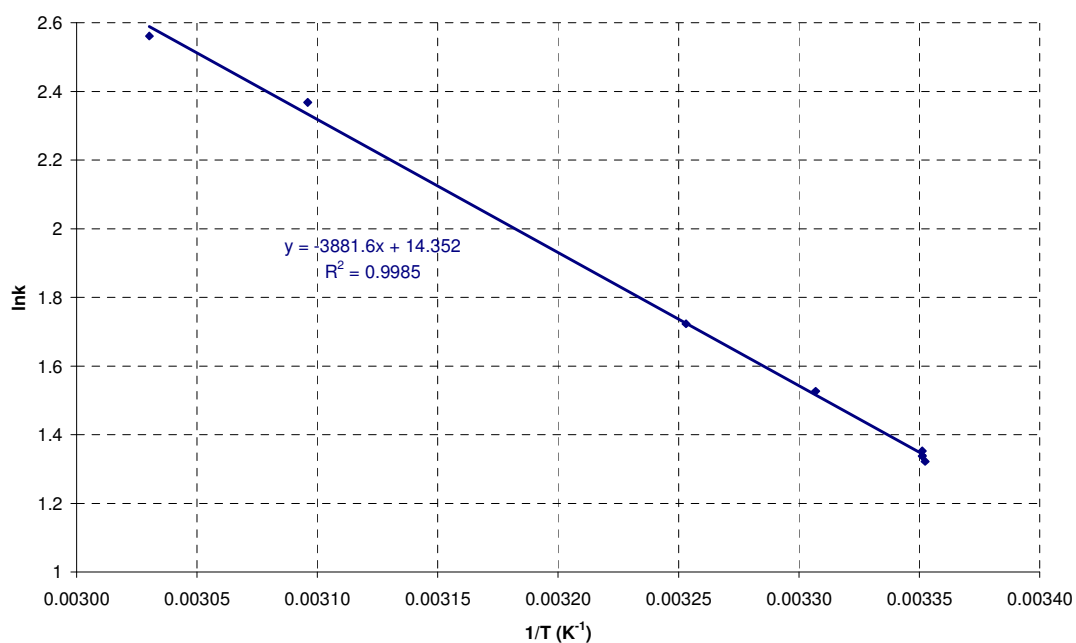
Figure 58: Eyring type plot for sulphurisation of triphenylphosphite with xanthane hydride in acetonitrile.

Previous work within our group has also determined activation parameters for the sulphurisation of triphenylphosphine with xanthane hydride and its dimethyl derivative in acetonitrile, summarised in table 35.[136]

Sample composition	$\Delta H^{\neq}$ (kJ mol^{-1})	$\Delta S^{\neq}$ (J mol^{-1} K^{-1})
Triphenylphosphite + xanthane hydride	36.5	-115
Triphenylphosphine + xanthane hydride	13.3	-121
Triphenylphosphine + dimethyl xanthane hydride	11.7	-128

Table 35: Activation parameters for sulphurisation of triphenylphosphite and triphenylphosphine with xanthane hydride and triphenylphosphine with dimethyl xanthane hydride in acetonitrile at 30°C.

170

In comparison, entropies of activation have been reported to be -146 and -142 J mol^{-1} K^{-1} for the reaction of diphenyl trisulphide with isopropyldiphenylphosphonite and diisopropylphenylphosphonite respectively in toluene.[141]

The activation parameters point to the first step being rate limiting, the relatively large negative entropy of activation being consistent with bimolecular formation of the transition state and generation of a charged species.

5.4.3 The effect of solvent polarity on the rate of sulphurisation

To further study the sulphurisation reaction, kinetic measurements were performed in acetonitrile with added *tetra-n*-propylammonium bromide salt to change the ionic strength of the acetonitrile to determine if medium effects influence the reaction. Classically a change in solvent would have been used to study the effect of solvent polarity, but due to the low solubility of xanthane hydride this was not possible.

Before a kinetic study was undertaken, conductance measurements of *tetra-n*-propylammonium bromide in acetonitrile were performed to confirm that the increase in conductance was linear with increasing salt concentration over the range studied (figure 59). The ionic strength of *tetra-n*-propylammonium bromide solution will be equal to its concentration as the salt is singly charged and this was found to be the case.

Conductance of *tetra-n*-propylammonium bromide in Acetonitrile at 30°C

$y = 0.1088x + 8E-05$
$R^2 = 0.9971$
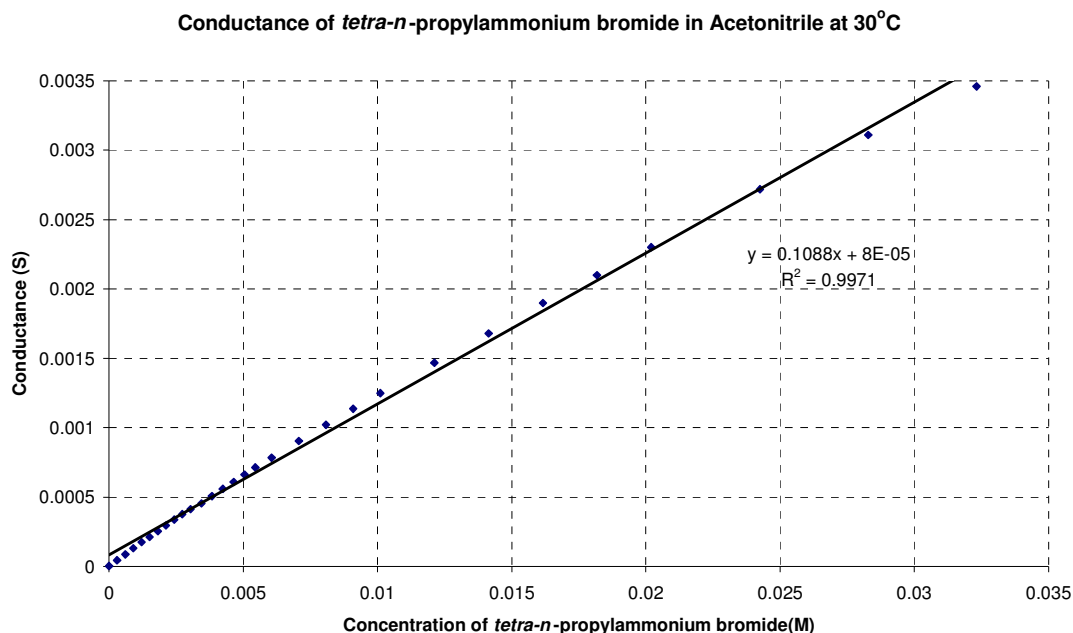
Figure 59: Conductance titration of *tetra-n*-propylammonium bromide to acetonitrile.

A plot of the observed rate constant as a function of phosphite concentration for the sulphurisation of triphenylphosphite with xanthane hydride in a range of *tetra-n*-propylammonium bromide salt solutions (figure 60), shows a decrease in the second order rate constants as the ionic strength of the reaction mixture is increased (table 36).

Sulphurisation of Triphenylphosphite with 9x10^{-5}M XH in Acetonitrile and t*etra-n*-propylammonium Bromide

$y = 3.6187x - 0.0019$
$R^2 = 0.993$

$y = 2.3245x - 0.003$
$R^2 = 0.9995$

$y = 1.6454x + 0.0021$
$R^2 = 0.9987$

$y = 1.1541x - 0.0004$
$R^2 = 0.9996$

$y = 0.8106x + 0.0007$
$R^2 = 0.9993$
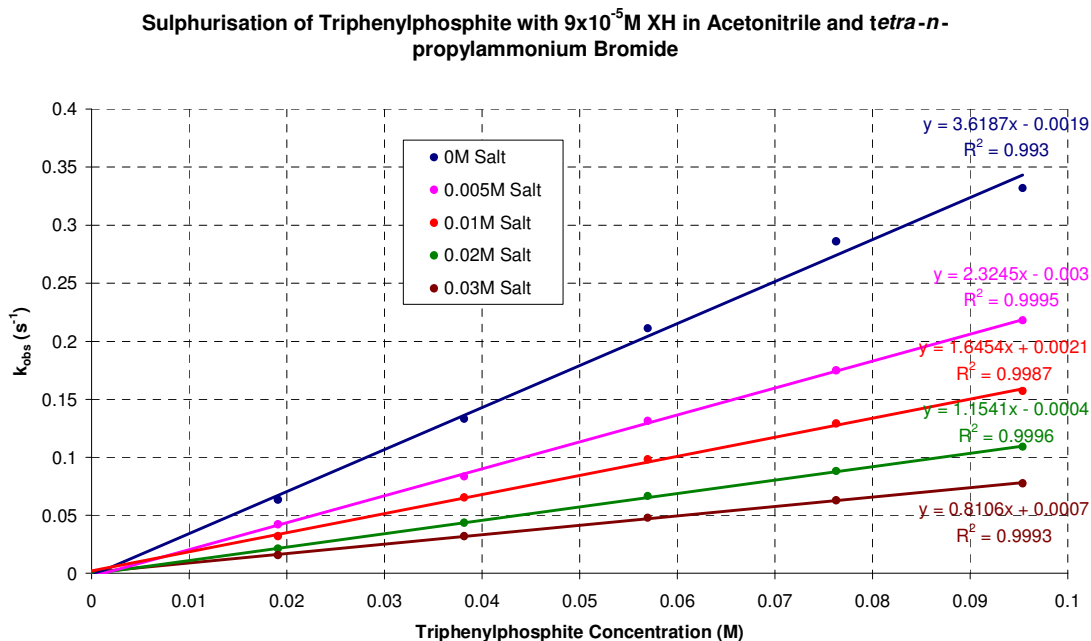
Figure 60: Sulphurisation of triphenylphosphite with xanthane hydride in acetonitrile with varying concentrations of *tetra-n*-propylammoniun bromide salt.

172

tetra-n-propylammonium bromide concentration (M)	k ($M^{-1} s^{-1}$)
0	3.6
0.005	2.3
0.01	1.6
0.02	1.2
0.03	0.8

Table 36: Second order rate constants for the sulphurisation of triphenylphosphite with xanthane hydride (9 x10^{-5} M) in solutions of tetra-n-propylammonium bromide in acetonitrile at 30°C.

These experiments were repeated for the sulphurisation of triphenylphosphine with xanthane hydride in acetonitrile. Again a plot of the observed rate constant as a function of phosphine concentration in a range of *tetra-n*-propylammonium bromide salt solutions (figure 61), shows a reduction in second order rate constant on increasing ionic strength (table 37).
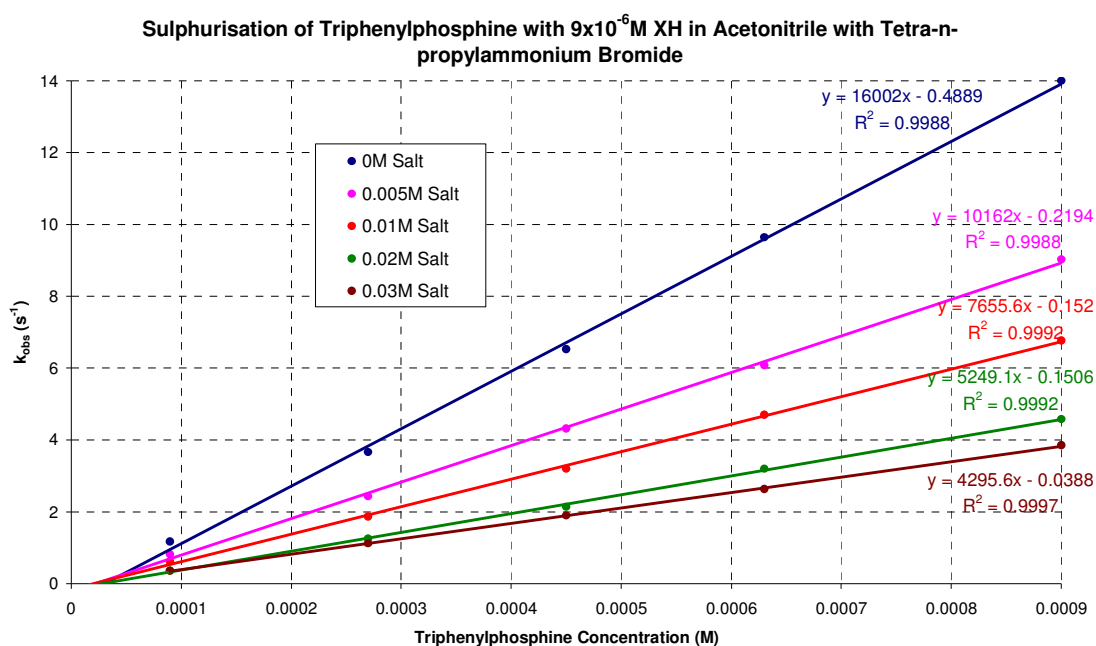
Figure 61: Sulphurisation of triphenylphosphine with xanthane hydride in acetonitrile with varying concentrations of *tetra-n*-propylammonium bromide salt.

tetra-n-propylammonium bromide concentration (M)	k (M^{-1} s^{-1})
0	16002
0.005	10162
0.01	7655
0.02	5249
0.03	4296

Table 37: Second order rate constants for the sulphurisation of triphenylphosphine with xanthane hydride (9 x10^{-5} M) in solutions of tetra-n-propylammonium bromide in acetonitrile at 30°C.

It was expected that increasing the ionic strength would increase the overall rate of reaction. The results show the opposite of this: increasing ionic strength decreases the rate of reaction. To further investigate the effect of ionic strength, activation parameters for the sulphurisation of triphenylphosphite with xanthane hydride were determined in solutions of acetonitrile of varying ionic strength.

Figure 61 shows Eyring type plots for the sulphurisation of triphenylphosphite with xanthane hydride in solutions of varying ionic strength. Good linear fits were obtained and calculated values for enthalpy and entropy are summarised in table 38.

Ionic strength (M)	$\Delta H^{\neq}$ (kJ mol^{-1})	$\Delta S^{\neq}$ (J mol^{-1} K^{-1})
0	32	-130
0.005	35	-122
0.01	38	-116
0.02	40	-113
0.03	39	-116

Table 38: Enthalpic and entropic data for the sulphurisation of triphenylphosphite with xanthane hydride in solutions of acetonitrile with varying ionic strength.

174
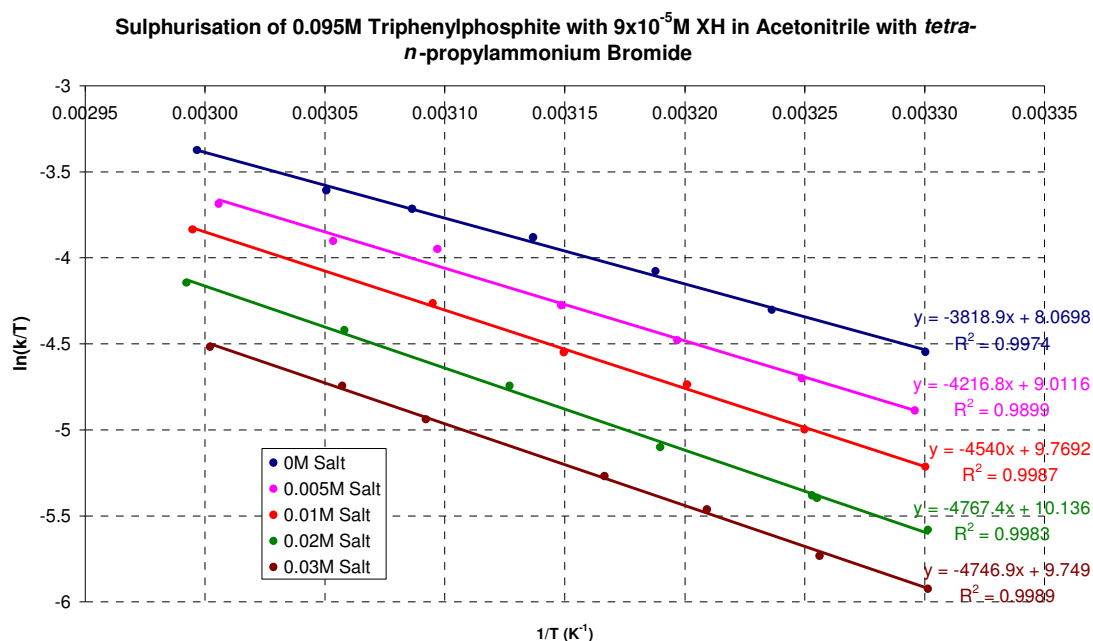
Figure 62: Eyring type plot for the sulphurisation of triphenylphsphite with xanthane hydride in acetonitrile with varying ionic strength.

It was expected that the activation energies would show a significant variation with an increase in solvent polarity due to the change in charge on transition state formation. But, the values for enthalpy and entropy are similar, although entropies of activation show a small decrease (-3 kJ mol^{-1}) and enthalpies a modest increase (+8 kJ mol^{-1}) with increasing ionic strength.

The effect of added salt on the reaction rate could, of course, be either a reactant or transition state effect. In order to examine the former, and using UV techniques described in section 2.5.3, the change in solubility of xanthane hydride in acetonitrile with changing ionic strength was studied. Figure 63 shows a plot of xanthane hydride solubility as a function of ionic strength. The plot shows a linear increase in solubility with increasing ionic strength.

Solubility of Xanthane Hydride in Acetonitrile Varying Ionic Strength with tetra-Propylammoniumbromide

$y = 0.6751x + 0.0147$
$R^2 = 0.9917$
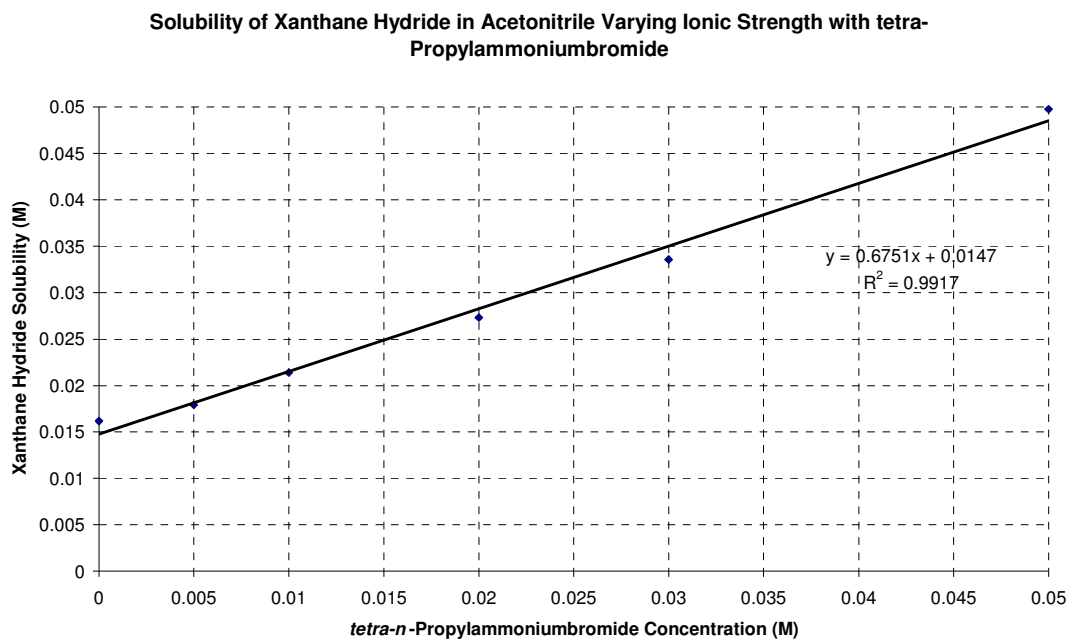
Figure 63: Solubility of xanthane hydride on increasing the ionic strength of acetonitrile.

The increase in solubility with increasing ionic strength is unexpected but indicates an increase in xanthane hydride stability. If the increase in xanthane hydrides solubility, and hence a decrease in energy, is greater than the increase in stability of the transition state then the difference in energy between reactants and transition state will increase. The increase in activation energy will cause a decrease in reaction rate on increasing ionic strength. This is summarised as an energy diagram in figure 64.
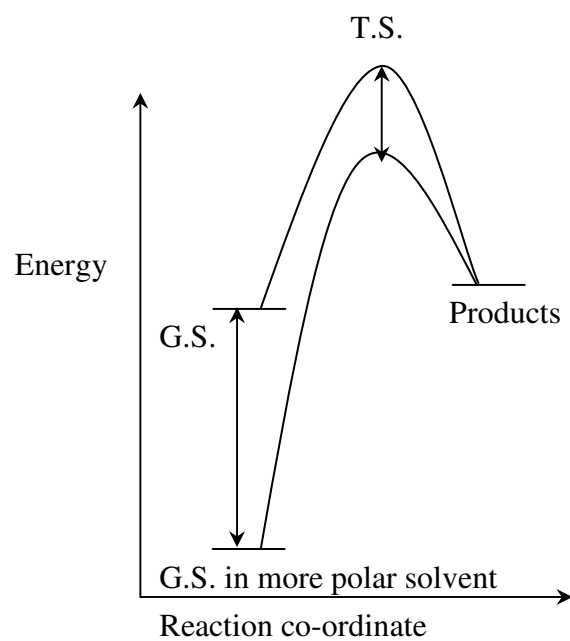
Figure 64: Energy diagram for the sulphurisation reaction showing a large decrease in the ground state (G. S.) energy than in the transition state (T. S.) energy on increasing polarity of solvent.

6   References

(1)   Devlin, T. M. *Textbook of Biochemistry: with Clinical Correlations*; 6th ed.; John Wiley & Sons, Inc., 2006.

(2)   Voet, D.; Voet, J. G.; Pratt, C. W. *Fundamentals of Biochemistry: Life at the Molecular Level*; 2nd ed.; John Wiley & Sons, Inc., 2006.

(3)   Berg, J. M.; Tymoczko, J. L.; Stryer, L. *Biochemistry*; 5th ed.; W. H. Freeman and Co., 2003.

(4)   Kvaerno, L.; Wengel, J. *Chem. Commun.* 2001, 1419.

(5)   Uhlmann, E.; Peyman, A. *Chemical Reviews* 1990, *90*, 543.

(6)   Stephenson, M. L.; Zamecnik, P. C. *Proc. Natl. Acud. Sci. U.S.A.* 1978, *75*, 285.

(7)   Zamecnik, P. C.; Stephenson, M. L. *Proc. Natl. Acud. Sci. U.S.A.* 1978, *75*, 280.

(8)   Micklefield, J. *Current Medicinal Chemistry* 2001, *8*, 1157.

(9)   Lonnberg, H. *Annu. Rep. Prog. Chem., Sect. B* 1999, *95*, 207.

(10)   Gryaznov, S.; Skorski, T.; Cucco, C.; Nieborowska-Skoska, M.; Chiu, C. Y.; Lloyd, D.; Chen, J. K.; Koziolkiewicz, M.; Calabretta, B. *Nucleic Acids Research* 1996, *24*, 1508.

(11)   van der Krol, A. R.; Mol, J. N. M.; Stuitje, A. R. *BioTechniques* 1988, *6*, 958.

(12)   Yamada, C. M.; Dellinger, D. J.; Caruthers, M. H. *J. Am. Chem. Soc.* 2006, *128*, 5251.

(13)   Monia, B. P.; Johnston, J. F.; Sasmor, H.; Cummins, L. L. *The Journal of Biological Chemistry* 1996, *271*, 14533.

(14)   Frey, P. A.; Sammons, R. D. *Science* **1985**, *228*, 541.

(15)   Iyengar, R.; Eckstein, F.; Frey, P. A. *J. Am. Chem. Soc.* **1984**, *106*, 8309.

(16)   Brill, W. K. D.; Nielsen, J.; Caruthers, M. H. *J. Am. Chem. Soc.* **1991**, *113*, 3972.

(17)   Beaton, G.; Brill, W. K. D.; Grandas, A.; Ma, Y. X.; Nielsen, J.; Yau, E.; Caruthers, M. H. *Tetrahedron* **1991**, *47*, 2377.

(18)   Ghosh, M. K.; Ghosh, K.; Dahl, O.; Cohen, J. S. *Nucleic Acids Research* **1993**, *21*, 5761.

(19)   Froehler, B. C. *Tetrahedron Letters* **1986**, *27*, 5575.

(20)   Froehler, B. C.; Ng, P. G.; Matteucci, M. D. *Nucleic Acids Research* **1986**, *14*, 5399.

(21)   Sergueev, D. S.; Ramsay-Shaw, B. *J. Am. Chem. Soc.* **1998**, *120*, 9417.

(22)   Sood, A.; Ramsay-Shaw, B.; Spielvogel, B. F. *J. Am. Chem. Soc.* **1990**, *112*, 9000.

(23)   Heidenreich, O.; Gryaznov, S.; Nerenberg, M. *Nucleic Acids Research* **1997**, *25*, 776.

(24)   Murakami, A.; Blake, K. R.; Miller, P. S. *Biochemistry* **1985**, *24*, 4041.

(25)   Stein, C. A.; Cohen, J. S. *Cancer Research* **1988**, *48*, 2659.

(26)   Blake, K. R.; Murakami, A.; Miller, P. S. *Biochemistry* **1985**, *24*, 6132.

(27)   Blake, K. R.; Murakami, A.; Spitz, S. A.; Glave, S. A.; Parameswara-Reddy, M.; Ts'o, P. O. P.; Miller, P. S. *Biochemistry* **1985**, *24*, 6139.

(28)   Agris, C. H.; Blake, K. R.; Miller, P. S.; Parameswara-Reddy, M.; Ts'o, P. O. P. *Biochemistry* 1986, *25*, 6268.

(29)   Bower, M.; Summers, M. F.; Powell, C.; Shinozuka, K.; Regan, J. B.; Zon, G.; Wilson, W. D. *Nucleic Acids Research* 1987, *15*, 4915.

(30)   Miller, P. S.; McParland, K. B.; Jayaraman, K.; Ts'o, P. O. P. *Biochemistry* 1981, *20*, 1874.

(31)   Agarwal, K. L.; Riftina, F. *Nucleic Acids Research* 1979, *6*, 3009.

(32)   de Vroom, E.; Dreef, C. E.; van der Elst, H.; van der Marel, G. A.; van Boom, J. H. *Recl. Trav. Chim. Pays-Bas* 1988, *107*, 592.

(33)   Bergstrom, D.; Romo, E.; Shum, P. *Nucleosides & Nucleotides* 1987, *6*, 53.

(34)   Bergstrom, D. E.; Shum, P. W. *J. Org. Chem.* 1988, *53*, 3953.

(35)   Obika, S.; Nanbu, D.; Hari, Y.; Andoh, J. I.; Morio, K. I.; Doi, T.; Imanishi, T. *Tetrahedron Letters* 1998, *39*, 5401.

(36)   Christensen, N. K.; Petersen, M.; Nielsen, P.; Jacobsen, J. P.; Olsen, C. E.; Wengel, J. *J. Am. Chem. Soc.* 1998, *120*, 5458.

(37)   Tolstikov, V. V.; Stetsenko, D. A.; Potapov, V. K.; Sverdlov, E. D. *Nucleosides & Nucleotides* 1997, *16*, 215.

(38)   Seela, F.; Chen, Y. *Helvetica Chimica Acta* 1997, *80*, 1073.

(39)   Balow, G.; Mohan, V.; Lesnik, E. A.; Johnston, J. F.; Monia, B. P.; Acevedo, O. L. *Nucleic Acids Research* 1998, *26*, 3350.

(40)   Letsinger, R. L.; Ogilvie, K. K. *J. Am. Chem. Soc.* 1967, *89*, 4801.

(41)   Letsinger, R. L.; Ogilvie, K. K. *J. Am. Chem. Soc.* 1969, *91*, 3350.

(42)   Reese, C. B.; Song, Q. *Bioorganic & Medicinal Chemistry Letters* 1997, *7*, 2787.

(43)   Reese, C. B.; Song, Q. *Nucleic Acids Research* **1999,** *27*, 963.

(44)   Reese, C. B.; Song, Q. *J. Chem. Soc., Perkin Trans. 1* **1999,** 1477.

(45)   Stawinski, J.; Hozumi, T.; Narang, S. A. *Can. J. Chem.* **1976,** *54*, 670.

(46)   Jones, S. S.; Rayner, B.; Reese, C. B.; Ubasawa, A.; Ubasawa, M. *Tetrahedron* **1979,** *36*, 3075.

(47)   Zarytova, V. F.; Knorre, D. G. *Nucleic Acids Research* **1984,** *12*, 2091.

(48)   Letsinger, R. L.; Finnan, J. L.; Heavner, G. A.; Lunsford, W. B. *J. Am. Chem. Soc.* **1975,** 3278.

(49)   Letsinger, R. L.; Lunsford, W. B. *J. Am. Chem. Soc.* **1976,** 3655.

(50)   Beaucage, S. L.; Caruthers, M. H. *Tetrahedron Letters* **1981,** *22*, 1859.

(51)   Matteucci, M. D.; Caruthers, M. H. *J. Am. Chem. Soc.* **1981,** *103*, 3185.

(52)   Tsukamoto, M.; Hayakawa, Y. *Frontiers in Organic Chemistry* **2005,** *1*, 3.

(53)   Sigurdsson, S.; Stromberg, R. *J. Chem. Soc., Perkin Trans. 2* **2002,** 1682.

(54)   Krotz, A. H.; McElroy, B.; Scozzari, A. N.; Cole, D. L.; Ravikumar, V. T. *Organic Process Research & Development* **2003,** *7*, 47.

(55)   Xu, Q.; Musier-Forsyth, K.; Hammer, R. P.; Barany, G. *Nucleic Acids Research* **1996,** *24*, 1602.

(56)   Michalski, J.; Dabkowski, W. *Top Curr Chem* **2004,** *232*, 93.

(57)   Garegg, P. J.; Lindh, I.; Regberg, T.; Stawinski, J.; Stromberg, R. *Tetrahedron Letters* 1986, *27*, 4051.

(58)   Garegg, P. J.; Regberg, T.; Stawinski, J.; Stromberg, R. *Chemica Scripta* 1985, *25*, 280.

(59)   Schwarz, M. W.; Pfleiderer, W. *Tetrahedron Letters* 1984, *25*, 5513.

(60)   McBride, L. J.; Caruthers, M. H. *Tetrahedron Letters* 1983, *24*, 245.

(61)   Hall, R. H.; Todd, A.; Webb, R. F. *Nucleotides* 1957, 3291.

(62)   Garegg, P. J.; Regberg, T.; Stawinski, J.; Stromberg, R. *Chemica Scripta* 1986, *26*, 59.

(63)   Kuyl-Yeheskiely, E.; Spierenburg, M.; van der Elst, H.; Tromp, M.; van der Marel, G. A.; van Boom, J. H. *Recl. Trav. Chim. Pays-Bas* 1986, *105*, 505.

(64)   Paul, C. H.; Royappa, A. T. *Nucleic Acids Research* 1996, *24*, 3048.

(65)   Adams, S. P.; Kavka, K. S.; Wykes, E. J.; Holder, S. B.; Galluppi, G. R. *J. Am. Chem. Soc.* 1983, *105*, 661.

(66)   Baik, M. H.; Friesner, R. A.; Lippard, S. J. *J. Am. Chem. Soc.* 2002, *124*, 4495.

(67)   Roger, M.; Hotchkiss, R. D. *Proc. Natl. Acud. Sci. U.S.A.* 1961, *47*, 653.

(68)   Septak, M. *Nucleic Acids Research* 1996, *24*, 3053.

(69)   Krotz, A. H.; Cole, D. L.; Ravikumar, V. T. *Nucleosides & Nucleotides* 1999, *18*, 1207.

(70)   Sproat, B. S.; Bannwarth, W. *Tetrahedron Letters* 1983, *24*, 5771.

(71)   Froehler, B. C.; Matteucci, M. D. *Nucleic Acids Research* 1983, *11*, 8031.

(72)   Kume, A.; Iwase, R.; Sekine, M.; Hata, T. *Nucleic Acids Research* **1984**, *12*, **8525.**

(73)   Crugeiras, J.; Maskill, H. *J. Chem. Soc., Perkin Trans. 2* **1998, 1901.**

(74)   Canle, M. L.; Demirtas, I.; Maskill, H. *J. Chem. Soc., Perkin Trans. 2* **2001, 1748.**

(75)   Crugeiras, J.; Maskill, H. *J. Chem. Soc., Perkin Trans. 2* **2000, 441.**

(76)   Crugeiras, J.; Maskill, H. *Can. J. Chem.* **1999,** *77*, **530.**

(77)   Dahl, B. H.; Nielsen, J.; Dahl, O. *Nucleic Acids Research* **1987,** *15,* **1729.**

(78)   Nurminen, E. J.; Mattinen, J. K.; Lonnberg, H. *J. Chem. Soc., Perkin Trans. 2* **1998, 1621.**

(79)   Nurminen, E. J.; Mattinen, J. K.; Lonnberg, H. *J. Chem. Soc., Perkin Trans. 2* **2001, 2159.**

(80)   Berner, S.; Muhlegger, K.; Seliger, H. *Nucleic Acids Research* **1989,** *17*, **853.**

(81)   Hayakawa, Y.; Kataoka, M. *J. Am. Chem. Soc.* **1997,** *119*, **11758.**

(82)   van der Knaap, T. A.; Bickelhaupt, F. *Phosphorus and Sulphur* **1984,** *21*, **227.**

(83)   Dahl, O. *Phosphorus and Sulphur* **1983,** *18*, **201.**

(84)   Nurminen, E. J.; Mattinen, J. K.; Lonnberg, H. *J. Chem. Soc., Perkin Trans. 2* **2000, 2238.**

(85)   Batyeva, E. S.; Al'fonsov, V. A.; Zamaletdinova, G. U.; Pudovik, A. N. *Russ. J. Gen. Chem. (Engl. Trans.)* **1976,** *46*, **2120.**

(86)   Beaucage, S. L. *Tetrahedron Letters* **1984,** *25*, **375.**

(87)   Korkin, A. A.; Tsvetkov, E. N. *Bull. Soc. Chim. Fr.* **1988, 335.**

(88)   Korkin, A. A.; Tsvetkov, E. N. *Russ. J. Gen. Chem. (Engl. Trans.)* **1987**, *57*, **1929.**

(89)   Hayakawa, Y.; Iwase, T.; Nurminen, E. J.; Tsukamoto, M.; Kataoka, M. *Tetrahedron* **2005**, *61*, **2203.**

(90)   Sanghvi, Y. S.; Guo, Z.; Pfundheller, H. M.; Converso, A. *Organic Process Research & Development* **2000**, *4*, **175.**

(91)   Pon, R. T. *Tetrahedron Letters* **1987**, *28*, **3643.**

(92)   Vargeese, C.; Carter, J.; Yegge, J.; krivjansky, S.; Settle, A.; Kropp, E.; Peterson, K.; Pieken, W. *Nucleic Acids Research* **1998**, *26*, **1046.**

(93)   Jin, Y.; Just, G. *J. Org. Chem.* **1998**, *63*, **3647.**

(94)   Dabkowski, W.; Tworowska, I.; Michalski, J.; Cramer, F. *Tetrahedron Letters* **2000**, *41*, **7535.**

(95)   Froehler, B. C.; Matteucci, M. D. *Tetrahedron Letters* **1983**, *24*, **3171.**

(96)   Stawinski, J.; Hozumi, T.; Narang, S. A.; Bahl, C. P.; Wu, R. *Nucleic Acids Research* **1977**, *4*, **353.**

(97)   Xie, C.; Staszak, M. A.; Quatroche, J. T.; Sturgill, C. D.; Khau, V. V.; Martinelli, M. J. *Organic Process Research & Development* **2005**, *9*, **730.**

(98)   Hayakawa, Y. *Bull. Chem. Soc. Jpn.* **2001**, *74*, **1547.**

(99)   Hayakawa, Y.; Kataoka, M.; Noyori, R. *J. Org. Chem.* **1996**, *61*, **7996.**

(100)   Hayakawa, Y.; Kawai, R.; Hirata, A.; Sugimoto, J. I.; Kataoka, M.; Sakakura, A.; Hirose, M.; Noyori, R. *J. Am. Chem. Soc.* **2001**, *123*, **8165.**

(101)   Hayakawa, Y.; Kataoka, M. *J. Am. Chem. Soc.* **1998**, *120*, **12395.**

(102)   Eleuteri, A.; Capaldi, D. C.; Krotz, A. H.; Cole, D. L.; Ravikumar, V. T. *Organic Process Research & Development* **2000**, *4*, **182.**

(103)   Stec, W. J.; Zon, G.; Egan, W.; Stec, B. *J. Am. Chem. Soc.* **1984**, *106*, 6077.

(104)   Connolly, B. A.; Potter, B. V. L.; Eckstein, F.; Pingoud, A.; Grotjahn, L. *Biochemistry* **1984**, *23*, 3443.

(105)   Iyer, R. P.; Phillips, L. R.; Egan, W.; Regan, J. B.; Beaucage, S. L. *J. Org. Chem.* **1990**, *55*, 4693.

(106)   Vu, H.; Hirschbein, B. L. *Tetrahedron Letters* **1991**, *32*, 3005.

(107)   Stec, W. J.; Uznanski, B.; Wilk, A. *Tetrahedron Letters* **1993**, *34*, 5317.

(108)   Vaman-Rao, M.; Macfariane, K. *Tetrahedron Letters* **1994**, *35*, 6741.

(109)   Zhang, Z.; Nichols, A.; Alsbeti, M.; Tang, J. X.; Tang, J. Y. *Tetrahedron Letters* **1998**, *39*, 2467.

(110)   Cheruvallath, Z. S.; Krishna-Kumar, R.; Rentel, C.; Cole, D. L.; Ravikumar, V. T. *Nucleosides, Nucleotides & Nucleic Acids* **2003**, *22*, 461.

(111)   Tang, J. Y.; Han, Y.; Tang, J. X.; Zhang, Z. *Organic Process Research & Development* **2000**, *4*, 194.

(112)   Hordvik, A. *Acta Chem. Scand.* **1963**, *17*, 2575.

(113)   Butler, A. R.; Glidewell, C. *J. Chem. Research* **1981**, 801.

(114)   Pon, R. T.; Yu, S.; Guo, Z.; Sanghvi, Y. S. *Nucleic Acids Research* **1999**, *27*, 1531.

(115)   Natt, F.; Haner, R. *Tetrahedron* **1997**, *53*, 9629.

(116)   Gait, M. J. *Oligonucleotide Synthesis: A Practical Approach*; IRL Press, **1984**.

(117)   Fahlberg, C.; Remsen, I. *ibid.* **1884**, *6*, 260.

(118)   Jencks, W. P.; Regenstein, J. *Handbook of Biochemistry*.

(119)   Chantooni, M. K.; Kolthoff, I. M. *Analytical Chemistry* **1979**, *51*, **133.**

(120)   Leito, I.; Kaljurand, I.; Koppel, I. A.; Yagupolskii, L. M.; Vlasov, V. M. *J. Org. Chem.* **1998**, *63*, **7868.**

(121)   Perdoncin, G.; Scorrano, G. *J. Am. Chem. Soc.* **1977, 6983.**

(122)   Jencks, W. P. *Accounts in Chemical Research* **1980**, *13*, **161.**

(123)   Jencks, W. P. *J. Am. Chem. Soc.* **1972**, *94*, **4731.**

(124)   Fife, T. H. *Accounts in Chemical Research* **1971, 5, 264.**

(125)   Fife, T. H.; Anderson, E. *J. Org. Chem.* **1971**, *36*, **2357.**

(126)   Nurminen, E. J.; Mattinen, J. K.; Lonnberg, H. *J. Chem. Soc., Perkin Trans. 2* **1999, 2551.**

(127)   Corbridge, D. E. C. *Phosphorus: An Outline of its Chemistry, Biochemistry and Technology*; Elsevier, **1978.**

(128)   Walker, B. J. *Organophosphorus Chemistry*; 1st ed.; Penguin Books Ltd, **1972.**

(129)   Bell, R. P.; Higgins, W. C. E. *Proceedings of the Royal Society of London. Series A, Mathematical and Physical Sciences* **1949**, *197*, **141.**

(130)   Catalan, J.; Abboud, J. L. M.; Elguero, J. In *Advances in Heterocyclic Chemistry*; Academic Press: New York, 1987; Vol. 41, p 187.

(131)   Schwetlick, K.; Noack, R.; Stebner, F. *J. Chem. Soc., Perkin Trans. 2* **1994, 599.**

(132)   Coetzee, J. F.; Padmanabhan, G. R. *J. Am. Chem. Soc.* **1965**, *87*, **5005.**

(133)   Peral, F.; Gallego, E. *Journal of Molecular Structure* **1997**, *415*, **187.**

(134)   Schwetlick, K.; Noack, R. *J. Chem. Soc., Perkin Trans. 2* **1995, 395.**

(135)   Spurlock, L. A.; Newallis, P. E. *J. Org. Chem.* **1968**, *33*, **2073.**

(136)   Hanusek, J.; Russell, M. A.; Laws, A. P.; Jansa, P.; Atherton, J. H.; Fettes, K.; Page, M. I. *Org. Biomol. Chem* **2007**, *5*, **478.**

(137)   Taft, R. W.; Taagepera, M.; Abboud, J. L. M.; Wolf, J. F.; DeFrees, D. J.; Hehre, W. J.; Bartmess, J. E.; McIver, R. T. *J. Am. Chem. Soc.* **1978**, *100*, **7765.**

(138)   Wiberg, K. B. *Physical Organic Chemistry*; 1st ed.; John Wiley & Sons, Inc., **1964.**

(139)   Hanusek, J.; Russell, M. A.; Laws, A. P.; Page, M. I. *Tetrahedron Letters* **2007**, *48*, **417.**

(140)   Bartlett, P. D.; Meguerian, G. *J. Am. Chem. Soc.* **1956**, *78*, **3710.**

(141)   Hall, C. D.; Tweedy, B. R.; Kayhanian, R.; Lloyd, J. R. *J. Chem. Soc., Perkin Trans. 2* **1992**, **775.**

(142)   Henderson, W. A., Jr.; Strueli, C. A. *J. Am. Chem. Soc.* **1960**, *82*, **5791.**

7   Appendix

7.1   Calculation   of K_{diss} by   conductance: Saccharin/diisopropylamine salt

In excess diisopropylamine only charged species will be present in solution as all of the saccharin will be ionised, therefore only K_{diss}, the dissociation of the ion pair into solvent separated free ions, needs to be considered

$$[\overset{\ominus}{S}\,\overset{\oplus}{DIAH}]_{ip} \xrightleftharpoons{K_{diss}} \overset{\ominus}{S} + DIA\overset{\oplus}{H}$$

The equation for the equilibrium constant is:

$$K_{diss} = \frac{[S^-][DIAH^+]}{[S^-\,DIAH^+]_{ip}} \qquad \ldots\ldots\ldots.1$$

Charges must balance, and this gives:

$$[S^-] = [DIAH^+]$$

Substituting for [DIAH⁺] in to equation 1 gives:

$$K_{diss} = \frac{[S^-]^2}{[S^-\,DIAH^+]_{ip}} \qquad \ldots\ldots\ldots.2$$

And,

$$[S^-DIAH^+]_{ip} = \frac{[S^-]^2}{K_{diss}}$$ 3

The mass balance for reaction can be written as:

$$[S^-H^+DIA]_{added} = [S^-] + [S^-\ DIAH^+]_{ip}$$ 4

Substituting for [S⁻DIAH⁺] equation 3 into mass balance,

$$[S^-\ DIAH^+]_{added} = [S^-] + \frac{[S^-]^2}{K_{diss}}$$ 5

Rearranging equation 5 into the form of a standard quadratic gives:

$$0 = \frac{[S^-]^2}{K_{diss}} + [S^-] - [S^-\ DIAH^+]_{added}$$ 6

The solution to which are

$$[S^-] = \frac{-b \pm \sqrt{b^2 - 4ac}}{2a}$$

Where

$$a = \frac{1}{K_{diss}} \qquad\qquad b = 1 \qquad\qquad c = -[S^-\ DIAH^+]_{added}$$

$$[S^-] = \frac{-1 + \sqrt{1^2 - 4\left(\frac{1}{K_{diss}}\right)\left(-[S^-\ DIAH^+]_{added}\right)}}{2\left(\frac{1}{K_{diss}}\right)}$$

$$[S^-] = \frac{\left(-1+\sqrt{1^2 + 4[S^- \ DIAH^+]_{added} \ / K_{diss}}\right) K_{diss}}{2} \qquad \ldots\ldots\ldots.7$$

And the concentration of the ion is directly proportional to the conductance of the system. Given by the equation:

$$[S^-] = \frac{(Mc - Bc)}{Sc}$$

Where,   Mc = Measured conductance of solution

Bc = Background conductance in the of saccharin and *N*-methylimidazole

Sc = Specific conductance of the analyt

7.2 Calculation of K$_{ass}$ by conductance: Saccharin/diisopropylamine salt

At lower diisopropylamine concentrations then two equilibria need to be considered,

$$SH + DIA \underset{}{\overset{K_{ass}}{\rightleftharpoons}} [S^{-} DIAH^{+}]_{ip} \underset{}{\overset{K_{diss}}{\rightleftharpoons}} S^{-} + DIAH^{+}$$

The equilibrium constant for the association of neutral molecules to form the ion pair is given by,

$$K_{ass} = \frac{\left[S^{-} DIAH^{+}\right]_{ip}}{[SH][DIA]} \qquad \ldots\ldots\ldots.1$$

The equilibrium constant for the dissociation of the ion pair into solvent separated free ions is again given by,

$$K_{diss} = \frac{\left[S^{-}\right]\left[DIAH^{+}\right]}{\left[S^{-} DIAH^{+}\right]_{ip}} \qquad \ldots\ldots\ldots.2$$

Again the charges must balance, provided that equal amounts of the stating materials are added.

$$[SH] = [HDIA] \text{ and } [S^{-}] = [DIAH^{+}]$$

Therefore equations 1 and 2 can be rewritten as:

$$K_{ass} = \frac{\left[S^{-} DIAH^{+}\right]_{ip}}{[SH]^{2}} \qquad \ldots\ldots\ldots.3$$

$$K_{diss} = \frac{[S^-]^2}{[S^- \; DIAH^+]_{ip}} \qquad \qquad \text{.........4}$$

From the mass balance for reaction, we can write:

$$[S^- \; DIAH^+]_{added} = [SH] + [S^-] + [S^- \; DIAH^+]_{ip} \qquad \qquad \text{.........5}$$

Rearranging equation 3 gives,

$$[SH]^2 = \frac{[S^- \; DIAH^+]_{ip}}{K_{ass}} \qquad \qquad \text{.........6}$$

Rearranging and simplifying equation 4 gives,

$$[S^- \; DIAH^+]_{ip} = \frac{[S^-]^2}{K_{diss}} \qquad \qquad \text{.........7}$$

Substituting equation 7 into 6 and simplifying gives,

$$[SH]^2 = \frac{[S^-]^2}{K_{ass} \; K_{diss}}$$

$$[SH] = \frac{[S^-]}{\sqrt{K_{ass} \; K_{diss}}} \qquad \qquad \text{.........8}$$

Substituting equations 7 and 8 into mass balance,

$$[S^- \; DIAH^+]_{added} = \frac{[S^-]}{\sqrt{K_{ass} K_{diss}}} + [S^-] + \frac{[S^-]^2}{K_{diss}} \qquad \qquad \text{.........9}$$

Simplifying equation 8 gives:

$$\left[S^- \; DIAH^+\right]_{added} = \left\{ 1+ 1\Big/\sqrt{K_{ass}K_{diss}} \; \right\}\left[S^-\right] + \frac{\left[S^-\right]^2}{K_{diss}} \qquad\qquad \ldots\ldots\ldots.10$$

Rearranging 9 into the standard format for a quadratic equation gives:

$$0 = \frac{\left[S^-\right]^2}{K_{diss}} + \left\{ 1+ 1\Big/\sqrt{K_{ass}K_{diss}} \; \right\}\left[S^-\right] - \left[S^- \; DIAH^+\right]_{added}$$

Where,

$$\left[S^-\right] = \frac{-b \pm \sqrt{b^2 - 4ac}}{2a}$$

$$a = 1\Big/ K_{diss} \qquad\qquad b = \left\{ 1+ 1\Big/\sqrt{K_{ass}K_{diss}} \; \right\} \qquad c = -\left[S^- \; DIAH^+\right]_{added}$$

$$\left[S^-\right] = \frac{-\left\{ 1+ 1\Big/\sqrt{K_{ass}K_{diss}} \; \right\} + \sqrt{\left\{ 1+ 1\Big/\sqrt{K_{ass}K_{diss}} \; \right\}^2 - 4\left(1\Big/K_{diss}\right)\left(-\left[S^- \; DIAH^+\right]_{added}\right)}}{2\left(1\Big/K_{diss}\right)}$$

$$\left[S^-\right] = \frac{\left(-\left\{ 1+ 1\Big/\sqrt{K_{ass}K_{diss}} \; \right\} + \sqrt{\left\{ 1+ 1\Big/\sqrt{K_{ass}K_{diss}} \; \right\}^2 + 4\left[S^- \; DIAH^+\right]_{added}\Big/K_{diss}}\,\right)K_{diss}}{2}$$

$$\ldots\ldots\ldots.11$$

And

$$\left[S^-\right] = \frac{(Mc - Bc)}{Sc}$$

Where,   Mc = Measured conductance of solution

Bc = Background conductance in the of saccharin and diisopropylamine

Sc = Specific conductance of the analyt

7.3   Calculation of K_{diss} by conductance: Saccharin/*N*-methylimidazole salt

When using *N*-methylimidazole as base the situation is further complicated by the possible involvement of homoconjugation.

$$[\overset{\ominus}{S}\ \overset{\oplus}{NMIH}]ip \ \xrightleftharpoons{K_{diss}}\ \overset{\ominus}{S}\ +\ \overset{\oplus}{NMIH}\ \xrightleftharpoons[\ +\ NMI\ ]{K_{homo}}\ \overset{\oplus}{NMIH}...NMI$$
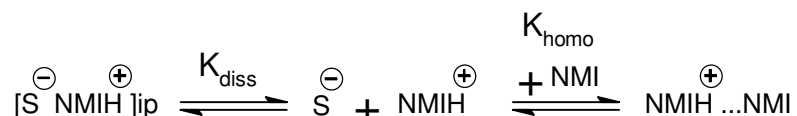
Again when excess *N*-methylimidazole is present the first equilibrium will be displaced across to the right, therefore, in excess *N*-methylimidazole only charged species will be present in solution therefore only K_{diss} will be in effect. However, now there will also be an extra term (K_{homo}) in the equation due to the homo-conjugation of excess *N*-methylimidazole molecules.

$$K_{diss} = \frac{\left[S^-\right]\left[NMIH^+\right]}{\left[S^-\ NMIH^+\right]_{ip}} \qquad \ldots\ldots\ldots 1$$

$$K_{homo} = \frac{\left[NMIH^+...NMI\right]}{\left[NMIH^+\right]\left[NMI\right]} \qquad \ldots\ldots\ldots 2$$

Charges must balance,

$$\left[S^-\right] = \left[NMIH^+\right] + \left[NMIH^+...NMI\right]$$

Therefore equation 1 becomes,

$$K_{diss} = \frac{\left(\left[NMIH^+\right] + \left[NMIH^+...NMI\right]\right)\left[NMIH^+\right]}{\left[S^-\ NMIH^+\right]_{ip}} \qquad \ldots\ldots\ldots 3$$

Rearranging equation 3 gives,

$$\left[S^- \ NMIH^+ \right]_{ip} = \frac{\left(\ \left[NMIH^+ \right] + \left[NMIH^+ ...NMI \right] \ \right) \left[NMIH^+ \right]}{K_{diss}} \qquad ....4$$

Rearranging equation 2 gives,

$$\left[NMIH^+ ...NMI \right] = K_{\hom o} \left[NMIH^+ \right] \left[NMI \right] \qquad ....5$$

The mass balance for reaction can be written as:

$$\left[S^- \ NMIH^+ \right]_{added} = \left[S^- \ NMIH^+ \right]_{ip} + \left[NMIH^+ \right] + \left[NMIH^+ ...NMI \right]$$

$$.........6$$

Substituting equations 4 and 5 into mass balance,

$$\left[S^- \ H^+ NMI \right]_{added} = \frac{\left(\ \left[NMIH^+ \right] + \left[NMIH^+ ...NMI \right] \ \right) \left[NMIH^+ \right]}{K_{diss}} + \left[NMIH^+ \right] + K_{\hom o} \left[NMIH^+ \right] \left[NMI \right]$$

$$.........7$$

Substituting equation 5 into equation 7,

$$\left[S^- \ NMIH^+ \right]_{added} = \frac{\left(\ \left[NMIH^+ \right] + K_{\hom o} \left[NMIH^+ \right] \left[NMI \right] \ \right) \left[NMIH^+ \right]}{K_{diss}} + \left[NMIH^+ \right] + K_{\hom o} \left[NMIH^+ \right] \left[NMI \right]$$

$$.........8$$

Simplifying equation 8 gives,

$$\left[S^- \ NMIH^+\right]_{added} = \frac{\left(\left[NMIH^+\right]^2 + K_{\hom o}\left[NMIH^+\right]^2\left[NMI\right] \right)}{K_{diss}} + \left[NMIH^+\right] + K_{\hom o}\left[NMIH^+\right]\left[NMI\right]$$

$$\left[S^- NMIH^+\right]_{added} = \frac{\left\{ 1 + K_{\hom o}\left[NMI\right] \right\}\left[NMIH^+\right]^2}{K_{diss}} + \left\{ 1 + K_{\hom o}\left[NMI\right] \right\}\left[NMIH^+\right] \ \ldots\ldots\ldots.9$$

Rearranging equation 9 for standard quadratic equation,

$$0 = \frac{\left\{ 1 + K_{\hom o}\left[NMI\right] \right\}\left[NMIH^+\right]^2}{K_{diss}} + \left\{ 1 + K_{\hom o}\left[NMI\right] \right\}\left[NMIH^+\right] - \left[S^- \ NMIH^+\right]_{added}$$

$$\ldots\ldots\ldots.10$$

Where,

$$\left[S^-\right] = \frac{-b \pm \sqrt{b^2 - 4ac}}{2a}$$

$$a = \frac{\left\{ 1 + K_{\hom o}\left[NMI\right] \right\}}{K_{diss}} \qquad b = \left\{ 1 + K_{\hom o}\left[NMI\right] \right\} \qquad c = -\left[S^- \ DIAH^+\right]_{added}$$

$$\left[S^-\right] = \frac{-\left\{ 1 + K_{\hom o}\left[NMI\right] \right\} + \sqrt{\left\{ 1 + K_{\hom o}\left[NMI\right] \right\}^2 - 4\left(\frac{\left\{ 1 + K_{\hom o}\left[NMI\right] \right\}}{K_{diss}} \right)\left(-\left[S^- \ DIAH^+\right]_{added} \right)}}{2 \left(\frac{\left\{ 1 + K_{\hom o}\left[NMI\right] \right\}}{K_{diss}} \right)}$$

$$[S^-] = \frac{\left(-\left\{1 + K_{\text{hom}_o}[NMI]\right\} + \sqrt{\left\{1 + K_{\text{hom}_o}[NMI]\right\}^2 + 4\left\{1 + K_{\text{hom}_o}[NMI]\right\}\left(-[S^- \ NMIH^+]_{added}\right)/K_{diss}}\right)K_{diss}}{2\left\{1 + K_{\text{hom}_o}[NMI]\right\}}$$

$$\ldots\ldots\ldots 11$$

And

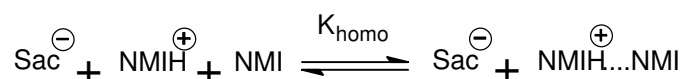$$[S^-] = \frac{(Mc - Bc)}{Sc}$$

Where,   Mc = Measured conductance of solution

Bc = Background conductance in the of saccharin and diisopropylamine

Sc = Specific conductance of the analyt

7.4   **Calculation of K_{homo}**

In the presence of excess *N*-methylimidazole it can be assumed that the equilibria is pulled through to the free ions (scheme 69).

$$\text{Sac}^{\ominus} + \text{NMIH}^{\oplus} + \text{NMI} \underset{\longleftarrow}{\overset{K_{homo}}{\longrightarrow}} \text{Sac}^{\ominus} + \text{NMIH}^{\oplus}...\text{NMI}$$

Scheme 69: *N*-methylimidazole homo-conjugation equilibrium.

Where,

$$K_{\hom o} = \frac{\left[Sac^-\right]\left[NMIH^+...NMI\right]}{\left[Sac^-\right]\left[NMIH^+\right]\left[NMI\ \right]}$$

$$K_{\hom o} = \frac{\left[NMIH^+...NMI\right]}{\left[NMIH^+\right]\left[NMI\ \right]} \qquad\qquad ....1$$

Mass balance,

$$\left[NMI\right]_{added} = \left[NMI\right] + \left[NMIH^+\right] + \left[NMIH^+...NMI\right] \qquad\qquad ....2$$

The concentration of the homoconjugate [NMIH$^+$…NMI] must be equal to the total concentration of saccharin/*N*-methylimidazole salt in solution, [NMIH$^+$]$_{total\ sol}$, less the concentration of the salt in solution which is not homoconjugated. The concentration of none-homoconjugated salt will be a constant, equal to the solubility of saccharin/*N*-methylimidazole salt in the absence of excess *N*-methylimidazole, [NMIH$^+$]$_{lim\ sol}$. Therefore,

$$[NMIH^+...NMI] = [NMIH^+]_{total\ sol} - [NMIH^+]_{\lim\ sol} \qquad \text{.........3}$$

The concentration of none-homoconjugated salt [H$^+$NMI] as discussed above will be equal to its limiting solubility, [NMIH$^+$]$_{\lim\ sol}$. Therefore,

$$[NMIH^+] = [NMIH^+]_{\lim\ sol} \qquad \text{.........4}$$

The concentration of none-homoconjugated N-methylimidazole, [NMI]$_{free}$, can be determined from,

$$[NMI]_{free} = [NMI]_{total} - [NMIH^+]_{\lim\ sol} - 2[NMIH^+...NMI] \qquad \text{.........5}$$

Where the total concentration of N-methylimidazole is given by

$$[NMI]_{total} = [NMI]_{solution} + [NMIH^+]_{total\ sol} \qquad \text{.........6}$$

Substitution of equations 6 and 3 into equation 5 gives,

$$[NMI]_{free} = [NMI]_{solution} + [NMIH^+]_{total\ sol} - [NMIH^+]_{\lim\ sol} - 2\left([NMIH^+]_{sol} - [NMIH^+]_{\lim\ sol} \right)$$

$$\text{.........7}$$

This simplifies to,

$$[NMI]_{free} = [NMI]_{solution} - [NMIH^+]_{total\ sol} - [NMIH^+]_{\lim\ sol} \qquad \text{.........8}$$

Substitution of equation 3, 4 and 8 into the equilibrium equation 1 gives,

$$K_{\text{hom}\,o} = \frac{\left(\left[NMIH^+ \right]_{total\ sol} - \left[NMIH^+ \right]_{\lim\ sol} \right)}{\left(\left[NMI \right]_{solution} - \left[NMIH^+ \right]_{total\ sol} - \left[NMIH^+ \right]_{\lim\ sol} \right) \left[NMIH^+ \right]_{\lim\ sol}}$$

$$\ldots\ldots\ldots 9$$

A plot of $[NMIH^+]_{total\ sol} - [NMIH^+]_{lim\ sol}$ versus $([NMI]_{solution} - [NMIH^+]_{total\ sol} - [NMIH^+]_{lim\ sol})[\ NMIH^+]_{lim\ sol}$ (figure 65) will give a slope equal to the equilibrium constant of homoconjugation K_{homo}.
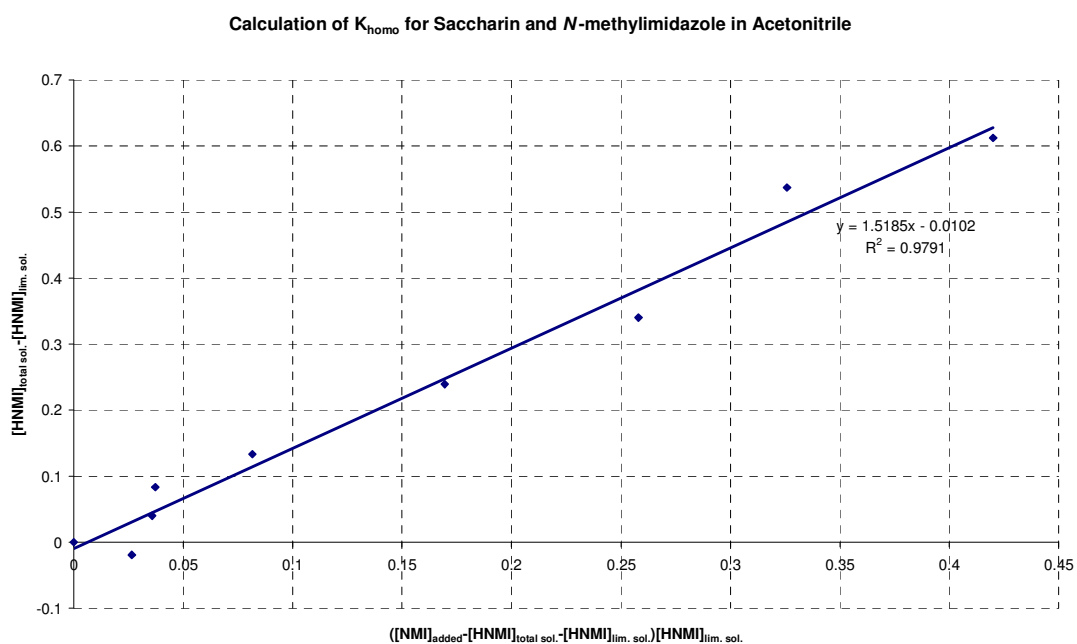
Calculation of K_{homo} for Saccharin and *N*-methylimidazole in Acetonitrile

Figure 65: Plot for calculation of K_{homo}.